

Nd:YVO₄ MICROCHIP LASERS AND AMPLIFIERS

A thesis submitted

by

Glenn Christopher Bowkett B. App. Sc. (RMIT)

for the degree of

DOCTOR OF PHILOSOPHY



Optical Technology Research Laboratory

School of Communication & Informatics

Victoria University of Technology

1999

23122832

FTS THESIS
621.3661 BOW
30001006994984
Bowkett, Glenn Christopher
Nd:YVO[subscript]4 microchip
lasers and amplifiers

Declaration

I, **Glenn Christopher Bowkett**, declare that this thesis titled,

Nd:YVO₄ microchip lasers and amplifiers,

is my own work, and has not been previously submitted, in whole or in part, in respect of any other academic award.

G.C. Bowkett

30 August 1999

Acknowledgments

Firstly, I would like to thank Prof. David Booth, then head of the Applied Physics department, along with the members of the academic staff who allowed me to undertake these research studies. I also thank them for their patience in allowing me to finish these studies. I am also greatly appreciative of the support offered by my supervisor Dr. Greg Baxter in his enduring encouragement, guidance and friendship.

Thanks also goes to my fellow post graduate students for their friendship and assistance, and for making it a pleasant and enjoyable environment in which to work.

I am appreciative of the friendship and help given by all academic, technical and administration staff of the department. Especially the technical help of Tibor Kovacs and Alex Shelamoff in the electronics and fibres fields, and Mark Kivinen and Donald Ermel in the construction of mechanical equipment.

I must also thank visiting research fellow Mingxin Qiu for his initial tests in the microchip area, and I am very grateful for the collaborative research efforts of Takunori Taira and T. Kobayashi, at Fukui University, Japan

I would like to thank my great family, including my late father Terry, my mother Joan and brother Michael, along with my in-laws Barry & Dawn, Robert, Tracy, Dani and Cheree.

A special thanks goes to my wife Anne for her patience, encouragement, love and understanding, and for the gentle push along from our new born son Tyler James.

And to God who makes all things possible, including an exciting universe worth investigating. Also thanks to my small groups at HNC for their encouragement and prayer.

Abstract

An investigation of microchip laser and amplifier systems using the material Neodymium doped Yttrium orthovanadate (Nd:YVO₄) has been performed. This project takes advantage of recent improvements in the growth of Nd:YVO₄ to investigate its potential as a compact and simple single longitudinal mode laser. Such lasers (termed microchip lasers) have important applications in laser seeding, communications and frequency doubled micro-laser systems. The material has also been investigated as a compact optical amplifier.

The optical properties of the Nd:YVO₄ material were initially investigated. The peak absorption of 94.6% of the pump light over the 0.5 mm length of the microchip was found to be at 808.51 nm, with π polarization. For σ polarized incident light the best absorption was 62.3% at a wavelength of 808.68 nm. These figures correspond to absorption co-efficients of 58.19 cm⁻¹ and 19.49 cm⁻¹, respectively. It was found that over a pump wavelength region of 1.8 nm, greater than 75% of the π polarized pump light was absorbed in the 0.5 mm length of the Nd:YVO₄ microchip.

Fluorescence from the Nd:YVO₄ sample was identified as sets of transitions from the upper laser level (⁴F_{3/2}) to the lower lying levels, ⁴I_{13/2}, ⁴I_{11/2} and ⁴I_{9/2}. Closer inspection of these regions (particularly to ⁴I_{13/2} ($\approx 1.34 \mu\text{m}$) and ⁴I_{11/2} ($\approx 1.06 \mu\text{m}$)) allowed the identification of the Stark split sub-levels responsible for the observed laser transitions. The main laser transitions were identified as originating from the lowest Stark sub-level of ⁴F_{3/2} to either the lowest Stark sub-level of ⁴I_{11/2} (1.06 μm transition) or the lowest Stark sub-level of ⁴I_{13/2} (1.34 μm transition). In the 1.34 μm case a second laser transition was observed, under certain pump power and crystal temperature conditions, which corresponded to a transition from the lowest Stark sub-level of ⁴F_{3/2} to the second lowest Stark sub-level of ⁴I_{13/2}.

Standard theoretical models for both lasers and amplifiers have been applied to the microchip situation. The laser model predicted values for incident pump power lasing threshold and incident versus output power slope efficiency. Two amplifier models predicted small signal gain against incident pump power, with the second model further considering the effect of high pump

intensities to better predict the observed results. The experimentally measured results have been compared to these models.

A piece of Nd:YVO₄ crystal coated to produce 1.06 μm lasing (the microchip laser) exhibited laser action across a large range of pump wavelengths, in both the 750 nm and 810 nm absorption bands, with both π and σ polarized incident pump light. The relative magnitude of the microchip laser output power across these wavelengths followed quite closely the relative absorption characteristics. It was found that the best laser output performance was achieved with π polarized incident pump light.

The highest microchip laser output power was approximately 80 mW for an incident pump power of 186 mW. The output spectrum remained single longitudinal mode at room temperature (≈20-21 °C) up to the maximum observed output power. The 1.06 μm laser demonstrated lowest thresholds of around 20 mW, and highest slope efficiency figures of approximately 50%. The output beam of the Nd:YVO₄ microchip laser was predominantly π polarized, with a divergence estimated to be 14 mrad (full angle), with a TEM₀₀ beam.

The separation between longitudinal modes was measured to be 0.52 nm (≈ 139 GHz), identical to that calculated. The laser's peak mode was temperature tunable at a rate of approximately 0.0056 nm/°C or -1.5 GHz/°C, comparing favourably with the calculated value of -1.64 GHz/°C. Single longitudinal mode output was maintained over a range of approximately 50°C for the 0.5 mm thick 1.06 μm microchip laser, at pumping powers of less than 200 mW.

A microchip coated to produce 1.34 μm lasing was pumped using the superior π polarization. An output power of 60 mW, at 1.342 μm, was obtained for a pump power of 422 mW. Here the output spectrum exhibited a second longitudinal mode, 20 dB less intense than the main peak. For output powers less than 40 mW the output spectrum displayed a single longitudinal mode. Lasing threshold levels of between 240 and 275 mW were observed, with a maximum slope efficiency of 40%. A second laser transition was occasionally observed at approximately 3.5 nm above the

main transition. The appearance of this transition was interdependent on the amplitude of the pump power and the microchip temperature.

To achieve single longitudinal mode lasing it was necessary to position one mode close to the centre of the gain profile. With 370 mW of incident pump power (approximately 40 mW output) single mode operation was achieved up to a temperature of approximately 30°C. For the 1.34 μm microchip laser the best operation, in terms of achieving single longitudinal mode operation, was obtained at room temperature.

The laser's output frequency was temperature tuned at approximately -2 GHz/°C, which corresponds to a tuning range of approximately 1.25 nm over the 0 to 100°C tested. A direct theoretical comparison of the frequency temperature tuning rate could not be made, since a figure for $\partial n_e / \partial T$ (change of refractive index with temperature) in Nd:YVO₄ at 1.34 μm could not be found in the literature. Therefore, from our experimentally measured frequency shift, the first known value of $\partial n_e / \partial T$ at 1.34 μm in Nd:YVO₄ is deduced to be $10.8 \pm 2.4 \times 10^{-6} / ^\circ\text{C}$.

Single pass gains in excess of 90 times (19.6 dB) were achieved at 1.06 μm with 30 μm diameter co-linear pump and signal beams. This was achieved in a 1 mm length of crystal with an incident pump power of 350 mW, and signal power of less than 10 μW . For a pumping diameter of 100 μm , the gain reduced to ≈ 3 (4.8 dB). Clearly indicating the need for small diameters (high intensities) to achieve high gains in this system.

Contents

	Page
CHAPTER 1 Introduction and Review	1
Introduction	1-2
1.1 Laser Materials	1-3
1.1.1 Rare-earth Dopant Ions	1-3
Rare-earth Ions.	1-4
Four Level Lasers	1-5
Neodymium (Nd ³⁺) Dopant Ion	1-6
1.1.2 Host Material	1-8
General	1-8
Nd:YVO ₄	1-9
Review of Nd:YVO ₄ Material	1-9
1.2 Narrow Bandwidth Lasers	1-13
Microchip Lasers	1-14
Microchip Lasers Review	1-15
1.3 Microchip Amplifiers	1-19
Review of Compact Optical Amplifiers	1-20
1.4 Scope of this Thesis	1-21
CHAPTER 2 Theory and Models	24
Introduction	2-25
2.1 Microchip Laser and Amplifier Principles	2-25
2.1.1 Microchip Lasers.	2-25
Longitudinal mode spacing	2-26
Spatial Output	2-28
Fluorescence profile	2-29
Temperature tuning	2-30

2.1.2 Microchip Amplifiers	2-32
2.2 Models	2-32
2.2.1 Laser Model	2-33
Laser rate equations	2-33
Gain	2-35
Establishing measurable laser parameters	2-37
Modifications to an ideal four-level system	2-38
Stark split upper laser level	2-38
Fluorescence branching ratio	2-39
2.2.2 Amplifier Model	2-40
Small signal single-pass Gain	2-40
Model One	2-40
Model Two	2-42
Saturation intensity	2-43
Conclusion	2-43
CHAPTER 3 Experiment	44
Introduction	3-46
3.1 Equipment	3-46
3.1.1 Pump Sources	3-46
3.1.2 Power Measurement	3-51
3.1.3 Absorption & Fluorescence Measurement	3-52
3.1.4 Beam Profiling	3-53
3.1.5 Microchips, Holders and Temperature Control	3-55
3.1.6 Miscellaneous Equipment	3-58
3.2 Experimental Techniques	3-61
3.2.1 Establishing pump spot size	3-61
3.2.2 Measurement of beam divergence	3-64

3.3 Measurement of Absorption	3-65
3.3.1 Using a White Light Source	3-65
3.3.2 Through Power Technique using a Ti:sapphire laser	3-70
3.4 Measurement of Fluorescence	3-71
3.5 Characterization of Microchip Lasers	3-72
3.5.1 Laser at 1.06 μm	3-73
3.5.2 Laser at 1.34 μm	3-76
3.6 Characterization of Microchip Amplifiers	3-77
3.6.1 Experimental Arrangement	3-78
3.6.2 Measurement of Gain	3-81
3.6.3 Measurement of Gain against Signal Power	3-82
3.6.4 Measurement of Gain against Pump Power	3-82
3.6.5 Amplification at 1.34 μm	3-83
Conclusion	3-85
CHAPTER 4 Characterization of the Nd:YVO₄ microchips	86
Introduction	4-87
4.1 Energy Levels of Nd:YVO ₄	4-87
4.2 Absorption Measurements	4-89
4.2.1 Discussion	4-94
4.3 Fluorescence Measurements	4-98
4.3.1 Discussion	4-103
4.4 Nd:YVO ₄ Microchip Quality	4-107
Conclusions	4-110
CHAPTER 5 Microchip Lasers	112
Introduction	5-113
5.1.1 1.06 μm Microchip Laser	5-113

Output versus Pump Wavelength	5-113
Output Power, Thresholds & Slope Efficiencies	5-115
Temperature Tuning	5-117
5.1.2 Model results for 1.06 μm microchip laser	5-119
5.1.3 Performance of 1.06 μm laser - Discussion	5-122
Output versus Pump Wavelength	5-122
Output Power, Thresholds & Slope Efficiencies	5-123
Output Beam	5-124
Temperature Tuning	5-125
5.2.1 1.34 μm Microchip Laser	5-127
Output versus Pump Wavelength	5-128
Output Power, Thresholds & Slope Efficiencies	5-128
Temperature Tuning	5-132
Second Transition	5-134
5.2.2 Model results for 1.34 μm microchip laser	5-135
5.2.3 Performance of 1.34 μm laser - Discussion	5-137
Output versus Pump Wavelength	5-137
Output Power, Thresholds & Slope Efficiencies	5-138
Output Beam	5-140
Temperature Tuning	5-140
Conclusion	5-141
CHAPTER 6 Microchip Amplifiers	143
Introduction	6-144
6.1.1 Amplification at 1.06 μm	6-144
Gain against Signal Power	6-144
Saturation intensity	6-145
Gain against Pumping Power	6-146

6.1.2 Model results for 1.06 μm amplifier	6-148
6.1.3 1.06 μm amplifier - Discussion	6-153
6.2.1 Amplification at 1.34 μm .	6-156
6.2.2 Model results for 1.34 μm amplifier	6-157
6.2.3 1.34 μm amplifier - Discussion	6-158
Conclusion	6-159

CHAPTER 7 Conclusions/Summary 160

Introduction	7-161
7.1 Nd:YVO ₄	7-162
7.2 Microchip lasers	7-163
7.3 Microchip Amplifiers	7-166
7.4 Current and Future Work	7-167

APPENDIX 1 - Review of research on Microchip devices (not covered in this work) A-1

APPENDIX 3 - Spot size calculations A-6

APPENDIX 3 - Casix WWW page (Nd:YVO₄ parameters) A-8

APPENDIX 4 - Publications resulting from this work A-9

REFERENCES R-1

Chapter 1 Introduction and Review

Introduction

1.1 Laser Materials

1.1.1 Rare-earth Dopant Ions

Rare-earth Ions

Four Level Lasers

Neodymium (Nd³⁺) Dopant Ion

1.1.2 Host Material

General

Nd:YVO₄

Review of Nd:YVO₄ Material

1.2 Narrow Bandwidth Lasers

Microchip Lasers

Microchip Lasers Review

1.3 Microchip Amplifiers

Review of Compact Optical Amplifiers

1.4 Scope of this Thesis

Chapter 1

Introduction and Review

Introduction

Lasers are generally described as being single frequency, however when investigated in more detail a laser is found to produce light which has a narrow range of frequencies (usually described by the bandwidth). In many applications it is advantageous to have this bandwidth as narrow as possible. Narrow bandwidth laser operation enables optical communication networks to achieve high data rates over large distances by minimizing chromatic dispersion along the length of an optical fibre (chromatic dispersion is the spreading of a light pulse in time due to the different frequencies present). The high coherence of the beam offered by a narrow bandwidth laser also enables it to be utilised for many applications requiring coherence measurement techniques, for example: interferometry, coherent spectroscopy, coherent lidar, and for other types of laser and optical fibre based sensing systems.

Narrow bandwidth laser operation is usually achieved through the addition of extra components to the laser system introducing added cost, volume and optical losses. In the case of a microchip laser, the short length of the lasing material results in a laser which inherently demonstrates single-longitudinal-mode operation, by providing a limited number of longitudinal modes within the gain region, thereby producing an extremely simple, narrow bandwidth laser source.

The development of microchip lasers has seen the emergence of a relatively cheap, easily manufactured and mass produced laser source with characteristics suitable for many laser applications [DeShazer (1994), Randolph(1995)]. In particular, the characteristics of the Nd:YVO₄ crystal make it well suited for use in a microchip laser configuration.

The advantageous lasing characteristics of Nd:YVO₄ crystals have been established for some time, [see for example the review by DeShazer (1994)], however until recently it was not possible to grow YVO₄ crystals of adequate size and quality. Recent developments in this area

have seen renewed interest in Nd:YVO₄ lasers and amplifiers. It is in this context that the present study examines the performance of Nd:YVO₄ as a gain material for microchip lasers, along with microchip amplifiers.

This chapter explores the suitability of rare-earth elements as dopant ions for solid-state lasers, with particular attention on neodymium, the most popular rare-earth dopant for laser applications. Following this, the properties required for a practical laser host material are described, leading to an introduction of the examined host material, yttrium orthovanadate (YVO₄). A discussion of various techniques which have been employed to achieve narrow bandwidth lasing is given in section 2, leading to an explanation of why the microchip laser is of particular interest within this group of lasers. A historical review of the literature covering the development and testing of various miniature and microchip lasers follows. Section 3 introduces the idea of microchip amplifiers, including a review of compact optical amplifiers. The final section of this chapter will outline the structure of the remainder of this thesis.

1.1 Laser Material

Lasers are a well developed technology, and there are many reference books covering the principles of lasers (see for example: Koechner (1992) or Siegman (1986)). Consequently, it is not intended to present all the principles here, but simply to develop an argument as to why the rare-earth element neodymium is particularly suitable as a dopant in laser materials, and why in combination with the host YVO₄ it is an extremely effective material for short absorption depth microchip devices.

1.1.1 Rare-earth Dopant Ions

Solid-state ionic lasers are sometimes referred to as doped-host lasers. They operate on an optical transition between two energy levels of an ion present as an impurity, or dopant, at relatively low

concentrations in a solid crystal or glass structure, which forms the host material. Here dopants which belong to the rare-earth elements group are reviewed.

Rare-earth Ions

Rare-earth ions are attractive as active ions in solid-state laser materials because they exhibit a wealth of sharp fluorescent transitions in the visible and near-infrared region. This arises from the fact that the outer most electrons ($5s^2$ and $5p^6$) of the rare-earth elements form a complete shell which is optically inactive, and sharp fluorescent transitions can be generated by the electrons in a partially filled inner shell (4f). Since the 4f shell is an inner shell it is well shielded, and as a consequence the associated energy levels are only weakly influenced by the external electric fields caused by neighbouring ions within the host material, in which the ion is placed. The associated transitions are therefore relatively sharp. When a rare-earth ion is placed in various host materials the energy levels, and corresponding transitions associated with the 4f electrons, remain very similar.

Atomic Number	Element	Outermost electrons					
		4d ¹⁰	4f ⁿ	5s ²	5p ⁶	-	6s ²
58	Cerium, Ce	4d ¹⁰	4f ²	5s ²	5p ⁶	-	6s ²
59	Praseodymium, Pr	4d ¹⁰	4f ³	5s ²	5p ⁶	-	6s ²
60	Neodymium, Nd	4d ¹⁰	4f ⁴	5s ²	5p ⁶	-	6s ²
61	Promethium, Pm	4d ¹⁰	4f ⁵	5s ²	5p ⁶	-	6s ²
62	Samarium, Sm	4d ¹⁰	4f ⁶	5s ²	5p ⁶	-	6s ²
63	Europium, Eu	4d ¹⁰	4f ⁷	5s ²	5p ⁶	-	6s ²
64	Gadolinium, Gd	4d ¹⁰	4f ⁷	5s ²	5p ⁶	5d ¹	6s ²
65	Terbium, Tb	4d ¹⁰	4f ⁹	5s ²	5p ⁶	-	6s ²
66	Dysprosium, Dy	4d ¹⁰	4f ¹⁰	5s ²	5p ⁶	-	6s ²
67	Holmium, Ho	4d ¹⁰	4f ¹¹	5s ²	5p ⁶	-	6s ²
68	Erbium, Er	4d ¹⁰	4f ¹²	5s ²	5p ⁶	-	6s ²
69	Thulium, Tm	4d ¹⁰	4f ¹³	5s ²	5p ⁶	-	6s ²
70	Ytterbium, Yb	4d ¹⁰	4f ¹⁴	5s ²	5p ⁶	-	6s ²

Table 1.1: *Electronic configuration of outer shells of Rare-Earth ions.**

Rare-earth ions usually exist in solids in either the trivalent or the divalent state. A divalent rare-earth ion is formed when the atom gives up its outermost 6s electrons. When a

* Electronic configuration of the elements taken from the CRC Handbook of Chemistry and Physics, 64th Ed., CRC Press Inc., Florida (1983-84).

trivalent ion is formed the atom also gives up a 4f electron (or the 5d electron in the case of Gd). This can be understood from Table 1.1, which shows the electronic configuration of the outer most shells.

The 4f shell is filled progressively for each successive rare-earth. While 4f levels remain unoccupied, electrons (already present in the 4f shell) can be raised by absorption of light into the empty 4f energy levels.

Four Level Lasers

Lasers which include rare-earth dopants as the optically active component will most commonly operate with what is generally described as a four level, optically pumped, laser scheme. The four-level scheme is the most common as lasers of this type do not require as high pumping powers, in comparison to two and three level laser systems. Figure 1.1 represents the different energy levels, within an ion, which make up the levels required for a four level lasing system. The ions are pumped from the ground state, 0, to an upper level, 3, from which they rapidly decay to a metastable level 2. From level 2 there is a slow decay to level 1, then a rapid decay back to the ground state. The laser transition responsible for producing the photons needed for laser action, is between levels 2 and 1, where an ion in level 2 is stimulated into a transition to level 1, resulting in the emission of a photon. For a laser, this stimulation is provided by photons which are reflected by a set of cavity mirrors, where the initial photons to begin the process are provided by spontaneous transitions between levels 2 and 1.

The upper level 3, commonly referred to as the pump level, may in fact be comprised of a number of higher energy levels, which together absorb the pumping power. When a large number of rare-earth ions within the laser material are being continually pumped to the upper level using incident light of an appropriate wavelength, most of the ions will be either in level 2 (the metastable state) or in the ground state, due to the short lifetimes of levels 3 and 1. This allows a large population inversion to be generated between levels 2 and 1.

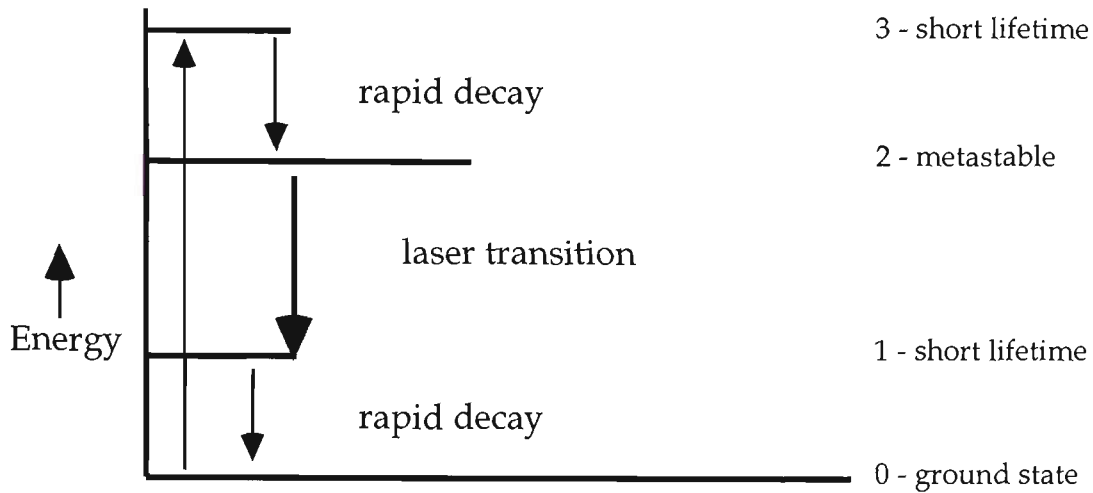


Figure 1.1: Energy levels within an ion, which represent a four-level laser. The length of the lines representing the levels are indicative of the population densities.

Neodymium (Nd³⁺) Dopant Ion

Neodymium is generally present in solid-state lasers in the form of Nd³⁺ ions. It was the first of the trivalent ions to be used in a laser [Johnson & Nassau (1961)], and remains by far the most common. Higher powers have been obtained from neodymium lasers than any other four-level laser system. The principal host materials used with neodymium have been yttrium aluminium garnet (Y₃Al₅O₁₂), better known as YAG, and glass; though there have been many others.

A simplified energy level scheme for the neodymium ion, shown in figure 1.2, indicates that there are four possible transitions from the ⁴F_{3/2} metastable level. The wavelength(s) of these transitions are centred at approximately 0.9, 1.06, 1.3 and 1.8 μm, corresponding to transitions from the metastable level to the lower levels ⁴I_{9/2}, ⁴I_{11/2}, ⁴I_{13/2} and ⁴I_{15/2} respectively, with the ⁴I_{9/2} level being the ground state. (A laser operating between the ⁴F_{3/2} and ⁴I_{9/2} levels may be considered to be a four level system if the Stark levels within ⁴I_{9/2} level are sufficiently spaced, resulting in the upper of these Stark levels being relatively unpopulated. If this is not the case, this laser transition would be more properly modelled as a three level laser.) Of the various transitions from the ⁴F_{3/2} metastable state to the lower lying levels, the 1.06 μm transition to the ⁴I_{11/2} level is the strongest, and the ≈1.8 μm transition to the ⁴I_{15/2} level is, by far, the weakest.

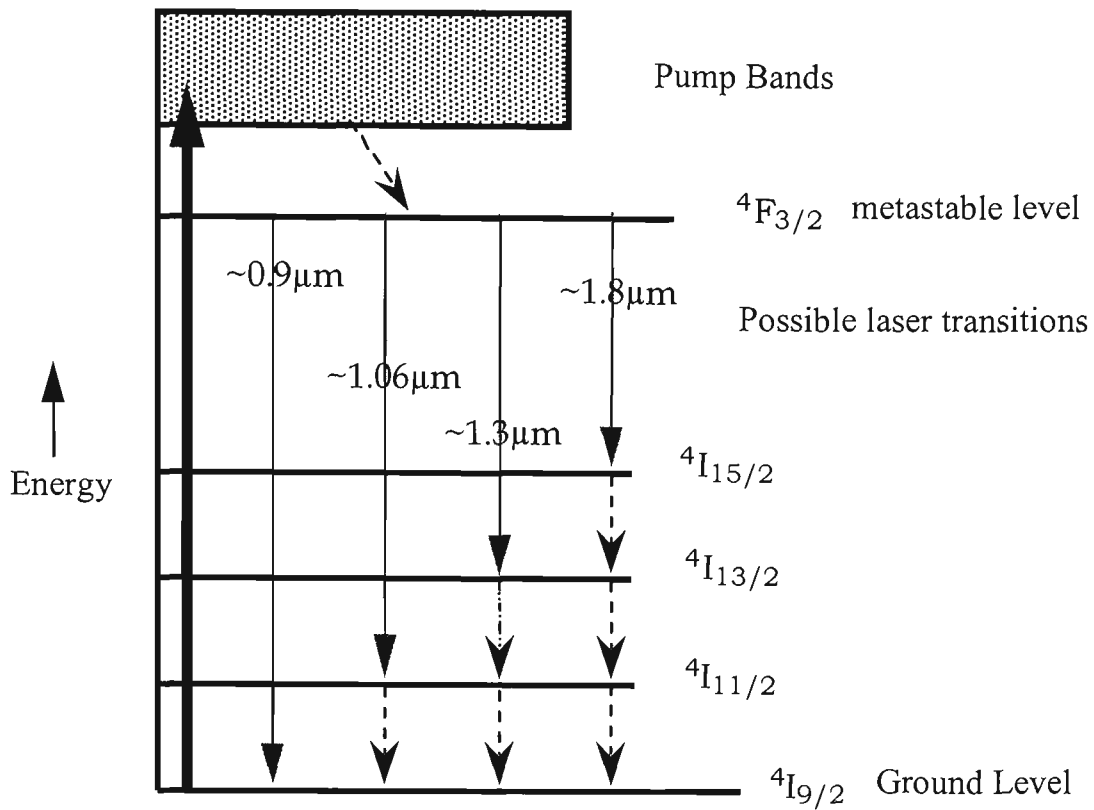


Figure 1.2: Neodymium (Nd^{3+}) energy level scheme. [not to scale]

Each of the energy levels shown in figure 1.2 may be further divided into a series of closely spaced sub-levels, known as Stark levels. This Stark splitting of the energy levels takes place in an electric field produced by the host environment in which the ion is placed. Consequently, the host material will determine the separation of Stark split sub-levels.

For the neodymium ion there are several strong absorption regions in the visible and near infrared (energy levels above the $4F_{3/2}$ level) which combined, or alone, form the possible pump band/s of a laser system. A broadband pump source may result in absorption of energy in many of these levels, or an appropriately chosen narrowband source in just one or two. From the pump bands the ion decays rapidly to the $4F_{3/2}$ metastable level.

1.1.2 Host Material

General

In rare-earth solid-state lasers the primary role of the host material is to hold the rare-earth ions in place, however they must also have several other properties conducive to successful laser action. The material must first have favourable optical properties, such as very low variation in refractive index throughout the material, and low absorption at the lasing wavelength. It must have good physical properties; these may include: hardness, chemical inertness and absence of internal strains. It must also have a high thermal damage threshold to withstand the heat generated by the pumping source.

The host material needs to have sites that can accept the dopant ions, ideally with the size and valance of the dopant ion matching that of the host ion it replaces. It must also be possible to grow the doped material to sufficient size with high optical quality, and then be cut and polished with great precision.

Solid-state host materials may be broadly grouped into glasses and crystalline solids. Glass is easily fabricated and from it a high quality optical finish can be produced. Laser ions placed in glass generally show a larger fluorescent bandwidth (broadening and flattening) than in crystals as a result of the lack of a unique and well-defined crystalline surrounding for the individual active ions. Therefore, the laser threshold for glass based lasers is generally higher than for lasers where the ion has been included in a crystalline host.

A laser based on a crystalline host material generally offers advantages over glasses in that it has a higher thermal conductivity, narrower fluorescence bandwidth, and in some cases, greater hardness. However, the optical quality and doping homogeneity of crystalline hosts are often poorer, and the absorption lines are generally narrower.

The crystal yttrium aluminium garnet doped with neodymium (Nd:YAG) has achieved a position of dominance among solid-state laser materials. YAG is a very hard, isotropic crystal, which can be grown and fabricated in a manner that yields rods of high optical quality. Up until recently, it has been the best commercially available crystalline laser host for Nd^{3+} , offering low

threshold and high gain. However, some other Nd³⁺ doped high-quality crystals are now becoming available which show better properties, in certain laser applications.

Nd:YVO₄

Nd³⁺ - doped yttrium orthovanadate (YVO₄) crystal is one of the materials to show some superior properties to Nd:YAG, in particular broader and stronger absorption. However, until recently Nd:YVO₄ could not be considered as a practical laser material because of growth difficulties associated with its production. Only over the past few years have these growth difficulties been overcome. Despite the fact that its thermal conductivity is much poorer than Nd:YAG, Nd:YVO₄ has recently been shown to out perform Nd:YAG, for low to medium power applications. A review of the characterization and development of YVO₄ as a host material for Nd³⁺ ions follows.

Review of Nd:YVO₄ Material

Neodymium is found to lase well in a large number of host materials [see for example, Kaminskii (1990) and Barnes *et al.* (1990)], and constitutes one of the most common laser dopants. Neodymium doped into Yttrium Aluminium Garnet (YAG) is by far the most common solid state laser material. However, it has been known for a long time that Neodymium doped into Yttrium Orthovanadate (YVO₄) does, in many respects, show better laser performance than Nd:YAG.

The first significant study of Nd:YVO₄ as a laser material was conducted by O'Connor (1966). The material demonstrated an increased oscillator strength at 1.06 μm when compared to that of Nd:YAG; at both room temperature and at 77 K. In addition, low threshold laser operation was observed at 90 K. From this initial study O'Connor concluded, "In view of its early stages of development, YVO₄:Nd³⁺ should become an important laser system".

Over the next few years several papers were published on Nd:YVO₄ by a group at the Institute of Crystallography, Academy of Sciences, USSR [Bagbasarov *et al.* (Feb 1968, Dec 1968), Kaminskii *et al.* (1969), Kaminskii (1969)]. In these papers room temperature laser action at 1.064 and 1.066 μm in Nd:YVO₄ was reported. The absorption and fluorescence characteristics of the crystal were determined and the Stark splitting of many of the levels, especially those

involved with the laser transition, were established. From this information, a partial energy level diagram between ${}^4I_{9/2}$ (0 cm^{-1}) and ${}^4D_{1/2}$ ($\approx 28,000\text{ cm}^{-1}$) was developed.

Though the Nd:YVO₄ crystal showed promise as a laser material, it was nearly totally abandoned for a period of five to six years due to problems associated with its growth. In a recent vanadate review article, DeShazer (1994) explains that during the Nd:YVO₄ crystal growth there occurred the biaxial metavanadate crystalline phase, YVO₃, within the uniaxial orthovanadate YVO₄ structure. This metavanadate phase is the origin of lossy, micron sized, scattering centres and absorbing color-centre defects within the crystal. These defects made the material ineffective as a laser crystal.

During the period, mid-seventies to early-eighties, researchers from the Center for Laser Studies, University of Southern California and the Aerospace Corporation, California, presented results generated with the use of larger, higher quality samples of Nd:YVO₄ grown by the Czochralski method at the Union Carbide Corporation. DeShazer *et al.* (1974) reported that by choosing incident light with π polarization (polarised parallel to c-axis, propagating along the crystallographic a-axis), Nd:YVO₄ had a stimulated emission cross-section approximately five times that of Nd³⁺ in YAG. It was noted that the YVO₄ exhibited a strongly birefringent uniaxial nature. This work determined the fluorescence lifetime of the ${}^4F_{3/2}$ state of Nd³⁺ in YVO₄ to be 94 μsec (Nd concentration not given), and demonstrated that long pulse, Q-switched and cw laser operation was possible.

Using small samples of Nd:YVO₄ Tucker *et al.* (1976) reported cw laser operation at 1.06 and 1.34 μm , with end pumping from an argon-ion laser. Despite a loss coefficient nearly ten times larger in the Nd:YVO₄ samples than that of high-quality Nd:YAG rods, the Nd:YVO₄ based laser performed equally as well at 1.06 μm , and even better at 1.34 μm , than similar Nd:YAG lasers. The authors observed that Nd:YVO₄ based lasers were still hindered by the lack of large, laser-grade crystals.

Following on from the spectroscopic studies performed to establish energy levels of Nd:YVO₄ in the late sixties, Yaney and DeShazer (1976) presented further energy level results. These results were obtained from analysis of polarised absorption and dye-laser excited

fluorescence investigations. Energy level positions, their identities and observed polarisation were noted. The principal laser line (1064 nm) was found to be predominantly π polarized with a stimulated emission cross-section of 30×10^{-19} ($\pm 20\%$) cm^2 , this being 4.6 times larger than the laser transition in Nd:YAG.

Further measurements of stimulated emission cross-section were made by Tucker *et al.* (1977). Comparative values were obtained on small samples of Nd:YVO₄ and Nd:YAG, with the cross-section of Nd:YVO₄ at 1064 nm measured to be approximately 2.7 times greater than that of Nd:YAG. This was a smaller difference than that previously reported (see note next paragraph), with the Nd:YVO₄ having a stimulated emission cross-section of $(12.0 \pm 2.4) \times 10^{-19}$ cm^2 at 1.06 μm and $(6.0 \pm 1.8) \times 10^{-19}$ cm^2 at 1.34 μm . The cross-section found for 1342 nm in Nd:YVO₄ was slightly greater than that for Nd:YAG at 1064 nm. Also reported was a reduction of the fluorescence lifetime of the $^4F_{3/2}$ level (upper laser level) with increasing neodymium concentration, from 98 μs with 1 at% Nd doping, to 57 μs with 3 at% Nd doping (at% - atomic percent). Sliney *et al.* (1979) also measured the lifetime of the $^4F_{3/2}$ level with different concentrations, measuring 100 μs with 0.4 at% Nd, down to 60 μs with 1.6 at% Nd {see footnote}.* Sliney found the lifetime to be constant with temperature at ≈ 100 μs over the range 90 to 300K, but had dropped to ≈ 87 μs at 453K. In further work, Tucker *et al.* (1981) measured the stimulated emission cross-section at 1.06 μm for a 1 at% doped sample, with a reported improved technique, and obtained a figure of $19.0 \pm 2.7 \times 10^{-19}$ cm^2 , with a fluorescence lifetime of 97 μs .

It is relevant to state that the measurement of the stimulated emission cross-section is not straight forward, nor is there a standard technique, and thus, different techniques often realize different values. This is because there is no direct measurement of the cross-section, it is based on the results of a combination of measurements, each with their associated errors. In addition, some of the techniques rely on determination of the stimulated emission cross-section value by comparison to that of other similar laser materials, which themselves are subject to variation depending on the technique used to establish their cross-section values.

* {The same trend of decreasing lifetime with increase in concentration is shown, consistent with Tucker, but at apparent lower concentrations of Neodymium. The manufactures specifications of Sliney's Nd:YVO₄ crystals were 1, 2 & 3 at% Nd concentration; but Sliney's own measurements gave 0.41, 0.72 & 1.6 at% ($\pm 15\%$). However, these concentration versus lifetime figures appear inconsistent with most other values found}.

The interest in YVO_4 as a host for Nd^{3+} ions (that was revived in the mid-seventies to early-eighties period, due primarily to improved techniques for growth of the YVO_4 crystal) began to wane due to the crystal's relatively low thermal conductivity. At this stage of laser technology development the low thermal conductivity was a particular problem since the standard method of pumping was by flash lamp, whose rather large spectral output produced a significant amount of unwanted heat. The late 80's saw the introduction of high power laser diodes for solid state laser pumping which, together with further improvements in the quality of YVO_4 crystal, again renewed interest in YVO_4 as a possible alternative host for the Nd^{3+} ion.

The first laser diode end-pumped $\text{Nd}:\text{YVO}_4$ laser was demonstrated by Fields *et al.* (1987). Comparative tests showed the YVO_4 system to have a lower threshold and a higher output power when compared to a similar $\text{Nd}:\text{YAG}$ laser. Measurements across a range of pump wavelengths showed a much wider pump absorption band than was available in $\text{Nd}:\text{YAG}$. The researchers concluded, "Our results reported here suggest that $\text{Nd}:\text{YVO}_4$, in presently obtainable material quality, is the laser crystal of choice for obtaining the highest cw power and lowest threshold from a DLEPL (diode-laser end-pumped laser) device." In the following year Jain *et al.* (1988) and Innocenzi *et al.* (1988) reported laser diode pumped $\text{Nd}:\text{YVO}_4$ lasing at $1.34 \mu\text{m}$.

Over the next few years several researchers including Fields *et al.* (1989), Barnes *et al.* (1990) and Mermilliod *et al.* (1992) compared the performance characteristics of various Nd ion host materials. Of six Nd host materials tested by Fields, $\text{Nd}:\text{YVO}_4$ showed the best output power versus input power slope efficiency, and the lowest threshold. Barnes concluded that the absorption efficiency of the π axis for $\text{Nd}:\text{YVO}_4$ was one of the highest of any laser material studied. Of eight Nd host materials studied by Mermilliod, $\text{Nd}:\text{YVO}_4$ had one of the highest laser efficiencies. In contrast to the other high efficiency materials, $\text{Nd}:\text{YVO}_4$ also had a large absorption bandwidth.

$\text{Nd}:\text{YVO}_4$ has now been brought to prominence for lasers with low to medium output powers, particularly with further improvement in the growth of vanadate crystals. Lasers are now being produced with smaller crystals because of the much improved efficiency offered by laser diode pumping and the strong absorption of pump radiation offered by the $\text{Nd}:\text{YVO}_4$.

The improvements in the techniques for producing Nd:YVO₄ have yielded significantly improved crystal quality, to the point where the material has become commercially available in the last five to six years. Higgins in *Laser Focus World* March 1993, and DeShazer in *Laser Focus World* February 1994, describe the improvement in quality of vanadate crystals and their subsequent availability. Many research groups have recently reported diode pumped Nd:YVO₄ lasers [see for example: Bernard *et al.* (June 1993, Dec 1993, Nov 1994), Feugnet *et al.* (1993, 1995) and Scheps *et al.* (Aug 1994, Sept 1994)]. The commercial availability of Nd:YVO₄ has resulted in it being utilized in commercial products; many of the devices currently available utilize the microchip concept and in this context, Nd:YVO₄ has proved especially useful.

1.2 Narrow Bandwidth Lasers

High resolution studies of the output from a passive laser resonator will generally reveal the laser operating in many longitudinal modes, which combined constitute the output frequency spread of the laser. Normally this bandwidth is characteristic of the gain profile which is naturally much larger than that for a laser made to operate in a single-longitudinal-mode. Very narrow laser bandwidth operation, in particular single-longitudinal-mode operation, is beneficial in many applications.

Narrowing of the output bandwidth of a laser is generally achieved by the introduction of additional components to the laser system. These additional components add to the optical losses, cost and volume of the complete laser system. Such components are used to provide high feedback for a single laser mode, actively discriminating against the other modes. This may be achieved by adding additional reflectors within the cavity or by inserting etalons within the cavity.

Other methods of narrowing the laser bandwidth modify the laser system so that it will preferentially select one, or a few, longitudinal laser modes; these are listed below:

- Cooling the laser, which has the effect of reducing the number of modes with sufficient gain to oscillate.

- Reducing the spatial hole burning. The problem of spatial hole burning is prevalent in crystals, where atoms located in the vicinity of the nodal planes of one longitudinal mode will preferentially contribute to other laser modes. Spatial hole burning may be eliminated by: employing a ring-laser cavity with unidirectional oscillation, by generating circularly polarized light in the rod, with mechanical motions, or with electro-optic phase modulations [Koechner(1992) p246]. Any technique reducing the effect of spatial hole burning will increase the likelihood of obtaining single longitudinal operation, but usually at the expense of added components or complexity to the system.
- Shortening the optical resonator, therefore increasing the difference in wavelength spacing between adjacent longitudinal modes, and thereby reducing the number of modes that are available within the gain region.

This final method of achieving single-longitudinal-mode oscillation is the one on which the microchip laser concept is based. For a successful microchip laser the material used must have very strong absorption of the pump light, and a high conversion efficiency of this pump energy into laser action. Such characteristics enable the microchip to be made sufficient thin so as to support only one longitudinal mode within the gain region, while still absorbing sufficient pump light. A fundamentally simple narrow bandwidth laser source may then be constructed by coating cavity mirrors on two opposite sides of the microchip surface (see section 2.1 for more detail on the operation of microchip lasers). Such a simple construction arrangement also lends itself well to mass production.

Microchip Lasers

Microchip lasers are a relatively new technology, with the name “microchip lasers” (as opposed to the computer or electronics microchip) being coined by Zayhowski and Mooradian (Jan 1989). Much of the work on microchip laser theory and other microchip based laser systems has been conducted by Zayhowski and fellow researchers at the Lincoln Laboratory, MIT. Although only a recent development, an impressive volume of work has grown around the microchip idea. The interest in microchip lasers is not only due to their useful spectral and output beam properties (low

divergence and TEM₀₀), but also because they have possibilities of substantial commercial gain for appropriate applications (due to their small size and easy construction).

Mooradian *et al.* (1995) in the magazine 'Optics and Photonics News' provides an informative review article on many aspects of microchip laser technology. The production and operation of a microchip laser is described along with the basic research which has taken place, including: tuning methods, Q-switching, output modulation, and two-dimensional microchip arrays.

Outlined below is the work leading to the development of the microchip laser, which is followed by a review of the major experimental and theoretical work conducted on microchip, and microchip based, lasers. Included in Appendix 1 is a review which covers research into aspects of microchips which are not central to the study of this thesis, but show the variety of investigations being undertaken into microchip devices. The Appendix covers the development of Q-switched microchip lasers, microchip laser arrays, dopants other than Neodymium used in microchips, and second harmonic generation with microchips.

Microchip Lasers Review

During the late seventies, Kubodera and Otsuka *et al.* (Feb, March & Dec 1979) reported on miniature lasers utilising small sections of the highly doped Nd laser material LiNdP₄O₁₂ (LNP). These lasers were developed initially to lase with a single transverse mode, where the material was placed behind an external input mirror and the other end-face of the material was cylindrically polished and coated to form a stable resonator. To achieve both single transverse and single longitudinal modes, a thin flat piece of the material was placed between a flat input mirror and a curved output mirror. At first the system was pumped with an argon-ion laser to produce single mode operation at 1.047 μm , following this single mode output was achieved at both 1.05 and 1.32 μm with low-power laser diode pumping. The authors noted "precise control of the crystal thickness is required to obtain single longitudinal mode operation".

Zayhowski and Mooradian (Jan 1989) reported a much simplified technique for a miniature single longitudinal mode laser, which was termed a microchip laser. The concept was

simply to include the highly doped laser material between two flat mirrors, normally coated directly onto the flat polished laser material. To demonstrate the feasibility of diode pumped microchip lasers, several different microchip lasers were constructed and operated cw at room temperature. These lasers included Nd:YAG at 1.06 and 1.3 μm using a 730- μm long cavity, Neodymium pentaphosphate at 1.06 μm using a 100- μm -long cavity, and Nd:GGG at 1.06 μm using a 625- μm -long cavity. Further work by Zayhowski and Mooradian (May 1989, June 1989) saw frequency modulation of a Nd:YAG microchip laser's output over several hundred megahertz by piezoelectrically squeezing the microchip so as to change its cavity length, and consequently output frequency. Zayhowski (1990) showed the oscillating mode, in a cw Nd:YAG microchip, to be a thermally guided mode, and developed a theoretical understanding of the mode waist size obtained in the microchip lasers.

Leilabady *et al.* (1990) found that by pumping a Nd:YAG microchip with a diode laser array the microchip laser output beam was a circularly symmetric Gaussian shape, even though the pump beam was irregularly shaped. This was consistent with the thermal lensing effect as was described earlier by Zayhowski (1990). Leilabady also demonstrated a dual wavelength source, at 1.064 and 1.319 μm , by placing two differently coated Nd:YAG microchips in series and pumping them both with a single diode laser array, using the pump power transmitted through the first microchip to pump the second.

As an aside from microchip lasers, where mirrors were coated on both sides of the thin gain material, Kintz and Baer (1990) looked at single-frequency operation of solid-state laser materials with short absorption depths, but not necessarily short cavity lengths. They demonstrated that in an external cavity, containing a short length of gain medium at one end of the cavity, single mode operation can be achieved due to the spatial overlap of longitudinal modes at the material/mirror interface where the material is pumped. They demonstrated this with a 2 mm sample of Nd:YVO₄ having a mirror coated on one end and a separate output coupler. Though this moved away from the simple flat/flat coated cavity design, it demonstrated the possibility of inclusion of other simple elements into a cavity whilst maintaining a single-longitudinal mode.

In late 1991 microchip lasing with the material Nd:YVO₄ was reported by Sasaki (1991), Sasaki *et al.* (1991) and Taira *et al.* (1991). Sasaki utilized Kintz and Baer's earlier principle of obtaining single mode operation by using a short absorption depth and not necessarily a short cavity length. The cavity consisted of a 1 mm length of Nd:YVO₄ with an input mirror coated on one side and an external output mirror placed so as to have a 10 mm cavity length. Having obtained single mode operation at 1064 nm with the laser system, Sasaki then inserted a frequency-doubling material in the cavity to produce a green (532 nm) laser output.* Taira utilised the original microchip concept of a monolithic design by having the mirrors coated on either side of the short length (0.5 mm) of Nd:YVO₄ gain material. Using a laser diode as the pump source, approximately 100 mW of single mode output was achieved, with thresholds lower than 10 mW and slope efficiencies greater than 32%. By heating the microchip crystal the laser output was found to be tunable across 100 GHz.

Zayhowski and Keszenheimer (1992), and Keszenheimer *et al.* (1992) examined the theoretical and practical effects, and uses of modulating the pump source of microchip laser systems. It was shown that for a microchip laser a large frequency modulation could be obtained, with only a small amount of modulation in the magnitude of the pump laser diode output power. Phase locking of two 1.32 μm Nd:YAG microchip lasers was obtained by controlling the frequency of one of the lasers, using feedback to control the current modulation of the pump laser diode.

By using laser diode arrays as the pump source, Leilabady *et al.* (1992) reported 1047 and 1053 nm lasing for a 0.75 mm thick Nd:YLF microchip laser. In this work the authors postulated that the 1313 and 1321 nm transitions of Nd:YLF, if achievable in microchip form, could be very useful in silica optical fibre communications, since existing fibres systems based around the 1300 nm telecommunications window had low dispersion at these wavelengths.

Research conducted here at Victoria University [Mingxin *et al.* (1993)] reported extensive performance studies of Nd:YVO₄ as a microchip laser material. This work forms part of this thesis, extending the studies of Nd:YVO₄ microchip lasers operating at 1.06 μm . The extensive

* {Substantial research has gone into Second Harmonic Generation (SHG) with microchip like configurations, a short review of significant work is given in Appendix 1}.

wavelength tuning range of a Ti:sapphire laser was used to pump a 0.5 mm thick Nd:YVO₄ microchip and test its output power variation with pump wavelength. The output power variation was compared to the measured absorption. With Ti:sapphire pumping, the microchip laser exhibited a threshold of 34 mW and slope efficiency of 41%, and 68 mW of single mode output power was obtained with 200 mW of incident pump power (π polarization). The temperature variation of the output power and spectrum were investigated from 0 to 100°C, where it was found that in order to obtain a single longitudinal mode from this laser it was necessary to select the crystal temperature so as to place a cavity mode at the centre of the laser gain profile.

Both Besnard *et al.* (1993) and He *et al.* (1994) examined polarization behaviour in microchip lasers. Besnard reported on the polarization states of microchip YAG lasers, their control by polarized feedback, and the dynamics of changes in the polarization states. He *et al.* observed dual-polarization modes in a diode-pumped, single-frequency, 2.0914 μm Ho,Tm:YAG microchip laser. The two modes were orthogonally polarized and separated by approximately 12 MHz. It was postulated that these were most likely due to stress induced birefringence in the YAG crystal.

Further work here at Victoria University (forming part of this thesis) in collaboration with researchers from Fukui University, Japan, produced the first reported results of 1.34 μm lasing from a Nd:YVO₄ microchip [Bowkett *et al.* (1993, 1994)]. A 0.5 mm thick crystal was operated with either Ti:sapphire or laser diode pumping, and produced a maximum 60 mW single mode output at approximately 1342.8 nm. Pumping thresholds as low as 155 mW and slope efficiencies as high as 40% were achieved. It was shown that two modes, and a second transition, were obtained at certain temperatures and pumping powers by comparing the non-lasing fluorescence spectrum to the longitudinal mode spacing. The output power versus the pumping wavelength was compared to the microchip absorption found across these wavelengths. The earlier publication (1993) made comparison of the performance between 1.34 and 1.06 μm lasing with the use of similar Nd:YVO₄ microchips.

Robrish (1994) used the crystal LiTaO₃ to construct a single-mode electro-optically tuned Nd:YVO₄ microchip laser. Given the increased absorption of Nd:YVO₄ over Nd:YAG, a

combined cavity as short as 0.6 mm was achieved (0.2 mm Nd:YVO₄ & 0.4 mm LiTaO₃). The laser was tuned electronically over a range greater than 10 GHz and thermally over a range greater than 100 GHz, without mode hopping.

High output power, single-longitudinal mode operation at 1.3 μm was achieved by Gavrilovic *et al.* (1994) with the use of highly doped Nd:YAG. Using two polarization-combined laser diodes to pump the 450 μm long 4.2% Nd doped YAG crystal, 210 mW of single-mode output was obtained. It was also possible to obtain lasing on two transitions, at 1.319 and 1.338 μm, and to switch between the two by heating or cooling the microchip.

Longhi *et al.* (1994) observed transverse output mode effects due to gain-guiding in a Nd:YVO₄ microchip laser as a function of the diameter of the incident pump beam. They found that the interplay of gain, laser detuning, and mode-pump overlap determine the threshold conditions and may lead, under appropriate conditions, to longitudinal mode-hopping and to sharp variations in the transverse laser field profile. Longhi *et al.* (1995) theoretically examined transverse effects in microchip lasers and predicted off-axis emission for narrow pump beam diameters; producing ring patterns in the 2D far-field intensity.

1.3 Microchip Amplifiers

The inverted population of an optically active (pumped) material may be utilized by passing a signal through that material to achieve signal amplification. The amplifier material is generally made of a similar material (same dopant, sometimes different host) to that used to produce the signal, so that the signal and amplifier gain regions overlap, which is necessary to achieve maximum signal gain. In essence an optical amplifier is a laser without mirrors, or with partially reflecting mirrors. Since the Nd:YVO₄ material offers strong absorption, and a correspondingly high gain, it is envisaged that with short lengths of the material, considerable signal gain can be achieved even for a single pass through the excited Nd:YVO₄ material. This provides the possibility to develop a simple compact optical amplifier. The amplifier length tested need not be much longer than that utilized for microchip laser systems, and thus they maybe appropriately

named 'microchip' amplifiers. Below is a review of the achievements with compact optical amplifier systems.

Review of Compact Optical Amplifiers

Following reports (Kane *et al.*(1986)) of a flash lamp pumped Nd:YAG laser amplifier capable of 62 dB gain in a multiple-pass slab geometry, Chan (1987) described a method of designing a miniature multiple-pass laser diode pumped Nd:YAG amplifier. The design used two sets of pump laser diode 2-D arrays, with 150 W or greater peak power, placed on opposite sides along the length of a slab of Nd:YAG. One of the smaller ends of the slab was reflection coated, and with two zig-zag passes through the 30 mm slab an approximate gain of 15 dB was estimated. Although this demonstrated an improvement in efficiency over the flash lamp pumped amplifier, it was not particularly efficient nor an easy design to construct.

Baer *et al.* (1992) using single and double pass "tightly folded resonator" configurations were able to achieve small signal gains of 15 and 28 dB, respectively, with a diode laser bar of ten 1W laser diode arrays and a 5 x 5 x 20 mm slab of Nd:YLF. The laser diode bar was close coupled to a long face of the crystal by a fibre lens. The input signal entered on the opposite face to the pump and was zig-zagged multiple times so that the points of reflection on the pump side corresponded to the location of the laser diodes. The amplified signal then exited on the opposite face to the pump laser diodes. To double pass the beam it was reflected back along the same path.

Work by Taira (1993) on a laser diode pumped microchip Nd:YVO₄ amplifier yielded gains as high as 6.2 dB for a pump power of just 146 mW. A 1 x 1 x 1 mm microchip was coated on one face for maximum transmission of pump light and maximum reflection of signal. The input signal was inserted from the opposite face and double passed through the amplifier microchip.

Plaessmann *et al.* (1993) devised a multiple-pass amplifier in which a small (between 3.5 and 7.5 mm long) piece of gain material, either Nd:YLF, YAG or YVO₄, was placed in the central axis of two 102 mm focal length mirrors. The gain material was pumped through one mirror and the signal passed through a hole in the other. The signal traversed multiple passes through the

gain material until it exited the cavity set by the mirrors. A small signal gain of 38 dB was obtained at 1.047 μm in Nd:YLF with 1.6 W of pump power, and 58 dB gain was obtained at 1.064 μm in Nd:YVO₄ with 13 W of pump power.

A simple diode pumped Nd:YVO₄ slab amplifier was demonstrated by Bernard *et al.* (June 1994). A quasi-cw 60W diode laser bar was used to pump one of the large faces of a 10.1 x 2.5 x 3.0 mm Nd:YVO₄ slab. The signal beam was projected in the direction of the longest edge making a single grazing reflection with the slab's pumped surface. In a single pass 26 dB gain was achieved with a Nd:YAG signal beam and 30 dB gain with a Nd:YVO₄ signal beam.

In work completed for this thesis Bowkett *et al.* (1995) reported amplification from a 1 mm long, Ti:sapphire pumped, Nd:YVO₄ microchip. Small signal single pass gains of greater than 19 dB were achieved using 260 mW of incident pump power, by overlapping the pump and signal beams co-linearly (minimum pump beam waist of $\approx 25 \times 20 \mu\text{m}$, minimum signal beam waist of $\approx 30 \times 25 \mu\text{m}$). Signal and pump beam diameter, and the overlap between the two, were seen to be significant factors in controlling and maximizing the achieved gain.

Brignon *et al.* (1995) examined multi-pass degenerate four-wave mixing in a laser diode pumped Nd:YVO₄ amplifier. A net double pass gain of 11 was achieved with 100 W of diode pumping using a 3 mm long crystal coated at one end.

1.4 Scope of this Thesis

Work on this thesis occurred across a period of time during which substantial other work was achieved with the material Nd:YVO₄ and with microchip based systems. Higher power laser diode pump sources, and improvements in Nd:YVO₄ material quality, has seen YVO₄ mature as a serious alternative laser material over the past five years allowing substantial research and product development to occur. As outlined in the microchip lasers review, this period has also seen substantial research into microchip based lasers. The studies performed in this thesis have made a timely contribution to work on Nd:YVO₄ microchip devices.

The current work describes performance studies of three Nd:YVO₄ microchip devices, a 1.06 μm microchip laser, a 1.34 μm microchip laser, and a microchip amplifier at the same

wavelengths. Of these, only the 1.06 μm laser had been studied previously, and only under restricted laser diode pumping. The work reported in this thesis forms part of a collaborative project with researchers at Fukui University, Japan, who had been testing a 1.06 μm Nd:YVO₄ microchip laser using laser diode pumping. Work began here in 1992 when the facilities available at the Optical Technology Research Laboratory within Victoria University enabled the extension of these studies.

To study the properties of Nd:YVO₄, and to understand the operation of the lasers and amplifiers which used the “new” Nd:YVO₄ material, absorption and fluorescence tests on an uncoated sample of the material were undertaken. The thickness of the uncoated Nd:YVO₄ sample was the same as that used in the microchip lasers (0.5 mm). Absorption tests established the pumping wavelengths for efficient (highest output) laser operation. Fluorescence tests were used to establish the gain bandwidth and to determine which Stark energy levels are responsible for laser action.

Each of the 1.06 and 1.34 μm Nd:YVO₄ microchip lasers reported in this work have been tested as outlined below. The microchip laser output power was studied as a function of the input pumping wavelength, and compared to the optical absorption through the microchip across the same wavelength range. The microchip laser output as a function of input pump power was determined at the wavelength of maximum absorption, from which the lasing threshold powers and slope efficiencies were established. The temperature of the microchip lasers was varied to determine the resultant change in the laser output wavelength, and modal spectrum. The operating conditions under which single-longitudinal-mode output may be observed, were determined.

A one millimetre cubic Nd:YVO₄ microchip, anti-reflection coated on opposite faces, was used as a gain medium to produce a miniature amplifier. At a signal wavelength of 1.06 μm , as provided by a microchip laser, the saturation intensity was experimentally determined by measuring the amplifier gain at different signal powers (same beam size). From this the small signal gain region was predicted. Gain versus incident pump power was measured for overlapping, co-linear pump and signal beams having minimum waist diameters of approximately 30 μm . Gain results were obtained for an increased pump beam minimum waist diameter of

approximately 100 μm . An attempt was made to obtain gain results at 1.34 μm , as provided by the other microchip laser, however only one gain result was obtained since the available equipment was unable to accurately measure the beam diameters and overlap at 1.34 μm .

A model to predict the performance of the Nd:YVO₄ microchip lasers was developed. Following an established theoretical model for a simple four-level laser system [Koechner (1992)], and introducing considerations for upper laser level Stark splitting and fluorescence branching ratios, the laser threshold and slope efficiency of the microchip laser systems have been predicted. The theoretical small signal single-pass gain of the microchip amplifiers has also been established. A first approximation model directly utilizes the small signal gain equation established within the laser model, and a second model further considers the high pump intensities to rewrite the gain equation and obtain a better match to the experimentally obtained gains. Theoretical predictions are compared to the experimental results by using the appropriate parameters for the Nd:YVO₄ material, including the dimensions and coating parameters of the microchips, and the beam parameters. The overlap between the pump and signal beams (as calculated from measurements given by a beam analyzer) has been introduced into the modelling.

The relationships which determine the behaviour of a microchip laser are outlined in chapter two, along with theoretical models to predict results for the lasers and amplifiers. Chapter three details the equipment needed for the experimentation, and lists the experimental techniques and procedures involved in the measurements. The results and discussion of absorption and fluorescence tests on the Nd:YVO₄ material are given in chapter four, along with an examination of the quality of the Nd:YVO₄ samples used. The experimental results, theoretical predictions and a discussion of the microchip lasers operation and performance are given in chapter five, while the same is given in chapter six for the microchip amplifiers. Finally chapter seven outlines conclusions that have been drawn from the work, and comments on current and future work in the field.

Chapter 2 Theory and Models

Introduction

2.1 Microchip Laser and Amplifier Principles

2.1.1 Microchip Lasers

Longitudinal mode spacing

Spatial Output

Fluorescence profile

Temperature tuning

2.1.2 Microchip Amplifiers

2.2 Models

2.2.1 Laser Model

Energy exchange processes

Laser rate equations

Gain

Establishing measurable laser parameters

Modification to an ideal four level system

Stark split upper laser level

Fluorescence branching ratio

2.2.2 Amplifier Model

Small signal single-pass Gain

Saturation intensity

Methods used to calculate gain

Conclusion

Chapter 2

Theory and Models

Introduction

This chapter outlines the theory behind the operation of microchip lasers and amplifiers, and adapts established models to theoretically predict their performance. The longitudinal mode properties of a microchip laser are shown to be established via a relationship between the physical microchip thickness and the gain curve of the microchip material. The effect of temperature of the microchip material on the laser output is also described. The operation of a microchip as a miniature optical amplifier is outlined. Equations are adapted from an established four-level laser model to theoretically predict the output power performance of a microchip laser, and the small signal single-pass gain of a microchip amplifier.

2.1 Microchip Laser and Amplifier Principles

The principles underlying the simple single longitudinal mode TEM₀₀ operation of a microchip laser, and the signal amplifying operation of a microchip amplifier, are presented within this section.

2.1.1 Microchip Lasers

As was outlined in section 1.2, the microchip laser is based on limiting the optical cavity length to achieve single longitudinal mode oscillation. Firstly, this section explains how longitudinal mode spacing is affected by cavity thickness. Secondly, the spatial output of the microchip laser is discussed and a short literature review undertaken which considers reasons for the observed transverse mode containment. Thirdly, an explanation is given of the relationship between the fluorescence profile, the cavity thickness and the laser's spectral output. Finally, the effect of temperature tuning of the laser output wavelength is discussed, establishing that by altering the temperature of the microchip laser, the relative positioning of the longitudinal laser modes and the material's fluorescence profile may be exploited to frequency tune the laser output.

Longitudinal mode spacing

The approximate output wavelength of a rare-earth based laser is determined by the difference in energy between the upper and lower levels involved in the stimulated emission, however the specific detail of the output depends on the laser resonator. If a Fabry-Perot interferometer formed from two plane parallel mirrors is considered, then the condition for constructive interference is:

$$2nL \cos\theta = q\lambda \quad (2.1)$$

where n is the refractive index, L is the distance between the mirrors, θ is the angle the beam makes with the normal to the mirrors, λ is the wavelength in vacuum and q is a positive integer.

Assuming the beam is at normal incidence, the cavity resonates at wavelengths λ , such that:

$$\lambda = 2nL/q, \quad (2.2)$$

or frequencies ν , such that:

$$\nu = qc/2nL \quad (2.3)$$

where c is the speed of light in vacuum.

These frequencies are called axial (or longitudinal) mode frequencies. The different integer values of q correspond to different axial or longitudinal modes of the cavity, with the q^{th} mode occurring at the frequency for which the spacing between the mirrors equals q half wavelengths.

The length L of typical laser cavities range from a few centimetres to a few metres, while the resonant wavelength is of the order of $1 \mu\text{m}$. Therefore, for most laser systems typical values of q , as determined by equation. 2.2, are of the order of 10^4 to 10^6 . An additional longitudinal mode occurs each time q increases by 1, then given the value of q is large and the bandwidth $\Delta\nu$ of the fluorescence is finite, many modes are likely to fall within the gain curve of the laser medium. This is shown by the typical spectral output of a Helium-Neon (HeNe) laser, as shown in Figure 2.1, which shows many longitudinal modes [Arecchi & Schulz-Dubois (1972)].

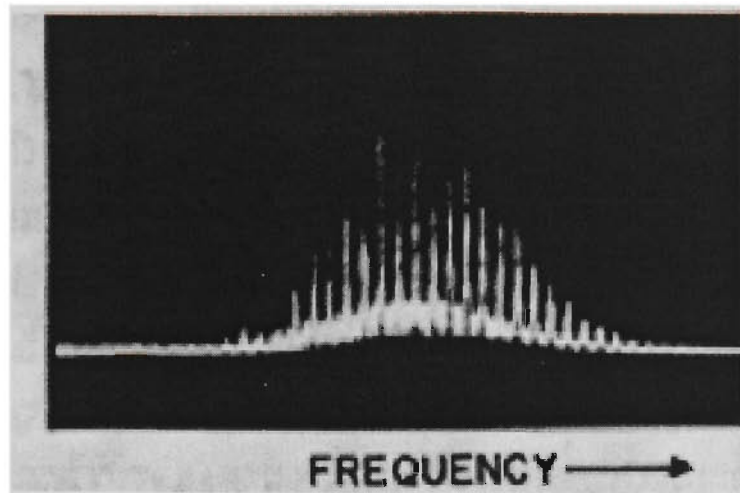


Figure 2.1: Typical output spectrum of a HeNe laser showing the many longitudinal modes produced in a typical length cavity.

The frequency spacing between two adjacent longitudinal modes is given by:

$$\Delta\nu_{long.} = \nu_{q+1} - \nu_q = c/2nL \quad (2.4)$$

or in terms of wavelength:

$$\Delta\lambda_{long.} = \lambda^2/2nL \quad (2.5)$$

This separation of adjacent longitudinal modes is inversely proportional to the length of the optical cavity. Therefore, if the cavity is made sufficiently thin the spacing of the modes will be increased such that only one longitudinal mode is present within the gain curve. Figure 2.2 illustrates how the longitudinal mode separation determines the number of modes that may lase. From the figure it can be seen that if the threshold level was lowered, or the mode separation made smaller, additional modes will be observed.

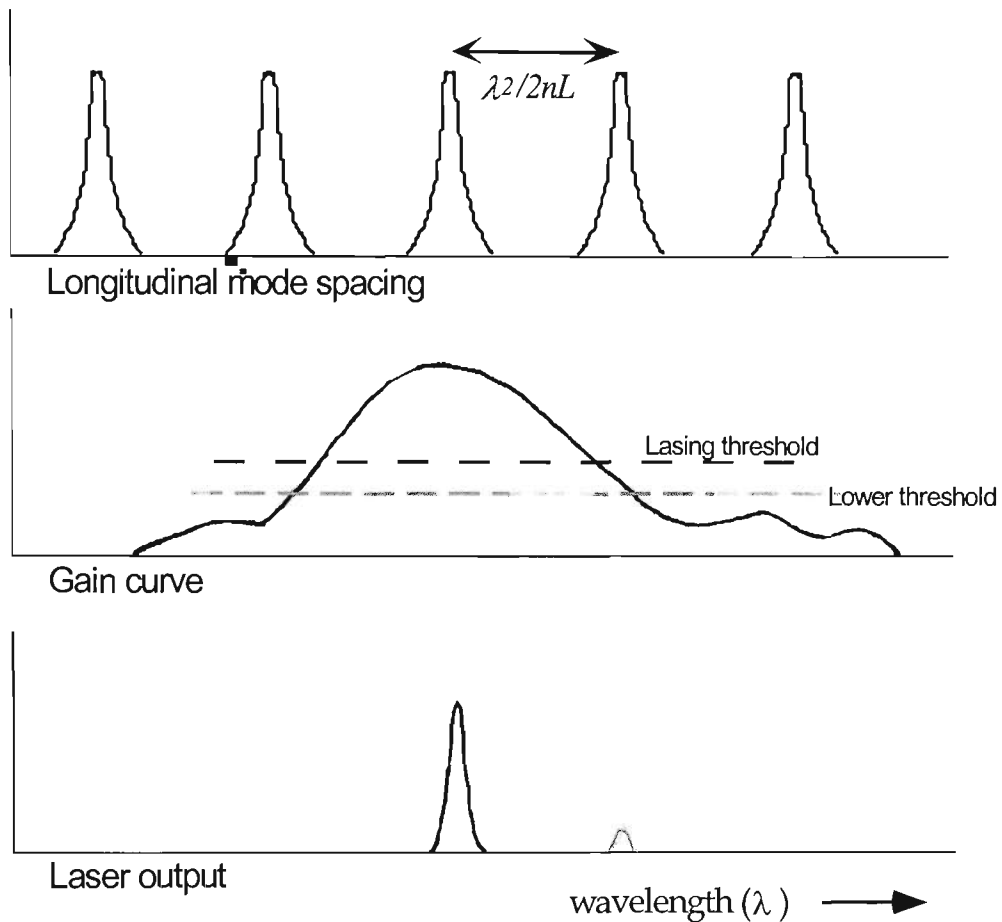


Figure 2.2: The combination of the mode spacing and the gain curve bandwidth govern the laser's output modes. The grey sections show that a relative shift of the gain curve against the lasing threshold level can result in the appearance of additional modes.

Spatial Output

Many laser applications favour the laser operating with a single spatial output mode, i.e. TEM_{00} mode. The TEM_{00} , or fundamental transverse mode, produces an output with the smallest beam divergence, the highest power density, and therefore, the highest brightness. Most practical lasers tend to operate with many higher-order transverse modes, however the nature of the microchip laser and its end pumping configuration strongly favour single transverse mode (TEM_{00}) operation.

The mirror coatings on either side of the microchip constitute a simple cavity arrangement of two plane parallel mirrors. This flat-flat mirror arrangement is only a marginally stable cavity,

and is not often used in practice because it has disadvantages of high sensitivity to alignment and relatively large loss of light due to diffraction “leakage” (or geometrical walkoff) of the optical beams. Zayhowski and Mooradian (Jan 1989) initially assumed the microchips relied on gain-guiding or non-linear optical effects to confine the transverse dimensions of the lasing mode. Zayhowski (March 1990) later showed that the oscillating mode in a cw Nd:YAG microchip laser was actually a thermally guided mode. The thermal guiding provided by the incident pumping energy stabilizes the laser cavity to operate in a single transverse mode through either a change of refractive index with temperature, causing thermally induced lensing, or a thermally induced bulge on the microchip mirror surface. The authors Chen *et al.* (1998) and Blows *et al.* (1998) both examine the thermal lensing effect in Nd:YVO₄ microchip lasers as the laser cavity stabilizing mechanism.

Exceptions to the theory of thermal guiding in microchips are suggested by Longhi *et al.* (1994, 1995), where it was found that in the case of very low or negative values of dn/dT (T the temperature) or for low pump intensities, gain-waveguide effects may dominate in defining the transverse dimension of the oscillating mode and the threshold conditions. Fan (1994) also found that in quasi-three-level (as opposed to the four-level laser used here) flat-flat cavity lasers the transverse mode dimensions were better described by an aperture guiding model, where mode shaping is driven by off-axis loss, as opposed to on-axis gain (gain-guiding).

Throughout this work single transverse mode operation (TEM₀₀) has been observed for the Nd:YVO₄ microchip lasers, one exception was observed when pumping with a laser diode having an unusual pump beam geometry. This characteristic could be eliminated by moving the relative position of the laser diode and focusing lens to improve the pump beam geometry. This work has not attempted to investigate the actual mechanism by which the transverse mode containment occurs, and therefore refers the reader to the above mentioned work for further information.

Fluorescence profile

The gain curve of the laser material is set by the profile and bandwidth of the fluorescence transition/s. The bandwidth and profile of the atomic transition depends on the mechanism of line

broadening. Optical transitions in solids can be broadened by lifetime, dipolar and thermal broadening effects, and/or by random inhomogeneities. Transitions to alternative Stark levels (other than those involved in the main transition) may also form part of the gain profile and the lasing threshold for these transitions (as opposed to modes) may also be exceeded at high pump powers. An indication of the gain bandwidth can be established by measuring the FWHM of the fluorescence profile.

Figure 2.3 shows the measured fluorescence for the transition associated with lasing near $1.06 \mu\text{m}$ in Nd:YVO_4 . From the FWHM of the fluorescence an estimate of the gain bandwidth can be obtained, and thus, the thickness of microchip needed to restrict the number of modes within the gain curve to one may be estimated.

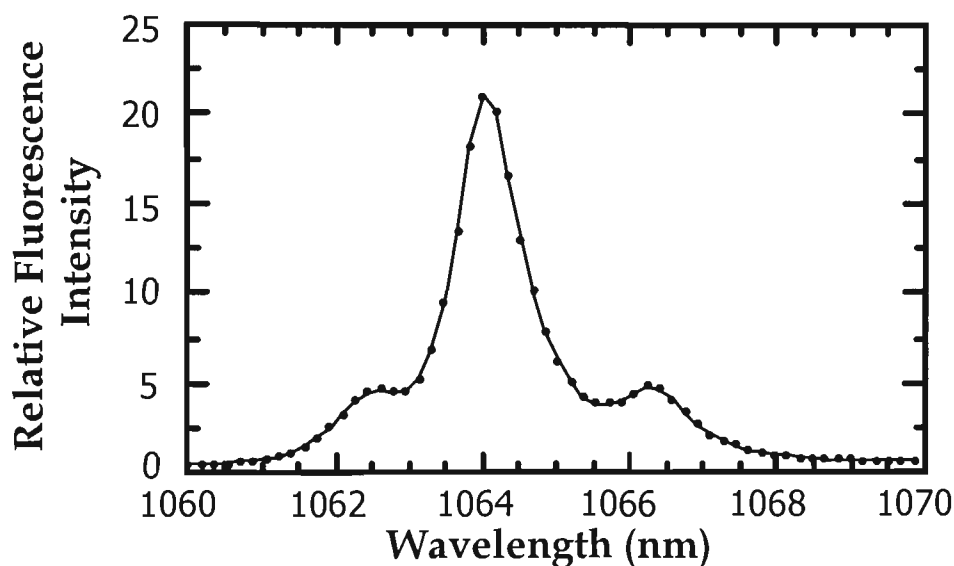


Figure 2.3: Typical Nd:YVO_4 fluorescence spectrum around $1.06 \mu\text{m}$. Here the dots are measured points and the solid line simply joins these points.

The above concept is illustrated by the following example. Taira *et al.* (1991) quoted a gain bandwidth of 257.0 GHz, or 0.96 nm, at $1.06 \mu\text{m}$. The refractive index of Nd:YVO_4 at this wavelength is 2.165, giving a mode spacing frequency (eqn 2.4) of $6.9 \times 10^7 / L$, where L is the length of the microchip. For a mode spacing equal to the gain bandwidth, the microchip length must be:

$$L = 6.9 \times 10^7 / 257.0 \times 10^9$$

$$\approx 2.7 \times 10^{-4} \text{ m or } 270 \text{ } \mu\text{m}$$

However, given that the microchips used by Taira (and myself) were 500 μm in length, it was possible to have two modes within the gain curve at once, with a corresponding mode spacing of:

$$\begin{aligned} \Delta\nu_{long} &= 6.9 \times 10^7 / 500 \times 10^{-6} \\ &= 1.38 \times 10^{11} \text{ Hz or } 138 \text{ GHz} \end{aligned}$$

It was possible to obtain only one lasing mode by centring the mode within the gain curve, since the mode spacing (138 GHz) was greater than half of the gain bandwidth (257 GHz).

Temperature tuning

Thermally induced changes occur in the refractive index and physical dimensions of the microchip material when its temperature is changed. This can therefore be a means by which to change the output of the microchip laser, where the longitudinal modes may be wavelength shifted with respect to the gain curve. With this method one longitudinal mode can be placed within the centre of the gain curve, so that this is the only mode to lase. The variation of laser frequency with temperature is dependent on the variation of both the refractive index and the cavity length, and can be expressed as [Taira *et al.* (1991)]:

$$\frac{d\nu}{dT} = -\nu \left(\frac{1}{n} \frac{\partial n}{\partial T} + \frac{1}{L} \frac{\partial L}{\partial T} \right) \quad (2.6)$$

The change in the refractive index with temperature ($\partial n / \partial T$) may be referred to as the thermal optical co-efficient, while the change in cavity length with temperature is referred to as the thermal expansion co-efficient ($1/L \partial L / \partial T$), often denoted by α . If the longitudinal modes are spaced as wide as, or wider than, the gain region, then temperature tuning also provides the ability to tune, with a single longitudinal mode, over the entire gain region.

Other frequency tuning schemes for microchip lasers have included application of transverse stress to modify the cavity length [Zayhowski and Mooradian (May 1989)], pump power modulation [Zayhowski and Keszenheimer (1992)], and electro-optically tuning via an inline LiTaO₃ element [Robrish (1994)].

2.1.2 Microchip Amplifiers

Conceptually there is no difference between a microchip amplifier and a normal optical amplifier, apart from the fact that it benefits from having high gain within a small path length. An optical amplifier may be considered a laser without mirrors, in which an incoming optical signal can access the inverted population of the pumped amplifier material to achieve signal gain. The signal propagating through the amplifier undergoes amplification by stimulated emission and emerges from the amplifier with greater signal intensity. Gain in an optical amplifier is generally achieved, in its simplest form, by a single pass through the excited (pumped) material, although double and multiple pass systems have been used to increase the interaction length, and therefore signal gain.

As the light signal passes through the amplifier, the signal intensity grows approximately exponentially. However, when the signal intensity in the amplifier becomes strong enough to change the inverted population level appreciably, the gain material begins to saturate, and the rate of signal growth begins to decrease. With increasing signal intensity the point is reached where the gain will become linear, rather than exponential, with the length traveled through the amplifier. Saturation effects therefore reduce the overall gain achieved, when compared to unsaturated (or small signal) gain. Saturation effects also occur when the pumping density is very large. This effect is less commonly observed but was the case for the amplifiers studied in this work.

For the amplifier tests conducted here, cw output from a Nd:YVO₄ microchip laser was utilized as the signal, and traversed a single pass through the pumped Nd:YVO₄ amplifier. Initial tests defined the ‘small signal’ regime, and subsequent tests determined the gain in this regime. A theoretical model to predict the expected small signal gain for this type of amplifier system is established in section 2.2.2.

2.2 Models

Existing theoretical models have been adapted to describe particular properties of the microchip lasers and amplifiers tested here. The microchip laser model, together with the appropriate material parameters, gives a theoretical expected value for the threshold and slope efficiency of lasing. Similarly, the amplifier model determines the theoretically expected small signal gain and

gives a value for the saturation intensity. Later, in chapters five (lasers) and six (amplifiers), the calculated theoretical results, established from these models, are compared to those measured experimentally.

2.2.1 Laser Model

As described in chapter 1, a neodymium laser operating on either the $1.06\ \mu\text{m}$ (${}^4\text{F}_{3/2} \rightarrow {}^4\text{I}_{11/2}$) or $1.3\ \mu\text{m}$ (${}^4\text{F}_{3/2} \rightarrow {}^4\text{I}_{13/2}$) transition may be represented by a four-level system. It is possible by manipulation of the well established rate equations for a four level system to establish mathematical relationships to predict the threshold, slope efficiency and output power of the laser. The laser model used here follows the work of Koechner (1992) in first establishing a rate equation to describe the system at threshold, then a small signal gain equation and saturation intensity. These equations are combined to give an equation describing the output power of the laser. This is then transformed into an equation containing experimentally measurable quantities. Modifications to the ideal four level system as described by Koechner are introduced to improve the model and achieve a better comparison with the experimental results. These modifications include the consideration of energy level Stark splitting and fluorescence branching ratios.

Laser Rate Equations

Here the population densities of each level are denoted, n_x , where x is the level, and the fluorescence transition lifetimes are denoted τ_{yz} , where y and z are the upper and lower levels of the transition. A diagram of an ideal four level laser system is given in figure 2.4.

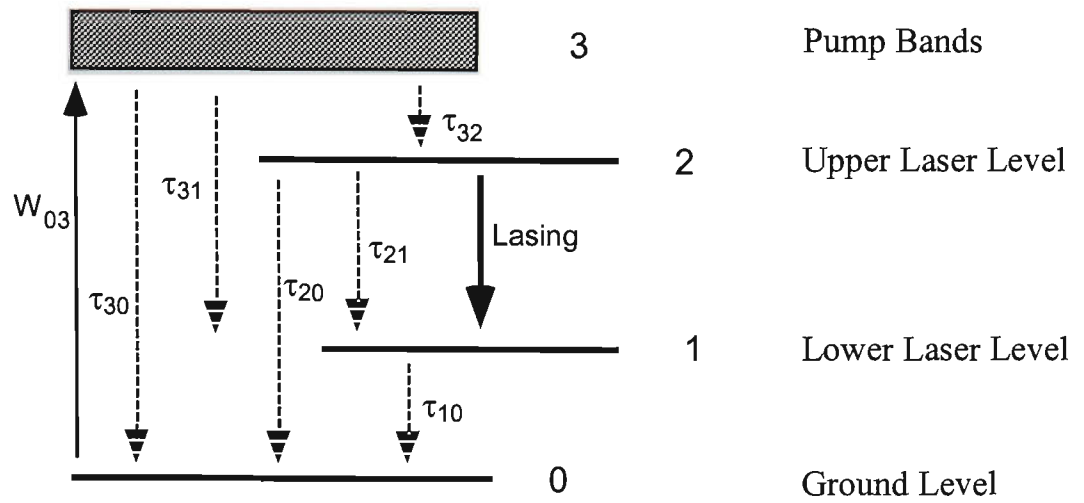


Figure 2.4: Four level system showing stimulated absorption (W_{03}) to the pump band and possible fluorescence transitions.

The transition from the pump bands to the upper laser level is generally rapid, ($\tau_{32} \ll \tau_{20} \& \tau_{21}$), hence the number of atoms in the pump band may be considered negligible, $n_3 \approx 0$, and $n_{tot} = n_0 + n_1 + n_2$. The rate at which the upper laser level becomes populated is then equal to the pump rate, W_p (see eqn. 2.11), multiplied by the ground level population, n_0 . The rate of change of the population density in the two laser levels may then be described by:

$$\frac{\partial n_2}{\partial t} = \underbrace{W_p n_0}_{\text{pumping}} - \underbrace{(n_2 - n_1) \sigma_{21} \phi c}_{\text{stimulated emission}} - \underbrace{n_2 \left(\frac{1}{\tau_{21}} + \frac{1}{\tau_{20}} \right)}_{\text{spontaneous emission}} \quad (2.7)$$

$$\frac{\partial n_1}{\partial t} = \underbrace{\frac{n_2}{\tau_{21}}}_{\text{spontaneous emission}} - \underbrace{\frac{n_1}{\tau_{10}}}_{\text{spontaneous emission to ground}} + \underbrace{(n_2 - n_1) \sigma_{21} \phi c}_{\text{stimulated emission}} \quad (2.8)$$

where σ_{21} is the stimulated emission cross-section and ϕ is the photon density.

The lower laser level in an ideal four-level system empties infinitely fast to the ground level, i.e. $\tau_{10} \approx 0$, and it follows that $n_1 = 0$. In this case the entire population is divided between the ground level, 0, and the upper laser level, 2. It follows that the rate equation for the ideal four-level system may now be written as:

$$\frac{\partial n_2}{\partial t} = W_p (n_0) - n_2 \sigma_{21} \phi c - \frac{n_2}{\tau_f} \quad (2.9)$$

where $\frac{1}{\tau_f} = \frac{1}{\tau_{21}} + \frac{1}{\tau_{20}}$ and (2.10)

$$W_p = \eta_Q W_{03} \quad (2.11)$$

Equation 2.11 allows for the fact that all atoms pumped to level 3 may not decay to the upper laser level 2. Here the pump quantum efficiency is defined as:

$$\eta_Q = \left(1 + \frac{\tau_{32}}{\tau_{31}} + \frac{\tau_{32}}{\tau_{30}} \right)^{-1} \leq 1 \quad (2.12)$$

This quantifies the fraction of the total atoms excited to level 3 dropping from there to level 2, thus becoming available for laser action. The second and third terms of 2.12 are the lifetime ratios of the possible downward transitions, as shown in figure 2.4. Gain results from a population inversion between levels one and two; $n = n_2 - n_1 \approx n_2$, since $n_1 \approx 0$. Accordingly, the population inversion rate equation may be approximated by:

$$\frac{\partial n}{\partial t} = W_p (n_{tot} - n) - n \sigma_{21} \phi c - \frac{n}{\tau_f} \quad (2.13)$$

When steady state condition is established (e.g. cw operation) then $\frac{\partial n}{\partial t} = 0$, and the

inverted population density becomes:

$$n = n_{tot} \left(W_p \left(W_p + \sigma_{21} \phi c + \frac{1}{\tau_f} \right) \right)^{-1} \quad (2.14)$$

A prediction of what happens at threshold can be made by neglecting the effect of stimulated emission, i.e. setting $\phi = 0$ (For operation at or near threshold the photon density, ϕ , is very small) then equation 2.14 becomes:

$$n = n_{tot} \left(W_p \tau_f \left(W_p \tau_f + 1 \right) \right)^{-1}, \quad (2.15)$$

Gain

Having established the behaviour of the population density of the levels within the laser system the behaviour of the gain can be determined. The small signal gain co-efficient, g_0 , is defined as the product of the stimulated emission cross section and the inversion population near threshold, i.e.

$$g_0 = \sigma_{21} n \quad (2.16)$$

Having established n , in equation 2.15, the small signal gain co-efficient becomes:

$$g_0 = \sigma_{21} \left[n_{tot} (W_p \tau_f) (W_p \tau_f + 1)^{-1} \right] \quad (2.17)$$

Above threshold where the photon density becomes appreciable, the gain of the system is reduced according to:

$$g = \frac{g_0}{1 + I/I_s} \quad (2.18)$$

$$\text{where } I \text{ equals the power density and } I_s = \left(W_p + \frac{1}{\tau_f} \right) \frac{h\nu_L}{\sigma_{21}} \quad (2.19)$$

The parameter I_s defines a signal intensity in the active material at which the saturated gain, g , becomes equal to half the small signal gain coefficient g_0 . (The frequency has been labelled ν_L to identify it as the laser transition frequency). Most commonly, in a four-level system $W_p \ll 1/\tau_f$, then I_s becomes:

$$I_s = \frac{h\nu_L}{\sigma_{21}\tau_f} \quad (2.20)$$

To obtain a term for the output power of the laser, the power density within the laser resonator may be considered. For the case where the transmission, T , of the output mirror is small, the power density in the gain medium is approximately equal to twice the power density of a wave propagating in either direction. ie. $I \approx 2I_z$

$$\therefore g = \frac{g_0}{1 + 2I_z/I_s} \quad (2.21)$$

and the output power of the laser resonator is:

$$P_{OUT} = AI_z T \quad (2.22)$$

where A is cross-sectional area.

Koechner uses equation 2.21, 2.22 and the equation $2gl \approx T+L$, where L is the loss in the laser cavity and l the cavity length, to form the following equation determining the laser power output:

$$P_{OUT} = \left(\frac{T}{T+L} \right) AI_s g_0 l - \frac{T AI_s}{2} \quad (2.23)$$

This gives the laser output power in terms of the saturation intensity, I_s , and the small signal gain co-efficient, g_0 . The following section shows how equation 2.23 may be transformed to establish the laser threshold and slope efficiency from experimentally measurable quantities.

Establishing measurable laser parameters

The Output power (P_{OUT}) from equation 2.23 can be found in terms of the absorbed pump power instead of g_0 and I_s , by mathematically establishing the pump rate required to maintain the laser at threshold. By using equation 2.17, the small-signal gain equation at threshold, and if $n_{tot} \approx n_0$ then one obtains:

$$g_0 = \sigma_{21} n_0 W_p \tau_f \quad (2.24)$$

assuming that $W_p \tau_f \ll 1$.

Using the pump rate given in equation 2.11 it can be seen that:

$$W_p n_0 = \eta_Q W_{03} n_0$$

The number of atoms transferred to the pump band per unit time and volume ($=W_{03}n_0$) is equal to the absorbed pump power divided by the pump photon energy times the pumped volume, ($P_{ab}/h\nu_p V$).

Then by using the ratio of laser energy to pump energy (known as the Stokes factor), $\eta_s = \frac{h\nu_L}{h\nu_p} = \frac{\lambda_p}{\lambda_L}$, the equation above can be written in terms of the laser transition frequency, to

later match in with the saturation intensity equation:

$$W_p n_0 = \eta_Q W_{03} n_0 = \eta_Q P_{ab}/h\nu_p V = \eta_Q \eta_s P_{ab}/h\nu_L V \quad (2.25)$$

where ν_L , ν_p , λ_L and λ_p are the laser and pump frequencies and wavelengths, respectively.

Equation 2.24 then becomes:

$$g_0 = \sigma_{21} \tau_f \eta_Q \eta_s P_{ab} / h\nu_L V \quad (2.26)$$

where P_{ab} is the absorbed pump power. P_{ab} is the product of the incident pump power P_{IN} , the beam overlap efficiency η_B , and an efficiency factor η_A . The beam overlap efficiency η_B , is a measure of the overlap between the pump beam and the laser mode distribution through the laser. The efficiency factor η_A , is a measure of the front mirror transmission at the pump wavelength and the fraction of the pump power absorbed in the laser material. Therefore equation 2.26 becomes:

$$g_0 = \sigma_{21} \tau_f \eta_Q \eta_s \eta_B \eta_A P_{IN} / h\nu_L V \quad (2.27)$$

Using equation 2.20 we get, $g_0 = \eta_Q \eta_s \eta_B \eta_A P_{IN} / I_s V$ (2.28)

so equation 2.23 becomes,

$$P_{OUT} = \left(\frac{T}{T+L} \right) \eta_Q \eta_s \eta_B \eta_A P_{IN} - \frac{T A I_s}{2} \quad (2.29)$$

where the area (A) and length (L) in equation 2.23 are cancelled out by the volume (V) in equation 2.28. From this power output equation the threshold power, P_{TH} , and slope efficiency, σ_s , may be established, where:

The Threshold Power, which defines the incident pump power at which lasing begins, i.e. P_{IN} when $P_{OUT} = 0$, is:

$$P_{TH} = \left(\frac{T+L}{2} \right) \frac{A I_s}{\eta_Q \eta_s \eta_B \eta_A} \quad (2.30)$$

and the Slope Efficiency, which defines the ratio of increase in laser output power with an increase in incident pump power above threshold, $\sigma_s = \frac{P_{OUT}}{(P_{IN} - P_{TH})}$, (2.31)

is:

$$\sigma_s = \left(\frac{T}{T+L} \right) \eta_Q \eta_s \eta_B \eta_A \quad (2.32)$$

Modifications to an ideal four-level system.

Comparison of the calculated threshold power from equation 2.30, to those observed experimentally (especially in the 1.34 μm case), showed the predicted threshold values to be substantially lower than those observed. Therefore the following additional considerations were necessary to better predict the threshold of the microchip lasers.

Stark split upper laser level

The upper laser level, which is considered to be a single level in the simple four-level laser model, is made up of two Stark split sub-levels for Nd:YVO₄. The manifold level population is consequently spread between the two Stark sub-levels following a Boltzman distribution. The initial upper laser level population must be considered according to the fact that the laser transition originates from just one of the Stark sub-levels. The parameter f_B defines the population

(fractional number of Nd³⁺ ions) in the appropriate Stark sub-level of the ⁴F_{3/2} state. In the laser material Nd:YVO₄ the lower Stark sub-level of ⁴F_{3/2} state is responsible for the laser transition and hence,

$$f_B = \frac{1}{1 + \exp[-(hc\Delta\bar{\nu}/KT)]}, \quad (2.33)$$

where h is Planck's constant, c the velocity of light, K Boltzman's constant, T the Kelvin Temperature, and $(\Delta\bar{\nu})$ is the level splitting in wave numbers between the upper and lower Stark sub-levels of the ⁴F_{3/2} state [Tucker (1977)].

This consideration creates an effective stimulated emission cross-section, where the cross-section is multiplied by the Boltzman distribution of the appropriate sub-level from which the transition occurs, i.e. $(\sigma_s \times f_B)$. Therefore, the threshold power is divided by f_B , and equation 2.30 becomes:

$$P_{TH} = \left(\frac{T+L}{2}\right) \frac{AI_s}{\eta_Q \eta_s \eta_B \eta_A f_B} \quad (2.34)$$

Conversely this population distribution of the upper laser level should not require any modification of the equations determining the slope efficiency because the close thermal coupling between the two Stark sub-levels ensure quick re-population between the levels for the steady state lasing condition. (In Nd:YVO₄ the ⁴F_{3/2} sub-level difference is $\approx 18 \text{ cm}^{-1}$).

Fluorescence Branching Ratio

For a system (such as neodymium) with additional lower levels, prior to the onset of lasing competition between the various fluorescence transitions will exist. This will cause an increase in the laser threshold by a factor equal to the reciprocal of the branching ratio, b , to the lower laser level. In figure 2.5 a schematic of an energy level diagram for Nd is shown, together with the branching ratio for each of the lower lying level in Nd:YVO₄. Therefore the threshold power calculation (eqn. 2.34) now becomes:

$$P_{TH} = \left(\frac{T+L}{2}\right) \frac{AI_s}{\eta_Q \eta_s \eta_B \eta_A f_B b}, \quad (2.35)$$

where b is the fluorescence branching ratio to the particular lower laser level.

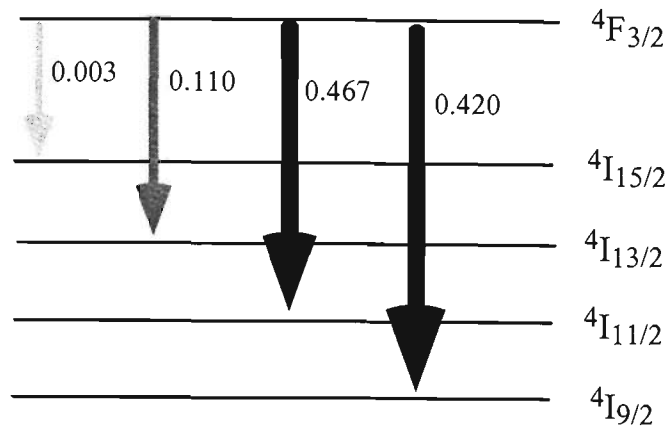


Figure 2.5: A Schematic of the fluorescence branching ratios of the $4F_{3/2}$ manifold of Nd:YVO₄ [branching ratio values from Lomheim & DeShazer (1978)].

2.2.2 Amplifier Model

This section examines the methods used to establish a theoretical prediction of a microchip amplifier's performance, when considered under CW steady-state pump and signal conditions. Two different models are established to predict the amplifier gain at small input signal levels. The first model equation is simply adapted from within the laser modelling, since an optical amplifier can be considered a laser without mirrors. The second model further considers the consequences of high pump beam intensities, as was the case for the work presented in this thesis. An equation which predicts the saturation intensity of the material is also examined to establish what signal levels can appropriately be described as 'small signal' levels. How these equations are used to obtain theoretical amplifier results for comparison to the experimentally measured data is described.

Small signal single-pass Gain

Model One

The small signal gain co-efficient (eqn. 2.16) g_0 , is related to the inverted population density n (the density of the upper laser level) by:

$$g_0 = \sigma_{21} n$$

where σ_{2l} is the stimulated-emission cross section at the signal frequency. For cw operation, by rearranging equation 2.27, g_0 can be given as:

$$g_0 = \frac{\sigma_{2l} \tau_f \eta_Q \eta_B \eta_A P_{IN}}{h\nu_p V} \quad (2.36)$$

where the previously introduced Stokes factor has been removed to give ν_p instead of ν_L (since strictly there is no self-generated laser output from an amplifier). In the case of cw amplification we can ignore the additional threshold considerations (Stark splitting and Fluorescence branching) which were required for lasers, as a steady-state has already been established. In the case of short-pulse amplification these additional factors would need to be considered.

Neodymium doped lasers are predominantly pumped at levels slightly above the ${}^4F_{3/2}$ upper laser level. The ${}^4F_{3/2}$ level is then populated by non-radiative transitions from these higher levels. This process is extremely rapid, and therefore fluorescence from these higher levels to levels below the ${}^4F_{3/2}$ upper laser level is not generally observed. It is therefore concluded that each absorbed pump photon produces a Nd^{3+} ion in the ${}^4F_{3/2}$ state, thus the pump quantum efficiency η_Q , is extremely high, and to a good approximation $\eta_Q = 1$. Therefore η_Q has been omitted from the following gain equations.

The small signal, single-pass gain is defined by:

$$G_0 = \exp (g_0 l) \quad (2.37)$$

where l is the length traveled through the amplifier material.

Therefore from 2.36,

$$G_0 = \exp \left[\frac{\sigma_{2l} \tau_f \eta_B \eta_A P_{IN}}{h\nu_p A} \right], \quad (2.38)$$

where A is the area of the beam.

Since amplifier gain is often quoted in units of dB the conversion is:

$$\text{Gain (dB)} = 10 \log G_0 \quad (2.39)$$

To a first approximation, the expected gain for a small signal on a single pass through a microchip amplifier may be calculated with these equations.

Model Two

When an amplifier is pumped at high power densities (P_{IN} large and A small) the approximation made at the top of page 2-36, that $W_p \ll 1/\tau_f$, is no longer valid. Therefore the small signal gain co-efficient of equation 2.17 must be used. This equation rearranged is:

$$g_0 = \sigma_{21} \left(\frac{n_{tot} W_p}{W_p + \frac{1}{\tau_f}} \right) \quad (2.40)$$

From equation 2.25 it has been established that $W_p n_{tot} = \frac{\eta_Q P_{ab}}{h \nu_p V}$, by assuming $n_{tot} \approx n_0$.

The pump rate W_p can be defined as the number of pump photons per unit area multiplied by the absorption cross-section, σ_{ab} .

$$\text{Therefore, } W_p = \frac{\eta_Q \sigma_{ab} I_p}{E_p} = \frac{\eta_Q \sigma_{ab} P_{ab}}{E_p A} = \frac{\eta_Q \sigma_{ab} P_{ab}}{h \nu_p A} \quad (2.41)$$

Where I_p is the intensity of the pump beam, and E_p is the energy of the pump photons. As for model one the pump quantum efficiency is approximated to unity ($\eta_Q = 1$), and is omitted from the following equations.

$$\text{Equation 2.40 becomes: } g_0 = \sigma_{21} \left[\frac{P_{ab}}{h \nu_p V} \middle/ \left(\frac{\sigma_{ab} P_{ab}}{h \nu_p A} + \frac{1}{\tau_f} \right) \right] \quad (2.42)$$

And the small signal single-pass gain equation from equation 2.37 becomes:

$$G_0(P_{ab}) = \exp(g_0 l) = \exp \left[\frac{\sigma_{21} \tau_f P_{ab}}{h \nu_p A} \middle/ 1 + \frac{\tau_f \sigma_{ab} P_{ab}}{h \nu_p A} \right] \quad (2.43)$$

The equation is then obtained in terms of the incident pump power, P_{IN} , by using the relationship $P_{ab} = \eta_A \eta_B P_{IN}$ as outlined in the laser model, and equation 2.43 becomes:

$$G_0(P_{IN}) = \exp \left[\frac{\sigma_{21} \tau_f \eta_A \eta_B P_{IN}}{h \nu_p A} \middle/ 1 + \frac{\tau_f \sigma_{ab} \eta_A \eta_B P_{IN}}{h \nu_p A} \right] \quad (2.44)$$

simplified 2.44 becomes:

$$G_0 = \exp \left[\frac{\sigma_{21} \psi P_{IN}}{1 + \sigma_{ab} \psi P_{IN}} \right] \quad (2.45)$$

with

$$\psi = \frac{\tau_f \eta_A \eta_B}{h \nu_p A} \quad (2.46)$$

Small signal single-pass gain in units of dB is then calculated from this equation by using equation 2.39.

Saturation Intensity

A small signal level is defined as when the input signal intensity times the gain is much less than the saturation intensity of the material, as defined in equation 2.20; ($I_s = \frac{h\nu L}{\sigma_{21}\tau_f}$). The numerical

value of the saturation intensity has been calculated in chapter six for the Nd:YVO₄ material used, and compared with experimental results obtained for the reduction in gain as the input signal level was increased.

Conclusion

The beginning of this chapter described the principles which govern the operation of the microchip lasers. Within this, it was shown that parameters including microchip thickness and temperature can be means by which to control the spectral output of the laser. The principles of an optical amplifier and how they apply to the microchip amplifier used in this work are given. Equations to predict the threshold and slope efficiency of the microchip lasers were established by manipulation of the rate equations for an ideal four level laser system. In chapter five results established from these theoretical equations are presented and compared with experimental data. Equations were established for the amplifiers to predict the saturation intensity and the small signal single-pass gain, with the results of these compared to the experimental data in chapter six.

Chapter 3 Experiment

Introduction

3.1 Equipment

3.1.1 Pump Sources

3.1.2 Power Measurement

3.1.3 Absorption & Fluorescence Measurement

3.1.4 Beam Profiling

3.1.5 Microchips, Holders and Temperature Control

3.1.6 Miscellaneous Equipment

3.2 Experimental Techniques

3.2.1 Establishing pump spot size

3.2.2 Measurement of beam divergence

3.3 Measurement of Absorption

3.3.1 Using a White Light Source

3.3.2 Through Power Technique using a Ti:sapphire laser

3.4 Measurement of Fluorescence

3.5 Characterization of Microchip Lasers

3.5.1 Laser at 1.06 μm

3.5.2 Laser at 1.34 μm

3.6 Characterization of Microchip Amplifiers

3.6.1 Experimental Arrangement

3.6.2 Measurement of Gain

3.6.3 Measurement of Gain against Signal Power

3.6.4 Measurement of Gain against Pump Power

3.6.5 Amplification at 1.34 μm

Conclusion

Chapter 3

Experiment

Introduction

This chapter focuses on the major equipment used and techniques utilized in performing the experimental examination of Nd:YVO₄ microchip lasers and amplifiers. The first section outlines the major pieces of equipment, and summarizes any functions or parameters which have been deemed necessary to comprehend their use, or method of operation. The remaining sections outline the techniques and procedures used throughout the work. These include the techniques used in establishing the pump beam spot size and the microchip beam divergence, the procedures used to measure the Nd:YVO₄ microchip absorption and fluorescence, and the details of the experimental tests to characterize the microchip lasers and amplifiers. Procedures used to measure some of the parameters necessary for modelling the amplifier performance are also included.

3.1 Equipment

3.1.1 Pump Sources

The microchip laser and amplifier systems studied in this work were optically pumped. In a practical microchip laser / amplifier system the pump source would be a small, relatively inexpensive laser diode; in keeping with the compact nature of the microchip system. However, in this work two different pump laser systems were employed. For the work on the microchip lasers a large, but versatile, argon ion/Ti:sapphire laser system was used. In the amplifier experiments a laser diode was used to pump the microchip laser which then provided the 'probe' signal, while the argon ion/Ti:sapphire laser system was used to pump the amplifier microchip under investigation. Outlined below are the characteristics, along with the advantages and disadvantages of each pump laser system.

Argon Ion / Ti:sapphire laser system

The argon ion / Ti:sapphire laser system is a combination of two different types of lasers, used in series to generate optical radiation at appropriate wavelengths in order to pump the Nd:YVO₄ microchips. This system is far too expensive and bulky for a practical microchip laser system, but because of its versatility is useful in the testing of the microchip lasers and amplifiers.

The argon ion laser (Spectra-Physics 2025-05) is a high power (in excess of 5 Watts multi-line) gas laser capable of producing laser action at several wavelengths between 454 and 514 nm (blue-green region). A tunable wavelength dispersive prism at the end mirror is used to select the desired transition. A high intensity source to pump the Ti:sapphire laser is produced by replacing the wavelength dispersive prism with a single end mirror, which allows all possible transitions to lase.

The Ti:sapphire laser (Spectra Physics 3900S) contains a titanium doped sapphire crystal which has broad absorption in this blue-green region. The Ti:sapphire laser is capable of tunable laser action over a broad region of the near infrared wavelength spectrum. A rotatable birefringent filter inside the laser cavity selects the operating wavelength. It is possible to use a series of etalons within the laser cavity to reduce the linewidth of the laser output (nominally less than 40 GHz), to less than 15 GHz when using a thin etalon, or less than 500 MHz when using a thick etalon. These etalons were not required in the experiments described in this work since the laser naturally had a linewidth much narrower than a 'standard' laser diode; which would be the basis for a practical microchip laser system. It is also already much narrower than the absorption band in Nd:YVO₄.

The laser system described above provides a very high quality tunable pump source for the microchip lasers and amplifiers. The Ti:sapphire output beam diameter is narrow and has low divergence (highly collimated), which allows easy modification to a known, controllable pump spot size. The output beam is also highly polarized (> 100:1 Horizontal), which was utilized for investigating polarized pumping of the microchips. The maximum output power of

the Ti:sapphire in the wavelength region required to pump the Nd:YVO₄ microchips (approximately 800 nm) is between 600 and 700 mW. This laser system would not be considered as a commercial pump source as it is very expensive to purchase, and costly to run (power and maintenance), and is much too large to incorporate into a commercial packaged microchip laser or amplifier end product. Table 3.1 below summarizes some significant parameters of the Ti:Sapphire laser output.

Available wavelengths	≈ 700 - 1000 nm #
Peak wavelength	790 nm
Peak power	≈ 750 mW * (with 5 W pump power)
Linewidth (no etalons)	< 40 GHz
Polarization	> 100:1 Horizontal
Beam diameter	0.95 mm * (1/e ² points)
Beam divergence	1.0 mrad * (full angle)

* at peak wavelength, # change of optics needed at ≈ 850 nm

Table 3.1: Beam parameters for Ti:sapphire laser.

Laser Diode

Using a laser diode to pump the microchip laser is comparatively a much cheaper alternative, both with respect to the initial unit price and also the running cost. The laser diode is compact and therefore suitable for development in a practical small microchip laser system. However, laser diodes have several characteristics, namely beam quality and controllability, spectral width and minimal wavelength tunability, which are not conducive to their use as a pump source in a laboratory based controllable test program.

A laser diode is a small semiconductor laser. The nature of its construction generally results in relatively poor beam quality (for a laser), with a highly divergent output beam. The beam is generally astigmatic, i.e. the divergence is usually greater in one direction than the other, resulting in an output beam which is difficult to focus to a small circular spot size.

Further difficulties arise if the beam diameter needs to be varied for experimental purposes. In comparison to the Ti:sapphire laser, a laser diode has a large spectral bandwidth, with optical power shared amongst a number of longitudinal modes, covering a region of several nanometres. Typical high power laser diodes operating in the 800 nm region have a FWHM output of approximately 2 nm. The Nd:YVO₄ material being investigated is one of the better laser materials for laser diode pumping since it has a relatively broad absorption region around 800 nm (greater than 50% absorption in a 0.5 mm length, over a region of approximately 3 nm). The performance of laser diodes is also sensitive to temperature, where the output wavelength can vary over several nanometres due to a change in the diode temperature. This property may be exploited to control the output wavelength, but may also be detrimental in some applications where the output power needs to be varied. Varying the output power requires changing of the diode drive current, which can result in a temperature change, and an unwanted shift in the wavelength of the output spectrum.

Two high power laser diodes were used to pump the microchip lasers, for the purpose of producing the 'probe' signals for use in the amplifier experiments. The laser diodes and their associated power supplies were constructed to operate in constant 'light' mode, where an internal photodiode monitored the output power of the laser. (As opposed to constant 'current' mode, where the supply current is kept constant, and the output power can vary). This mode of operation protects the laser diode from being over-powered, but has the drawback that any light entering back into the laser diode (for example back reflections from a lens or mirror) is measured by the monitor photodiode. The drive current of the laser diode is subsequently decreased because the system measures that it is producing more output power than is actual. This results in a lower than indicated output power, and restricts the maximum achievable output power. Tests with these systems confirmed that the laser diode's performance was greatly affected by back reflections into their output facet. An anti-reflection coated lens was thus used in front of the laser diodes.

The characteristics of the two laser diodes used are summarized in figure 3.1 and table 3.2 below. A 500 mW laser diode (Sony SLD-303XT-25) was sufficient to pump a 1.06 μm

microchip laser and generate the small microchip output powers required for the amplifier experiment. A higher power 1 Watt laser diode (Sony SLD-304XT-25) was necessary for pumping the higher threshold 1.34 μm microchip laser.

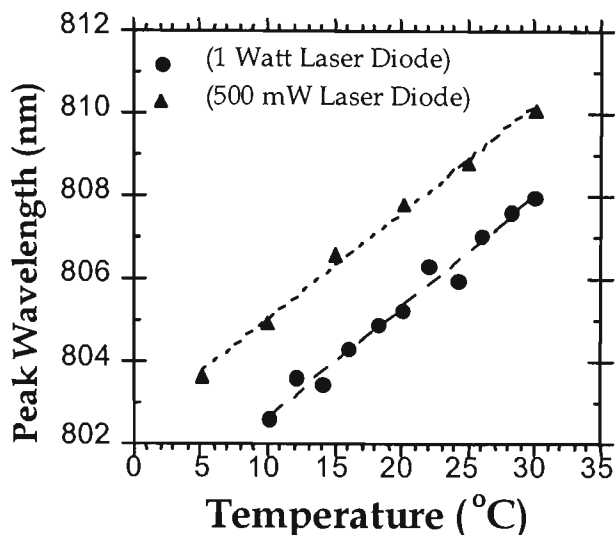


Figure 3.1: Peak wavelength of pump laser diodes versus temperature.

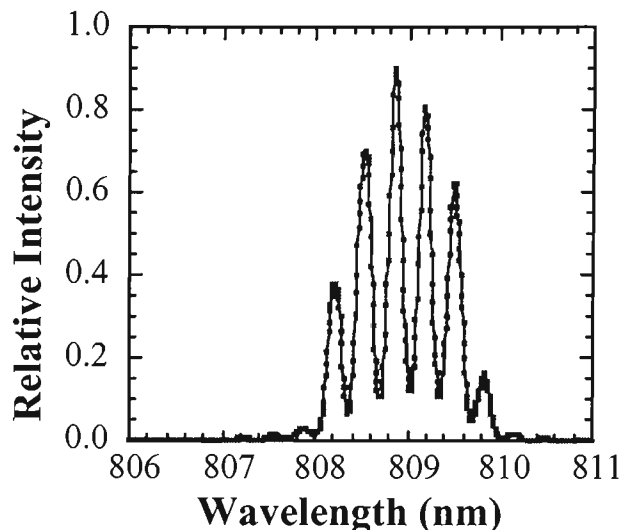


Figure 3.2: Typical multimode output spectrum of the pump laser diodes. (Model 303XT at 25°C, with 377 mW output).

Figure 3.1 shows the peak output wavelength of the two laser diodes used to pump the microchip lasers. The 500 mW laser diode was operated at an output power of approximately 378 mW and the 1 Watt laser diode at an output power of approximately 703 mW (powers recorded according to internal photodiode). This was close to the maximum outputs available, given the reduction in output power from back reflections, and the instrument set limits. Given that the maximum absorption in the pump band above $^4F_{3/2}$ in Nd:YVO₄ is between 808 and 809 nm, this graph shows that the lower power laser diode had the best wavelength match to the absorption spectra of the Nd:YVO₄ microchips. The maximum pumping efficiency was achieved with the laser diode at a temperature of approximately 25°C. The output wavelength of the 1 Watt laser diode matched the greatest absorption region of the Nd:YVO₄ microchip and achieved maximum pumping efficiency when operated just beyond the laser diode's maximum recommended temperature (30°C). Figure 3.2 shows a typical output spectrum from these laser diodes; this particular spectrum is from the 500 mW laser diode at an output power

of approximately 377 mW at a temperature of 25°C. The output parameters for the two laser diodes are listed in table 3.2.

Type:	SLD-303XT-25	SLD-304XT-25
Rated. Max. Power	500 mW	1 Watt
Divergence* (parallel)	9.6°	12.7°
(perpendicular)	29.7°	26.1°
Peak wavelength as measured at 20 °C	807.86 nm	805.27 nm

* at 25 °C (450 mW for 303, 900 mW for 304)

Table 3.2: Laser diode parameters as supplied.

3.1.2 Power Measurements

To measure pump power and output power, and to maximize the light intensity coupled into a fibre (for fibre coupled instruments, e.g. optical spectrum analyzer), several different optical power measuring devices were used.

A series of Coherent base units and detector heads were used to measure free space optical power. A LM-10 Thermal detector head was used when making adjustments to the argon ion/Ti:sapphire laser system, and to measure the pump power delivered to the microchips. Typically a LM-2 Silicon, or LM-2 Germanium, detector head was used when measuring output power from the microchips. Wavelength selective filters were placed after the microchip to minimize the transmitted pump power before the detector head used to measure the power level of the output laser beam or amplified signal beam. Each of the measurement base units allowed for wavelength calibration of the power measurement.

An AWA analog fibre coupled power meter was used where it was necessary to measure light that had been coupled into fibres. This power meter had an FC fibre receptacle input and, by detecting the power transmitted at the far end of a fibre, it was possible to

maximize the coupling of light into the fibre. The meter was very effective at detecting low intensities of light in a fibre, with a dynamic range of around 70 dB and a minimum reading of -72 dBm.

3.1.3 Absorption & Fluorescence Measurements

Three main pieces of equipment were used in the measurement of the absorption of the Nd:YVO₄ microchip, these were: a white light source, a parallel beam mount and an optical spectrum analyzer (OSA). (Note: a power measurement technique was also used, which utilized the Ti:sapphire laser and a power meter, both of which have been outlined earlier). Each of these instruments is described below, while the procedure for the measurement of absorption is given in section 3.3. The main equipment used for the measurement of fluorescence was the Ti:sapphire laser (outlined in section 3.1.1), and the OSA. The fluorescence measurement procedure is given in section 3.4.

White Light Source

The Ando AQ-4303B White Light Source is a broad band light source which has an FC receptacle output. The emission wavelengths are from 400 to 1800 nm with the lighting element being a Halogen globe. This light source was used in conjunction with a parallel beam mount and an OSA to obtain transmission (and corresponding absorption) measurements of the microchips and other coated optical components (filters, beamsplitters, etc.).

Parallel Beam Mount

By connecting the input of the Ando AQ-9314 Parallel Beam Mount to the white light source and output to the OSA, with optical fibres, measurement of the wavelength dependent transmission properties of a material could be obtained. The parallel beam mount is a light proof container which holds the object under test within an expanded, collimated beam of light

from the white light source. Once the light has passed through the object it is focused back into a fibre, to be entered into the spectrum analyzer for analysis.

Optical Spectrum Analyzer

The Ando AQ-6310B Optical Spectrum Analyzer (OSA) can measure input light with wavelengths from around 400 to 1750 nm. It has a FC fibre receptacle input, so any light that is to be investigated needs first to be coupled into a fibre.

The OSA has three sensitivity settings; high sensitivity-off, high sensitivity-fast, and high sensitivity-slow. Each respective setting allows a lower reading limit, but corresponds to a slower reading time. The minimum reading level is -100 dBm, though the noise floor limit appears to vary between -90 and -95 dBm across the region 500 to 1500 nm. The OSA can be set to detect at a resolution as narrow as 0.1 nm. It also has an averaging function to improve the signal to noise ratio for measurement at low signal levels.

The OSA was used to perform many functions including: transmission and fluorescence measurements, monitoring of the laser output spectrum, and to conduct comparative amplifier gain measurements. Data from the OSA is transferable to computer via GPIB. It was also used to study the spectral output of laser diodes and to set the wavelength of the Ti:sapphire laser. The OSA has a wavelength self calibration function using an input He-Ne laser at 632.8 nm, and was also checked against other known wavelength laser sources.

3.1.4 Beam Profiling

Well determined pump beam diameters were required to perform repeatable tests on the microchip lasers and amplifiers, and to accurately model the observed performance. Three methods of beam profiling were employed. These methods evolved throughout the research program described as the need for more sophisticated methods became evident. The methods were: 1) calculations, 2) manual x,y scanning of the beam using a small pin-hole, and 3) use of a commercial beam analyzer.

Initially it proved sufficient to use standard Gaussian beam theory, and simple spot size estimates, to determine the pump beam diameter (outlined in section 3.2.1). This was sufficient for a well defined Ti:sapphire beam and a single focusing lens. Subsequent experiments using a laser diode pump source required experimentally verifiable methods to establish the beam size, as the diode beam parameters were complex and multiple lens systems were required.

In order to establish the spot size of a focused laser diode a nominal 12 μm pin hole attached to a power meter was traversed across the beam in two orthogonal directions in a number of locations around the perceived beam waist. It was then found where the power level dropped to half the maximum power and a rough measure of the beam size established. This process was very time consuming when trying different focusing arrangements to achieve the beam size that was required. It also had limited accuracy, since it gave very little idea of the actual beam shape, and small beam sizes would produce a convolution effect with the pin hole.

Thus in order to get accurate, real time, measurements of the beam dimensions down to very small diameters, a beam analyzer/profiler was purchased. An investigation of commercial CCD camera based profiling systems found that they did not have the ability to measure the required small beams, due to pixel size limitations. The system purchased was a Melles Griot Super BeamAnalyzer, designed to measure the position, power, profile and width of a continuous wave (cw) laser beam. It utilized seven scanning knife-edges and tomographic reconstruction to provide high resolution, three-dimensional views of the entire intensity distribution of the beam. The resolution of the three-dimensional reconstruction paralleled that of the CCD camera systems, yet provided an order of magnitude improvement in accurate minimum beam size measurement.

A silicon detector (9 mm square) is mounted behind a drum with different orientation knife-edges. With the drum rotating, multiple scans generate seven profiles each representing the intensity profile of the beam in a different direction.

For measurements of higher power beams, filters can be inserted between the drum of knife-edges (measurement plane) and the detector, which prevents distortion of the measured intensity profile that may result from imperfections in the filter.

The figures given in the specifications for the maximum measurable power density at the detector, closest to our intended wavelength use are:

96 $\mu\text{W}/\text{mm}^2$ @ 830 nm

165 $\mu\text{W}/\text{mm}^2$ @ 1064 nm

These figures seem rather low when considering this device can measure beams of the order of 30 μm in diameter, as was required during this work. So in addition to the 10% and 0.5% transmission neutral density (ND) filters supplied, a second filter holder (like those supplied) was constructed and fitted with a higher density ND3.0 filter. The percentage transmission versus wavelength figures were measured for the ND3.0 filter and inserted into the beam analyzer software to produce a calibrated power reading.

In addition to the measurement of beam diameters, the beam analyzer was used to measure beam profiles, where measurements of the beam shape were taken in steps along the path of the beam. It was also used to establish the relative position of two beams, to achieve the optimum pump and signal overlap within an amplifier microchip.

3.1.5 Microchips, Holders & Temperature Control

Microchips

The microchips were acquired through TEM Incorporated, Japan, who performed the optical coating of the chips, however the Nd:YVO₄ microchips themselves were test samples from NEC, Japan. At the time the material was not commercially available, and was acquired through collaborative links with Fukui University, Japan. The microchips used were constructed from rods of YVO₄ crystal with $1.0 \pm 0.1\%$ Nd³⁺ doping. The rods were diced and polished to the required thickness, with dielectric mirrors then coated onto the laser and

amplifier microchips. A number of different Nd:YVO₄ microchips were used in this work: an uncoated test sample for absorption and fluorescence tests, two samples mirror coated for lasing at particular wavelengths, and one larger anti-reflection coated microchip for use in the amplifier tests, the characteristics of each of these are outlined below in table 3.3.

Nd:YVO₄ is a uniaxial birefringent material. This means that incident light which is polarized parallel to the single optic axis (thus uniaxial) experiences a different refractive index to that light which is polarized perpendicular to the axis. In Nd:YVO₄ the crystallographic c-axis is the optic axis, and these microchips were thus constructed to have this axis parallel to the input and output faces of the microchip to maximize the pump absorption.

The quality of the reflective coatings on the microchips and the microchips themselves was rather varied. This was seen by inspecting the microchips under a microscope (which was necessary to determine the orientation of the crystal c-axis, and the input and output sides), and was confirmed by the greatly varied results obtained when traversing the pump beam across the microchips. The coatings on the Nd:YVO₄ microchips, and to a smaller extent the microchips themselves, were cracked and rough. This is especially visible around the edges of the microchips. Although the quality of the coated Nd:YVO₄ microchips was “not the best”, optimum pumping locations on the microchips were found by scanning the surface of the crystal with the pump beam, and from this good results were achievable. {For discussion of Nd:YVO₄ quality see section 4.4}

Microchips	Dimensions	Coatings
Test sample	3 x 3 x 0.5 mm	uncoated
1.06 μm laser	3 x 3 x 0.5 mm	(3 x 3 mm faces coated) face 1) 1.064 μm Reflection = 99.92% 808 nm Transmission = 99% 2) 1.064 μm Reflection = 99±0.2%

1.34 μm laser	1 x 1 x 0.5 mm	(1 x 1 mm faces coated) face 1) 810 nm Transmission \approx 98% 1.06 μm Transmission \approx 96% 1.34 μm Reflection = 99.95% 2) 1.06 μm Transmission \approx 96% 1.34 μm Reflection \approx 98.1%
Amplifier	1 x 1 x 1 mm	(2 opposite faces AR coated) 810 nm Transmission \approx 98.8% 1.06 μm Transmission \approx 99.8% 1.34 μm Transmission \approx 99.9%

Table 3.3: Summary of the size and coating of microchips used.

Microchip holders

A holder was designed for the very small and quite easily damageable microchips. The holder protected the chips from possible handling damage, produced a suitable thermal mass for temperature control, and allowed a large fraction of the chip area to be investigated. Aluminium holders were constructed which conducted heat away and allowed access to both coated (or polished) sides of the microchips through a hole in the holder slightly smaller than the microchip. These holders also allowed for easy mounting to other equipment, including a heat sink and positioning equipment. As shown in figure 3.3, the microchip was positioned in a groove, slightly wider than the microchip, machined into the base and was held in place by lightly securing the cover.

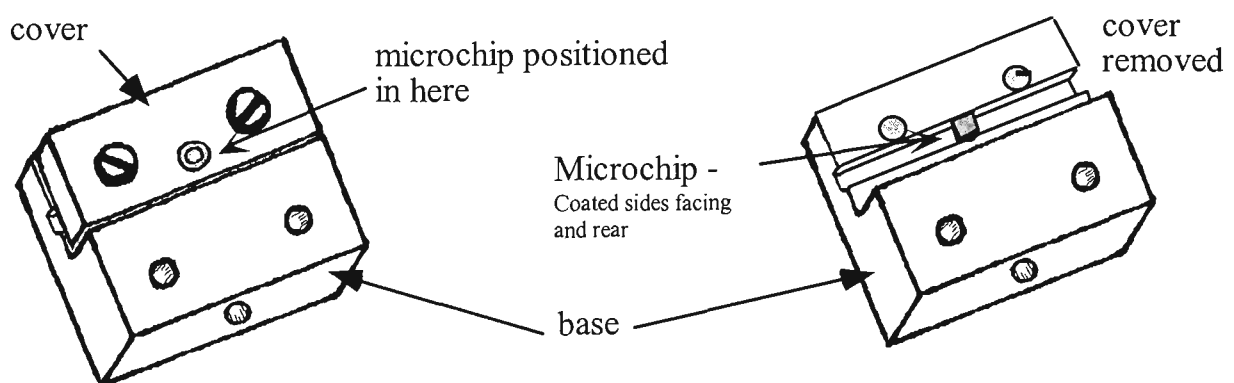


Figure 3.3: Microchip holder

Temperature Control

A Peltier device with an area of approximately 1 x 1 cm was mounted between the aluminium microchip holder and a heat sink to facilitate the heating and cooling of the microchip. A current source (+ve or -ve) could cause the Peltier device to heat or cool, thus heating or cooling the microchip. A thermocouple device was placed into a hole drilled up through the bottom of the holder base towards the microchip position in order to measure the temperature as near to the microchip as possible.

3.1.6 Miscellaneous Equipment

Fibres

Multimode fibres (50 or 100 μm core diameter) were used to transport light to and from the microchip to perform the transmission/absorption measurements. They were also used to transport light to the optical spectrum analyzer for setting the Ti:sapphire laser wavelength, observing fluorescence, and for monitoring the microchip laser, or amplifier, spectral outputs.

Filters

Unabsorbed pump radiation was “filtered out” by high pass filters when monitoring the microchip laser or amplifier outputs. The high pass filters was used to discriminate the pump power from the output power when using a power meter. A filter was also used when coupling the microchip output into the OSA to reduce any unabsorbed pump power so as not to exceed the input level limit of the OSA of approximately 1 mW. And to also limit the creation of alias peaks of secondary or tertiary light in the OSA caused by a high level of pump light at around 800 nm. (These alias peaks are generated by the other diffraction orders of the grating used to cover the spectral range of the OSA. They are greatly reduced by internal filtering, but are still seen to be present at high input intensities). The properties of the filters used are listed in table

3.4, and were all measured, or confirmed against specifications, using a white light source and the OSA.

Manufacturer	Filter ID	Transmission		
ORIEL	58863	$\approx 0\%$ at 800 nm	$\approx 85.7\%$ at 1064 nm	$\approx 84.5\%$ at 1342 nm
ORIEL	LP1000	0.3% at 807 nm	$\approx 65\%$ at 1060 nm	89% at 1343 nm
ORIEL	57897	5% at 804 nm	86.5% at 1060 nm	86% at 1340 nm
MicroCoatings	MC-1060-R	notch filter - max 59% at 1059.65 nm, with 10.9 nm FWHM		
ORIEL	52842	notch filter - max 55% at 1064 nm, with 9.8 nm FWHM		

Table 3.4: *Transmission properties of filters used.*

Beamsplitter / mirror

To allow simultaneous monitoring of the pump beams spectral content and its use as a pump beam for the microchip lasers, a glass microscope slide was used as a beamsplitter to reflect away a small amount of light. The microscope slide was placed on an angle within the beam path and the surface reflection coupled into fibre to the OSA; the beam transmitted through the slide contained the majority of the power and was used to pump the microchip.

To bring together the signal and pump beams from different directions onto the amplifier microchip a wavelength selective beamsplitter (combining mirror) was needed. This required one beam (signal beam) to travel through the combining mirror and the other (pump beam) to be reflected from it (see fig 3.12). A multi-layer coating was designed to achieve this task, using FTG Software's program 'Filmcalc'. Filmcalc determines the reflectivity/transmission of a coating given the number of layers, the layer thicknesses, the layer materials, and the substrate characteristics. Using this information the author deposited an eleven layer coating onto a glass microscope slide to produce the combining mirror. The coating procedure was performed in a standard thin film vacuum coating system. A measured

transmission spectrum of the constructed mirror, when placed at 45° to the incident beam (as it was positioned in the amplifier set-up), is shown in figure 3.4. The combining mirror has a transmission of approximately 5% at 808.8 nm, 76% at 1064 nm and 85% at 1343 nm.

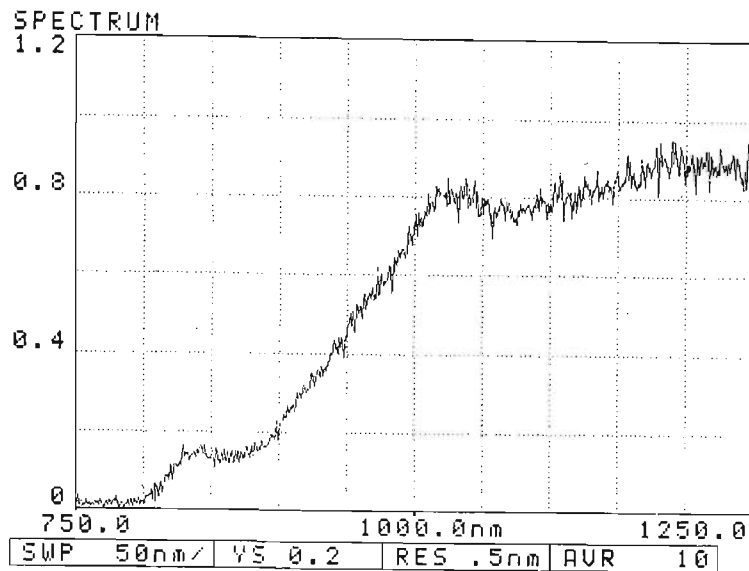


Figure 3.4: Recorded transmission spectrum of the constructed wavelength selective combining mirror for the amplifier arrangement. (light incident at 45°).

Polarizing cube

A polarizing cube was inserted into the Ti:sapphire pump beam to ensure controlled linear polarization when conducting microchip laser tests. This was required as the Nd:YVO₄ crystal is uniaxial and its absorption depends on the polarization of the incident pump light. Although the Ti:sapphire output is specified to be greater than 100:1 horizontally linearly polarized, a broadband (620 - 1000 nm) polarization beamsplitting cube, with an average extinction ratio of greater than 1000:1, was inserted to ensure that only a single polarization orientation was being used to pump the microchips under test. It is noted that in a small practical microchip laser system the insertion of a polarizing device is unnecessary as the Nd:YVO₄ will absorb both polarizations. However the microchip will need to be oriented to achieve the strongest absorption depending on the dominant polarization of the pump source.

3.2 Experimental Techniques

3.2.1 Establishing pump spot size

A well determined pump beam diameter from the Ti:sapphire laser output beam was required to perform repeatable tests on the microchip lasers and amplifiers, and to accurately model the observed performance. It was possible, by assuming a simple diverging gaussian beam and using the characteristics of gaussian beams and the thin lens equation, to calculate the positioning and the correct focal length of the lens to use for achieving the small spot sizes required. The summary given below, which establishes the correct arrangements to produce a required spot size, follows the detailed work of O'Shea (1985), 'Elements of Modern Optical Design'.

Gaussian Beams

A gaussian beam converging at an angle θ should collapse to a point under the laws of geometrical optics; however this does not occur due to diffraction effects. At the intersection of the asymptotes that define θ , a minimum diameter is obtained; the beam waist diameter.

Considering a TEM₀₀ mode, the beam waist d_0 depends on the beam divergence angle in the following way:

$$d_0 = \frac{4\lambda}{\pi\theta} \quad (3.1)$$

where λ is the wavelength, π has its normal mathematical meaning and θ is given in radians.

The variation of the beam diameter in the vicinity of the beam waist is:

$$d^2 = d_0^2 + \theta^2 z^2 \quad (3.2)$$

where d is the diameter at a distance z away from the waist along the beam axis, as shown in figure 3.5.

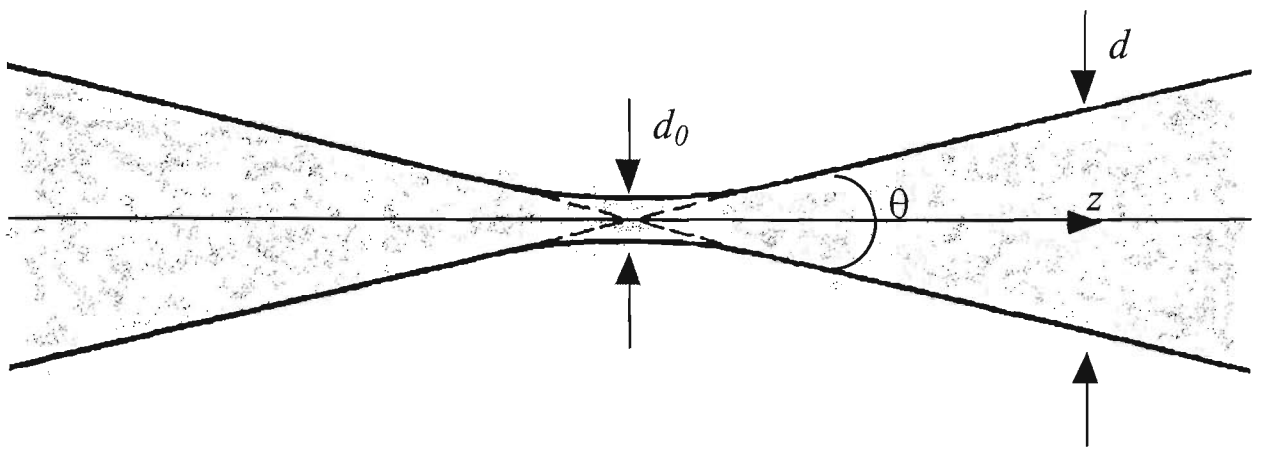


Figure 3.5: Gaussian beam waist and divergence

Rayleigh Range

The parameter Rayleigh range is used to characterize the extent of the beam waist. The radius of curvature of the wavefronts in a gaussian beam are considered as a function of the distance z . When the distance z from the beam waist is large the wavefronts are nearly planar, also at the beam waist they are planar. Therefore, the radius of curvature of the wavefronts changes from near infinity at large distances through a minimum and returns to infinity at the beam waist. This minimum corresponds to the Rayleigh range, Z_R , and it can be shown to be the distance from the waist to where the beam diameter is $\sqrt{2}$ times that of the waist. The Rayleigh range may be expressed in a number of ways:

$$Z_R = \frac{d_0}{\theta} = \frac{4\lambda}{\pi\theta^2} = \frac{\pi d_0^2}{4\lambda} \quad (3.3)$$

The three characteristics of a gaussian beam, d_0 , θ and Z_R , are dependent on each other in such a way that given any of the three quantities, and the wavelength, the behaviour of the beam can be completely described.

Calculating the spot size of a focused beam

The beam emerging from the Ti:sapphire laser was modified to obtain the required pump beam spot size at the microchip. The simplest method to achieve this is by using a single lens, therefore the thin lens equation is considered:

$$-xx' = f^2 \quad (3.4)$$

where x is the distance from the front focal point to the object, and x' is the distance from the back focal point to the image. The thin lens equation can be used for gaussian beams with some minor redefinitions and the addition of a term to account for the effects of diffraction. The optical diagram in figure 3.6 shows the terms associated with using the thin lens equation on a refocused gaussian beam. Replacing the object and image distances with the positions of the input and output beam waists, the lens equation becomes:

$$(Z_2 - f)(Z_1 - f) = f^2 - f_0^2 \quad (3.5)$$

where $f_0 = \frac{d_0'}{\theta}$ (or $\frac{d_0}{\theta'}$) is the term introduced to account for diffraction. Note: f_0^2 is also equal to $Z_R Z'_R$, where Z'_R is the new waist's Rayleigh range.

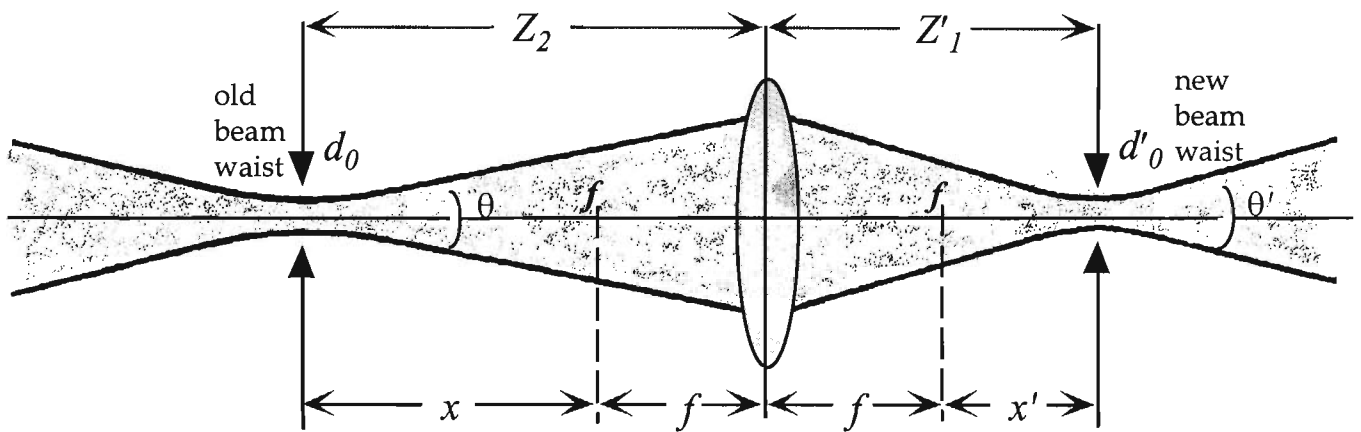


Figure 3.6: Refocussing to a new beam waist.

The relationship between the beam waists and their locations from the lens may be written:

$$\frac{(Z_2 - f)}{(Z_1 - f)} = \frac{d_0'^2}{d_0^2} \quad (3.6)$$

and when used in conjunction with equation 3.5, with the substitutions of $f_0^2 = \frac{d_0'^2}{\theta^2}$ and

$\theta^2 = \frac{d_0^2}{Z_R^2}$ (from equation. 3.3), it can be found that the new beam waist (d'_0) in terms of the

old beam waist (d_0) is:

$$d_0'^2 = m^2 d_0^2 \quad (3.7)$$

where $m = \frac{|f|}{\sqrt{(Z_2 - f)^2 + Z_R^2}} \quad (3.8)$

The function m , is termed the beam waist magnification, and is related to the input beam (Z_R), the lens (f) and the beam-lens position (Z_2-f).

To obtain the required spot size for pumping a value of m needs to be established, considering the size of the old beam waist. The new beam waist parameters may then be established.

$$d'_0 = md_0 \quad (3.9)$$

$$\theta' = \frac{\theta}{m} \quad (3.10)$$

$$Z'_R = m^2 Z_R \quad (3.11)$$

Once the magnification constant (m) has been determined; there are a large number of combinations of focusing geometries that will provide the required new beam waist. A relationship between the choice of the lens focal length and the location of the lens from the old beam waist (the beam waist of the Ti:sapphire laser) exists. By solving equation 3.8 for Z_2 the distance from the old beam waist to the lens becomes:

$$Z_2 = f + \frac{1}{m} \sqrt{f^2 - f_0^2}, \quad (3.12)$$

and by using equations 3.6 and 3.7 the distance from the lens to the new beam waist becomes:

$$Z'_1 = f + m^2 (Z_2 - f) \quad (3.13)$$

However, to avoid the diffraction limit set by f_0^2 , the choice of focal length must be greater than the diffraction limit:

$$f > f_0 = \sqrt{Z_R Z'_R} = \frac{d'_0}{\theta} = \frac{d_0}{\theta'} \quad (3.14)$$

By considering the focal length of lenses available and the old beam waist to lens, and lens to new beam waist distances, equations 3.12 to 3.14 can determine the most appropriate geometry to achieve the new spot size required. Appendix 2 contains a sample calculation to determine the focusing geometry for the pumping of the 1.06 μm microchip laser.

3.2.2 Measurement of beam divergence

A simple procedure to obtain an estimate of the beam divergence from the microchip laser was achieved by placing an infrared detector card in the beam at several distances from the microchip laser. At these locations the diameter of the beam was estimated against the marked

scale on the detector card. These results were then analyzed graphically and/or mathematically to determine a best fit, or average result, for the beam divergence. The later introduction of a beam analyzer saw the same method adopted, but with more accurate and reliable measurements of the beam diameter at a number of positions along the path of the output beam.

3.3 Measurement of Absorption

To investigate the absorption properties of the Nd:YVO₄ material a non-coated sample was used. This sample contained the same dopant concentration as the other Nd:YVO₄ microchips and was the same thickness (0.5 mm) as the laser microchips.

3.3.1 Using a White Light Source

To obtain the absorption spectra, the output from a white light source was coupled via an optical fibre to a parallel beam mount, into which a microchip holder assembly was placed. The light passing through the Nd:YVO₄ microchip sample in the holder was coupled into a fibre, then transferred to an optical spectrum analyzer. The arrangement of equipment used for this procedure is shown in figure 3.7.

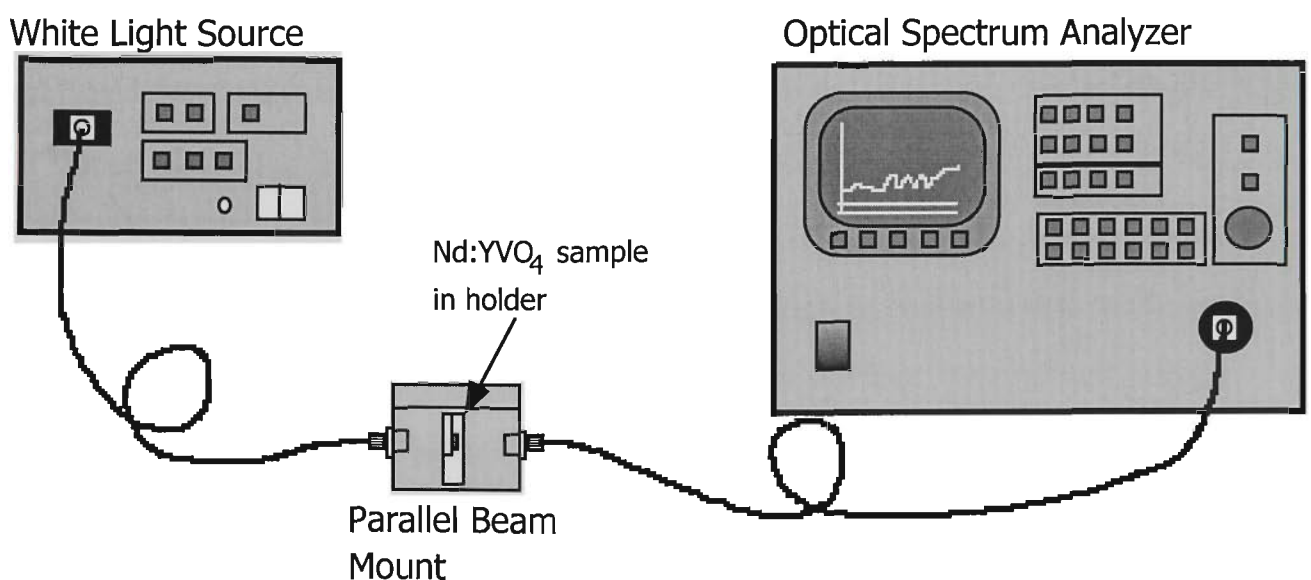


Figure 3.7: Absorption measurement arrangement.

Two input light versus wavelength spectra were obtained on the optical spectrum analyzer to negate the effects of wavelength intensity variations of the white light source, and the transmission through the hole of the microchip holder. The first spectrum considered the transmission with the holder in place but containing no sample, and the second with the holder containing the Nd:YVO₄ sample. In this way the difference in the two spectra is attributed to any differences caused by the Nd:YVO₄ sample alone. A spectrum was generated which gave a measure of the Nd:YVO₄ sample's effect on the transmission across the measured wavelength range by using the optical spectrum analyzer's ability to subtract data on one spectrum from that on another. The data from the OSA was transferred to a computer for manipulation and better presentation in a graphing program. A wavelength absorption spectrum for the Nd:YVO₄ sample was produced using the procedure described below. The data transferred to disk were modified to take into account the reflections from the air/microchip and microchip/air boundaries, which arise when the non-coated microchip is in place, but not when the microchip is removed.

The percentage reflection at each surface is given by:

$$\left(\frac{1-p}{1+p} \right)^2 \times 100\%,$$

where $p = n_1/n_2$, n_1 and n_2 are the refractive indices of air and the microchip. The refractive index of air is assumed to be 1.00 ($n_1 = 1.00$), while n_2 is wavelength dependent and was established from known refractive index values of the Nd:YVO₄ material, as shown in table 3.5. Since Nd:YVO₄ is a uniaxial crystal, exhibiting birefringence, the refractive index does not just depend on the wavelength of the incident light, but also on the incident direction and polarization. The microchips were fabricated so that light incident normal to the microchip face, and polarized parallel (π) to the c-axis, is an extra-ordinary ray (refractive index = n_e), where as light normal, and polarized perpendicular (σ) to the c-axis, is an ordinary ray (refractive index = n_o). Randomly polarized incident light would clearly be a combination of both.

Wavelength (nm)	Refractive Index	
	n_o	n_e
532	2.0210	2.2560
808	1.9721	2.1858
1064	1.9573	2.1652

Table 3.5: Refractive index values for Nd:YVO₄. (CASIX (1996))

Although a full Sellmeier equation for the refractive index change in Nd:YVO₄ would be the most accurate means by which to correct the measured absorption spectra, a full set of Sellmeier coefficients were, as yet, unavailable. Therefore to obtain an approximation of the refractive index across the measurement region (400-1100 nm) the known values of the refractive index against wavelength for Nd:YVO₄ were fitted with a 2nd order polynomial. From this the following equations were obtained to predict n_2 for π polarized light (n_e), σ polarized light (n_o) and randomly polarized light (n_r), assuming $(n_e + n_o)/2$.

$$n_e = n_2 = 2.5318 - 6.9231 \cdot 10^{-4} \times \lambda + 3.2684 \cdot 10^{-7} \times \lambda^2$$

$$n_o = n_2 = 2.2117 - 4.7782 \cdot 10^{-4} \times \lambda + 2.2436 \cdot 10^{-7} \times \lambda^2$$

$$n_r = n_2 = 2.3718 - 5.8507 \cdot 10^{-4} \times \lambda + 2.7560 \cdot 10^{-7} \times \lambda^2$$

where λ is the wavelength. Figure 3.8 shows an example of the relationship between the refractive index and wavelength, in this case for π polarized light (n_e) incident on the Nd:YVO₄ sample as described above. The 2nd order polynomial fit established here from the known refractive index values within the 400 to 1100 nm region of interest is at most 2% different from the Sellmeier equation for pure YVO₄, as given by CASIX(1996), and therefore seems to be a sufficient approximation in this wavelength dependent absorption correction.

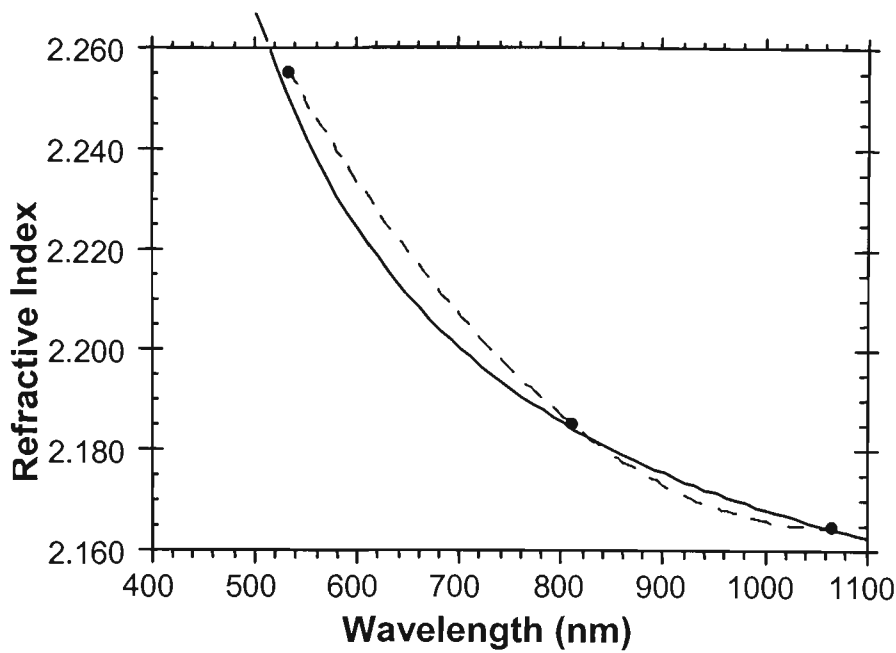


Figure 3.8: Graph of refractive index (n_e) for Nd:YVO₄. Dots represent given values, dashed line is a 2nd order polynomial fit. The solid line is generated from the Sellmeier equation for pure YVO₄ as given by CASIX (1996).

In order to determine the absorption co-efficient $\alpha(\lambda)$ from the acquired data careful consideration of the effect of reflections at the interfaces was required. The relative magnitude of the reflection from the second interface is sufficiently large as to effect the absorption measurement. As is shown in Figure 3.9 the measured intensity is a sum of a series of contributions, where I_0 is the input intensity, and all the right side terms will add to I_D , the detected intensity.

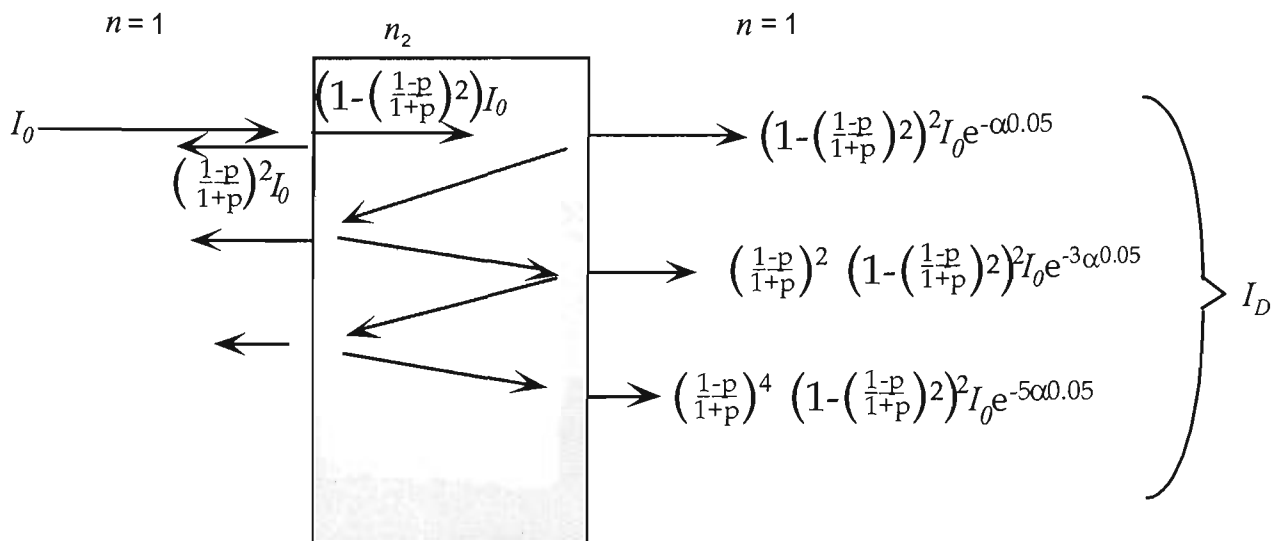


Figure 3.9: Consideration of reflections from microchip/air boundaries in absorption measurements.

A single pass calculation is sufficient for wavelengths where there is significant absorption through the Nd:YVO₄ sample, with subsequent terms being negligible, but for wavelengths with low absorption multiple passes may become important. (If there was no absorption then the third term will equal approximately 0.025% of the original input intensity for a n_2 value of 2.165). Consequently, calculations have been performed which take into account three reflections from the input and output faces, as shown in figure 3.9. The ratio I_D/I_0 corresponds to the data from the resultant transmission difference spectrum obtained on the optical spectrum analyzer (or to the difference in power measurements in the through power technique using the Ti:sapphire (see next heading)). A computer mathematical package (MAPLE) was used to solve the equations as shown in figure 3.9, given the values for the refractive indices and I_D/I_0 , to establish the absorption coefficient α . The corrected absorption of the 0.5 mm length of Nd:YVO₄ can be calculated from the absorption coefficient with the following equation;

$$\text{Absorption} = 1 - \exp(-(\alpha \times 0.05)),$$

with α given in cm⁻¹. Each corrected absorption data point is then reconstructed in a graphing program to constitute an absorption versus wavelength graph.

Initial absorption tests were broadband, with randomly polarized incident light, to investigate the general regions of absorption across the spectrum. Though the energy levels of neodymium are well documented, each host material shifts these levels slightly, and shifts the Stark sub-levels by different amounts. The absorption tests described above gave an overview of the energy level positions in the specific Nd:YVO₄ microchips used for this work, and the relative absorption intensity of each of the levels present.

The high absorption peaks in Nd:YVO₄ found at around 750 - 760 nm and 810 nm were investigated more closely as these lie within the wavelength range provided by the Ti:sapphire laser used for pumping the microchip lasers. Due to the uniaxial nature of the Nd:YVO₄ microchip, and its consequent polarization dependent absorption, a piece of linearly polarizing sheet was placed in the parallel beam mount in front of the microchip holder. To

obtain absorption spectra for parallel (π) polarized incident light the transmission axis of the polarizing sheet was aligned with the crystalline c-axis of the microchip, and for perpendicular (σ) polarized incident light the sheet was rotated through 90°. Polarization dependent absorption spectra were obtained for both the 755 nm and 810 nm regions.

Higher resolution absorption spectra were obtained around the highest absorption region near 810 nm, by decreasing the OSA's range and increasing its sensitivity, to find the greatest absorption intensity peak. Having established the wavelength/s with the highest absorption these then determine the most efficient pump wavelengths for the microchip laser.

3.3.2 'Through Power' Technique using the Ti:sapphire Laser

It was found that in the region of highest absorption around 810 nm, very little signal was reaching the optical signal analyzer for the technique described in 3.3.1, consequently a different technique was devised to give a more accurate measurement of the absorption. As shown in figure 3.10, a 'Through Power' technique was used. This was a simple point by point technique that only needed to cover a small wavelength region, and was simpler than using the Ti:sapphire as the source in the above method. This in itself would have been a point by point method, but with the added drawbacks of relying on a free-space coupling into the OSA for measurement, and the introduction of a neutral density filter to protect the OSA from high input powers.

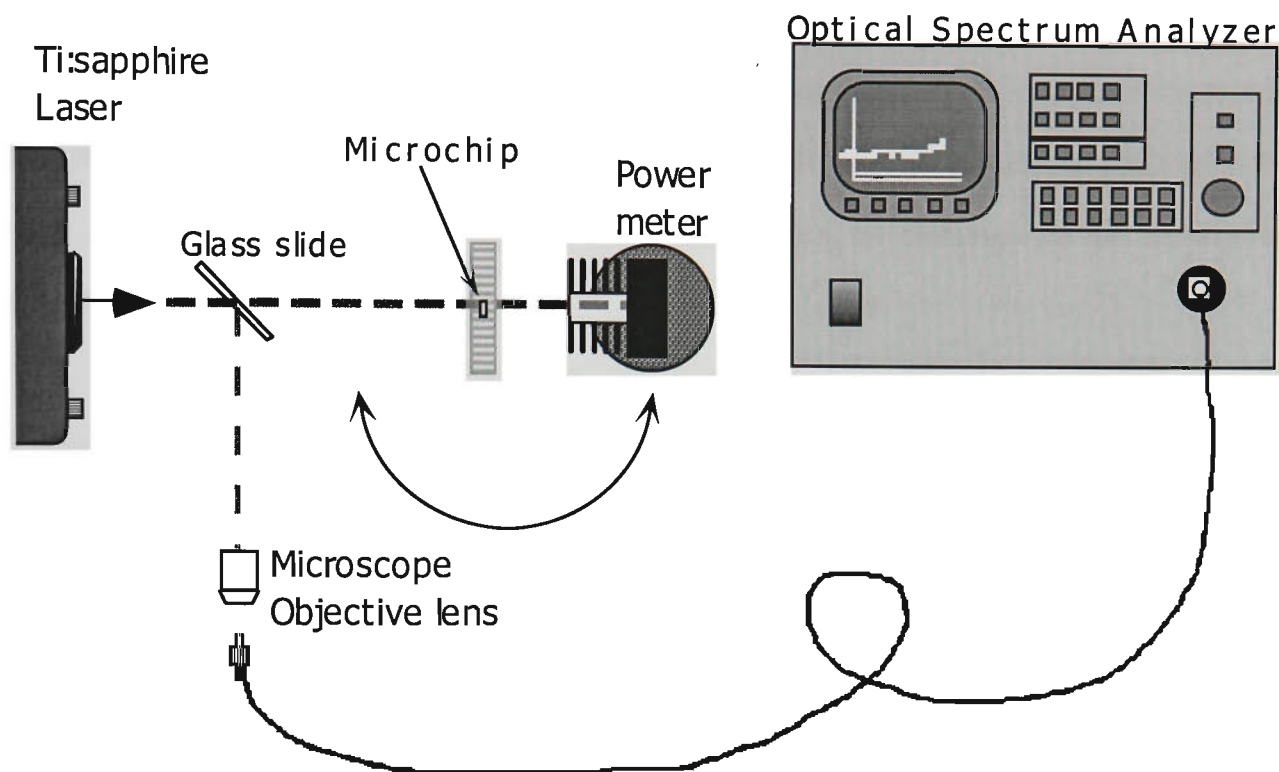


Figure 3.10: Arrangement for Through Power absorption measurements. The double head arrow indicates the two locations for the power meter as described in the text.

The tunable Ti:sapphire laser was used as the light source and was tuned, in 0.05 to 0.1 nm steps, over the regions; 800 to 815 nm for σ incident polarization absorption test, and 806 to 815 nm for π incident polarization absorption tests. In this case, since the Ti:sapphire output is naturally linearly polarized, the sample was rotated through 90° for opposing polarization measurements. At each wavelength, (measured by the OSA), a power meter measured the power before and after the microchip. The ratio of the before and after power corresponds to I_D/I_0 as described in the previous section. Then following the same calculation steps previously outlined, an absorption result was obtained.

3.4 Procedures for the Measurement of Fluorescence

Measurement of the relative fluorescence intensity resulting from transitions between the $^4F_{3/2}$ metastable level of Nd^{3+} and lower levels (predominately $^4I_{11/2}$ around 1.06 μm and $^4I_{13/2}$

around 1.3 μm) were conducted using the techniques described below. The non-coated microchip was mounted so that the linearly polarized light from the Ti:sapphire laser was incident parallel (π) to the Nd:YVO₄ crystal c-axis. The pump wavelength and polarization were set to correspond with the highest pump absorption as obtained in the absorption experiments.

A high pass filter was placed after the microchip to reduce the intensity of light transmitted at the pump wavelength. Light from the microchip was coupled with a microscope objective lens into an optical fibre which was connected to the optical spectrum analyzer. A series of traces, each with a span of 100 nm, were taken to show detail of the fluorescence generated by the Nd:YVO₄ material across the wavelength region, 0.8 to 1.5 μm .

The strong fluorescence regions were identified then examined individually. The individual traces acquired were transferred to computer and analyzed by a graphing program enabling clear presentation of the fluorescence versus wavelength data.

The energies of the Stark split sub-levels, as given in Kaminskii (1990), were used to find the wavelength values for each possible transition between Stark levels. From this, the wavelength of each transition was compared to the intensity peaks within each fluorescence region. It was possible to determine which particular Stark transition was responsible for the laser action of the 1.06 and 1.34 μm microchip lasers through identifying the maximum peak in the fluorescence regions around 1.06 and 1.3 μm . The width of the maximum intensity peaks was measured to give an estimate of the gain bandwidth, and therefore an indication of the number of possible longitudinal lasing modes.

3.5 Procedures for the characterization of Microchip Lasers

A number of experimental tests were performed with the purpose of understanding and specifying the operation of the Nd:YVO₄ microchip lasers. Each test series was designed to vary a different operational parameter. These included changing the pump wavelength, the

pump power and the microchip temperature, while monitoring the output power and spectrum of the microchip laser.

3.5.1 Laser at 1.06 μm

Appropriate pump wavelengths were determined from the measurement of absorption. Likewise, the probable lasing wavelengths were determined from the fluorescence measurements. The microchip coated for laser action in the high fluorescence 1.06 μm region was tested under several varying pumping and temperature parameters.

Pump Beam Parameters

The experimental arrangement designed to produce a pump beam diameter of approximately 200 μm was obtained by using the specified divergence, beam waist diameter and the presumed waist location of the Ti:sapphire laser, following the theory and calculations outlined in section 3.2.1. Calculations showed that with a 250 mm focal length lens placed 962.5 mm from the beam waist of the Ti:sapphire pump laser, the beam will focus a 200 μm diameter at a distance of 281.6 mm after the lens. (See Appendix 2 for calculations).

The beam size, when using the arrangement from the above calculations, was later measured using the Beam Analyzer to be 265 ± 3 μm in diameter and not the arbitrary 200 μm as intended. This difference between the calculated and measured beam size may possibly be attributed to the Ti:sapphire laser's divergence and beam waist diameter being different from that specified (specifications were for the peak wavelength of 790 nm). The 1.06 μm microchip laser results reported are therefore for a 265 μm minimum pumping spot diameter. (The laser modelling calculations have been adjusted to reflect this larger pumping diameter.)

A polarizing beamsplitter cube with greater than 1000:1 extinction ratio was inserted into the beam path to insure single linear polarization of the pump beam when pumping the microchip laser.

The arrangement of the microchip laser and the pumping configuration is shown in figure 3.11. The mounting post attached to the aluminium heat sink block, to which the

microchip holder is attached, was placed into a mounting system where adjustment of x , y and z position was possible.

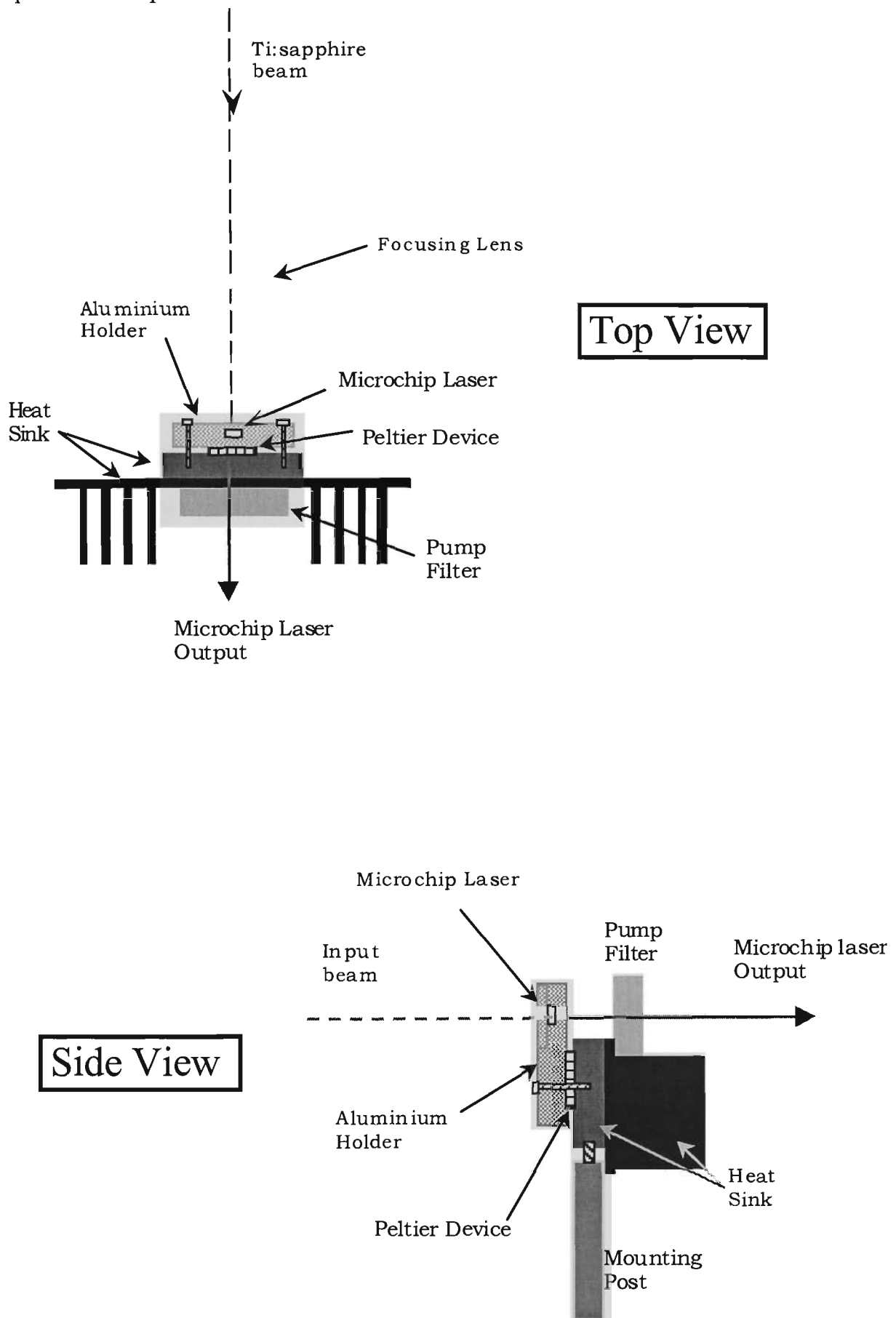


Figure 3.11: Experimental arrangement for microchip lasers.

Laser Output versus Pump Power

The pump beam was scanned across the surface of the microchip to find the area producing the best performance. This was necessary due to the variable quality of the Nd:YVO₄ sample and coating. Measurements were made of the input pump power versus the output power of the microchip laser whilst pumping within the peak wavelength absorption region. The input current, and thus output power, of the argon laser was changed to increase or decrease the input power to the microchip. Changing the power of the argon laser varies the output power of the Ti:sapphire laser in a uniform way which has a minimal effect on the wavelength and beam profile of the Ti:sapphire output (these being monitored). The incident pump power was measured between the polarizing cube and the focusing lens (the approximate 8% loss of power through the lens was taken into account in the analysis of the results). A band pass or high pass filter was placed before the detector to filter out any transmitted pump power when measuring the output power of the microchip laser. The transmission of the filter at the lasing wavelength was measured and used to correct the laser output data. Graphs of microchip laser input versus output power were obtained using this data, and important parameters such as slope efficiencies and thresholds were established. Results were obtained for each input polarization by rotating the crystal through 90°.

Laser Output versus Pump Wavelength

The microchip laser was also pumped at wavelengths other than that in the region of maximum absorption. Keeping the pumping power constant, the Ti:sapphire pump wavelength was varied over its tuning range of 700 to 850 nm, whilst the output power of the microchip laser was monitored. The microchip laser output power was plotted against pump wavelength, and also compared to the absorption at these wavelengths. This procedure was repeated for each pumping polarization.

Laser Wavelength Temperature Dependence

The temperature of the microchip was varied by adjusting the current to the Peltier device, positioned between the microchip holder and a heat sink (see fig 3.11). Measurements of the laser output spectrum were taken at different temperatures having allowed the system time to settle to a constant temperature. To measure the temperature a thermocouple was mounted up through the bottom of the microchip holder. The microchip laser's output power and spectrum were recorded for temperatures between 0 and 100 °C with a constant pump power.

3.5.2 Laser at 1.34 μm

Some initial tests on the 1.34 μm microchip laser were performed with the same pump beam diameter as the 1.06 μm laser ($265\pm 3 \mu\text{m}$). For a co-publication with Taira and colleagues at Fukui University, Japan, (in which they used a laser diode pump source on the same microchip for comparison to our Ti:sapphire pump source results) a smaller pump beam diameter was required (approximately 150 μm) [Bowkett *et al.* (1994)]. Consequently all subsequent 1.34 μm microchip laser results presented here are obtained with this smaller pump beam diameter.

Pump Beam Parameters

To obtain a 150 μm pump spot size the theory and equations found in section 3.2.1 were used to calculate the lens required and its distance from the Ti:sapphire and microchip. The same lens as used in the 1.06 μm laser tests (250 mm focal length), was placed 1516.7 mm from the beam waist of the Ti:sapphire, to produce the 150 μm diameter spot at a distance 281.6 mm after the lens.

Later measurements with the beam analyzer found the minimum pump diameter using these above results to be $165\pm 3 \mu\text{m}$, the difference in sizes attributed to the same reasons noted in the 1.06 μm case.

Performance Tests

The same series of experiments which were performed for the 1.06 μm laser were repeated for the 1.34 μm laser, with any variation from these noted below.

As the microchip laser's output power against input pump power was measured the output spectrum of the microchip laser was monitored. The output was coupled with a microscope objective lens into a fibre and to the OSA to observe the spectrum. Through this observation the modal behaviour of the laser output was determined as the power increased.

The peak wavelength, or wavelengths in the case of more than one mode, were monitored with change in temperature of the microchip. In the case of the 1.34 μm laser it was common to observe more than one longitudinal mode, where as the 1.06 μm laser was generally single mode. At each measurement temperature the wavelength and relative intensity of each mode present was recorded.

In some of the 1.34 μm laser output spectra a peak appeared at a wavelength about 3.5 nm higher than the main transition peak. As a consequence, a closer examination of the fluorescence (tested on the non-coated microchip) in the region of lasing was undertaken to better understand this extra peak.

3.6 Procedures for the characterization of Microchip Amplifiers

This section begins with a description of the experimental arrangement that was employed to test the microchip devices when used as optical amplifiers. A physical interpretation of the gain is described, along with the techniques used to measure it. Outlined are procedures for testing the amplifier with varying input signal intensities to experimentally establish the saturation intensity and to determine the 'small signal' region. The method of measuring the gain against pump power is outlined. Finally, the experimental problems encountered when testing the microchip amplifier at 1.34 μm are described, together with the ways in which the arrangement and procedures differed from the 1.06 μm case.

3.6.1 Experimental Arrangement

The Nd:YVO₄ amplifier microchip was made of the same gain material as the microchip lasers, however in this case it was anti-reflection coated at the signal wavelength to avoid oscillation. The microchip used had dimensions of 1 x 1 x 1 mm, and was anti-reflection coated on two opposite faces to permit single-pass amplification measurements. As shown by the experimental arrangement in figure 3.12, the pump and signal beams were passed co-linearly through the amplifier microchip.

A 1.06 μm Nd:YVO₄ microchip laser was pumped with a laser diode, and its output used to provide a signal for the amplifier. The pump laser diode (Sony SLD-303XT-25) was extremely sensitive to back reflections, since it was configured to be controlled in light mode. The focusing lens which was placed between the laser diode and the microchip laser was anti-reflection coated, by the author, at the pump wavelength to reduce the amount of light reflected back into the laser diode.

The laser diode pumped microchip laser arrangement was not thoroughly investigated, or maximized for best efficiency, but was sufficiently optimized to provide approximately 10 mW of single longitudinal mode output. The pump energy for the amplifier microchip was provided by the Ti:sapphire laser.

A multilayer coated combining mirror was constructed by the author and used to combine the signal and pump beams, which were required to overlap co-linearly in the amplifier chip, see figure 3.12. This mirror allowed the signal to pass through it, while the pump beam was reflected, so when placed at 45°, the two beams incoming at 90° could be combined.

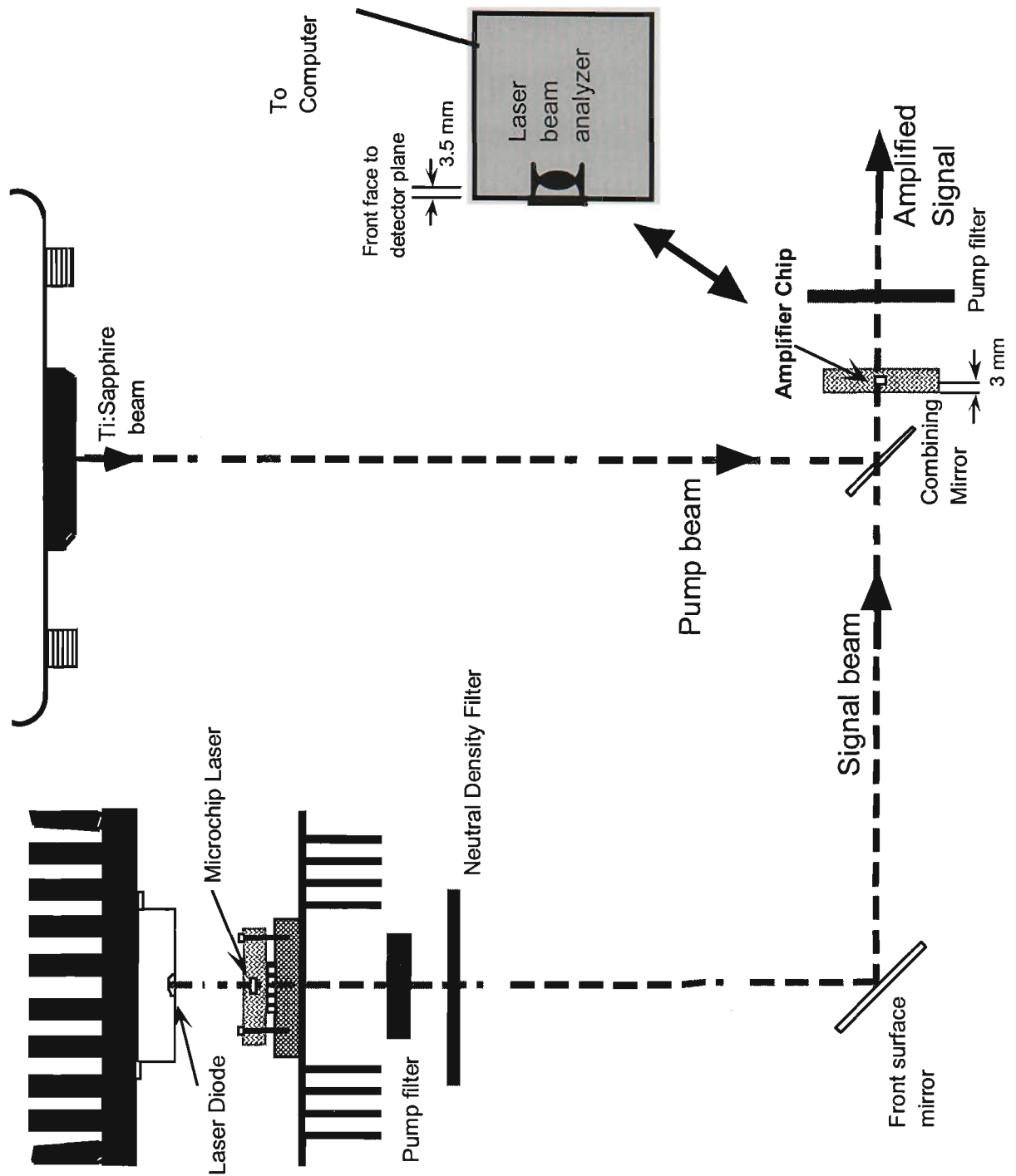


Figure 3.12: Experimental arrangement for the microchip amplifiers. A Ti:sapphire laser provided the pump beam. The signal beam was from a laser diode pumped microchip laser. The two beams were combined with a coated mirror to pass co-linearly through the Amplifier chip. The Laser beam analyzer takes the position of the amplifier microchip and holder to measure the beam profiles through the microchip position.

Pre-test calculations suggested that a small pump beam spot size was necessary to achieve considerable amplification, so this required that the signal and pump beams be reduced in size. Three lenses were placed in each beam path, the first to expand the beam, the second to collimate, and the third to reduce the beam to the required spot size. By inspection of the beams with an IR viewing card, the combining mirror and the lens assemblies of each beam were adjusted to approximately overlap the two beams over a distance of approximately 10 cm beyond the combining mirror. This insured a general co-linearity between the two beams. By using the beam analyzer to measure the beam diameter, and varying the position and focal length of the lenses, the required beam sizes were obtained. The minimum spot size of each beam was made to lie at the same distance beyond the combining mirror (nominated the z direction). The centres of the two beams (as given by the beam analyzer) were also overlapped at their common point of minimum spot size. This was achieved by blocking off one beam whilst noting the centre position of the other. The blocking of the beams was then swapped and the second beam adjusted to match the centre position of the first (generally the x and y position of the final lens of the pump beam was adjusted to match the location with the signal beam). In general the minimum beam diameter of both the pump and signal beams was approximately $30\ \mu\text{m}$ for the amplifier tests.

Prior to the removal of the beam analyzer its position was noted and the amplifier chip (in its holder) was mounted in approximately the same position. The aim was to approximately match the detector plane of the analyzer and the front surface of the microchip. It was noted, and accounted for in the positioning, that the detection plane of the beam analyzer was $\approx 3.5\ \text{mm}$ from the front surface of its outside housing, and that the front face of the microchip $\approx 3.0\ \text{mm}$ from the front of its holder. Then while monitoring the signal output through the amplifier (with pumping) the amplifier was moved in the z direction (towards and away from the beamsplitter) to maximize the amplifier gain. The amplifier position was then varied in x and y to find the best position for maximum gain. The overlap of the two beams was then also 'tweaked' to achieve maximum gain (normally by adjusting final lens in the pump beam).

3.6.2 Measurement of Gain

The Gain was measured in terms of the increase in the output signal. This is often referred to as the 'Gross Gain', and does not consider the losses experienced by the signal when passing through the amplifying system, which should be minimal in a four-level system.

Initially the signal, which had passed through the amplifier microchip, was focused with a microscope objective lens into a fibre and entered into the OSA. A filter was placed before the microscope objective, to block most of the transmitted pump light, protecting the OSA from damage and spurious peaks produced by high input power at the pump wavelength. The amplifier signal output was observed with, and without, pumping of the amplifier and the signal gain determined. This method was proposed to insure measurement of only signal gain, and not a combined measurement of gain and transmitted pump power. This first method of using the OSA to measure the gain was useful in that it insured that any transmitted pump power was not being included in the measurement of gain, since the spectral output of the amplifier could also be observed. However, the comparison of these gain measurements against those obtained with a power meter and appropriate pump filter, showed the original gain measurements to be exaggerated by a factor of approximately 2. This was thought to be due to one of two reasons, or a combination of both. First, on coupling the output signal into the fibre, which transports the light to the OSA, the coupling is maximized. This may mean that only the most intense part of the beam is entered into the fibre, i.e. not all the beam. When the pump is turned on this may be the portion of the beam which undergoes the maximum amplification. Or second, the coupling may become improved due to beam reshaping or displacement on amplification. Thus the power meter measurement technique was adopted. With this technique the power transmitted through the amplifier microchip was measured with both the pump and signal beams incident on the amplifier, then the transmitted power was measured with only the pump beam incident. The second value was then subtracted from the first, and then divided by the measured transmitted power of the signal alone, to obtain a measure of the gain.

Measurement of the pump power was obtained using a thermal detector head placed before the focusing optics. From this reading the measured losses of all the optics through to the input of the microchip were subtracted to obtain the incident pump beam power. The output signal power for the 1.06 μm amplification was measured using a silicon detector head through a 1064 nm notch filter (to cut out most of the pump). The 1.06 μm output signal power was therefore obtained by dividing the measured signal by the measured transmission of the filter at 1.06 μm . For 1.34 μm amplification the signal was measured with a germanium detector head, with a corresponding notch filter to stop any transmitted pump power. Any pump power transmitted through the notch filter was determined by running the pump beam alone, and then this was subtracted from the output amplified signal power.

3.6.3 Measurement of Gain against Signal Power

To determine the saturation characteristics of the gain the intensity of the signal was varied with neutral density (ND) filters. This method was chosen to avoid the problems associated with varying the pump laser diode, since any change in the laser diode may change the output spectrum of the microchip generated signal. The ND filters were inserted into the signal path after the pump filter and before the first lens, see figure 3.12. The insertion of the ND filters did not noticeably change the signal beam minimum spot-size or position, but after the swapping of the filters the beam overlap, and the crystal position were “tweaked” to achieve the maximum gain.

Amplification saturation occurs due to the signal intensity within the amplifier, and is not simply reliant on the input signal intensity, therefore tests were run with several different pump powers, to observe the effect on the gain saturation.

3.6.4 Measurement of Gain against Pump Power

The above tests established that with an incident pump power of around 250 mW, gain saturation would begin to occur at non-pumped output signal powers greater than approximately 10 μW (see fig 6.1). Thus the tests described below were performed with the

minimum signal achievable with the use of a single ND filter placed in the signal beam. This was a Melles Griot OD3.0 filter which reduced the output signal to approximately 7 μW .

The output signal gain was measured against the incident pump power with the beams overlapped as described in the experimental arrangement. To compensate for any beam movement due to argon ion, and/or Ti:sapphire beam shifts the beam overlap and crystal position were “tweaked” for maximum gain after each adjustment of the incident pumping power.

In a further series of tests the pump beam was made considerably larger than the incoming signal, to investigate the effect of pump beam size or intensity. The minimum diameter of the incident pump beam was increased to $\approx 100 \mu\text{m}$. The waist of each beam was again overlapped and the amplifier microchip placed within the beams. Signal gain versus incident pump power was again recorded.

3.6.5 Amplification at 1.34 μm

To obtain a signal to test the amplifier microchip at 1.34 μm , the 1.34 μm microchip laser was pumped by a 1 Watt laser diode. The laser diode was run at high power and high temperature to achieve lasing from the microchip, with a maximum signal power of around 1 mW obtained.

In the 1.06 μm amplifier tests the beam analyzer allowed the measurement of beam size and beam overlap, however since the beam analyzer contained a silicon detector, such measurements were not obtained at 1.34 μm . Consequently, this inability to measure and controllably adjust, the small beam diameters and pump-to-signal overlap that was necessary to produce high gains, made these tests extremely difficult.

In an attempt to determine the 1.34 μm beam size and location, the 1.06 μm signal was run in tandem, with the arrangement shown in figure 3.13. A front surface mirror was rotated through 90° to run either the 1.06 μm signal or the 1.34 μm signal which originated from opposite directions. With the 1.06 μm signal beam focused and adjusted to give maximum gain from the amplifier, the 1.34 μm signal beam was adjusted to try and emulate the 1.06 μm

beam. This was achieved by placing two iris diaphragms in the beam path between the front surface mirror and the amplifier chip and trying to match the beam dimensions. By this method a small amount of $1.34 \mu\text{m}$ signal gain was achieved.

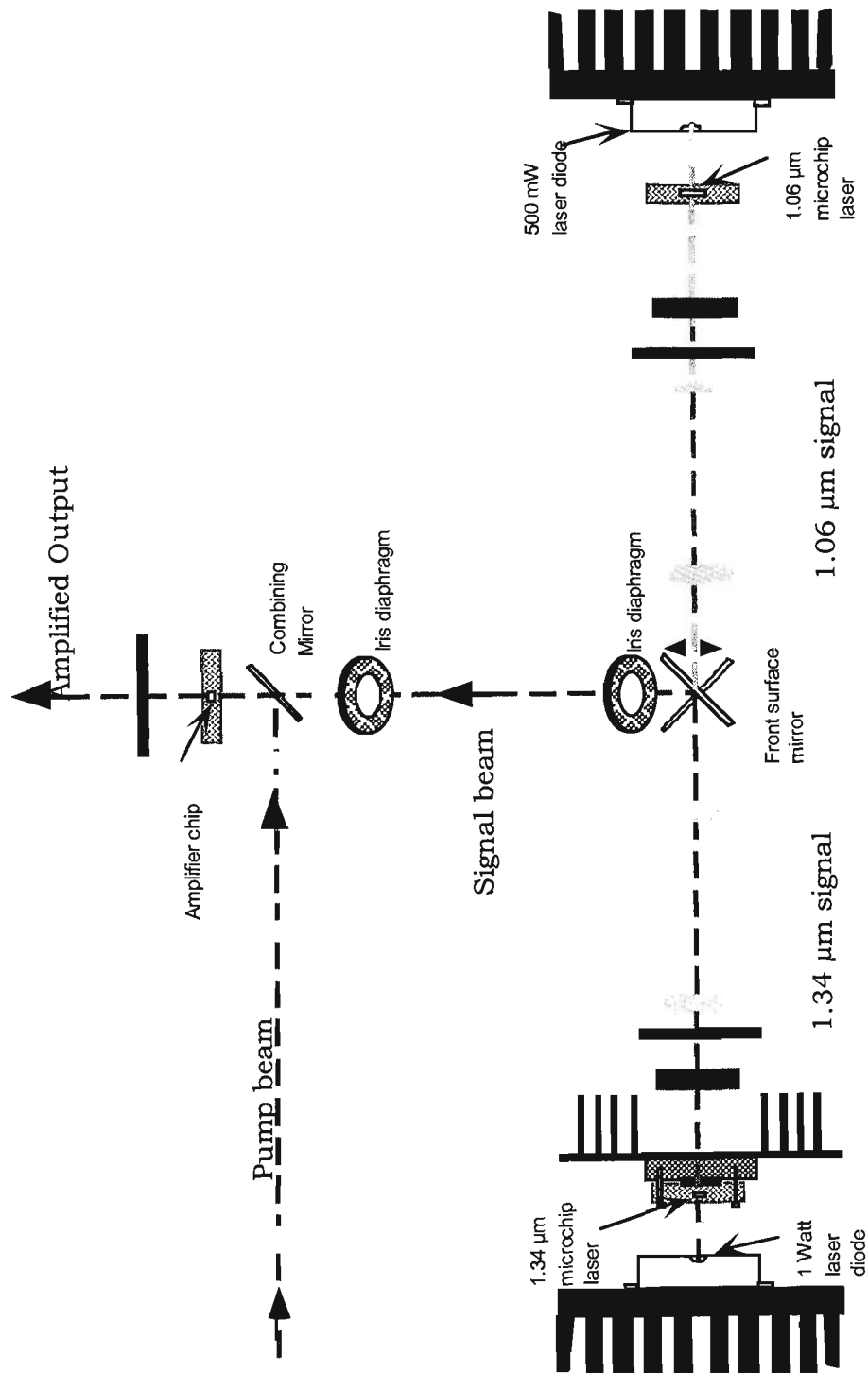


Figure 3.13: Diagram of the $1.34 \mu\text{m}$ amplifier arrangement. The pump beam is provided by a Ti:sapphire laser. The $1.34 \mu\text{m}$ (bottom right) and $1.06 \mu\text{m}$ (top right) signals were produced by laser diode pumped microchips. Rotation of the front surface mirror governs which signal reaches the amplifier microchip. The iris diaphragms positioned within the signal beam were used to try and match the diameters of the 1.06 and $1.34 \mu\text{m}$ signal beams.

Conclusion

This chapter describes the equipment used and the experiments performed. It also describes the techniques used to establish beam parameters, be that pump spot size or output divergence. The procedures established for the measurement of absorption and fluorescence were used to obtain the results in the following chapter which characterizes the Nd:YVO₄ microchip material. The procedures outlined to characterize the microchip lasers were used in obtaining the results presented in chapter five, while the procedures for obtaining the necessary beam parameters and characterizing the microchip amplifiers were used in obtaining the results and modelling contained in chapter six.

Chapter 4 Characterization of the Nd:YVO₄ microchips

Introduction

4.1 Energy Levels of Nd:YVO₄

4.2 Absorption Measurements

4.2.1 Discussion

4.3 Fluorescence Measurements

4.3.1 Discussion

4.4 Nd:YVO₄ Microchip Quality

Conclusions

Chapter 4

Characterisation of the Nd:YVO₄ Microchips

Introduction

Absorption and fluorescence tests on a non-coated sample of Nd:YVO₄ were undertaken in order to study its properties, and to better understand its operation as a gain material for the microchip lasers and amplifiers tested. In section 4.1 a diagram of the energy levels of Nd:YVO₄ is reproduced. This diagram has been used as a reference to relate the absorption or fluorescence spectra with their corresponding transitions between energy levels. The absorption results outlined in section 4.2 were used to find the optimum pump wavelength, and to aid comparison of laser operation whilst pumping at different wavelengths. The fluorescence results outlined in section 4.3 were used to establish a measure of the gain bandwidth, and also to determine the Stark energy levels responsible for the laser transitions observed. Finally, the physical quality of the Nd:YVO₄ microchips used has been examined.

4.1 Energy Levels of Nd:YVO₄

A partial energy level diagram of neodymium doped into YVO₄ has been presented in Figure 4.1. The energy levels and corresponding Stark levels have been taken from Kaminskii (1990), and then plotted diagrammatically against an increasing energy scale. The spectroscopic notation for each level (the level identification), and the number of Stark levels within that energy level has been placed on the right hand side of the diagram. The energy levels shown were established at a temperature of 77 K, at this temperature the effect of broadening on the spectra is small, therefore identification of individual Stark levels is made easier. These energy levels, and the calculated wavelength differences between them, are compared in the following sections to the absorption and fluorescence measurements.

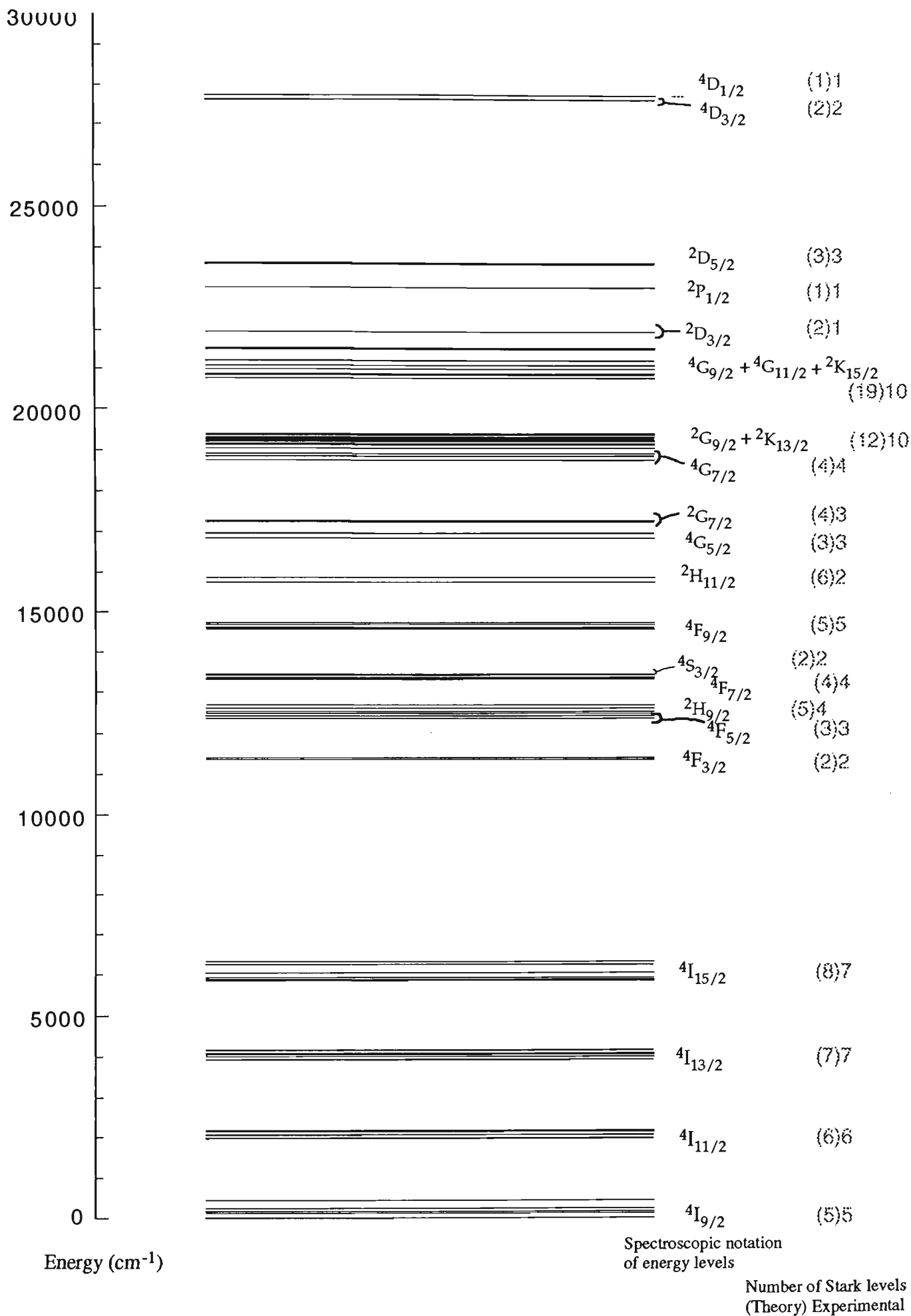


Figure 4.1: Nd:YVO₄ energy level diagram. The values of the energy levels are from Kaminskii (1990). To the right of the energy levels is their spectroscopic notation and the number of Stark-split levels within that particular level. In this case theory predicts $J+1/2$ Stark levels (J is the bottom right hand term of the spectroscopic notation), the experimental number is as found by Kaminskii.

4.2 Absorption Measurements

Absorption tests were carried out on the Nd:YVO₄ crystal to establish at what wavelengths, and to what extent, the energy levels would absorb pump energy and be best utilized in a laser system. The Absorption spectrum below (fig 4.2) was obtained with a white light source (producing unpolarized light) and an Optical Spectrum Analyzer (OSA). It shows the peak absorption regions of the material above 10000 cm⁻¹ (less than 1000 nm), i.e. the visible and near infrared regions that are the most likely candidates for use as pump bands. The spectrum was produced with an OSA resolution of 0.5 nm. Above 560 nm the sensitivity was set to fast with 10 times averaging, below 560 nm the sensitivity was slow with 5 times averaging. The setting were changed below 560 nm since the white light source drops in intensity at shorter wavelengths. The spectrum was produced with a non-coated Nd:YVO₄ sample of length 0.5 mm.

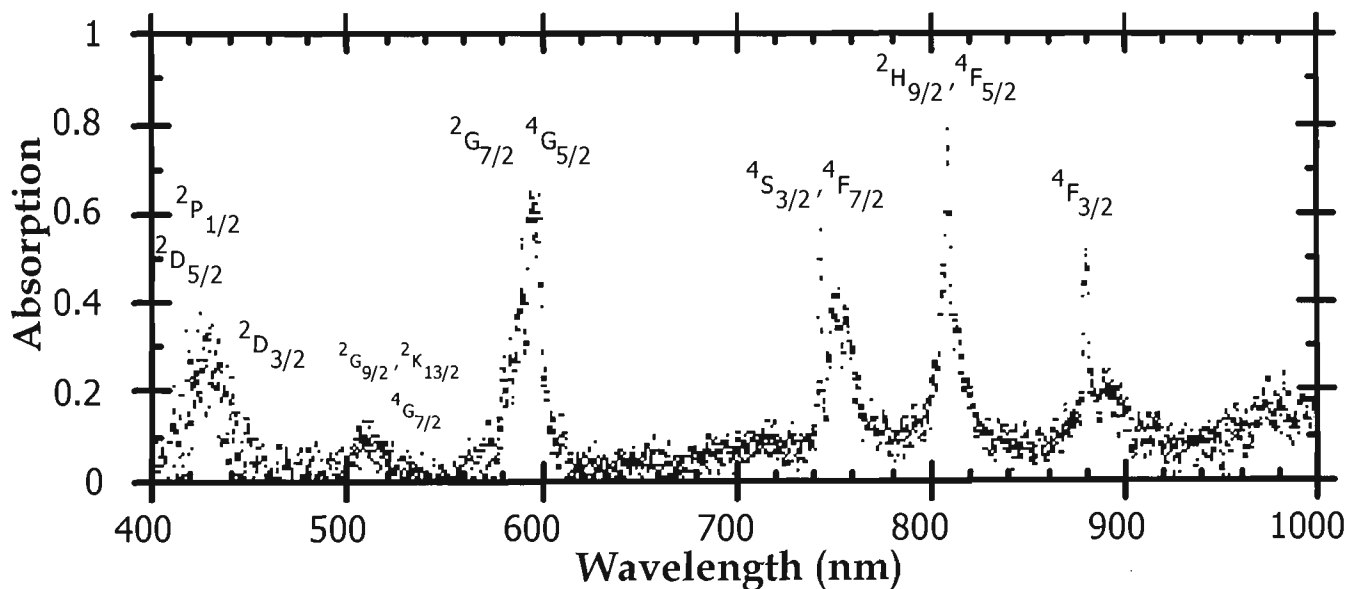


Figure 4.2: Nd:YVO₄ Absorption Spectrum for randomly polarized light. Obtained from a 0.5 mm long non-coated Nd:YVO₄ sample. The energy levels shown are at a wavelength corresponding to absorption from the ground ($4I_{9/2}$) level.

The absorption peaks in figure 4.2 directly correspond to the excited state energy levels since it can be reasonably assumed that the initial electron population was overwhelmingly in

the $^4I_{9/2}$ ground level. This correspondence may be simply determined given the difference in energy levels from the energy level diagram, figure 4.1.

Neodymium based materials generally show high absorption in the region around 800 nm; the material Nd:YVO₄ is no exception. High absorption in this region is very convenient because of the large selection of commercially available laser diodes with spectral output around this wavelength, which may therefore be used as pump sources. The absorption spectrum of figure 4.2 also shows that the Nd:YVO₄ material can be pumped in several other regions. The Ti:sapphire laser, with a spectral output range of 700 to 1000 nm, may be used to pump several of the peak absorption regions shown.

Absorption in the region 730 to 830 nm was investigated in greater detail as these wavelengths are easily pumped by the Ti:sapphire laser. Absorption spectra of the region 730 to 830 nm were recorded for different incident polarizations because of the uniaxial nature of the Nd:YVO₄ crystal. The resultant spectra are shown in figure 4.3. They were recorded with a resolution of 1 nm, the sensitivity of the OSA was set to slow, with 10 times averaging.

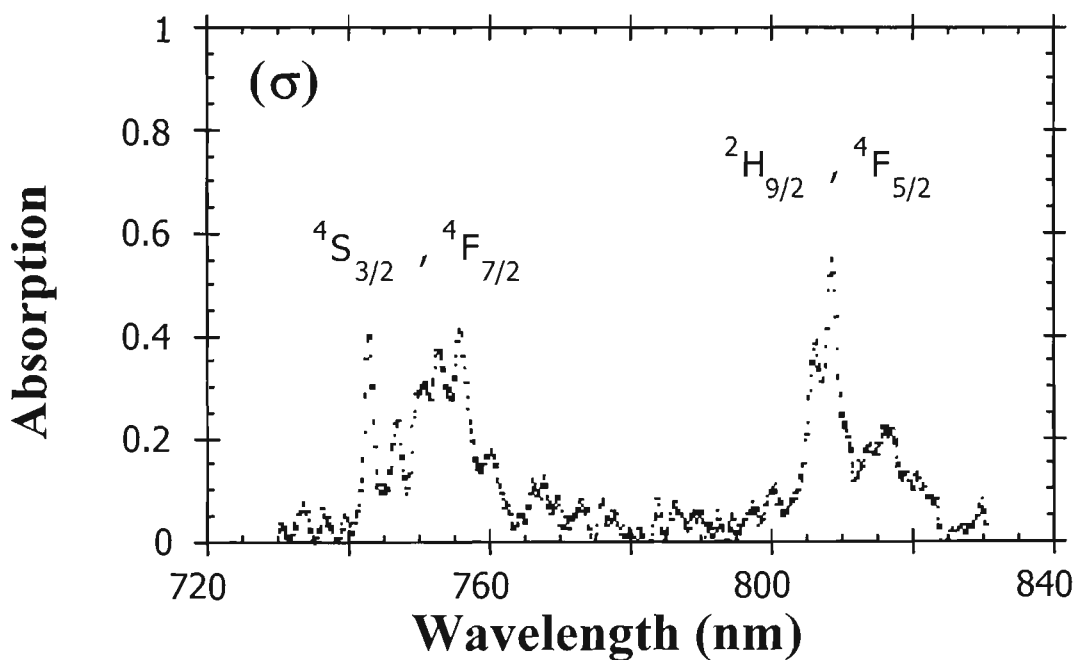
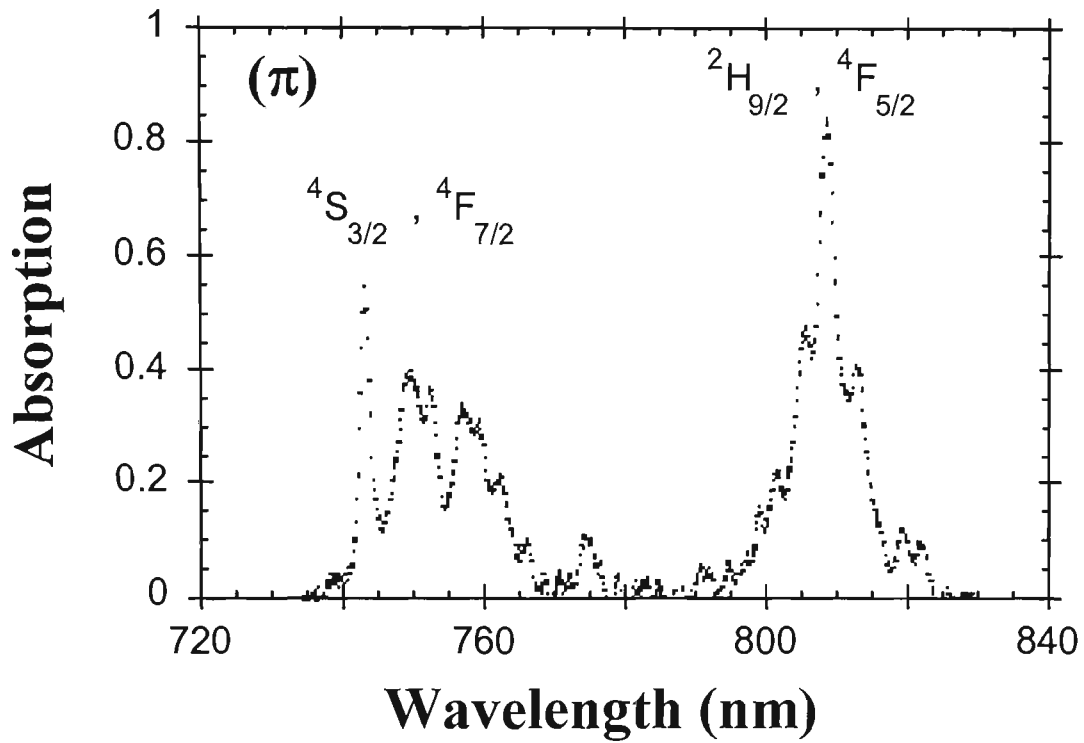


Figure 4.3: Absolute absorption through a 0.5 mm long non-coated Nd:YVO₄ microchip with 1 atm% doping (corrected for surface reflections). Shown is absorption in the $^4S_{3/2};^4F_{7/2}$ and $^2H_{9/2};^4F_{5/2}$ bands, for incident light parallel (π) and perpendicular (σ) to the c axis.

The transitions associated with these regions of absorption are from the ground level ($^4I_{9/2}$) to the $^4S_{3/2};^4F_{7/2}$ (≈ 750 nm) and $^2H_{9/2};^4F_{5/2}$ (≈ 810 nm) bands. As can be seen from these absorption graphs the maximum absorption is between 800 and 820 nm, particularly for

incident light which is π polarized. The graphs presented in figure 4.4 show these regions in greater detail, in which the data was recorded with an OSA resolution of 0.5 nm, sensitivity set to slow and 10 times averaging. The graphs show structure associated with absorption from, and to, Stark split levels within the energy bands involved, i.e. the ground level (${}^4I_{9/2}$) and the upper band ${}^2H_{9/2}; {}^4F_{5/2}$.

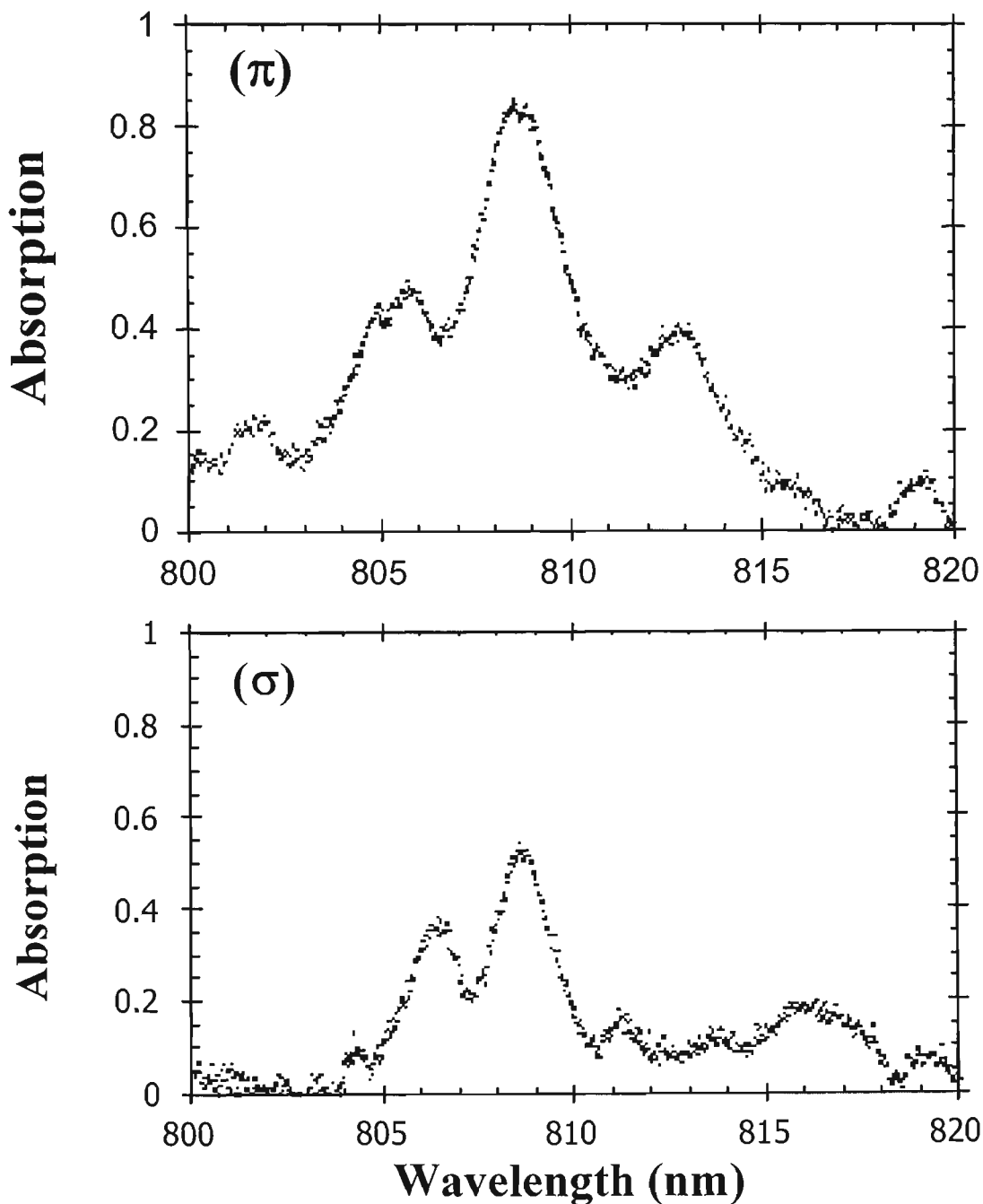


Figure 4.4: Absolute absorption through a 0.5 mm long non-coated Nd:YVO₄ microchip with 1 atm% doping. Shown is the absorption in the high absorption ${}^2H_{9/2}; {}^4F_{5/2}$ bands, for parallel (π) and perpendicular (σ) polarized incident light.

The regions of high absorption shown on the graphs were measured with signals which were close to the noise floor of the OSA; since the Nd:YVO₄ absorbed the majority of the white light signal at these wavelengths. Thus a 'through power' technique with the Ti:sapphire and a power meter taking measurements every 0.05 to 0.1 nm was adopted to better examine the absorption in this region. (Note: the bandwidth of the Ti:sapphire was <40 GHz or <0.08 nm at a wavelength of 800nm). Pump saturation with the higher power Ti:sapphire was not evident in these measurements, as no decrease in the absorption ratio expected from pump saturation was observed. From the measurements of power before and after the microchip, along with a correction for microchip surface reflections, figure 4.5 was generated, showing the highest absorption region for each polarization of incident light.

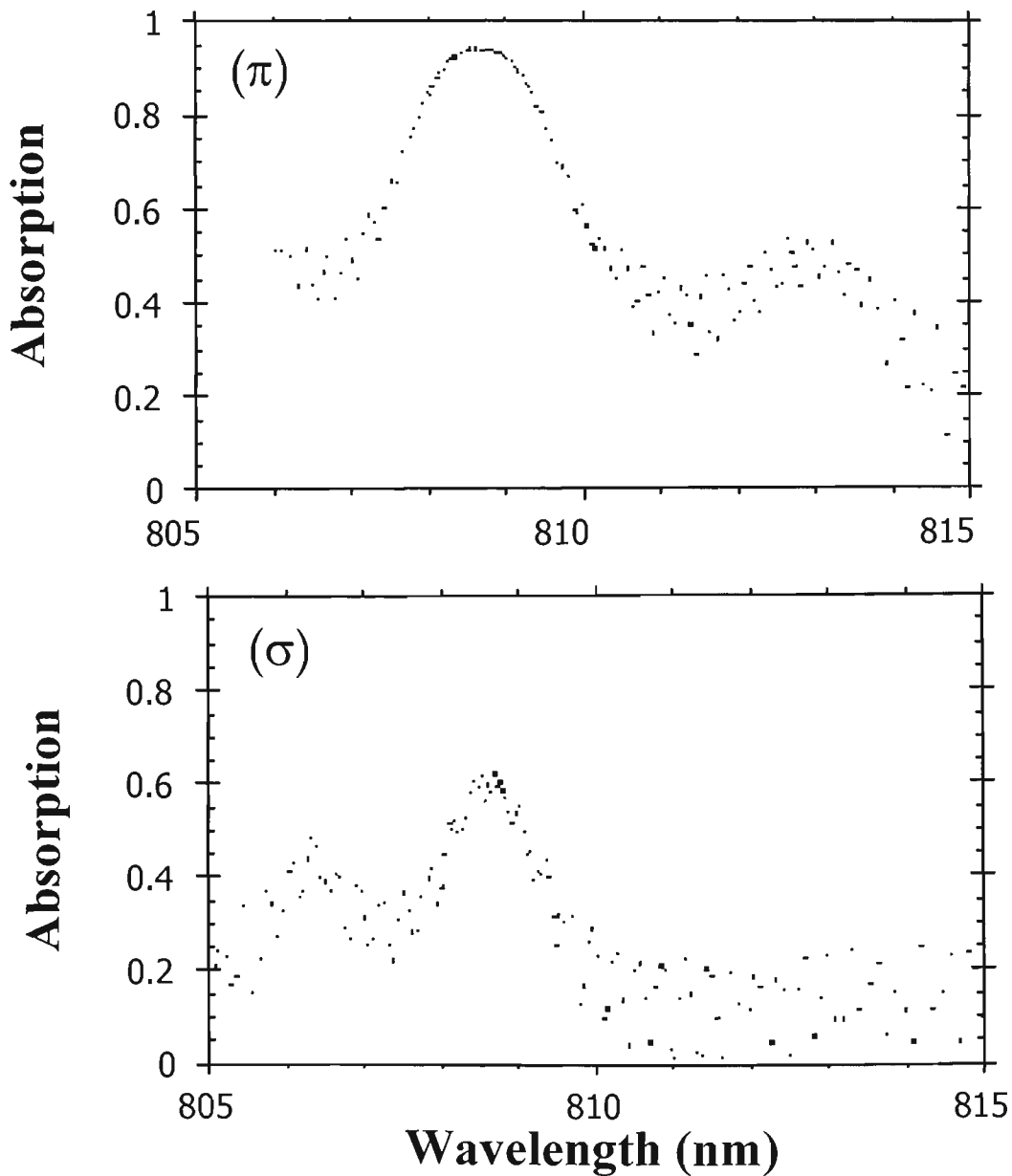


Figure 4.5: Absolute absorption through a 0.5 mm long non-coated Nd:YVO₄ microchip with 1 atm% doping. Shown is the absorption in the ²H_{9/2}:⁴F_{5/2} bands using a ‘through power’ technique, for parallel (π) and perpendicular (σ) polarized incident light.

Π polarized incident light was shown to be absorbed at much higher levels than the σ polarized light, with the maximum absorption close to 95% of the incident light. Table 4.1 outlines the percentage absorption figures in the highest absorption region.

Incident Pump Polarization	Absorption
π polarization	max absorption of $\approx 94.5\%$ $> 90\%$ between 808.20 and 809.10 nm $> 80\%$ between 807.89 and 809.44 nm
σ polarization	max absorption of $\approx 62.3\%$ $> 55\%$ between 808.37 and 808.82 nm $> 45\%$ between 808.03 and 809.13 nm

Table 4.1: Percentage absorption outlined in high absorption region for 0.5 mm length of Nd:YVO₄ with 1 atm% doping.

4.2.1 Absorption Discussion

As was outlined in the Nd:YVO₄ review in chapter 1, many researchers have compared Nd:YVO₄ to the laser industry standard Nd:YAG and found it to have superior absorption properties, in that it has broader and stronger absorption. With the absorption regions for pumping typically broader than Nd:YAG, more flexibility in choice of laser diode pump source is offered, and increased absorption of a broad laser diode pumping source is possible. By utilizing these absorption properties a more efficient laser system can be produced, potentially leading to higher output powers and/or savings in component and running costs.

The Nd:YVO₄ microchip shows several regions of absorption through the visible and near infrared region of the spectrum, as was shown in figure 4.2. These regions are centred near 425, 505, 595, 810 and 890 nm. Having demonstrated relatively high levels of absorption in the regions 400-450 nm, 575-600 nm and from 740 through to 900 nm, the material would appear to be a very good candidate for broadband pumping with a flash lamp or arc lamp, such as Nd:YAG has proved to be. However Nd:YVO₄ has quite poor thermal conductivity, and since broadband pumping generates a lot of unused energy which creates heating, Nd:YVO₄ has proved to be less effective with this type of pump source [Higgins (1993)]. Alternatively, an argon-ion laser with output wavelengths between 454 and 514 nm can be used as a pump source in the small absorption peak just beyond 500 nm. However, the absorption is not very strong, and the quantum efficiency is relatively low (c.f. 800 nm pump), proving a very inefficient process.

A Nd:YVO₄ laser becomes a much more attractive alternative with direct pumping of the absorption regions using a relatively narrow bandwidth pump source, in which considerably less heat is introduced into the laser material. Direct pumping of solid-state laser materials has become more viable with the advent of laser diodes and the increased availability, and price reduction, of higher power laser diodes. The match of the availability of laser diodes at wavelengths around 800 nm, with the strong absorption in neodymium materials at these wavelengths, has encouraged the production of more efficient and practical lasing systems based on laser diode pumping. While a Ti:sapphire laser was used in this research to provide the flexibility to pump the Nd:YVO₄ laser over a wide range of wavelengths and to investigate the absorption in closer detail across 730 to 830 nm, once the wavelength of the maximum absorption is established an appropriate laser diode could be selected to perform the pumping task, and produce a more practical sized laser system.

Absorption tests performed with both π and σ incident polarized light showed that in general the π polarized light had a higher absorption level. The absorption spectra showed structure associated with the absorption from, and to, Stark levels within each energy level. For the 0.5 mm length of Nd:YVO₄ sample tested, within the 750 nm absorption band, the π

polarized incident light had a greatest absorption of approximately 56% at 742.9 nm, and the σ polarized light a greatest absorption of approximately 41% at 755.3 nm. These percentage absorption figures correspond to absorption co-efficients of 16.3 cm^{-1} and 10.7 cm^{-1} respectively.

The initial tests between 730 and 830 nm showed the ${}^2\text{H}_{9/2}:$ ${}^4\text{F}_{5/2}$ bands (around 810 nm) to have the highest levels of absorption, correspondingly more detailed tests were conducted in this region. The “power through” absorption measurements revealed very high absorption in the 808 to 809 nm region for π polarization (80 to 90 % for a 0.5 mm length). The best absorption was measured to be 94.6% for π polarized incident light at 808.51 nm, and 62.3% for σ polarized light at 808.68 nm. These correspond to absorption co-efficients of 58.19 cm^{-1} and 19.49 cm^{-1} respectively.

Table 4.2, gives peak absorption co-efficient values from literature for Nd:YVO₄, and some Nd:YAG results for comparison. The peak absorption co-efficients measured for this work appear larger than those published with similar neodymium doping concentrations. The results of both DeShazer (1994) and Dallas (1994) for Nd:YVO₄, however, give no indication of the pump polarization, and may well be for unpolarized light, thus reducing the figure from that of π polarization pump alone. The values from this work were produced with the narrow bandwidth of the Ti:sapphire laser and in general will allow the Nd:YVO₄ to be pumped in a narrower portion of the absorption spectrum than any laser diode pump, as was the case with Robrish (1994). The results for Nd:YVO₄ with 3 at% Nd doping show the increased absorption with an increase in neodymium concentration, this must be considered against a reduction in the fluorescence lifetime, which results from the increased neodymium concentration.

Author	Material / Absorption co-efficient (cm^{-1})		Nd doping conc. (at%)
	Nd:YVO ₄	Nd:YAG	
This work	58 (π), 19.5 (σ)		1±0.1%
DeShazer (1994)	40.7	8	1%
Dallas (1994)	31	4.8	1.1%
Robrish (1994)	≈50 (π)		1.5%
Kintz & Baer (1990)	111(π), ≈30(σ)		3%
Bernard et.al.(1993)	≈75(π), ≈30(σ)		3%

Table 4.2: Peak absorption co-efficient, α , for neodymium doped host, taken from the data of various authors.

The results in table 4.2 show that comparatively the magnitudes of the peak absorption of the material Nd:YVO₄ are substantially higher than Nd:YAG. Both materials are accessible by conventional laser diodes for pumping, with the wavelength of the peak absorption for both materials at around 808 nm. These high absorption figures show why Nd:YVO₄ is an excellent material for compact laser systems, since such a large amount of input light can be absorbed in a small length of material. In addition, the peak absorption found within the 750 nm absorption band of Nd:YVO₄ is also stronger than in Nd:YAG at the 800 nm band, giving the added benefit of pump flexibility, if required.

Not only does Nd:YVO₄ have strong absorption peaks, but it also has rather wide absorption regions, in comparison to other Nd laser materials. DeShazer (1994) uses a comparative unit of (FW75%), to compare various Nd doped materials, this corresponds to a wavelength range over which at least 75 % of the pump light is absorbed in a 5 mm path length through the crystal. A value of 2.5 nm is quoted for Nd:YAG and 15.7 nm for Nd:YVO₄, both having a 1 at% Nd doping concentration. An absorption of 75% in a 5 mm length corresponds to approximately 13% absorption through a 0.5 mm length, therefore the data from figure 4.4 shows a (FW75%) bandwidth of 14 nm for π polarization pumping and a bandwidth of 4.8 nm

for σ polarization pumping. To illustrate the usefulness of Nd:YVO₄ in microchip form, it was found that over a region of approximately 1.8 nm, greater than 75% of π polarized pump light could be absorbed in the 0.5 mm length of microchip used in the present work.

4.3 Fluorescence Measurements

Fluorescence from the sample was measured while pumping the non-coated Nd:YVO₄ sample within the very high absorption region at 808.8 nm. The fluorescence generated is at lower energies (higher wavelengths) than the pump energy. The following fluorescence spectrum was composed of 7 traces, each covering a wavelength range of 100 nm, and was observed on the OSA with a resolution of 1 nm (Figure 4.6). A filter was placed in the system to block most of the unabsorbed pumping power. Consequently, the filter has also reduced some of the fluorescence in the region 870 to 880 nm, which can be seen in the more detailed fluorescence spectrum of that region (Figure 4.7). The pump power remaining after the filter may be observed as a sharp peak just below 810 nm in the spectrum.

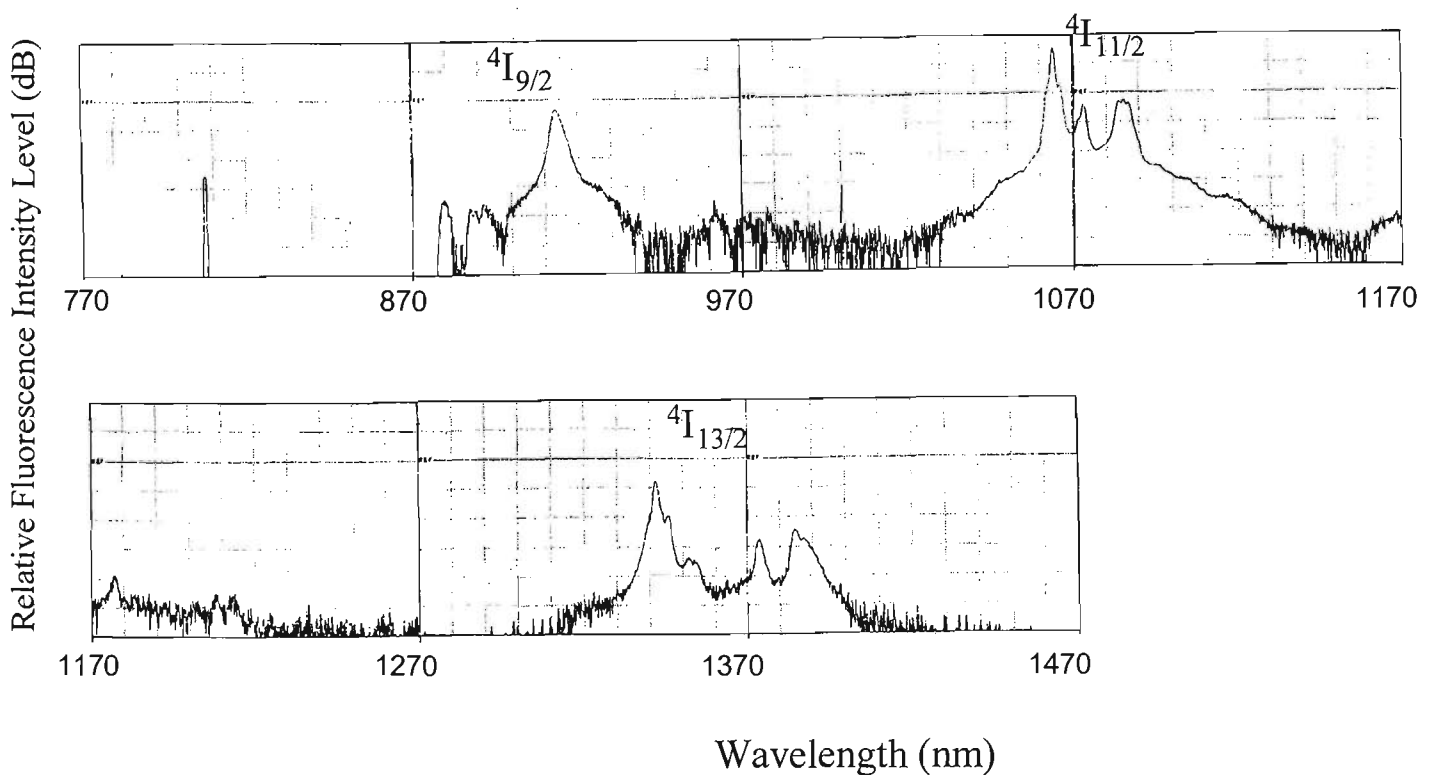


Figure 4.6: Nd:YVO₄ fluorescence produced with constant pump power from a Ti:sapphire laser at 808.8 nm.

Above each fluorescence region in figure 4.6 is noted the lower level of the transition (from the $^4F_{3/2}$ metastable level) which produced the observed fluorescence. A more detailed look was taken at each of the fluorescence regions to better identify the contained peaks. The peak structure is associated with individual Stark sub-level transitions between the two levels responsible for the fluorescence. The first region from 860 to 930 nm is shown in figure 4.7, and was observed on the OSA with a resolution of 0.5 nm and sensitivity set to fast, with 5 times averaging.

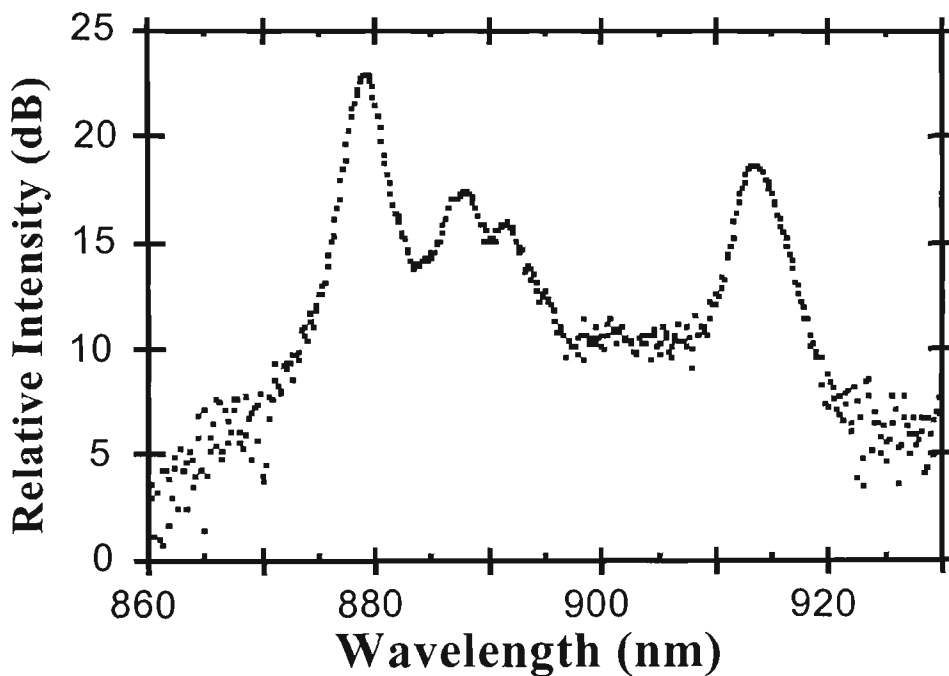


Figure 4.7: Fluorescence associated with the $^4F_{3/2}$ to $^4I_{9/2}$ transition.

The spectrum in figure 4.7 shows fluorescence resulting from transitions from the metastable $^4F_{3/2}$ level to the ground level $^4I_{9/2}$. Below is a simplified energy level diagram showing the possible Stark transitions involved (Figure 4.8). To the right of this, table 4.3 gives the calculated wavelength of each of these transitions, as given by the difference in the Stark energy levels of Kaminskii (1990). It can be seen by careful comparison with figure 4.7 that the transitions from the $^4F_{3/2}$ level to the lowest stark level (denoted 'a') in $^4I_{9/2}$ are dominant.

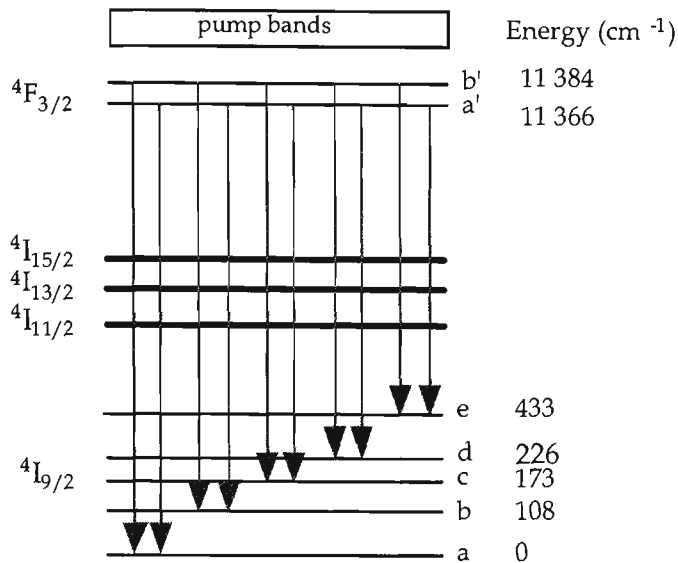


Figure 4.8: Transitions from ${}^4F_{3/2}$ to ${}^4I_{9/2}$.

Transition	Energy Difference (cm ⁻¹)	Wave-length (nm)
b' → a	11 384	878.4
a' → a	11 366	879.8
b' → b	11 276	886.8
a' → b	11 258	888.3
b' → c	11 211	892.0
a' → c	11 193	893.4
b' → d	11 158	896.2
a' → d	11 140	897.7
b' → e	10 951	913.2
a' → e	10 933	914.7

Table 4.3: Energy and wavelength of transitions.

The next fluorescence region (figure 4.9) contains the strongest fluorescence intensity peak, and consequently the most common lasing wavelength in neodymium doped materials. The fluorescence found at wavelengths from 1050 to 1100 nm corresponds to transitions from the ${}^4F_{3/2}$ metastable level down to the ${}^4I_{11/2}$ level. Again the fluorescence was measured with an OSA resolution of 0.5 nm, sensitivity on fast and 5 times averaging. Figure 4.10 is a simplified energy level diagram showing the possible Stark transitions involved. The wavelength of each of these transitions is given in table 4.4. Transitions to the lower Stark levels of ${}^4I_{11/2}$ may be identified as dominant, as is discussed in more detail in the following section of this thesis.

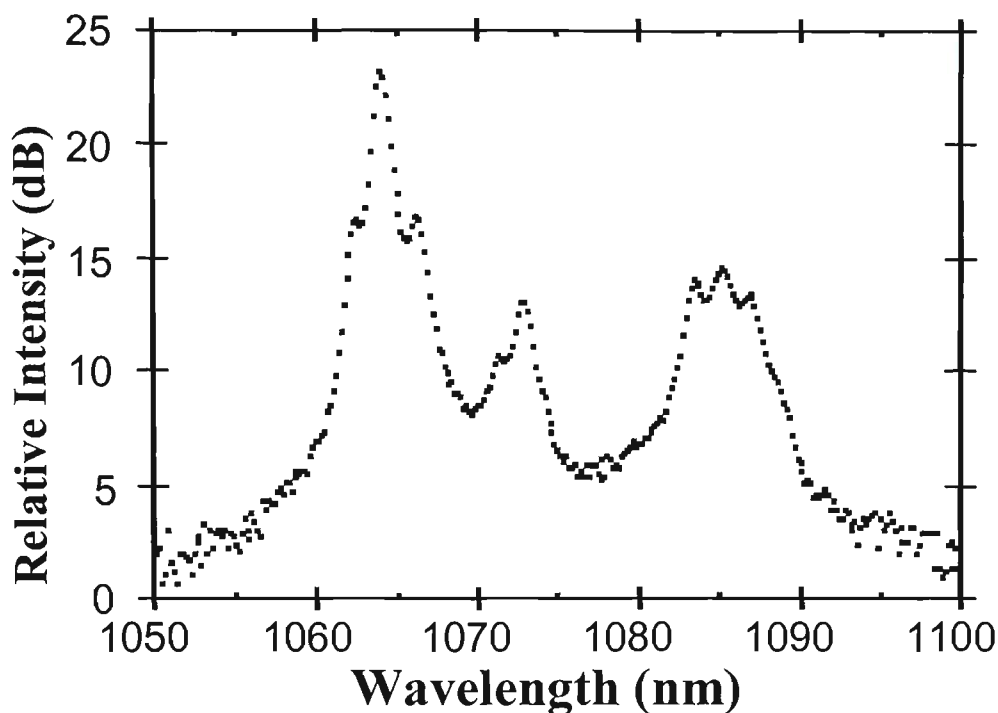
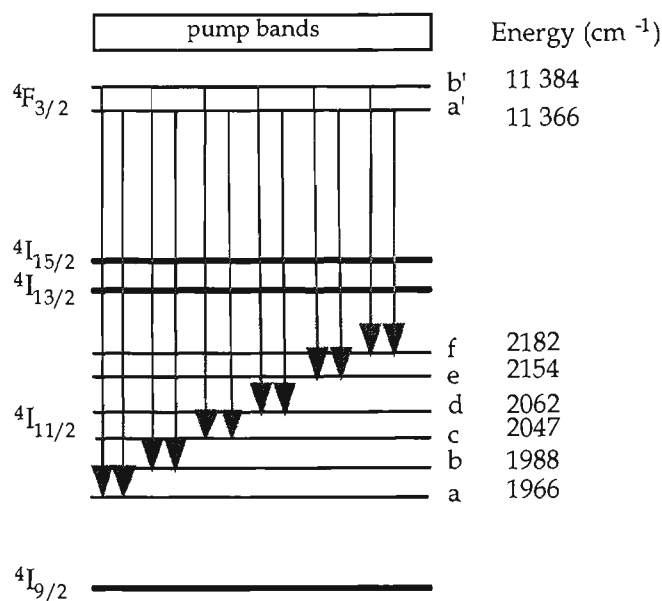


Figure 4.9: Fluorescence associated with the ${}^4F_{3/2}$ to ${}^4I_{11/2}$ transition.



Transition	Energy Difference (cm ⁻¹)	Wave-length (nm)
b' → a	9418	1061.8
a' → a	9400	1063.8
b' → b	9396	1064.3
a' → b	9378	1066.3
b' → c	9337	1071.0
a' → c	9319	1073.1
b' → d	9332	1072.7
a' → d	9304	1074.8
b' → e	9230	1083.4
a' → e	9212	1085.5
b' → f	9202	1086.7
a' → f	9184	1088.9

Table 4.4: Energy and wavelength of transitions.

Figure 4.10: Transitions from ${}^4F_{3/2}$ to ${}^4I_{11/2}$.

Lastly, the fluorescence in the region 1330 to 1410 nm was observed. Due to the output in this region being 5 to 10 dB lower in intensity than near 1060 nm (ie. a weaker or less probable transition) the OSA sensitivity was set to slow, again with 5 times averaging and 0.5 nm resolution. The fluorescence corresponds to transitions from the metastable ${}^4F_{3/2}$ level

to the ${}^4I_{13/2}$ level, these being the levels responsible for the 1.34 μm laser action. Figure 4.12 shows a simplified energy level diagram to demonstrate the possible Stark transitions between the two levels, and table 4.5 shows the wavelength of these transitions, which can be related back to the fluorescence spectrum. Again the dominant transitions are those down to the lower Stark levels.

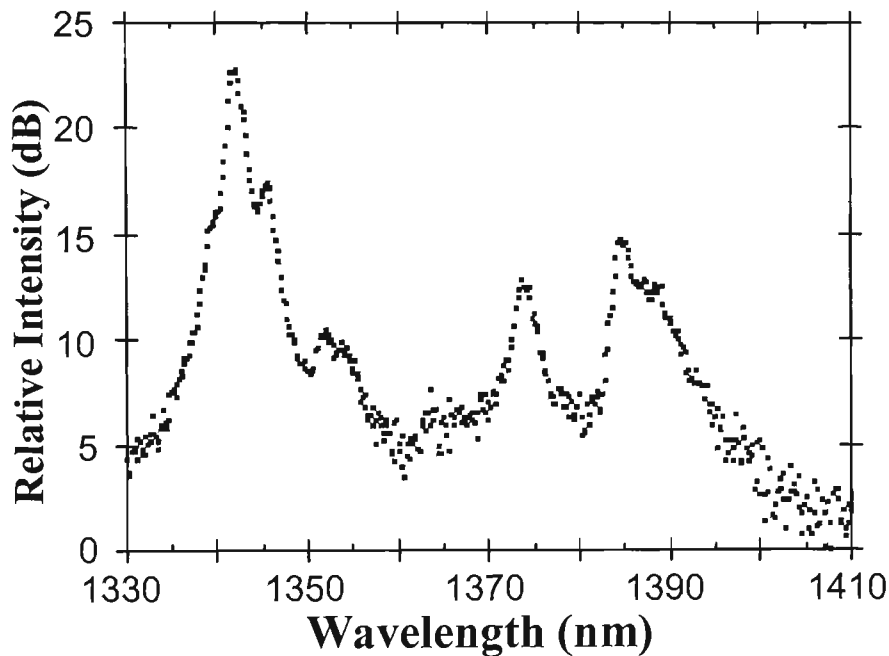


Figure 4.11: Fluorescence associated with the ${}^4F_{3/2}$ to ${}^4I_{13/2}$ transition.

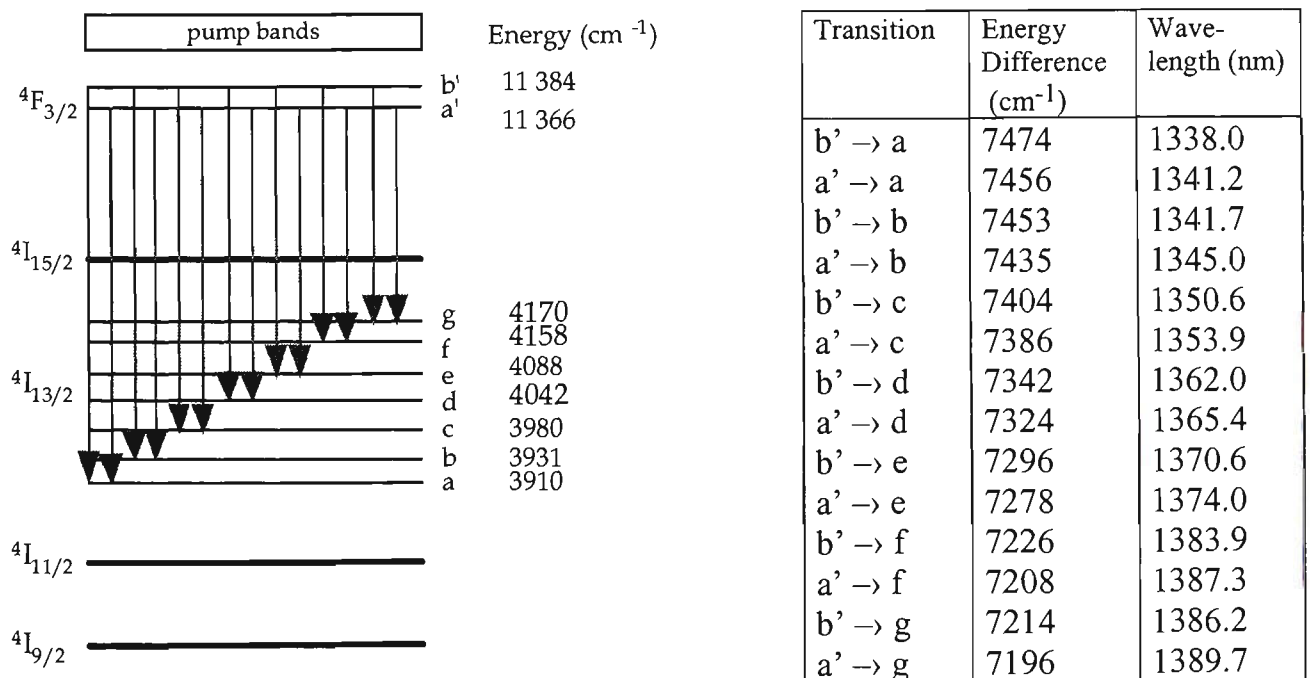


Figure 4.12: Transitions from ${}^4F_{3/2}$ to ${}^4I_{13/2}$.

Table 4.5: Energy and wavelength of transitions.

4.3.1 Fluorescence Discussion

From the fluorescence diagram, figure 4.6, the energy levels positioned below the ${}^4F_{3/2}$ metastable level (see figure 4.1) can be identified. Each group of peaks corresponds to a transition from the ${}^4F_{3/2}$ level down to a particular level, with the peaks within each group corresponding to a particular transition between a Stark level of the metastable level and a Stark level of the particular lower level. The figure shows fluorescence down to the ${}^4I_{13/2}$, ${}^4I_{11/2}$ and ${}^4I_{9/2}$ levels, but not to the ${}^4I_{15/2}$ level, which would be positioned slightly beyond 1500 nm. This particular transition falls outside the scope of the present study.

Closer investigation of the fluorescence allows the identification of each peak corresponding to a transition from, and to, individual Stark levels. Not all the Stark transitions were resolved at room temperature since the peaks were relatively broad and their close spacing made them difficult to individually identify. The fluorescence tests would need to be performed at lower temperatures, where thermal broadening is minimized, to better resolve each individual Stark transition, as has been done to obtain the energy level values found in Kaminskii (1990), which have been used here as a comparison to identify the levels. The energy levels, and therefore calculated wavelengths of the transitions, taken from Kaminskii were established at 77K, however the relative positions of the Stark levels should remain unchanged for the room temperature measurement performed here.

Analyzing the relative intensity level of the peaks of the observed fluorescence can enable a prediction of which peaks are most likely to reach threshold first within a laser system. (Note also, that within a laser system the mirrors may need to discriminate against other transitions having high fluorescence output). It may be determined which levels and sub-levels (Stark levels) are associated with any lasing by comparing the major peak back to the energy level diagram, or calculated wavelength table (eg. tables 4.4 or 4.5).

The first region investigated in more detail in figure 4.7 was around 860 to 930 nm, and corresponds to fluorescence down to the ground level (${}^4I_{9/2}$). A laser developed to operate on this transition would correspond to a three level laser system, or possibly a quasi-four level laser system if the upper Stark levels of the ground level (${}^4I_{9/2}$) were unpopulated and the laser

operated on a transition down to these upper Stark levels. Lasers working on this ${}^4F_{3/2} - {}^4I_{9/2}$ transition have been previously developed, but were not investigated here given our limited availability of microchip samples. Therefore, of more interest are the regions 1050 to 1100 nm (figure 4.9) and 1330 to 1410 nm (figure 4.11), which are known to correspond to the most likely lasing transitions in neodymium doped materials. The region near 1.06 μm , which has the highest fluorescence intensity, is shown in figure 4.13. By overlaying lines corresponding to the wavelengths in table 4.4, equal to the energy difference in the Stark transitions shown in figure 4.10, we can infer which transitions are responsible for particular peaks.

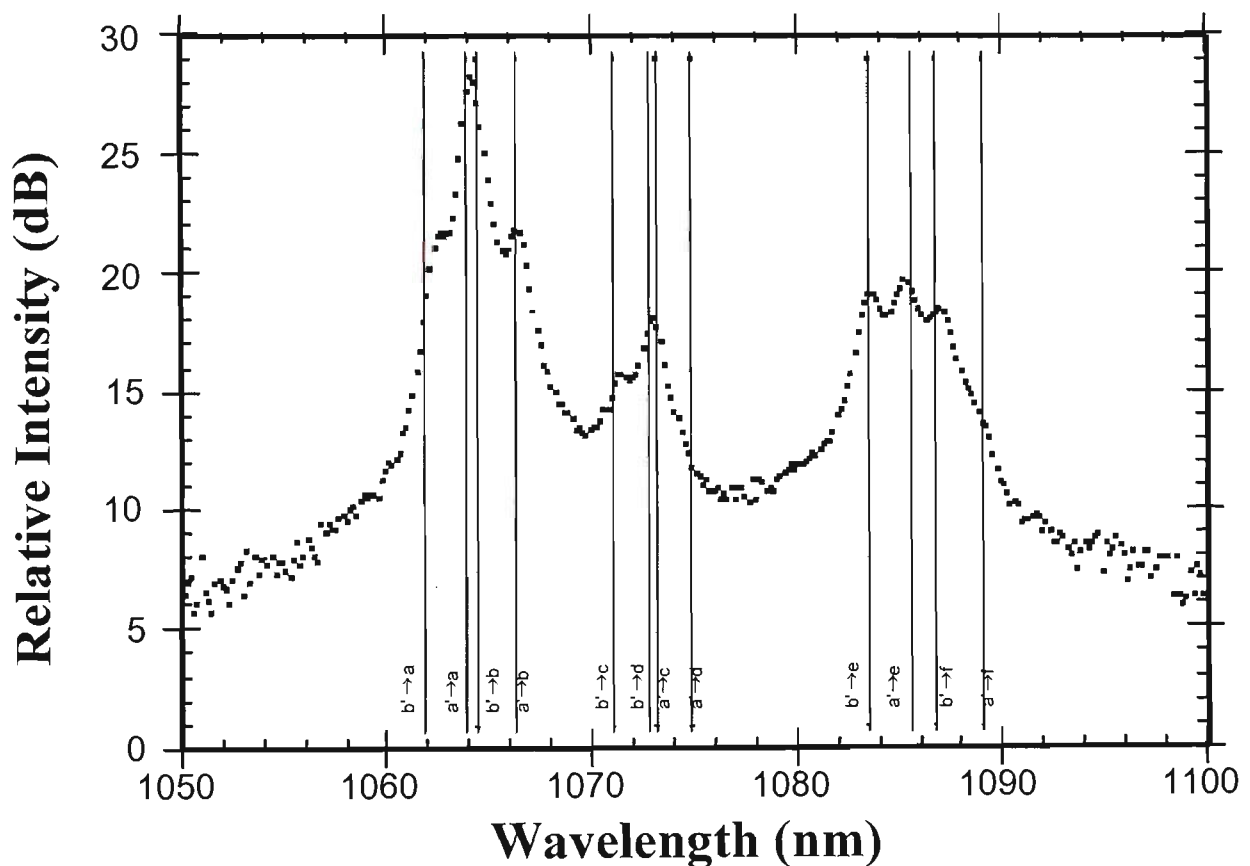


Figure 4.13: Fluorescence around the 1.06 μm transition, also shown are theoretical Stark transition wavelengths (vertical lines) transferred from table 4.4.

Similarly figure 4.14 considers the region around the 1.34 μm transition, and by taking the information from figures 4.11 and 4.12, and table 4.5, the wavelengths of each Stark transition have been overlayed onto the fluorescence spectrum.

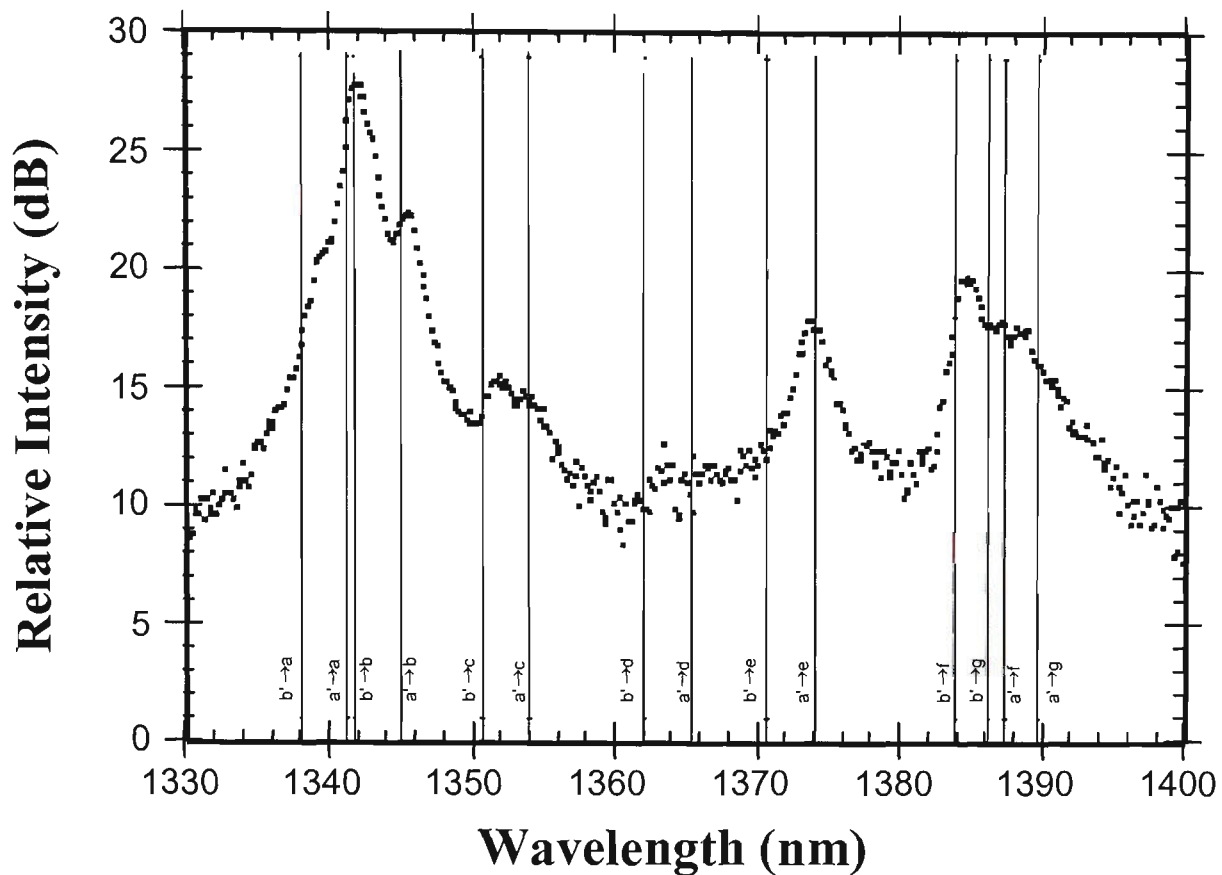


Figure 4.14: Fluorescence around the 1.34 μm transition, also shown are theoretical Stark transition wavelengths (vertical lines) transferred from table 4.5.

In both cases, there is a reasonable comparison between the measured fluorescence peaks and the wavelength of the Stark transitions as calculated from the energy levels given by Kaminskii, though some peaks are shifted in wavelength slightly, and others are not visible. In general it appears that the calculated wavelength of the Stark transition for the 1.34 μm fluorescence region are systematically about 0.5 nm less than that observed here. These differences may well be accounted for by the difference in measurement temperatures, or differences in the actual composition, or quality, of the Nd:YVO₄ material measured.

The major peak in each spectrum (which is likely to be responsible for the dominant laser transition) correspond to the Stark transitions a'-a and b'-b. In a paper by Yaney and DeShazer (1976) the a'-a transition was shown to swamp the much weaker b'-b transition, and thus the transition between the two lowest Stark levels of each level is believed to be responsible for laser action. Note: Other transitions may also produce lasing if the pumping

power is sufficiently high, as was demonstrated by the lasing on the second transition in the 1.34 μm microchip laser tests (see section 5.2.1).

The bandwidth of relevant fluorescence transitions has also to be considered since a primary interest of this work is single-longitudinal mode lasing. The bandwidth, together with the longitudinal mode spacing governed by the microchip thickness, will effect the number of modes within the fluorescence peak. The fluorescence peak which reaches beyond threshold in the laser system may also be referred to as the gain region or profile. An estimation of the gain bandwidth can be made by measuring the FWHM of the peak fluorescence. The fluorescence FWHM at 1.06 μm was between 0.86 and 0.93 nm when measured with an incident pump power between 40 and 200 mW (using the OSA with 0.1 nm resolution). An example of the measured fluorescence around the 1.06 μm transition is shown in figure 4.15. These bandwidth results compare favourably with the value of 0.96 nm from Taira *et al.*(1991), 0.95 nm from Kintz & Baer(1990), and ≈ 0.8 nm from O'Connor(1966). The measured fluorescence FWHM at 1.34 μm was 1.6 nm, again measured with an OSA resolution of 0.1 nm (see figure 5.13).

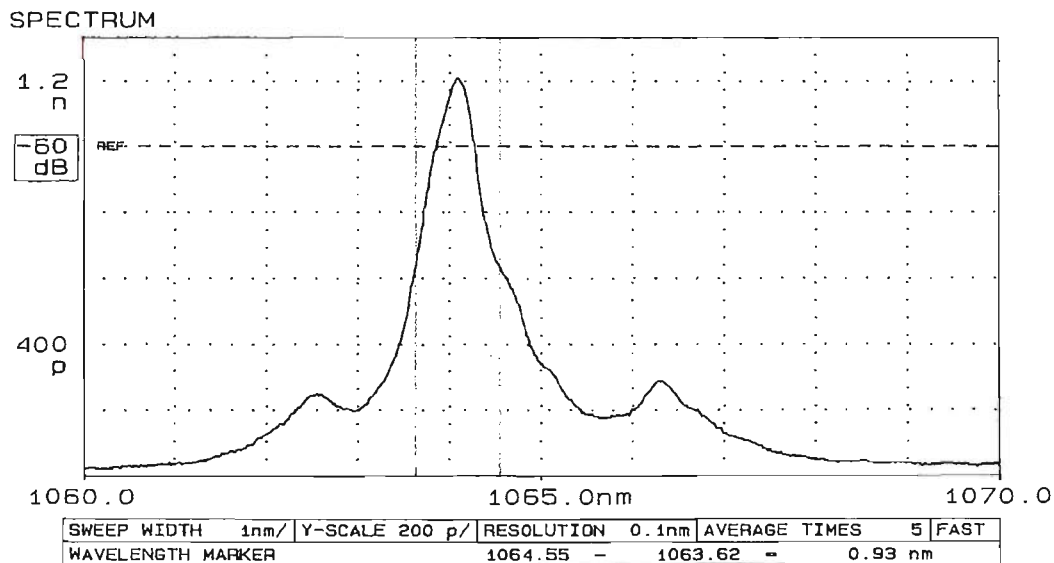


Figure 4.15: A optical spectrum analyzer trace of the Nd:YVO₄ fluorescence spectrum around the main peak of the 1.06 μm transition, showing a measure of the FWHM (0.93 nm). (Taken with an incident pump power of ≈ 200 mW on a non-coated, 1 at% doped, Nd:YVO₄ microchip).

4.4 Nd:YVO₄ Microchip Quality

Greatly varied results were observed when pumping different locations on the microchips. Thus, with both lasers and amplifiers, it was necessary to traverse the microchip in the incident beam so as to maximize the laser output or amplifier gain. Recently other authors of Nd:YVO₄ literature have also commented on this. Mermilliod et.al. (1992) states, "... it is worth noting the inhomogeneity of the samples since their output power and their laser efficiency can vary much from one boule to another and even inside the laser sample itself. 30 to 50% variations have been noted in the output power of certain samples." They also refers to "the poor quality of our YVO₄ crystal", and it is noted that the Nd:YVO₄ crystal used in this work came from the same source at probably about the same time, NEC Japan.

In a Laser Focus World article in February 1994, DeShazer (1994), reporting on the work of Fincher and Fields states, "In the past, orthovanadate crystal exhibited variations as large as 50%. Fields states that finding the "sweet spot [for efficient lasing] appears to be no problem" for his crystal." Further in the article it is noted that great improvements in quality of Nd:YVO₄ has occurred in the past few years. Given that Nd:YVO₄ is now commercially available, it is expected that currently available crystals have improved over those used in the present work (1992) to the extent that they would not exhibit the large variations demonstrated by our samples.

Visual Inspection

All the microchips used were initially inspected under a microscope to determine their orientation and mounting direction. Most of them had been marked in some small way so as to be able to determine the crystal c-axis, and the input and output ends of the coated laser microchips. At this time it was possible to see that the coatings, and to a smaller extent the physical microchips themselves, were cracked and rough. This was especially visible around the edges of the microchips. Whether the quality of the Nd:YVO₄ crystal itself was poor, was difficult to determine.

Following completion of experiments using the microchips, several were photographed under a microscope in order to show their visible quality. The first of series of photographs (figure 4.16) is of the non-coated Nd:YVO₄ crystal sample. The actual size of the sample was 3 x 1.5 mm, and 0.5 mm thick. The photographs of the crystal show slight edge damage probably attributed to the cutting process and quite possibly mounting. Many marks appear on the surface of the crystal, some of which are dirt or dust, others are dents or damage. There also appears to be internal darkened marks, but this is difficult to define. Each of the observed marks is small in comparison to the overall size of the microchip.



Figure 4.16: Photographs of the non-coated Nd:YVO₄ microchip through a microscope.

The second set of photographs is of the microchip coated for 1.06 μm lasing (Figure 4.17). The microchip is 3 x 3 mm in size and 0.5 mm thick, and has been placed in an aluminium holder with a circular access aperture slightly less than 3 mm in diameter. The two photographs are focussed approximately on opposite faces of the microchip. Again the picture shows many marks over the microchip surface, some which appear to be dirt, some which appear to be damage.

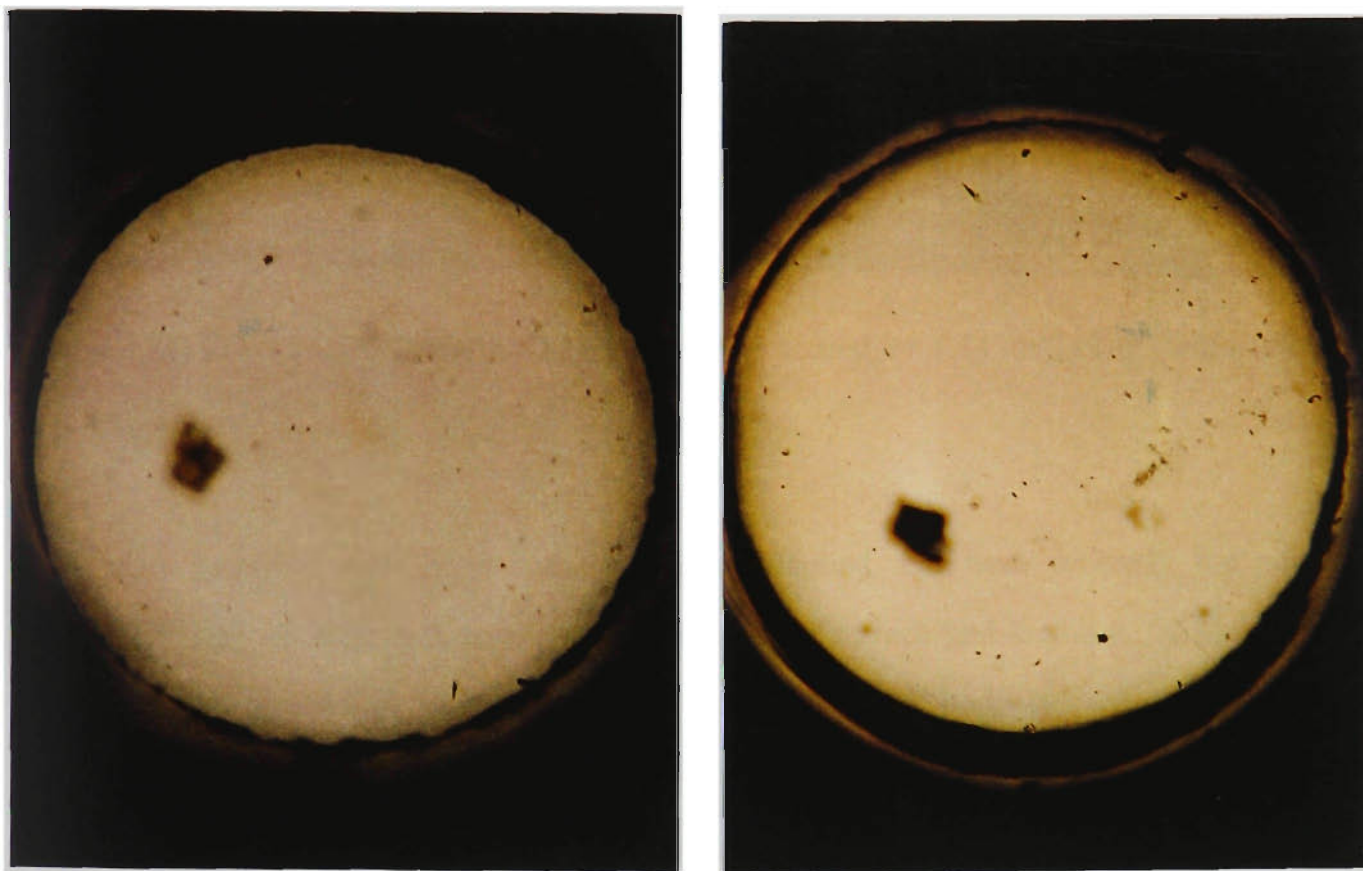


Figure 4.17: Photographs of the Nd:YVO₄ microchip coated for 1.06 μm lasing, contained within an aluminium holder.

The final photographs are of the microchip laser coated for 1.34 μm lasing (Figure 4.18). This microchip is 1 x 1 mm and 0.5 mm thick, and is also held within an aluminium holder. Again these photographs are focussed on either side of the microchip. These photographs show best the damage that was on many of the edges of the laser and amplifier microchips. Chipping of the crystal around the edges and corners is shown, along with the

cracking and peeling of the dielectric coatings. This microchip also shows marks on the surface, though one side looks rather clean.

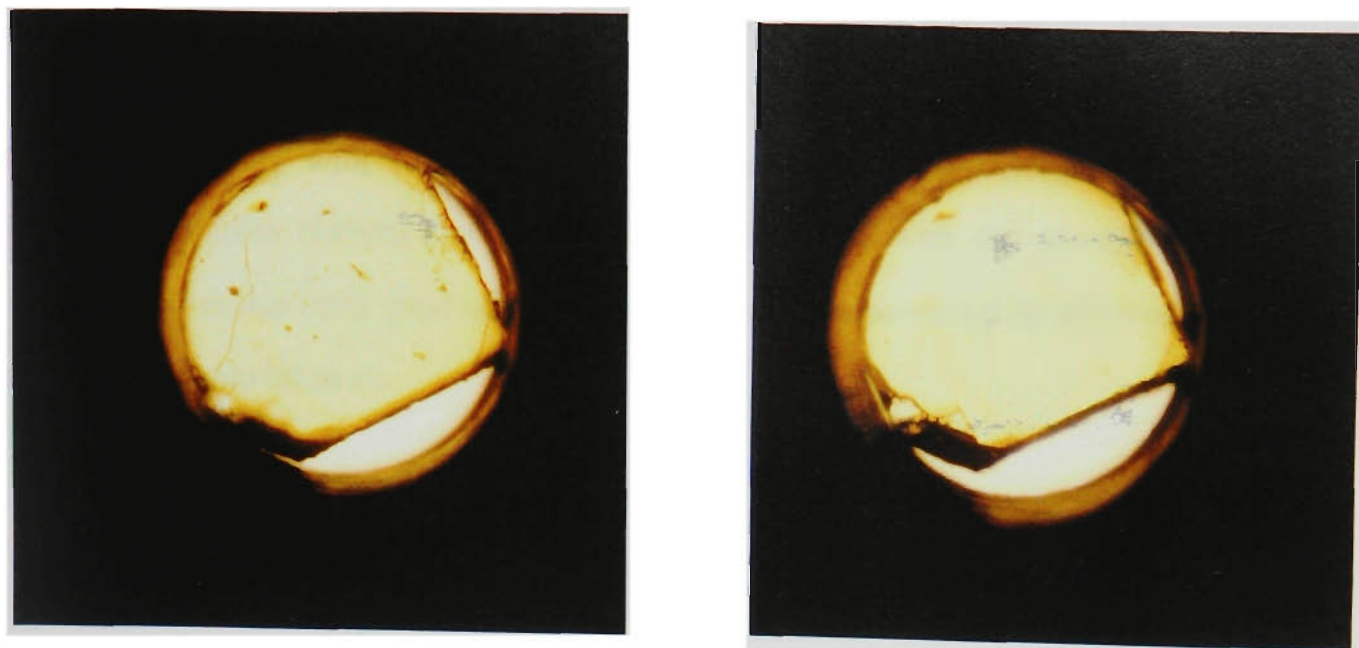


Figure 4.18: Photographs of the Nd:YVO₄ microchip coated for 1.34 μm lasing, held within an aluminium holder.

The amplifier microchips, were not photographed, but were probably the poorest quality in terms of chips and cracks of the microchip surface and coatings. Although the quality of the coated Nd:YVO₄ microchips was considered to be rather poor, pumping locations on the microchips could be found to yield results comparable to those predicted.

Conclusions

Absorption measurements of the Nd:YVO₄ material were used to determine the most efficient pumping wavelengths. This absorption is compared in chapter five to the laser output performance achieved across different pump wavelengths. The absorption results obtained were compared to those found in the literature for Nd:YAG, showing the superior absorption properties of Nd:YVO₄. The fluorescence measurements were used to establish the probable

lasing regions, and then to identify the Stark sub-levels involved in the main laser transitions to be between the lower Stark levels of both the upper and lower laser levels. The fluorescence profiles found in the lasing regions were used to give a measure of the gain bandwidth and are in good agreement with values found in the literature. Closer visual inspection of the Nd:YVO₄ samples showed that quality problems existed with our samples, however as reported later in this work good laser and amplifier performance could be achieved with careful selection of pump location.

Chapter 5 Microchip Lasers

Introduction

5.1.1 1.06 μm Microchip Laser

Output versus Pump Wavelength

Output Power, Thresholds & Slope Efficiencies

Temperature Tuning

5.1.2 Model results for 1.06 μm microchip laser

5.1.3 Performance of 1.06 μm laser - Discussion

Output versus Pump Wavelength

Output Power, Thresholds & Slope Efficiencies

Output Beam

Temperature Tuning

5.2.1 1.34 μm Microchip Laser

Output versus Pump Wavelength

Output Power, Thresholds & Slope Efficiencies

Temperature Tuning

Second Transition

5.2.2 Model results for 1.34 μm microchip laser

5.2.3 Performance of 1.34 μm laser - Discussion

Output versus Pump Wavelength

Output Power, Thresholds & Slope Efficiencies

Output Beam

Temperature Tuning

Chapter 5

Microchip lasers

Introduction

The microchip laser tests were initiated out of collaboration with a group of researchers at Fukui University Japan. While their initial investigations focussed on Laser Diode pumping of the microchip lasers [Taira *et al.* (1991)], the tests performed here at Victoria University utilized the versatile wavelength tunability of a Ti:sapphire laser as the pump source to further characterize these devices. In this chapter the operation of Nd:YVO₄ microchip lasers at both 1.06 and 1.34 μm , with the use of a Ti:sapphire laser for pumping, are studied. Based on the laser model established in chapter 2, the theoretically expected output power performance of these lasers is determined, given the material, mirror and dimensional properties of the microchips. These theoretical predictions are compared to the experimental output powers obtained. This is followed by discussion of the operating performance of the microchip laser devices.

5.1.1 1.06 μm Microchip Laser

The following results were obtained using a 0.5 mm thick $1.0\pm 0.1\%$ Neodymium doped YVO₄ microchip, which was coated for 1.06 μm lasing. The reflection / transmission properties of the coatings are outlined in table 3.3.

Output versus Pump wavelength

The output power of the microchip laser was measured for different pump wavelengths from 730 to 830 nm. The power output data shown in figure 5.1 was obtained with a constant incident pump power of 200 mW, and was taken for both parallel (π) and perpendicular (σ) polarization of the incident pump beam on the Nd:YVO₄ microchip. As a comparison, the figure also shows the Nd:YVO₄ absorption across the 730 to 830 nm wavelength region.

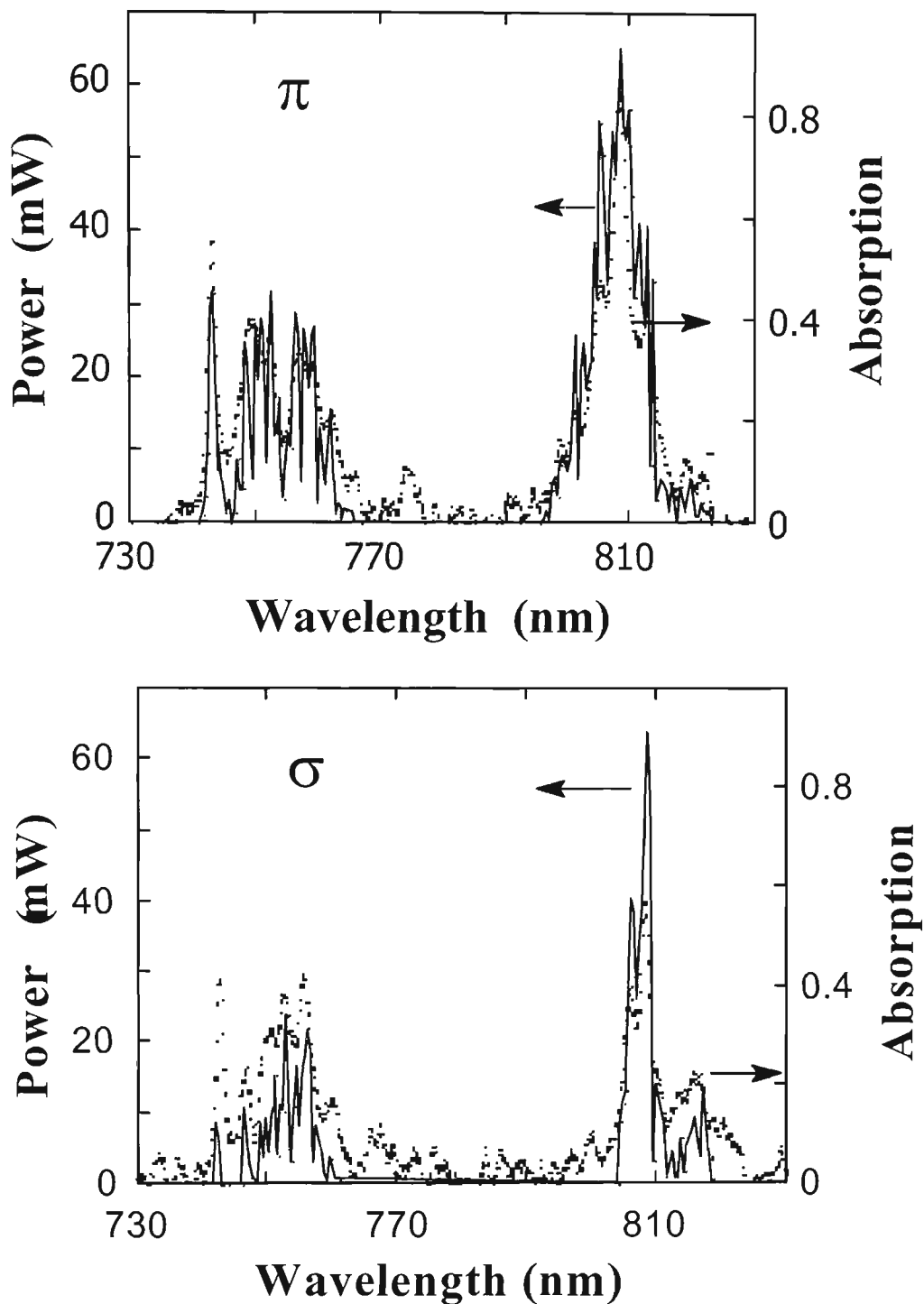


Figure 5.1: Power output (line) & absorption (dots) against pump wavelength, for parallel (π) and perpendicular (σ) polarized incident light. The output power was measured at pump wavelength steps of approximately 0.4 to 0.5 nm, with a line joining these points. This was done with a constant incident pump power of 200 mW and a linewidth of <15 GHz. The absorption was measured in 0.17 nm steps, with 0.2 nm resolution.

In general, substantially higher output power and lower thresholds were obtained with π polarized pump light. The full widths of the output power profiles for the π polarization pump are consequently wider by a factor of approximately 3 compared to that for the σ orientation. The magnitude of the output power that can be obtained when pumping the $^4F_{7/2}:^4S_{3/2}$ bands near 750 nm is, at best, approximately half that which can be achieved for the same pump power in the $^4F_{5/2}:^2H_{9/2}$ bands near 810 nm. The reduced output power in the shorter wavelength bands can be seen from figure 5.1 to be consistent with the reduced absorption of the pump radiation at these wavelengths, in combination with the reduction in the Stokes factor. The maximum output power was seen to be consistent with the region of maximum absorption, thus all subsequent pumping of the microchips was based in the region bounded by the wavelengths 808.70 and 808.85 nm.

Output Power, Thresholds & Slope efficiencies

The incident pump power versus microchip laser output power data for the two incident polarizations at a pump wavelength of 808.7 nm are shown in figure 5.2, both measured with the microchip at room temperature ($\approx 21^\circ\text{C}$). The laser thresholds for π and σ orientations were 34 ± 7 and 46 ± 10 mW, respectively. The corresponding slope efficiencies (the ratio of change in output power to change in incident power) are $41 \pm 4\%$ and $32 \pm 4\%$ respectively. The estimates of uncertainty are generated from the maximum and minimum lines of best fit to the data, when error bars of ± 2.5 mW are introduced in the output power data. (the ± 2.5 mW is a slight overestimate of the variance observed in some of the output power measurements from the microchip laser). The output power obtained with a pump power of 200 mW for the better performing π orientation was 68 mW. The beam divergence of the microchip laser when operated at an output power of 68 mW was measured to be 14 ± 2 mrad (full angle), from several measurements at different distances from the microchip output.

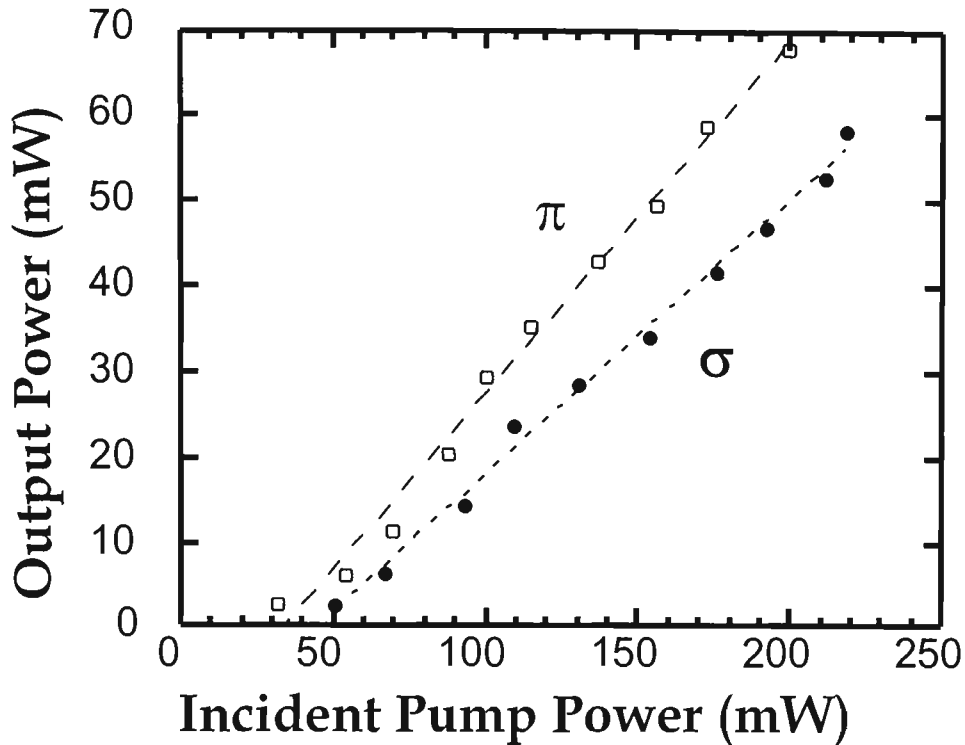


Figure 5.2: Output power against incident pump power for the 1.06 μm microchip laser.

The following graph (fig. 5.3) shows the best observed output data obtained for the 1.06 μm microchip laser, and was for the better π pumping polarization. This data corresponds to a different pumping position on the microchip to that used above. The line of best fit, also considering ± 2.5 mW error bars to estimate uncertainty, predicts a threshold of 34 ± 8 mW and a slope efficiency of $53 \pm 6\%$. However, an apparent decrease in slope at low pump powers provides a lower threshold of ≈ 20 mW. This decrease in slope efficiency at low pump powers was not uncommon in the tests performed, in these cases providing a threshold lower than would be predicted by a straight line of best fit. At higher pump powers the slope efficiency increases to greater than 50%, and an output power of approximately 78 mW is produced with 185.6 mW of incident pump power. (The dashed line shown is a line of best fit for all points, including low pump powers, thus the slope efficiency of 52.8% predicted by this line may be an under estimate for higher pump powers).

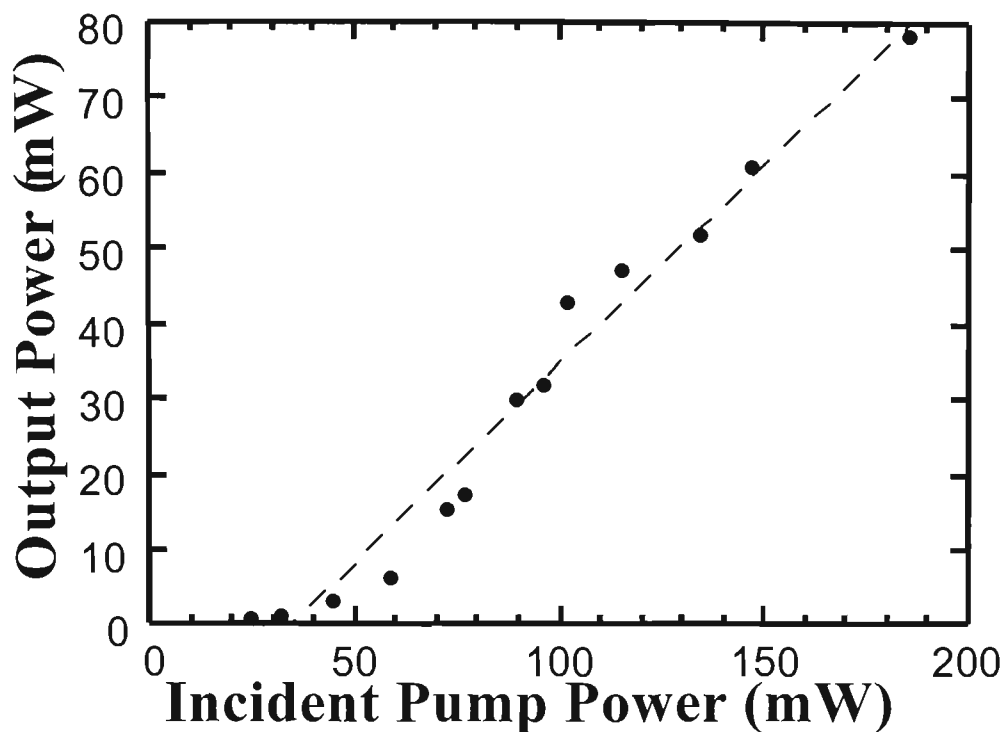


Figure 5.3: 1.06 μm microchip laser output power versus incident pump power, π polarization data with lowest threshold and greatest slope efficiency.

Temperature Tuning

The variation of the output power (π pump polarization) caused by the microchip temperature, along with the change in wavelength of the major peak in the output spectrum, are shown in figure 5.4. These results were achieved with a pump power of 220 mW at a wavelength of 808.7 nm. The output power at 100 °C is approximately half that achieved at 1.3 °C.

In terms of frequency the microchip laser output varied at a rate of approximately -1.5 GHz/°C. Using the expression given in equation 2.6 the frequency change with temperature was calculated to be -1.64 GHz/°C, where the thermal optical co-efficient ($\partial n_e / \partial T$) is given as $3.0 \times 10^{-6} / ^\circ\text{C}$, and the thermal expansion co-efficient (α_a) as $4.43 \times 10^{-6} / ^\circ\text{C}$ [CASIX(1996)].

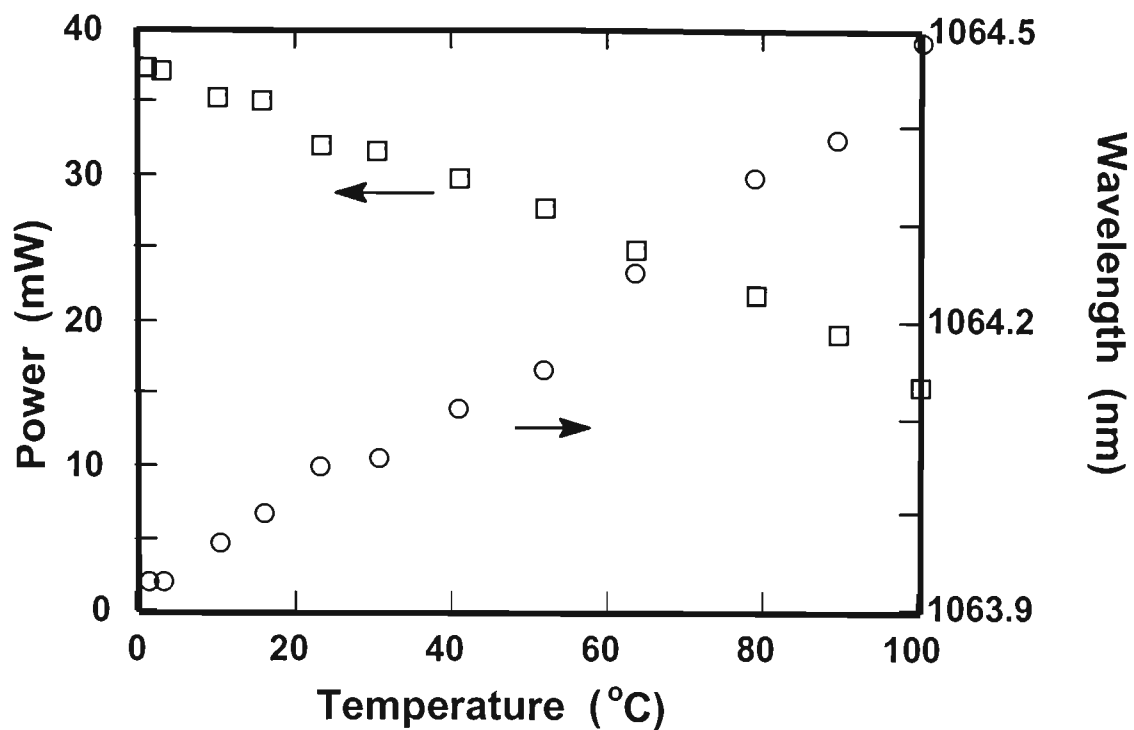


Figure 5.4: Change in output power, and peak wavelength, with a change in microchip temperature.

As the temperature was increased, the spectrum of the output changed as the longitudinal modes of the cavity moved with respect to the laser gain profile. Figure 5.5 illustrates this behaviour showing the output spectrum for temperatures of 1.3, 45.4, and 100 °C. At 1.3 °C there was a small, longer wavelength secondary peak at less than 10% of the height of the main peak. At 45.4 °C small peaks appear at both sides of the main peak at less than 5% of the height of the main peak. At 100 °C there are clearly two modes with the shorter wavelength mode approximately 50% of the height of the longer wavelength mode. With the incident pump power of 220 mW used, which is well above the threshold pump power of 20-40 mW, the microchip laser does not exhibit pure single longitudinal operation.

The spacing between the peaks of the two modes that are evident in the high temperature spectrum is 0.52 nm. This corresponds to the longitudinal mode spacing of the laser resonator, and is identical to that calculated by theory (equation 2.5). In order to obtain a single longitudinal mode with this laser it is therefore necessary to adjust the crystal temperature to place a cavity mode near the centre of the laser gain profile. One must also

consider the magnitude of the pump power above the threshold value, since this may increase the gain bandwidth sufficiently to allow another longitudinal mode to lase, as is seen in this case.

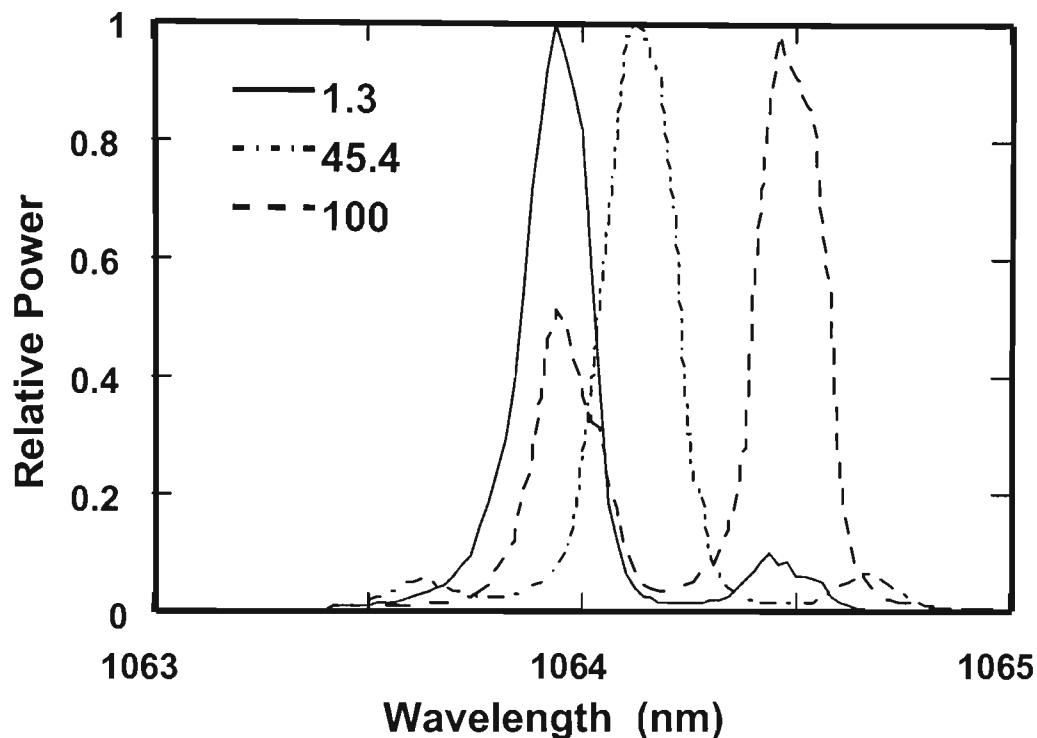


Figure 5.5: Normalized output mode spectrum of microchip laser (pumped with 220 mW of incident pump power) at the temperatures specified (°C).

5.1.2 Model results for 1.06 μm microchip laser

Using the laser equations established in section 2.2.1 and the parameters of the Nd:YVO₄ microchip and its coatings given in table 3.3 (for 1.06 μm lasing), theoretical results for the laser threshold and slope efficiency may be determined. Equation 2.35 gives the predicted incident pump power at threshold, while equation 2.32 gives the predicted slope efficiency. By using the calculated results from the two equations, a theoretical incident pump power versus output power graph was established, and is shown in figure 5.6. The following table shows the parameters used to model the 1.06 μm microchip laser:

Parameter	Reason	Value
T	(Transmission loss of the output coupler at the lasing wavelength) = 1% Microchip specification gives a reflectivity of $99 \pm 0.2\%$	0.01
L	(Resonator losses) intrinsic material loss (CASIX (1996)) 0.02 cm^{-1} @ $1.06 \mu\text{m}$ round trip cavity length is 1 mm, therefore intrinsic loss = 0.002 front mirror reflection = 99.92%, therefore mirror loss = 0.0008 Total resonator loss = 0.0028	0.0028
A	(Cross-sectional area of pumping (πr^2)) = $\pi \times (265 \mu\text{m} / 2)^2$	$5.515 \times 10^{-8} \text{ m}^2$
I_s	(Saturation intensity ($\frac{h\nu_L}{\sigma_{21}\tau_f}$)) = $\frac{6.626 \times 10^{-34} \times 2.8195 \times 10^{14}}{15.6 \times 10^{-23} \times 100 \times 10^{-6}}$ $\nu_L = \frac{c}{\lambda_L} = \frac{3 \times 10^8}{1064 \times 10^{-9}} = 2.8195 \times 10^{14} \text{ Hz}$ σ_{21} (Stimulated-emission cross-section) literature varies between 10 to $20 \times 10^{-19} \text{ cm}^2$, $15.6 \times 10^{-19} \text{ cm}^2$ from DeShazer (1994) τ_f (Fluorescence lifetime) $100 \mu\text{s}$ for 1 at% Nd doped YVO_4 [DeShazer (1994)]	$1.2 \times 10^7 \text{ W/m}^2$
η_Q	(Pump Quantum efficiency) ≈ 1 The fractional number of Nd^{3+} ions in the $^4\text{F}_{3/2}$ state per absorbed photon. Neodymium doped lasers are predominantly pumped at levels slightly above the $^4\text{F}_{3/2}$ upper laser level. The $^4\text{F}_{3/2}$ level is then populated by non-radiative transitions from these higher levels. This process is so rapid that fluorescence from the higher levels is not observed. Therefore it is concluded that each absorbed pump photon produces a Nd^{3+} ion in the $^4\text{F}_{3/2}$ state, thus the pump quantum efficiency η_Q , is extremely high, and to a good approximation $\eta_Q = 1$.	1
η_S	(Stokes factor (λ_P/λ_L)) = $808.72 / 1064$	0.76
η_B	(Beam overlap efficiency) Assumed to be ≈ 1 This is a good assumption for end pumping configurations.	1
η_A	(Fraction of incident pump power absorbed) absorption at pump wavelength $\approx 95\%$ front mirror transmission $\approx 99\%$ $0.95 \times 0.99 = 0.9405$	0.9405
f_B	(Population of the Stark sub-level within the upper laser level responsible for the laser action - given by equation 2.33) $T = 294 \text{ K}$, $(\Delta\bar{\nu}) = 18 \text{ cm}^{-1}$	0.52
b	(Fluorescence branching ratio to the lower laser level $^4\text{I}_{11/2}$, see figure 2.5)	0.467

Table 5.1: Parameters used for the modelling of the $1.06 \mu\text{m}$ microchip laser.

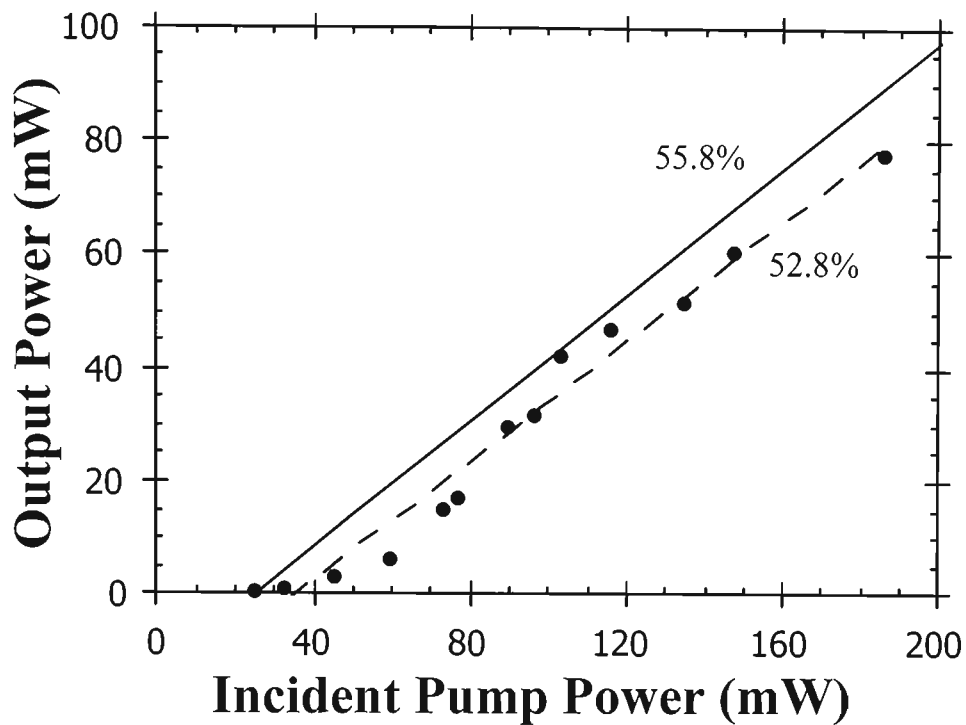


Figure 5.6: Model (solid line) and experimental (dots and dashed line of best fit) results for incident pump power versus output power. The corresponding slope efficiencies are shown beside each line.

Figure 5.6 shows model results for the Nd:YVO₄ 1.06 μm microchip laser, along with experimental data translated from figure 5.3. The lasing threshold predicted by the model calculations corresponds to an incident pump power of 24.4 mW, this compares well to the 20 to 25 mW experimental threshold shown. It is noted that the line of best fit from the full set of measured points suggests a threshold of ≈ 35 mW, however, a slight change in slope efficiency just above threshold dictates the lower threshold. The calculated slope efficiency of 55.8% is comparable to the slope efficiency of 52.8% obtained from the line of best fit applied to the experimental data. In practice the experimental slope efficiency may be closer to the calculated value since the line of best fit includes those points just above threshold which have a lower slope efficiency. By removing the first two points from the line of best fit calculation the slope efficiency becomes $\approx 56.6\%$.

5.1.3 Performance of 1.06 μm laser - Discussion

Output versus Pump Wavelength

The 1.06 μm microchip laser has been shown to lase over a large range of pump wavelengths, in both the 750 and 810 nm absorption bands, with both π and σ polarized incident light. The microchip laser output power across these wavelengths followed quite closely to the absorption of pump light at these wavelengths, and therefore the reduced output in the lower absorption band is consistent with the reduced magnitude of absorption. This is also consistent with the idea that each absorbed photon produces an upper laser level electron in the $^4F_{3/2}$ state, with very little, if any, loss due to fluorescence from the absorption levels. For a practical device based on a microchip system where maximum microchip output power is not the only consideration, a range of laser diode wavelengths could be used as the pump source, since the pump wavelength is not so critical in obtaining lasing. The Nd:YVO₄ microchip will be very suitable for absorbing the output of relatively wide bandwidth laser diodes due to its wide absorption region. Typical high power laser diodes (hundreds of milliwatts to several watts) have bandwidths of approximately 2 nm, therefore, with less stringent requirements on the pump source, production of microchip laser systems based on laser diode pumped Nd:YVO₄ material should prove more economical.

Fields *et al.* (1987) found that the small Stark splitting of YVO₄, combined with comparatively large inhomogeneous broadening, effectively created a wide continuous absorption band. In comparison the broader Stark splitting and highly resolved bands of Nd:YAG created a spiky absorption band. Fields concluded that the Nd:YVO₄ material was therefore more tolerant to laser diode pump wavelength variation, which is advantageous for multiple diode devices and aging effects in diodes which shift the output wavelength. Mermilliod *et al.* (1992) also found that of eight neodymium materials tested Nd:YVO₄ showed the least variation in pump efficiency with a laser diode temperature variation of 20°C. Nd:YVO₄ also demonstrated the maximum main absorption bandwidth of all the materials.

It has been generally shown that absorption, and therefore laser output performance, is best for π polarized incident pump light. Thus the mounting of any pump source (or conversely microchip) with preferential lasing in one linear polarization was considered so as to operate with the best laser performance. Higher power laser diodes which may be used generally have a dominant polarization which should be investigated initially to provide the best output from a microchip laser system.

Output Power, Thresholds & Slope Efficiencies

The experiments demonstrated a best microchip laser output power of approximately 80 mW for an incident pump power of around 186 mW, this output figure would have undoubtedly increased, with increased pump power. The output spectrum remained single longitudinal mode up to this maximum observed output power for the input versus output tests performed at room temperature ($\approx 20\text{-}21^\circ\text{C}$). By choosing other pumping areas on the microchip multi-longitudinal-mode output beams could be readily produced, however the areas of best output performance generally corresponded to the best modal output (single mode).

In comparison, with a similar Nd:YVO₄ 1.06 μm microchip laser, Taira *et al.* (1991) demonstrated a maximum single longitudinal mode output power of approximately 103 mW, and a maximum multimode power of 154 mW, when pumped by a 500 mW laser diode. In the initial microchip laser tests performed by Zayhowski & Mooradian (Jan, May 1989), a 730 μm long, 1.1 weight% doped Nd:YAG microchip laser demonstrated a maximum single mode output of only 22 mW.

Lasing threshold values of 34 mW and 46 mW of incident pump power were determined respectively for π and σ polarized pumping as shown in figure 5.2. Different locations on the crystal revealed slightly lower thresholds, however this most often corresponded with a change to a lower slope efficiency at low pump powers (just above threshold). For example, figure 5.3 shows a lower threshold of around 20 mW for π polarization pumping. These values are in quite good agreement with the theoretically

calculated threshold value for π pumping of 24.4 mW of incident pump power. Taira *et al.* (1991) achieved a threshold of approximately 5.3 mW with their laser diode pumped Nd:YVO₄ microchip laser, showing the potential for low threshold lasing, however this was probably with a smaller pump diameter than was used here, and therefore higher pump intensity. Zayhowski & Mooradian (Jan, May 1989) achieved lasing thresholds of less than 1 mW with their Nd:YAG microchip. This was achieved with a pump spot diameter of approximately 50 μm (greater than ten times the pump power intensity used here), and similar, or better, threshold levels should be expected from good quality Nd:YVO₄ samples.

Slope efficiencies of 41% (π) and 32% (σ) are given by the data shown in figure 5.2, however figure 5.3 shows the possibility of figures better than 50% for π polarization. From the line of best fit of all the experimental measured points in figure 5.3 the slope efficiency is 52.8%, however if the first two points are removed, which demonstrate a reduced slope efficiency, the slope efficiency value becomes 56.6%. This higher slope efficiency value was also in good agreement with the 55.8% slope efficiency predicted by the theoretical calculations. The 1.1 weight% doped Nd:YAG microchip of Zayhowski & Mooradian (May 1989) showed a maximum slope efficiency of 48%, also reported was a Nd:LNP (LiNdP₄O₁₂) microchip laser which demonstrated 28% slope efficiency.

The best of the experimentally obtained values for lasing threshold and slope efficiency compared well with the predictions given by the theoretical calculations. It should be expected that with the better quality Nd:YVO₄ crystals and more uniform microchip coatings that are now reported to be available, consistently high quality results across most of the crystal area should be obtainable.

Output Beam

The output divergence of the microchip laser was estimated to be approximately 14 mrad (full angle), with a TEM₀₀ beam. This corresponding to a M^2 value of approximately 1.002, where M^2 is a measure of the beam quality. [$1/M^2 = \lambda/(\pi\omega_0\theta)$, where λ equal laser wavelength, ω_0 is half beam waist and θ is far field divergence half angle]. The divergence

was measured by estimating the size of the output beam on an infrared detector card at several distances from the laser. The beam size on the detector card is not a very accurate measure of beam size, and it is suggested that the measured size of the beam was probably a slight overestimate of the actual $1/e^2$ beam size. It is therefore suggested that the divergence was actually a little less than is estimated. The microchip laser's very low divergence gives it a distinct advantage over typical laser diode outputs, in that it is much easier to focus, or butt couple, into an optical fibre. Also, complicated optics would not be required in measurement systems where collimated or circularly symmetric beams were required.

Spectroscopic studies and analysis of laser states in bulk Nd:YVO₄ samples conducted by Yaney and DeShazer (1976) found that the principal laser line from the possible transitions around 1064 nm was predominately π polarized. This was found also to be the case with the output beam of the Nd:YVO₄ microchip laser. This linearly polarized beam may be a distinct advantage for things like simple second harmonic generation and electro-optic Q-switching (because there is no need for an intracavity polarizer), and allows simple arrangements for systems which may utilize a polarization based measurement technique. Apart from the fact that the microchip laser output can be single longitudinal mode, which makes it good for coherence measurement techniques, the above favourable beam characteristics (low divergence, single transverse mode and single polarization) make the microchip output much more useful in many applications, and introduces new applications where laser diodes have not been suitable.

Temperature Tuning

The laser output modal spectrum is governed by the crystal thickness, which sets the longitudinal mode spacing, compared to the materials gain bandwidth (outlined in section 2.1.1). The frequency and wavelength spacing of the longitudinal modes is given by equations 2.4 and 2.5, respectively. With a microchip thickness of 0.5 mm and a refractive index of 2.165 at 1.06 μm , the frequency separation of modes is ≈ 139 GHz and the wavelength separation is ≈ 0.52 nm. This wavelength separation compares well with that shown

experimentally in figure 5.5. When compared to the measured FWHM bandwidth of the fluorescence (\approx gain bandwidth) of between 0.86 and 0.93 nm, or 228 to 246 GHz, this shows that more than one longitudinal mode may be situated within the gain bandwidth, thus producing a multimode output. However, with the microchip thickness used here single mode output is possible over a wide temperature range, when a single longitudinal mode is positioned close to the centre of the gain region. A thinner microchip would give a better tuning range with a single longitudinal mode output, but with a consequential reduction in absorption and output power. For example, a microchip with the same neodymium concentration having a thickness of 270 μm would have a longitudinal mode spacing approximately equal to the Nd:YVO₄ gain bandwidth at 1.06 μm , and approximately 79% maximum absorption. (cf. \approx 95 % absorption in the 0.5 mm thickness used in this work).

At a pump power of 220 mW, as was used to perform the temperature tests on the 1.06 μm microchip laser, side modes are evident through out the temperature range, this can be seen in figure 5.5. The incident pump power used was approximately ten times the threshold pump power, however as is illustrated in figure 2.2, and found experimentally, a slight reduction in the pump power will reduce the magnitude or occurrence of side modes. (These tests therefore give an indication of the temperature region where single longitudinal mode operation would occur given a slightly lower pump power). From approximately 3°C to around 50°C side modes were very small (less than 5% of the peak mode magnitude). Then by increasing the temperature further the intensity of the lower wavelength mode grew, through to where it was around half the height of the main mode at 100°C. The laser's peak mode was tunable at approximately 0.0056 nm/°C or -1.5 GHz/°C. This value compares favourably with the calculated value of -1.64 GHz/°C, which considered the refractive index and cavity length change with temperature (equation 2.6). The work of Taira *et al.* (1991) on a similar Nd:YVO₄ microchip demonstrated a tuning rate of \approx -1.6 GHz/°C.

The illustrated drop in output power with an increase in the microchip temperature, as shown in figure 5.4. is expected due to thermal broadening of the gain profile thereby reducing the peak gain on the lasing transition, and consequently reducing the output power. This effect

is combined with the frequency shift of the lasing mode away from the peak in the gain profile, also reducing the output power.

With a 0.5 mm thick Nd:YVO₄ 1.06 μm microchip laser, at pumping powers of less than 200 mW, single longitudinal mode output may be obtained over a temperature range of approximately 50°C. In this case the temperature range for single mode output conveniently covered operation at room temperature so that in general temperature control was unnecessary to maintain single mode operation. If single mode operation at room temperature had not been the case, temperature tuning would have offered a simple method to insure single mode output. Temperature control conversely offers a degree of tuning of the output wavelength without loss of single longitudinal mode operation.

Temperature tuning of practical microchip devices may prove quite useful if the microchip laser output wavelength/frequency needs to be varied, or locked at a particular value. The process is simply achieved by mounting an electrically controlled Peltier temperature control device next to the microchip or its holder. In a developed microchip product it is conceivable that the microchip may be mounted directly onto a temperature control device.

Other forms of microchip laser output tuning are possible, though not considered in this work (described in microchip laser review section 1.2). Some include: Mechanically changing the length of the microchip, to change the longitudinal mode spacing, or, pump power modulation, which can vary the energy deposited in, and therefore the temperature of the microchip.

5.2.1 1.34 μm Microchip Laser

The following results were obtained using a 0.5 mm thick 1.0±0.1% Neodymium doped YVO₄ microchip, which was coated for 1.34 μm lasing. The reflection / transmission properties of the coatings are outlined in table 3.3.

Output versus Pump Wavelength

The variation of output power as a function of Ti:sapphire pump wavelength for an incident pump power of approximately 370 mW is shown in figure 5.7. Also shown is the absorption of the Nd:YVO₄ crystal in this region of the ⁴F_{5/2}:²H_{9/2} absorption bands. Lasing was obtained on the 1.34 μm transition only when pumping at wavelengths in the region from 808 to 809.5 nm, for which there is very high absorption. In terms of the high lasing threshold value found at the maximum absorption region (240-280 mW) the pump power used here is not large, and it would be expected that this pump wavelength lasing region would increase with an increase in the incident pump power.

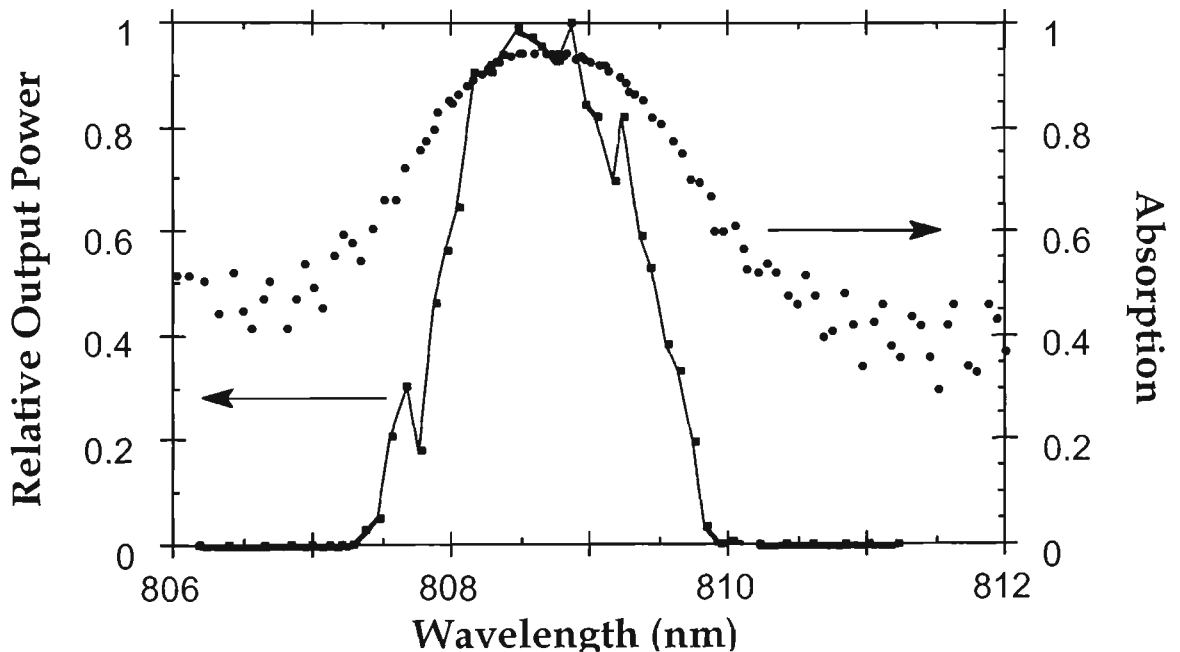


Figure 5.7: Output power (incident pump of 370 mW) and crystal absorption versus pump wavelength for the 1.34 μm Nd:YVO₄ microchip laser.

Output Power, Threshold & Slope Efficiency

The variation of output power of the Nd:YVO₄ laser with increasing incident pump power from a Ti:sapphire laser is shown in figure 5.8. This data was obtained after varying the position of the microchip in a 370 mW pump spot to obtain maximum output power. The Ti:sapphire pump wavelength was 808.8 nm, and the Nd:YVO₄ crystal temperature was

operated at room temperature ($\approx 21^\circ\text{C}$). The incident pump power for laser threshold, estimated from the line of best fit, was 275 ± 10 mW, and the slope efficiency obtained was $40 \pm 5\%$. (Lower thresholds than 275 mW were observed, as low as ≈ 240 mW, however these were generally associated with lower slope efficiency at low pumping powers, which then improved at higher pump powers). With 422 mW of pump power, the cw output power obtained was 60 mW at 1342.8 nm. At this stage the output spectrum was beginning to show evidence of a second longitudinal mode (see fig 5.9). The intensity of the second longitudinal mode is seen to be small, i.e., less than 1.5% of that of the main mode. The output beam was circularly symmetric, with a full-angle divergence of 12 ± 1 mrad established from measurements at different distances from the microchip output.

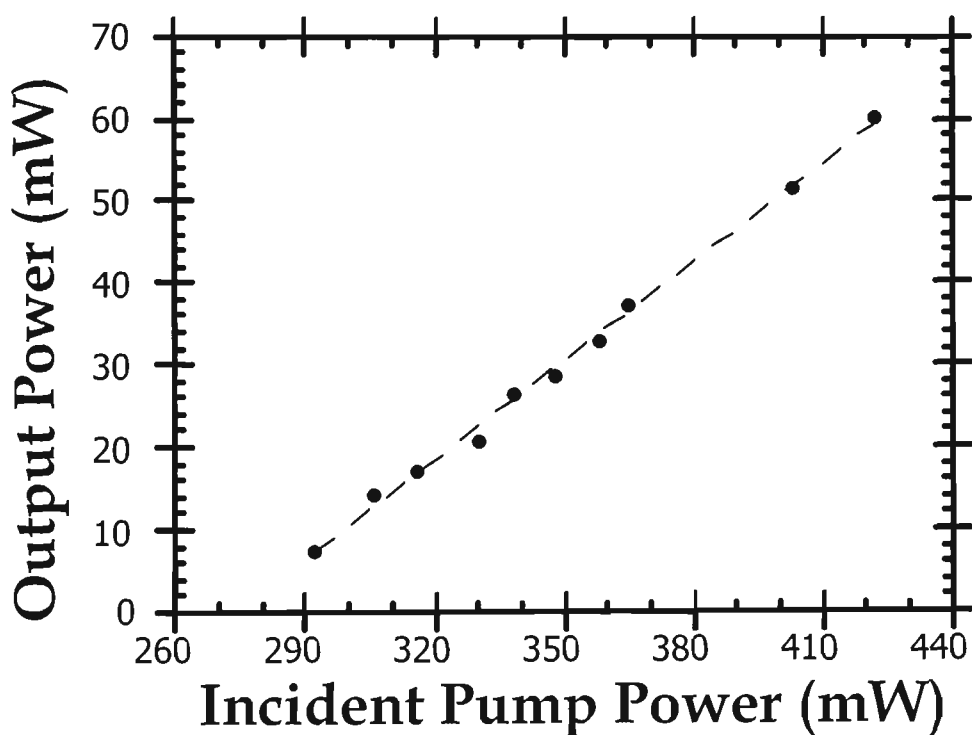


Figure 5.8: Output power against incident pump power for the 1.34 μm microchip laser.

An unexpected second laser transition was noted in the laser output spectra generated during these measurements (fig. 5.9). (Note the spectra are plotted on a dB scale to better show the appearance of other modes or transitions). At pump powers of 316, 330 and 338 mW, a second transition was observed at about 3.5 nm higher than the peak mode wavelength.

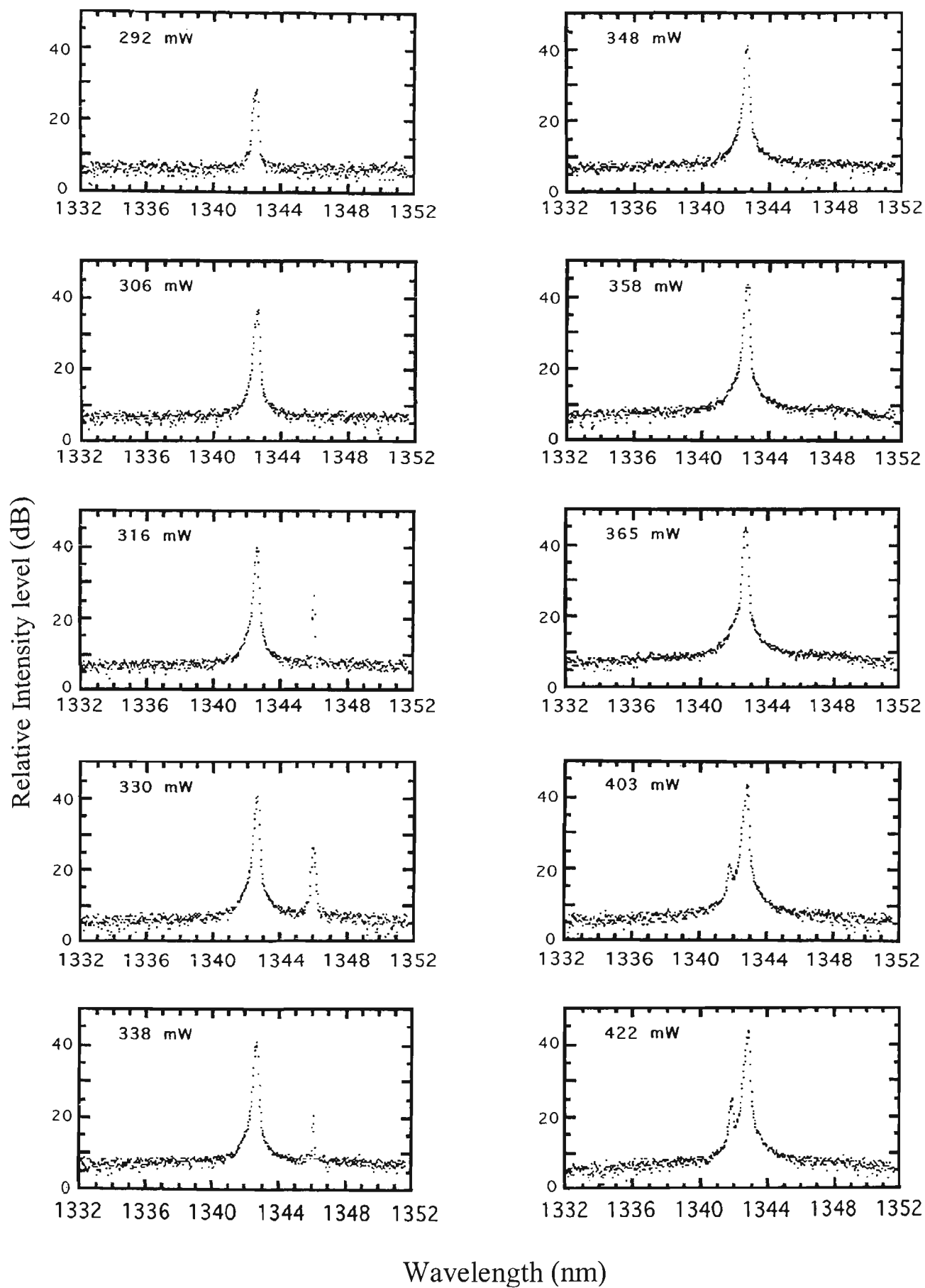


Figure 5.9: Laser output spectrum plotted for increasing pump power. The number in top left corner of each graph is the incident pump power.

The following output spectra in figure 5.10 were generated by pumping a different location on the microchip. Here, no second transition was observed and the output was single mode over the entire range. A second longitudinal mode at a shorter wavelength would reasonably be expected to appear if the incident pump power were to be increased further.

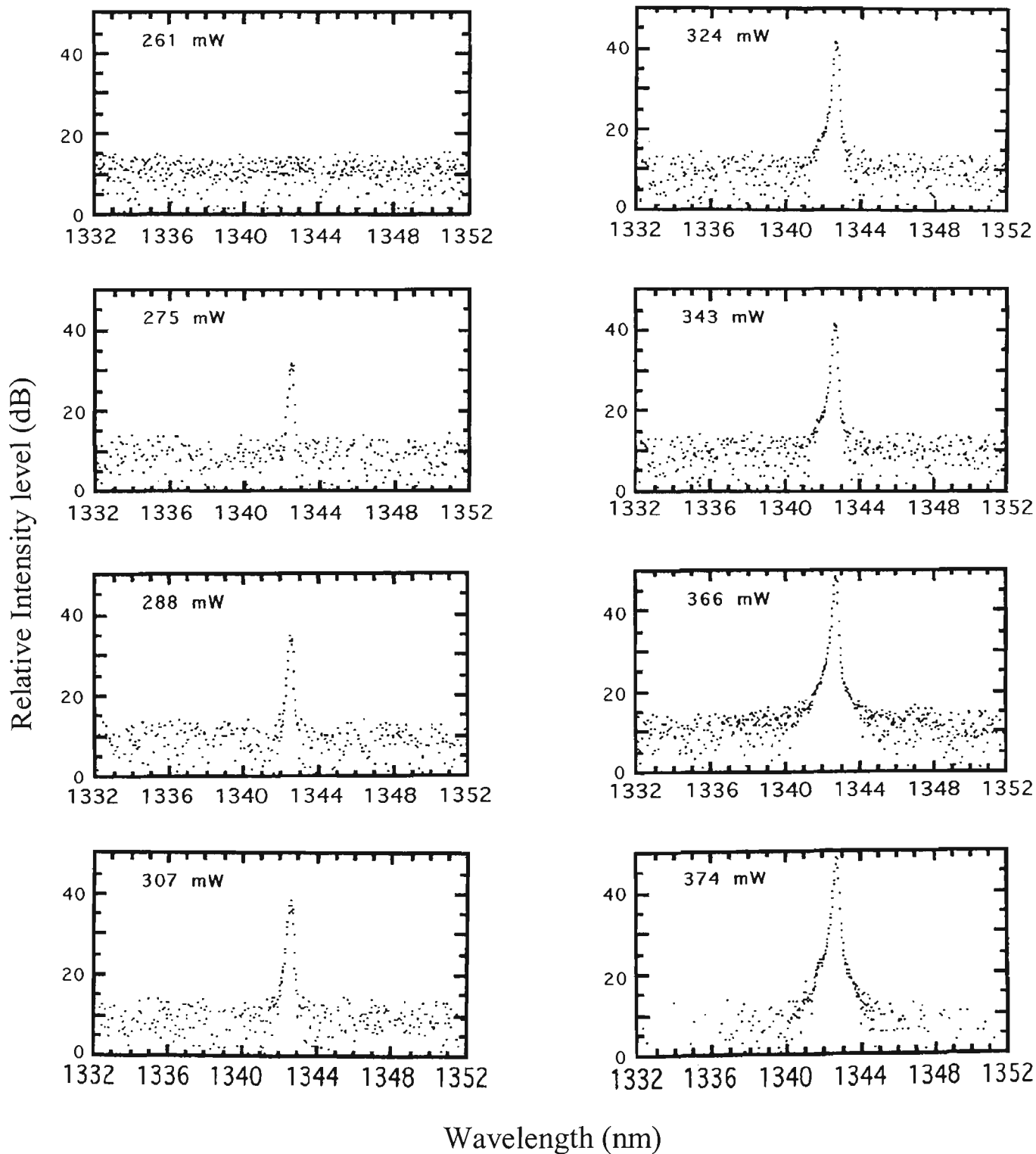


Figure 5.10: Laser output spectrum plotted for increasing pump power. The number in the top left corner of each graph is the incident pump power.

Figure 5.10 shows a slight increase in output wavelength with an increase in pump power (≈ 0.2 nm from 275 to 374 nm pump power). This increase in output wavelength can be attributed to an increase in the temperature of the microchip as the pump power is increased. By utilizing the fact that the microchip output wavelength varies with temperature, temperature may be used as a means to control, or tune, the output wavelength of the laser.

Temperature Tuning

The output spectrum of the laser was measured as the microchip temperature was varied between 3.8 and 100°C whilst maintaining the Ti:sapphire laser pumping at 370 mW. Figure 5.11 shows three representative spectra obtained using the optical spectrum analyzer with a 0.1 nm resolution. Each temperature spectrum has had its peak value output normalized to 1. The laser output consists of a single longitudinal mode at 3.8 °C and is just beginning to operate on two modes at 32°C. At 100°C two well defined laser modes are evident.

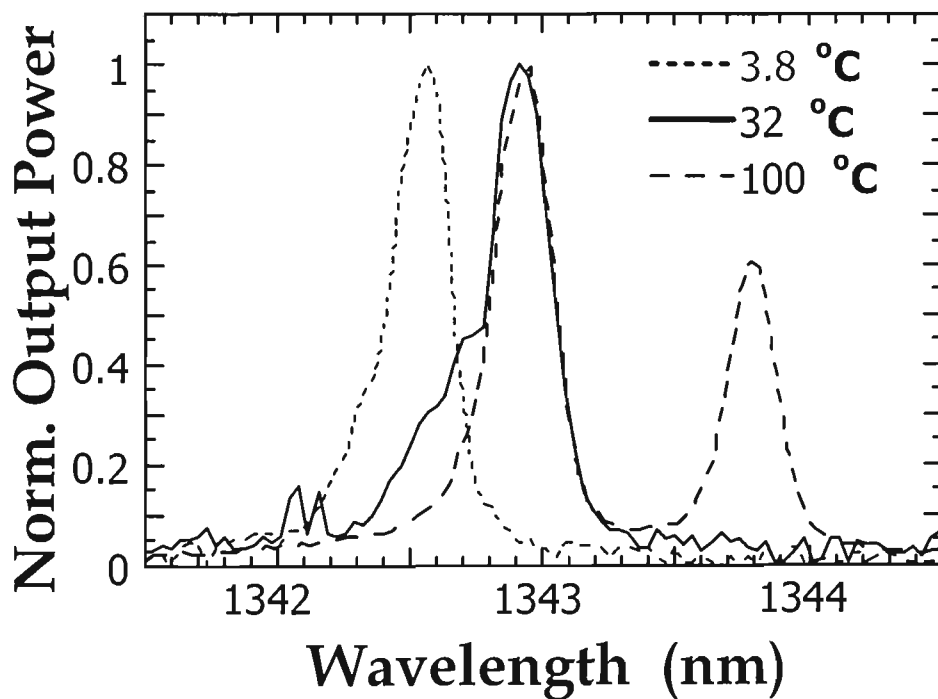


Figure 5.11: Normalized output spectrum for 3 specified temperatures showing longitudinal mode structure from the 1.34 μm microchip laser.

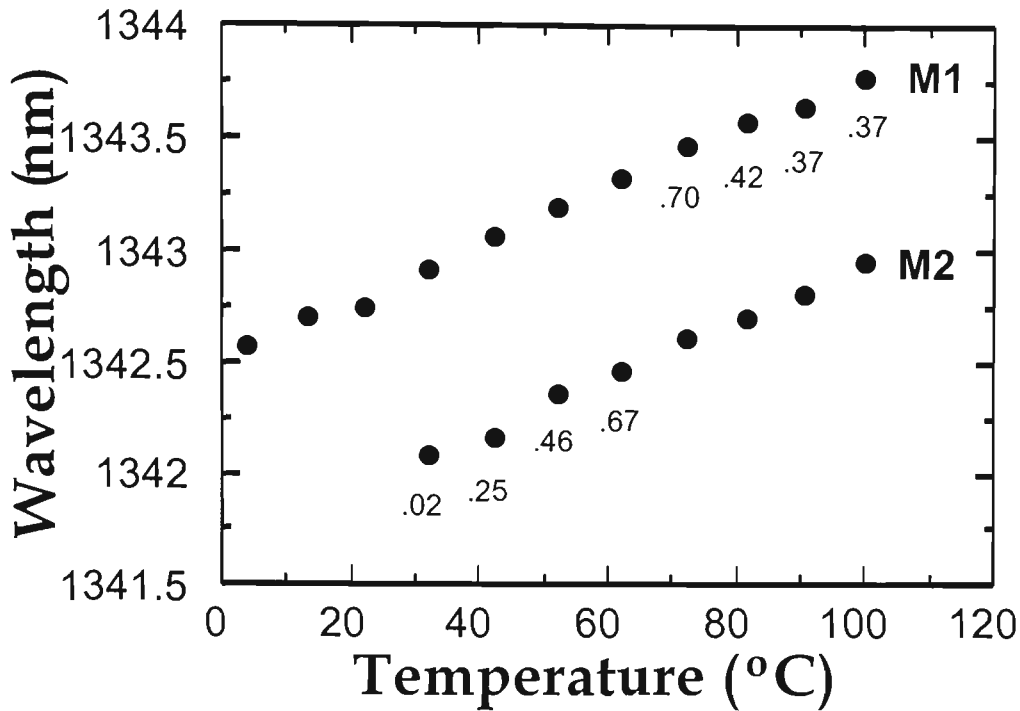


Figure 5.12: Peak wavelength of modes for increasing temperature. Numbers indicate intensity relative to the other mode at that temperature.

Figure 5.12 summarizes the data for the number of modes lasing and the wavelength of these modes over the entire temperature range studied. Data are plotted for 370 mW of Ti:sapphire pumping at a wavelength of 808.8 nm. Single longitudinal mode operation is observed between 3.8 and 32°C. Above 32°C the laser output consists of two longitudinal modes. The output wavelength of the higher wavelength mode (M1) increased by ≈ 1.2 nm between 3.8 and 100°C. The measured frequency shift with temperature was approximately -2 GHz/°C for each mode. In comparison, the calculated value of frequency shift as given by equation 2.6, when using $\partial n_e / \partial T = 3.0 \times 10^{-6}/^\circ\text{C}$ and $\alpha_a = 4.43 \times 10^{-6}/^\circ\text{C}$ both given at $1.06 \mu\text{m}$ [CASIX(1996)], was -1.3 GHz/°C ($n_e = 2.154$). However, since the refractive index of the material changes with wavelength, it is likely that the refractive index change with temperature ($\partial n_e / \partial T$) is also wavelength dependent. Therefore, the value of $\partial n_e / \partial T = 3.0 \times 10^{-6}/^\circ\text{C}$ is probably not applicable in this case. With no known literature reference of $\partial n_e / \partial T$ at $1.34 \mu\text{m}$ in Nd:YVO₄, no direct theoretical comparison of the frequency shift can be made, however, since the thermal expansion co-efficient (α_a) can not be wavelength dependent,

$\partial n_e / \partial T$ at 1.34 μm may be experimentally determined from the present data to be $10.8 \pm 2.4 \times 10^{-6}/^\circ\text{C}$ (with the error estimated from applying a ± 0.05 nm wavelength error bar to the data of figure 5.12 and finding maximum and minimum lines of best fit before converting to a frequency shift).

Second Transition

Other peak wavelength versus temperature measurements were conducted, and many of these (especially the initial 265 μm spot size results) yielded spectra which contained the second transition over portions of the lower temperature region. The second transition was positioned at approximately 3.5 nm higher than the main mode (M1) and demonstrated the same temperature dependent behaviour as described above.

The strongest lasing transition (1342.8 nm at room temperature) has been identified as transitions from the lower Stark level of the $^4F_{3/2}$ level (a') to the lowest Stark level of $^4I_{13/2}$ (a). The fluorescence spectrum around the 1.34 μm region, figure 4.14, shows a small peak to the right (longer wavelength) side of the main peak and is identified as fluorescence from the lower Stark level of $^4F_{3/2}$ (a') to the second lowest Stark level of $^4I_{13/2}$ (b). The fluorescence in this specific region has been remeasured on the OSA with a 0.1 nm resolution and plotted on a linear scale in figure 5.13. The figure shows the main fluorescence peak with the small peak to the right, in the region 1345 to 1346 nm, being that due to the fluorescence on the second transition (a' to b). This is identified as being the transition responsible for the second lasing transition observed in some of the laser spectra.

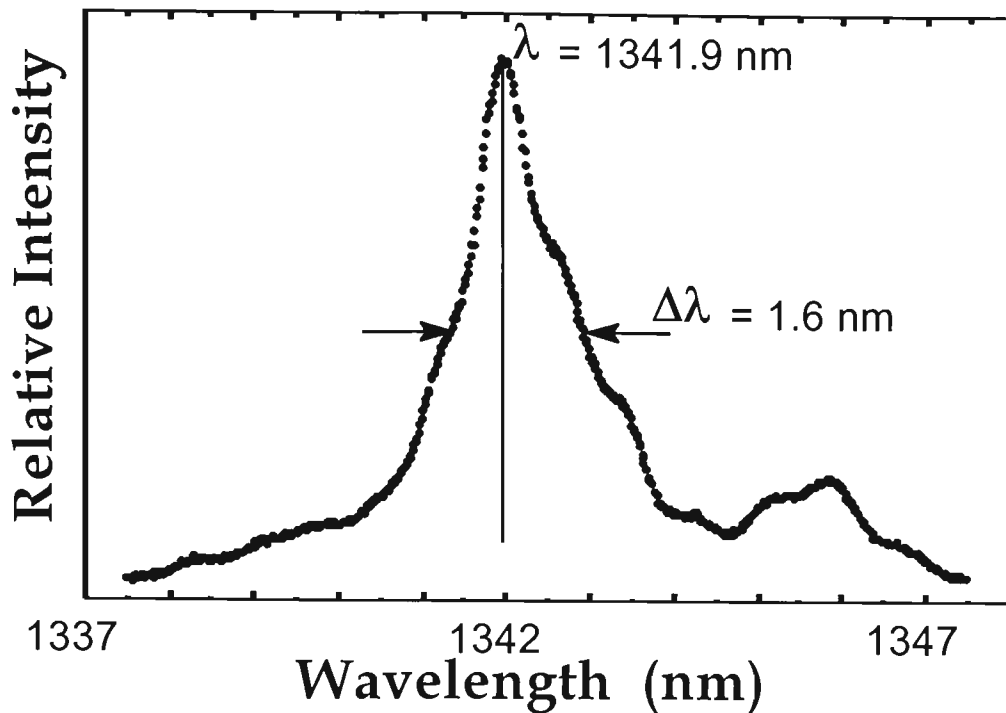


Figure 5.13: Fluorescence spectrum of a non-coated Nd:YVO₄ microchip around the 1.34 μm laser transition region. A second laser transition occurred in the small peak region to the right of the spectrum (1345 to 1346 nm) during some of the tests.

5.2.2 Model results for 1.34 μm microchip laser

Theoretical results for the laser threshold (eqn 2.35) and slope efficiency (eqn. 2.32) were determined using the laser equations established in section 2.2.1 and the parameters of the Nd:YVO₄ microchip and its coatings (for 1.34 μm lasing). From these results a graph of the laser's predicted incident pump power versus output power has been produced and is shown in figure 5.14. The following table lists the parameters used to model the 1.34 μm microchip laser:

Parameter	Reason	Value
T	(Transmission loss of output coupler at the lasing wavelength) = 1.9% Specification gives a reflectivity of approximately 98.1 % at 1.34 μm	0.019
L	(Resonator losses) intrinsic material loss (CASIX(1996)) 0.02 cm^{-1} @ 1.06 μm * round trip cavity length is 1 mm, therefore intrinsic loss = 0.002 * Material loss co-efficient greater than 3 times higher at 1.34 μm than at 1.06 μm [Tucker (Dec 1977)], therefore intrinsic loss taken as 0.006 front mirror reflection = 99.95%, therefore mirror loss = 0.0005 Total resonator loss = 0.0065	0.0065
A	(Cross-sectional area of pumping (πr^2)) = $\pi \times (165 \mu\text{m} / 2)^2$	$2.138 \times 10^{-8} \text{ m}^2$
I_s	(Saturation intensity ($\frac{h\nu_L}{\sigma_{21}\tau_f}$)) = $\frac{6.626 \times 10^{-34} \times 2.2355 \times 10^{14}}{6 \times 10^{-23} \times 100 \times 10^{-6}}$ $\nu_L = \frac{c}{\lambda_L} = \frac{3 \times 10^8}{1342 \times 10^{-9}} = 2.2355 \times 10^{14} \text{ Hz}$ σ_{21} (Stimulated-emission cross-section) $\approx 6 \times 10^{-19} \text{ cm}^2$ literature: Tucker (Dec 1977) $6 \pm 1.8 \times 10^{-19} \text{ cm}^2$ Jain <i>et al.</i> (1988) $7 \pm 2 \times 10^{-19} \text{ cm}^2$ Innocenzi <i>et al.</i> (1988) $6 \times 10^{-19} \text{ cm}^2$ τ_f (Fluorescence lifetime) 100 μs for 1 at% Nd doped YVO ₄	$2.47 \times 10^7 \text{ W/m}^2$
η_Q	(Pump Quantum efficiency) -see note in 1.06 μm parameters -table 5.1.	1
η_S	(Stokes factor (λ_p/λ_L)) = 808.8 / 1342	0.60
η_B	(Beam overlap efficiency) Assumed to be ≈ 1	1
η_A	(Fraction of pump power absorbed) absorption at pump wavelength $\approx 95\%$ front mirror transmission $\approx 98\%$ $0.95 \times 0.98 = 0.931$	0.931
f_B	(Population of the Stark sub-level within the upper laser level responsible for the laser action - given by equation 2.33) $T = 294 \text{ K}$, $(\Delta\bar{\nu}) = 18 \text{ cm}^{-1}$	0.52
b	(Fluorescence branching ratio to the lower laser level $^4I_{13/2}$ - see figure 2.5)	0.110

Table 5.2: Parameters used for the modelling of the 1.34 μm microchip laser.

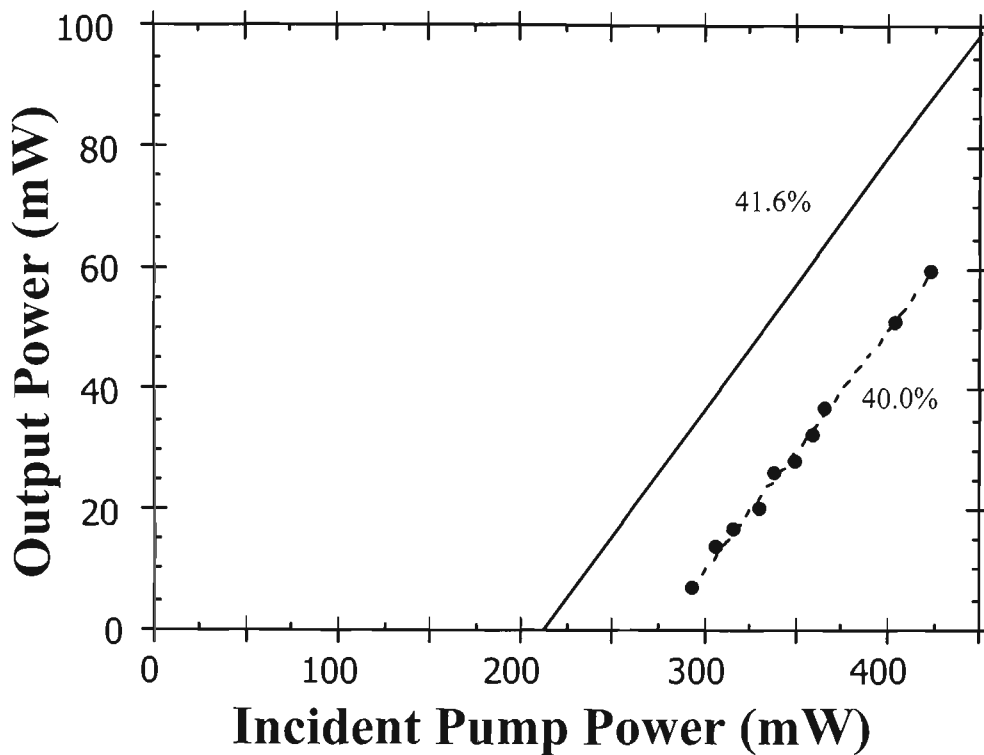


Figure 5.14: Model (solid line) and experimental (dots and dashed line of best fit) results for output power against incident pump power, with the slope efficiency written next to each.

Figure 5.14 shows the model results for the 1.34 μm Nd:YVO₄ microchip laser along with the experimental data from figure 5.8. The theoretically calculated threshold value of 211 mW was between 12 and 25% below the measured threshold values of between 240 and 280 mW. The experimental slope efficiency of 40% was in good agreement with the calculated value of 41.6%.

5.2.3 Performance of 1.34 μm laser - Discussion

Results for the 1.34 μm microchip laser were only considered for the superior π polarization pumping, since it was established that considerably better performance was obtained with π polarization pumping at 1.06 μm and similarly in preliminary testing at 1.34 μm .

Output versus Pump Wavelength

Microchip laser output at 1.34 μm was observed only when the microchip was pumped in the very high absorption region of the 810 nm band from around 807.5 to 810 nm, and not at all on

the 750 nm band. It must be considered that in this case the pump power of approximately 370 mW was only approximately 100 mW above the high threshold pump power needed to achieve lasing at 1.34 μm , at the maximum absorption. (In the same test at 1.06 μm , the pumping was at 5 to 10 times above the threshold pumping power). With the pump power used here, lasing was achieved over a pump wavelength span of greater than 2 nm. This pump wavelength region of lasing is expected to increase with increased pump power.

Output Power, Threshold and Slope Efficiency

A maximum microchip output power of 60 mW, at 1.342 μm , was obtained using a maximum incident pump power of 422 mW. At this level the output spectrum was demonstrating a second longitudinal mode at a level of approximately 20 dB below the main mode. For output powers less than 40 mW the output spectrum was completely single mode. Extrapolating the data of figure 5.8 the 1.34 μm laser demonstrates a threshold incident pumping power of approximately 275 mW, though several tests demonstrated a decrease in the slope efficiency at low pumping powers, and thus lower threshold levels, generally around 240 mW. The laser also demonstrated a maximum slope efficiency of 40%.

Comparison can be made between the present work and that of Taira *et al.* at Fukui University, Japan [see Bowkett *et al.* (1994)], who performed tests on a similar Nd:YVO₄ microchip using laser diode pumping. Their work produced a maximum output of 91 mW with a pump power of 820 mW. The output was multimode at this output power. The laser had a threshold of approximately 285 mW and a slope efficiency of approximately 3%, until a pump power of around 555 mW, where the slope efficiency changed to 46%. Damage to the dielectric coating was noted at the high pump power used.

Zayhowski and Mooradian (May 1989) demonstrated a 1.32 μm Nd:YAG microchip laser with a threshold of approximately 13 mW of absorbed pump power and a slope efficiency of 44%. The microchip had 1.6 weight% Nd doping and a 1 mm cavity length. The most significant difference was the pumping spot size of 50 μm , compared with the 165 μm spot size used in this research, resulting in a greater than 10 fold increase in pump power

density. Gavrilovic *et al.* demonstrated 1.3 μm lasing from a 450 μm cavity length, 4.2% doped, Nd:YAG microchip laser. A minimum threshold of 105 mW, a slope efficiency of 45%, and a maximum single frequency output of 170 mW was achieved with a pump spot size of 25 μm .

For each data point shown in figure 5.8 (input versus output data), the microchip laser output spectrum was measured, and was reproduced in figure 5.9. At pump powers well above threshold a second longitudinal mode reaches threshold and begins to lase, as was evident in the last two spectra. This phenomenon is not unexpected, being consistent with the trends observed for the 1.06 μm laser. Lasing on a second transition, which was shown in the three spectra between 316 mW and 338 mW was not expected. Lasing on this second transition occurred in several of the tests performed, and generally with pump powers in the low to mid 300 mW's region. This second lasing transition never occurred in any tests above approximately 40°C. In contrast, figure 5.10, which was also performed at room temperature ($\approx 20\text{-}21^\circ\text{C}$), but with the pump beam positioned at a different location on the microchip, shows no second transition at any pump power. This location gave a slightly lower threshold of ≈ 270 mW and slope efficiency of $\approx 30\%$, and possibly corresponded to a local difference in material or coating characteristics which discriminates against the second transition.

Gavrilovic *et al.* (1994) also reports simultaneous lasing on two transitions at around 1.3 μm . This is achieved from a 4.2% doped Nd:YAG microchip. At low pump powers (less than three times above threshold) the laser would operate at either 1.319 or 1.338 μm depending on the crystal temperature, at higher pump powers both transitions would operate simultaneously with both transitions operating on a single longitudinal mode.

The measured gain bandwidth at 1.34 μm determined from the data of figure 5.13 was 1.6 nm, or 266 GHz. The calculated mode spacing using equations 2.4 and 2.5 was determined to be 0.84 nm, or 139 GHz. From these values it is clear that more than one mode may occur within the gain bandwidth. Consequently to achieve single longitudinal mode lasing it may be necessary to position one mode close to the centre of the gain profile by changing the microchip temperature.

Output Beam

The full-angle divergence of the 1.34 μm microchip laser output beam was measured to be approximately 12 mrad, and exhibited a TEM_{00} transverse mode structure. This corresponding to a M^2 value of approximately 1.0002, where M^2 is a measure of the beam quality. This output divergence is similar to that observed at 1.06 μm (14 mrad), however it was measured with a more accurate technique. The $1/e^2$ intensity dimensions of the output beam were measured at several locations along the beam path with a beam analyzer, and from these results the beam divergence was calculated.

Temperature Tuning

A tuning rate of the laser output of approximately $-2 \text{ GHz}/^\circ\text{C}$ was given by the data in Figure 5.12, which corresponds to a tuning range of approximately 1.25 nm over the 0 to 100°C tested. With no known literature figure for $\partial n_e / \partial T$ in Nd:YVO₄ at 1.34 μm a direct theoretical comparison could not be made. However, from our experimentally measured frequency shift, the first known value of $\partial n_e / \partial T$ at 1.34 μm in Nd:YVO₄ was deduced to be $10.8 \pm 2.4 \times 10^{-6}/^\circ\text{C}$.

With a pump power of 370 mW single mode operation was achieved up to a temperature of approximately 30°C , at higher temperatures a shorter wavelength mode develops, growing in strength relative to the main mode. Above approximately 70°C the shorter wavelength mode becomes dominant. Similar tests with a slightly lower pump power, approximately 340 mW, show a single mode output up to a temperature of approximately 50°C , but also show lasing on the second transition below 10°C .

The best operation for the 1.34 μm laser, in terms of achieving single longitudinal mode operation, was obtained at room temperature, as was the case for the 1.06 μm laser. However, the presence of lasing on the second transition was a complicating factor. The second transition could be avoided by picking a particular location on the microchip, where the

microchip or coating properties differed, but this did not generally coincide with selecting the best output performance pumping location. Alternatively the second transition could be avoided by using pump powers outside the low to mid 300 mW range (with the same pump beam diameter). Finally it was found that by insuring a low microchip temperature single-mode operation was maintained, with the maximum temperature for single mode lasing depending on the level of incident pump power.

Conclusion

This chapter examined the operation of Nd:YVO₄ microchip lasers operating at 1.06 μm and 1.34 μm . The 1.06 μm microchip laser was shown to be able to lase over a large range of pump wavelengths, in both the 750 and 810 nm absorption bands, with both π and σ polarized incident light. For the 1.34 μm microchip laser output was observed only when the microchip was pumped in the very high absorption region of the 810 nm band. For both lasers the best performance was achieved for π polarized incident pump light.

The 1.06 μm experiments demonstrated a best microchip laser output power of approximately 80 mW for an incident pump power of around 186 mW, with thresholds as low as 20 mW and slope efficiency figures better than 50%. At 1.342 μm a maximum microchip output power of 60 mW was obtained with an incident pump power of 422 mW. The laser demonstrated a minimum incident pumping power threshold of 240 mW, and a maximum slope efficiency of 40%. The model equations established in chapter two were compared to the laser results, and were found to give a good representation of what happened in practice.

The output beams were measured to have low divergence (12 to 14 mrad full angle) and a single transverse mode. This is a distinct advantage in many laser applications, when compared to the typical output of a laser diode.

The output variation caused by the microchip temperature was examined. The longitudinal modes were seen to shift within the gain profile to determine the output modal structure. The lasers were shown to operate with single longitudinal mode output over a range of microchip temperatures, with both lasers having single mode output at room temperature.

Chapter 6 Microchip Amplifiers

Introduction

6.1.1 Amplification at 1.06 μm

Gain against Signal Power

Saturation intensity

Gain against Pumping Power

6.1.2 Model results for 1.06 μm amplifier

6.1.3 1.06 μm amplifier - Discussion

6.2.1 Amplification at 1.34 μm

6.2.2 Model results for 1.34 μm amplifier

6.2.3 1.34 μm amplifier - Discussion

Chapter 6

Microchip Amplifiers

Introduction

The amplification performance of the same Nd:YVO₄ material was tested using the previously characterised microchip lasers as the signal source. A 1 mm cavity length, antireflection coated microchip was tested at both 1.06 and 1.34 μm , as could be provided by the microchip lasers. Unfortunately, no substantial experimental results were obtained at 1.34 μm due to the inability to accurately measure the size and location of the 1.34 μm beam with the available equipment. Results of the experimental investigation of the saturation intensity and the small signal gain are presented here for the 1.06 μm signal. The theoretically expected saturation and the single pass small signal gain for the microchip amplifier has been calculated at both wavelengths. The gain is first modelled using the small signal gain equation established within the laser model, and secondly by re-writing the small signal gain equation to account for the high pump beam intensities in the microchip. The model results are compared with data obtained experimentally.

6.1.1 Amplification at 1.06 μm

Gain against Signal Power

The amplifier operation was measured with different signal powers to investigate where the gain of the amplifier could be considered to be within the small signal gain region. The concepts of small signal gain and saturation intensity are outlined in section 2.2.2. Tests were also conducted at different pumping powers, since the gain saturation is not simply governed by the non-amplified signal intensity (input), but by the signal intensity reached within the amplifier (i.e. higher gain results in a higher signal intensity). The following graph (figure 6.1) shows the gain achieved for increasing signal power at three pump powers. The signal power

indicated is a measure of the signal after the amplifier microchip with no incident pump power, and the gain is the ratio of the signal after the microchip with and without pumping.

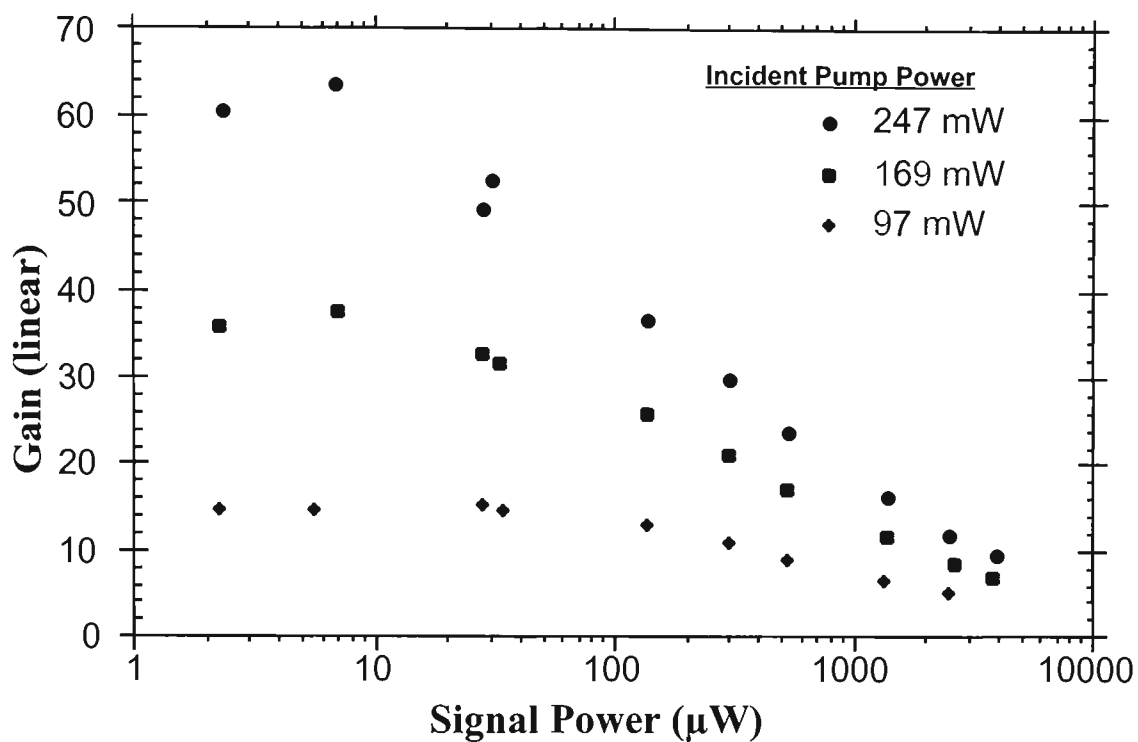


Figure 6.1: Amplifier Gain versus the transmitted non-amplified signal power, for three different incident pumping powers, using a 1 mm length of AR coated, $1.0 \pm 0.1\%$ doped Nd:YVO₄ crystal. Minimum pump and signal beam diameters were approximately 30 μm.

In figure 6.1 it can be seen that for small signal powers initially an almost constant gain level is achieved for increasing signal powers (corresponding to a region of small signal gain), then a drop in gain is observed as the signal power further increases. For each increase in incident pumping power the reduction in gain begins at a lower signal power. This is attributed to a higher signal intensity within the amplifier due to the larger gain provided by the increased pumping power, causing an earlier onset of saturation effects.

Saturation Intensity

From figure 6.1, an estimate of the saturation intensity for the pump diameter of $\approx 30 \mu\text{m}$ can be made. The saturation intensity is defined as the signal level at which the small signal gain level has dropped to half its initial value. Examining the 97 mW incident pump power case,

the maximum gain is approximately 14. At a signal level of around 1 mW (1000 μ W) the gain has dropped to half this level (7). Therefore the amplified signal level reached in the amplifier microchip would be around $7 \times 1 \text{ mW} = 7 \text{ mW}$, corresponding to the saturation power. Given a beam diameter of 30 μm , this equates to a saturation intensity of $1.0 \times 10^7 \text{ W/m}^2$.

At an incident pump power of 169 mW, a maximum gain of approximately 37 was obtained, while at a gain level of half this (18.5) the signal level was approximately 0.4 mW. Therefore the saturation power was around $18.5 \times 0.4 \text{ mW} = 7.4 \text{ mW}$. Similarly at a pump power of 247 mW, the maximum gain was around 62, with the signal level at half this gain being approximately 0.25 mW. The saturation power was therefore $31 \times 0.25 \text{ mW} = 7.75 \text{ mW}$. These results are summarized in table 6.1 below. Therefore to stay within the small signal gain regime the signal power reached within the amplifier microchip should be kept well below the 7 mW level.

Incident Pump Power (mW)	Maximum Gain	Half Maximum Gain	Approximate Signal Power at Half Maximum Gain (μ W)	Saturation Power (mW)	Saturation Intensity (W/m^2)
97	≈ 14	7	1000	$7 \times 1 = 7$	1.0×10^7
167	≈ 37	18.5	400	$18.5 \times 0.4 = 7.4$	1.05×10^7
247	≈ 62	31	250	$31 \times 0.25 = 7.75$	1.1×10^7

Table 6.1: Summary of experimentally determined saturation power and intensity results, with a pump diameter of $\approx 30 \mu\text{m}$.

Gain against Pump Power

The Gain versus incident pump power graph given as Figure 6.2 was generated from the gain data achieved with both pump and signal beams focused to minimum beam diameters of $\approx 30 \mu\text{m}$, and an unamplified signal power of approximately $6.5 \mu\text{W}$. The output signal was multiplied by approximately four (6 dB) with an incident pump power of less than 35 mW, and a gain of greater than 92 (19.6 dB) was achieved with an incident pump power of 347 mW. A change in the slope of the gain curve is observed above approximately 100 mW of incident

pump power. The level of the amplified output signal fluctuated at very high gains, with a maximum fluctuation of approximately $\pm 10\%$ (or $\approx \pm 0.5$ dB) at the greatest measured gain.

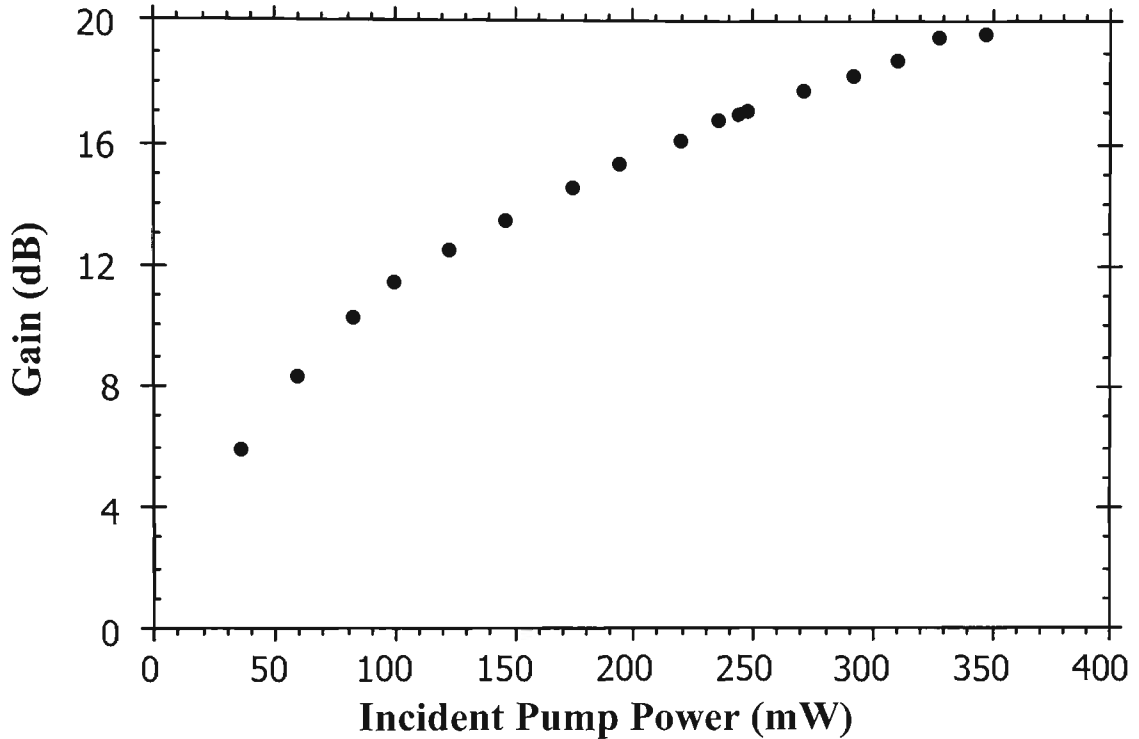


Figure 6.2: Gain (dB) versus incident pump power for 30 μm minimum pump and signal beams, using a signal power of $\approx 6.5 \mu\text{W}$ at 1.06 μm .

The diameter of the pump beam was then made considerably larger than that of the signal beam (30 μm), with the pump beam minimum diameter increased to 100 μm . Figure 6.3 was generated from the gain data obtained with this larger pump beam size. The unamplified signal power during this test was approximately 7.2 μW . In this case the maximum gain achieved was approximately 4.8 dB with 386 mW of incident pump power. The decrease in the slope of the gain with increase in pump power was more pronounced here in comparison to having 30 μm pump and signal beams where the spatial overlap of the pump and signal power are better matched.

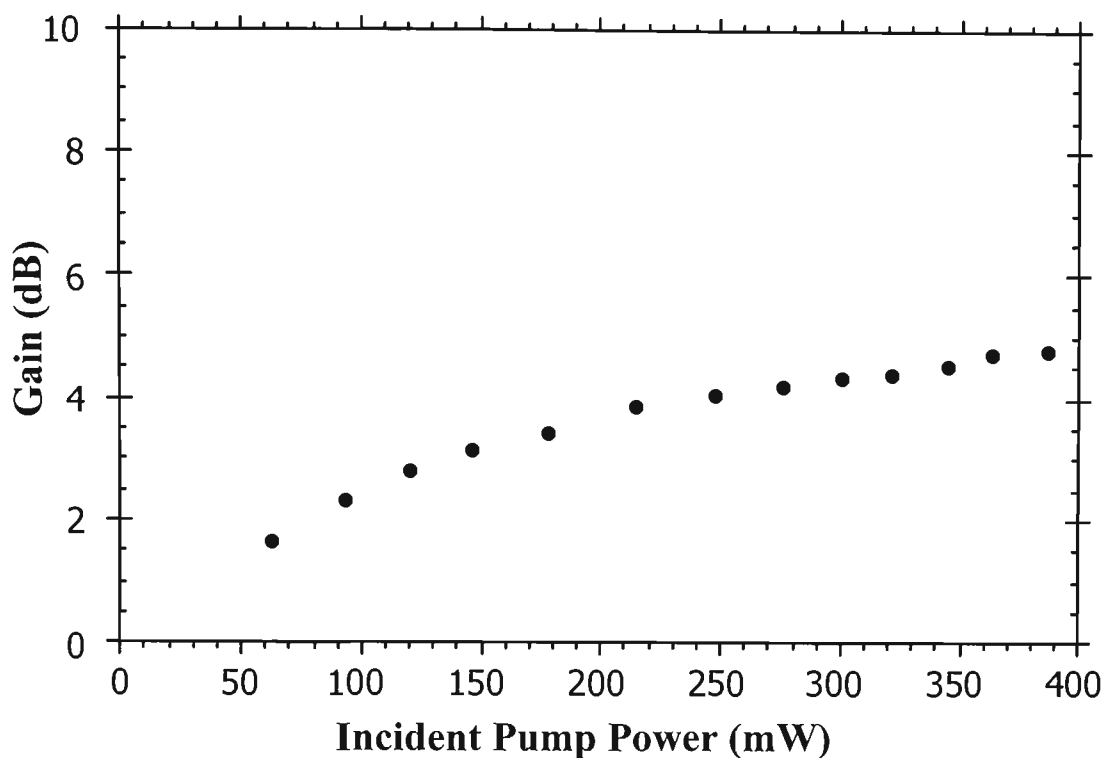


Figure 6.3: Gain (dB) versus incident pump power for pump and signal minimum beam diameters of 100 and 30 μm , respectively, while using a signal power of $\approx 7.2 \mu\text{W}$. Achieved at 1.06 μm using a 1 mm length of 1.0 ± 0.1 doped Nd:YVO₄ microchip.

6.1.2 Model results for 1.06 μm amplifier

The saturation intensity of the microchip amplifier has been calculated based on the theory outlined in section 2.2.2, in order to verify whether the signal intensity of the data recorded was within the region normally considered as small signal gain. Assuming small signal intensity levels the expected gain trends of the Nd:YVO₄ microchip amplifier were modelled. The modelling results assume a constant beam diameter through the amplifier and unity overlap between the pump and signal beams. Though this is not strictly the case, it is a good assumption for this simple model, and provides a single calculation for the entire amplifier length. The amplifier small signal gain was first calculated using the small signal gain equation established within the laser model. A second model further considers the high intensity pump beam of the amplifier and rewrites the small signal gain equation to better represent the experimentally obtained results.

Saturation intensity

The saturation intensity, which is given by equation 2.20, has been established in the laser modelling section (5.1.2) for gain at 1.06 μm in Nd:YVO₄ to be equal to $1.2 \times 10^7 \text{ W/m}^2$ (see Table 5.1). Assuming a constant beam area through the amplifier microchip of πr^2 , where r equals approximately 15 μm , then the **theoretical signal saturation power** for the amplifier at 1.06 μm (with a 30 μm beam spot size) is:

$$1.2 \times 10^7 \times \pi (15 \times 10^{-6})^2 \approx 8.5 \times 10^{-3} \text{ W or } \mathbf{8.5 \text{ mW}}$$

Calculated Gain

Model One

The first model used to predict the amplifier single pass small signal gain utilized the gain equations established within the laser model. To calculate results for the predicted gain, equation 2.38 from section 2.2.2 (Amplifier Model) is used:

$$G_0 = \exp \left[\frac{\sigma_{21} \tau_f \eta_B \eta_A P_{IN}}{h \nu_p A} \right]$$

in combination with equation 2.39

$$\text{Gain (dB)} = 10 \log G_0$$

Model Two

The second model which rewrites the gain equation, no longer assuming that $W_p \ll 1/\tau_f$, uses equations 2.45 and 2.46 to calculate the gain:

$$G_0 = \exp \left[\frac{\sigma_{21} \psi P_{IN}}{1 + \sigma_{ab} \psi P_{IN}} \right],$$

where

$$\psi = \frac{\tau_f \eta_A \eta_B}{h \nu_p A}.$$

These are again used in combination with equation 2.39 to obtain the gain in units of dB.

The 1.06 μm Nd:YVO₄ amplifier parameters used within these equations are as follows:

Parameter	Reason	Value
σ_{21}	(Stimulated emission cross-section) literature varies between 10 to 20x10 ⁻¹⁹ cm ² , 15.6x10 ⁻¹⁹ cm ² from DeShazer (1994)	15.6x10 ⁻¹⁹ cm ²
σ_{ab}	(Absorption cross-section at 808 nm)	2.7x10 ⁻¹⁹ cm ²
τ_f	(Fluorescence lifetime) 100 μs for 1 at% Nd doped YVO ₄ [DeShazer (1994)]	100x10 ⁻⁶ s
P_{IN}	(Incident pump power)	Varied
η_A	(Fraction of pump power absorbed) absorption at pump wavelength $\approx 99.7\%$ front mirror transmission $\approx 99\%$ $0.997 \times 0.99 \approx 0.987$	0.987
η_B	(Beam overlap efficiency) assumed to be unity	1
h	(Planck's constant) = 6.626176x10 ⁻³⁴ Js	6.626176x10 ⁻³⁴ Js
ν_P	(Pump frequency) $\frac{c}{\lambda_P} = \frac{3 \times 10^8}{808.8 \times 10^{-9}} = 3.709 \times 10^{14}$ Hz	3.709x10 ¹⁴ Hz
A is the area of the pump.		

Table 6.2: Parameters used for modelling of 1.06 μm amplification.

First model

As a simple first model the signal and pump beams are considered to have unity overlap ($\eta_B = 1$) and equivalent constant beam diameters. This allows for a single calculation to obtain the gain predicted through the 1 mm microchip at any particular pump power level. Figure 6.4 was produced by applying this calculation over a large portion of the available pumping range. The figure shows the predicted gain under the above conditions with beam diameters of 30 μm and 50 μm , where $A(\text{Pump area}) = \pi r^2$. (The 50 μm calculation is provided

as a comparison so that the significant effect of changing the beam size within this calculation may be appreciated).

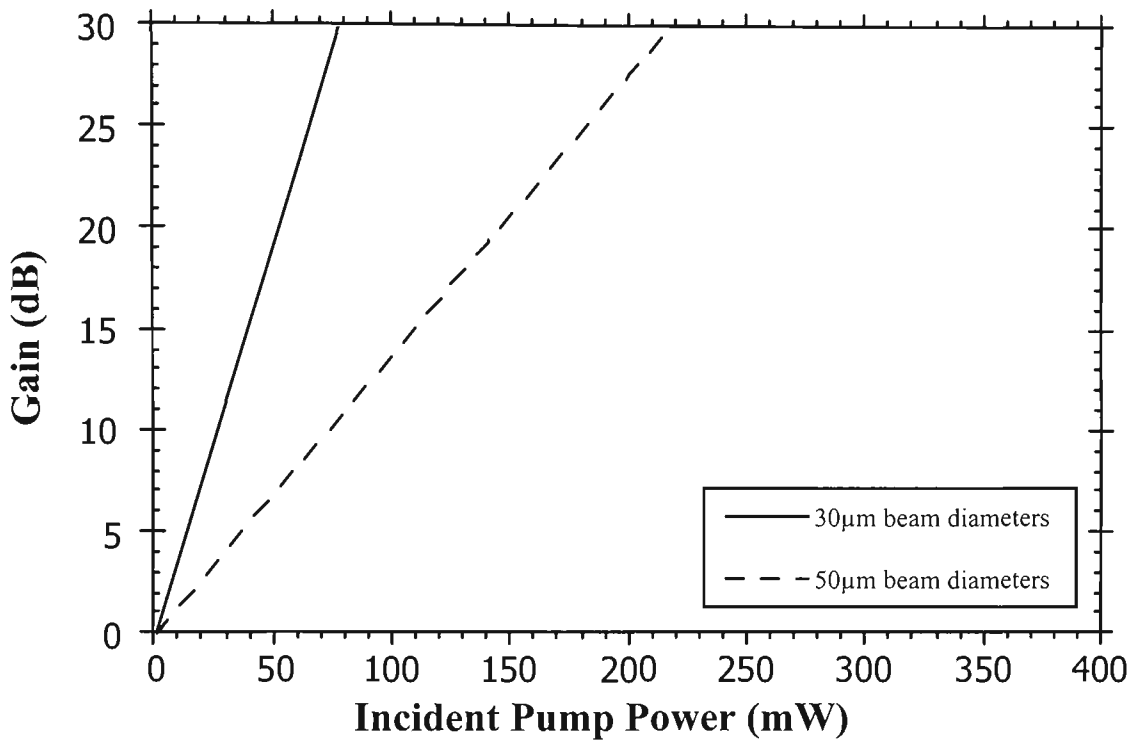


Figure 6.4: Calculated amplifier Gain (dB) at $1.06\ \mu\text{m}$ for a 1 mm length of $1.0\pm 0.1\%$ doped Nd:YVO₄ with constant beam diameters and unity overlap (model one).

Second model

For the second model the overlap between the pump and signal beams (η_B) was still assumed to be unity and the beam diameter constant. The calculated gain as a function of incident pump power using the second model is shown in figure 6.5 for a beam diameter of $30\ \mu\text{m}$. This model deviates greatly from the first model, especially as the incident pump power increases. There is a 3 dB difference at just over 25 mW incident pump power, and greater than 10 dB difference at 60 mW incident pump. The asymptotic behaviour of this model is obtained by considering the pump power saturation brought about by the high intensity pump beam.

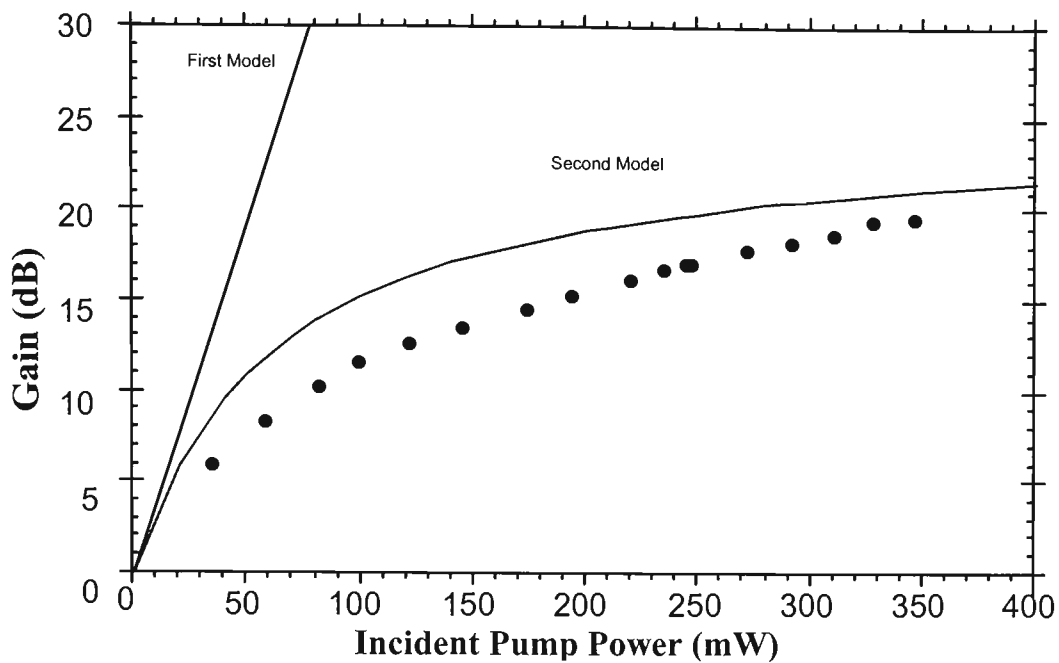


Figure 6.5: Experimentally measured amplifier Gain (dB) (dots) from a 1 mm long $1.0 \pm 0.1\%$ doped Nd:YVO₄ microchip, compared with that predicted by the two models.

In figure 6.5 the experimental data has been reproduced along side the results of the above theoretical model calculations. From this graph the virtue of considering the pump power intensity, and therefore pump power saturation, within a second simple model can be seen.

100 μm pump diameter

The results obtained for an increased pump beam minimum diameter of approximately 100 μm were also modelled using only stage two of the modelling, and have been displayed in figure 6.6. The line shows the predicted small signal gain based on the pump beam size and incorrectly assumes unity overlap between the signal and pump beams. The effect of two gaussian beams of different radii on the average gain for the signal is complex. A reasonable fit to the experimental data could be achieved by assuming that an average of 50% of the absorbed pump beam was contributing to the gain of the signal. In comparison, the 1/e point of the signal overlaps with 31% of the pump beam intensity. To carefully model the interaction between the dissimilar signal and pump beams would require a point by point analysis across the beam surface, and was considered beyond the scope of this thesis.

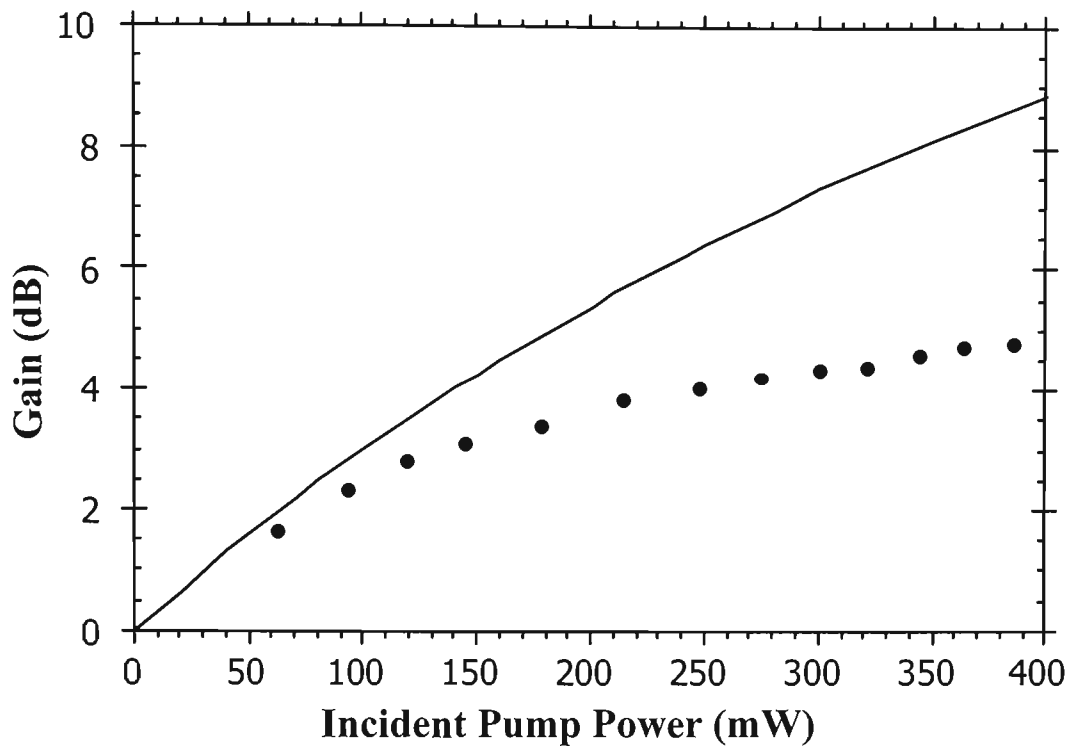


Figure 6.6: Measured Gain (dB) (dots) from a 1 mm long, $1.0 \pm 0.1\%$ doped, Nd:YVO_4 microchip, compared with the calculated gain from model two (minimum pump beam diameter of $100 \mu\text{m}$, minimum signal beam diameter of $30 \mu\text{m}$).

6.1.3 $1.06 \mu\text{m}$ amplifier – Discussion

Saturation Intensity

Meaningful comparison between theory and experiment for an optical amplifier may be achieved in the small signal regime. Consequently, it was important to determine the small signal regime for the particular experimental parameters of this work. In theory this region is considered to be when the signal level was well below the Saturation intensity (eqn. 2.20). Assuming a constant beam diameter of $30 \mu\text{m}$ through the amplifier microchip the saturation signal power was calculated to be approximately 8.5 mW (saturation intensity = $1.2 \times 10^7 \text{ W/m}^2$). This theoretical calculated value is in good agreement with the experimental saturation signal power values of between 7 and 7.75 mW as determined from the data of figure 6.1. The saturation power was defined as the signal power within the amplifier when the gain had dropped to half of its initial small signal gain value.

To remain in the small signal gain region the pumping power must also be considered, since this determines the rate of signal growth within the amplifier. It can be shown, from figure 6.1, that for a pump level of 97 mW one needs to start with an unamplified signal of less than $\approx 100 \mu\text{W}$ to avoid saturation. Similarly, for a pump level of 169 mW one needs to start with an unamplified signal of less than $\approx 11 \mu\text{W}$ to avoid saturation. For a pump level of 247 mW it was difficult to establish where the small signal gain begins to drop with just two points at very low signal power, but with an unamplified signal of less than $\approx 10 \mu\text{W}$ one should avoid signal saturation.

Amplifier Gain

Careful adjustment of the crystal position and beam overlap were needed to achieve high gain amplification. High gain values were obtained with both pump and signal beam minimum diameters of approximately $30 \mu\text{m}$ (≈ 92 times gain (19.6 dB) for 347 mW of incident pump power). However, at these high gain values the amplified output signal suffered variations in magnitude of approximately $\pm 10\%$ (± 0.5 dB). At a lower pump power of 292 mW, a gain of 62.6 (18 dB) was achieved and there was less than 5% variation in the output amplified signal level. Further reduction of the pump power to 244 mW resulted in 50.3 times gain (17 dB). Here the output signal variation was reduced to less than 2%. These fluctuations in the output amplified signal may have a number of causes. Firstly, since the signal and pump beam overlap is critical any variations in this, caused by pump or signal beam movement, will result in rather large variation of amplified signal output. Secondly, output fluctuations may occur because of small variations in the level, or spatial property, of the signal provided by the laser diode pumped microchip laser. These may be caused by variations in the laser diode output, or temperature variations in the laser diode or microchip laser.

The initial amplifier modelling (equations 2.38 and 2.39) which utilized the gain equation established in the laser model predicted very large gains for the system, with in excess of 50 dB gain at an incident pump power of just over 130 mW ($30 \mu\text{m}$ diameter beam). This was a very large over estimate of the gains which had been achieved experimentally.

With the data appearing to asymptote, a saturation effect seemed evident. The signal power level had been tested and then set at a level to avoid signal saturation, the effect of pump power saturation was therefore considered. In establishing the small signal gain within the laser model, it is normally assumed that the pump rate is significantly smaller than the reciprocal of the fluorescence lifetime. This condition was found not to be valid with the high pump intensities used in the microchip amplifier. The gain equation was subsequently re-established using equation 2.17.

From figure 6.5 it can be seen that this second model demonstrates a saturation effect. On comparison to the experimental data the second model deviates by a maximum of approximately 3.5 dB. The model fit is reasonable considering the broad assumptions that were placed on the model. The assumed constant beam diameter actually varies through the length of the microchip, and the beam overlap assumed to be unity varies as the two beams converge and diverge at different angles. Also the beam waist diameter will differ within the microchip amplifier material to that measured in free space.

In an attempt to test what could be considered a more practical amplifier, where the alignment and overlap of the signal beam would not be so critical, a larger minimum pump beam diameter was used, along with the same 30 μm diameter signal. However, with a larger pump minimum size of around 100 μm diameter, large gains were not obtained, with the maximum gain being approximately 5 dB. The larger pumping diameter resulted in a much smaller pump intensity, and thus the inversion intensity was greatly reduced within the amplifier. Figure 6.6 shows the measured gain results compared to the gains predicted by the second small signal gain model. The model predicts much reduced gains when compared to the 30 μm pump beam, however the gain line does not yet (at these incident pump powers) show an asymptote, due to the reduced pump beam intensity. The data does not follow the model as closely as in the previous case. This is thought to be due to the initial assumption of unity beam overlap, where here there is a signal beam with a minimum waist diameter of 30 μm and a pump beam with a minimum waist diameter of 100 μm .

Practically it may also be possible to use Nd:YVO₄ microchips to amplify signals from a Nd:YAG laser source, since there is a close match between the Nd:YVO₄ and Nd:YAG gain profiles at 1.06 μm. This principle has been demonstrated in bulk samples of Nd:YVO₄ by Will Grossman of Lightwave Electronics Corp. [DeShazer (1994)] and Bernard *et al.* (1994).

The gain co-efficient achieved at 1.06 μm in this Nd:YVO₄ microchip amplifier work is substantially greater than is found in previously reported work on miniature Neodymium doped amplifiers. Where the gain co-efficient is defined in equation 2.37, and is equal to $\ln G_0 / \text{length}$. Chan (1987) predicted a gain co-efficient value of 0.4 cm⁻¹ from his Nd:YAG slab amplifier design with laser diode side pumping of 300W. Baer *et al.* (1992) obtained a figure of 0.34 cm⁻¹ from a tightly folded resonator configuration Nd:YAG amplifier which was effectively end pumped by an array of 10, 1W diodes. Using a multipass end pumped Nd:YVO₄ amplifier Plaessmann *et al.* (1993) achieved a figure of 2.3 cm⁻¹ using 13 W of laser diode pump power. Brignon *et al.* (1995) achieved approximately 4 cm⁻¹ from an end pumped two-pass Nd:YVO₄ amplifier with 100 W laser diode pumping. From a laser diode side pumped Nd:YVO₄ amplifier Bernard *et al.* (June 1994) achieved a figure of approximately 7 cm⁻¹ with 60 W of pump power. Using a laser diode pumped double pass Nd:YVO₄ microchip amplifier Taira (1993) obtained a figure of 7.14 cm⁻¹. From this work a figure of approximately 45 cm⁻¹ has been achieved (gain of 92, over 1 mm length) with a pump power of 347 mW. This figure is substantially higher than previously reported figures, however it relies heavily on the good overlap of signal and pump beam afforded by the well collimated nature of the Ti:sapphire pump beam, which allows high gain to be achieved in a short length. To achieve high gains laser diode pumped systems have generally had to utilize increased interaction length, with multiple passes or zig-zag paths.

6.2.1 Amplification at 1.34 μm

Attempts were made to operate the amplifier at a signal wavelength of 1.34 μm, as was offered by the Nd:YVO₄ microchip laser, however without an ability to accurately analyze the relative

location and properties of the signal beam, with respect to the pump, this task was very difficult. (The detector housed within the beam analyzer was not sensitive to light near 1.34 μm). Alternative methods, as outlined in section 3.6.5, were undertaken in an attempt to obtain a measure of the 1.34 μm beam size and location. A maximum gain of 1.40 (1.46 dB) was achieved with an incident pump power of ≈ 160 mW. This was with an unamplified signal power of approximately 29 μW . The expected small signal gain at 1.34 μm was modelled, and is outlined below.

6.2.2 Model results for 1.34 μm amplifier

Saturation intensity

The saturation intensity which is given by equation 2.20, has been established in the laser modelling section (5.2.2) for gain at 1.34 μm in Nd:YVO₄ to be equal to 2.47×10^7 W/m² (see Table 5.2). Assuming a constant beam area through the amplifier microchip of πr^2 , where r equals approximately 15 μm , then the **theoretical signal saturation power** for the amplifier at 1.34 μm (with a 30 μm beam spot size) is:

$$2.47 \times 10^7 \times \pi(15 \times 10^{-6})^2 \approx 17.5 \times 10^{-3} \text{ W or } 17.5 \text{ mW}$$

Calculated Gain

The same modelling technique from section 2.2.2 has been applied for the 1.34 μm case as was used in the 1.06 μm case, with the stimulated-emission cross-section, σ_{21} , changed to 6×10^{-19} cm² [Innocenzi *et al.* (1988)] within the gain equation. The calculations have been based on a beam diameter of 30 μm , though the beam diameter of the experimental result was not accurately known. Figure 6.7 shows the gain predicted from both the first and second models, along with the data point obtained. The models show a greatly reduced gain in comparison with that obtained at 1.06 μm .

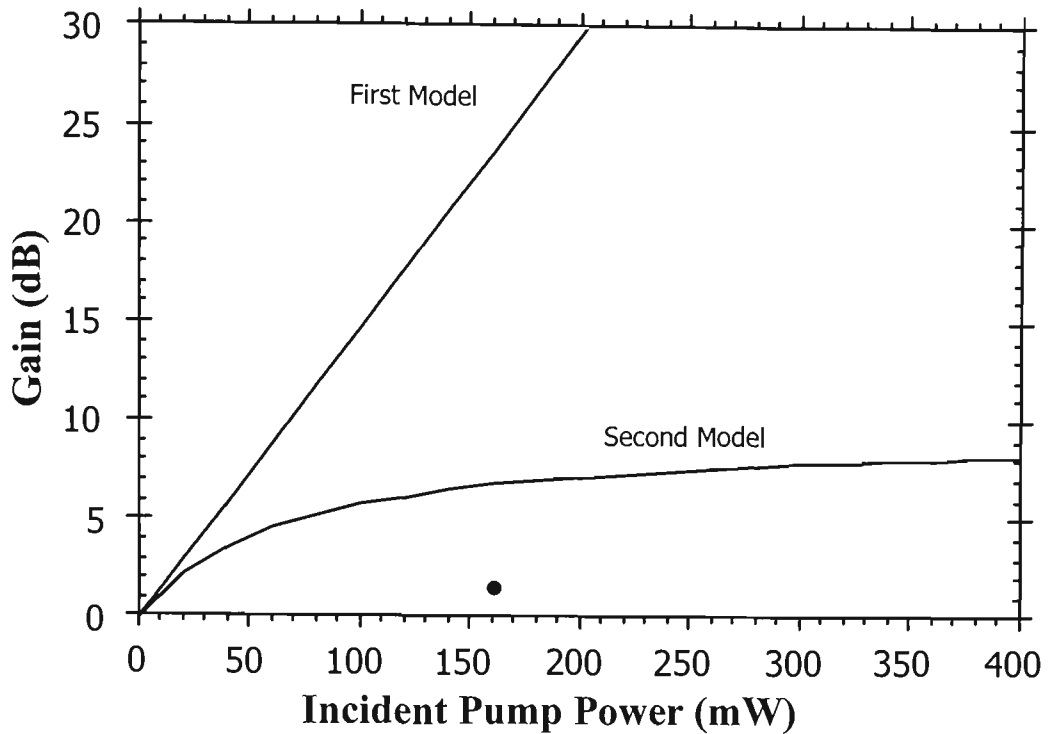


Figure 6.7: Graph of the predicted single-pass small signal amplifier Gain (dB) at 1.34 μm from a 1 mm length of $1.0 \pm 0.1\%$ doped Nd:YVO₄. The dot is the only experimental result.

6.2.3 1.34 μm amplifier - Discussion

The beam analyzer contained a silicon detector, and was thus not able to measure at a wavelength of 1.34 μm , this therefore allowed no accurate means by which to measure and establish the small beam diameters and the high degree of beam overlap which were required. Therefore, as outlined in section 3.6.5, a 1.06 μm signal was aligned for maximum achievable gain from the amplifier, then the 1.34 μm signal was set up in parallel in an attempt to get similar input signal beams, and thus similar beam sizes and overlaps. During these attempts a maximum gain of 1.40 (1.46 dB) was achieved with an incident pump power of approximately 160 mW. The difficulty with this method was that although the two beams may have looked similar on an IR detector card at several different points along the beam path (two locations where the beams were expanded), they probably started with different beam waist sizes and beam divergences at their respective laser microchips. They would therefore converge with different spot sizes and at slightly different locations. The gain result achieved was

approximately 3.6 times below the small signal gain predicted for that pump power at 1.34 μm , assuming a 30 μm diameter beam (figure 6.7). Obtaining results with better agreement would require an accurate measurement of the 1.34 μm signal beam size and location.

The higher theoretically predicted saturation signal power at 1.34 μm of ≈ 17.5 mW, in comparison to ≈ 8.5 mW at 1.06 μm (for 30 μm beam diameter), suggests that there would be a ‘roll-off’ of the gain results from the predicted small signal gain line due to signal saturation at a higher pump power than for 1.06 μm . This may to some extent compensate for the lower gains predicted at 1.34 μm .

The predicted gain is substantially lower than that for a 1.06 μm signal, this is because of a stimulated emission cross-section value which is approximately 2.5 times lower than at 1.06 μm . The calculations gave a predicted gain of ≈ 7.3 dB with 200 mW incident pump power at 1.34 μm , in comparison to ≈ 18.9 dB gain for the same pump power at 1.06 μm .

Conclusion

This chapter examined the performance of the material Nd:YVO₄ as a microchip amplifier. Firstly the signal saturation within the amplifier was tested to determine the small signal region. The signal saturation intensity levels found were in good agreement with that predicted. Small signal single pass gains as high as 19.6 dB were achieved with the 1mm long Nd:YVO₄ microchip amplifiers at a signal wavelength of 1.06 μm for 30 μm pump and signal minimum beam diameters. An increase in the pump beam minimum diameter to 100 μm saw a large reduction in the gain, with the best gain being approximately 5 dB. A small signal single pass gain model based on the gain equation established directly from the laser model gave a gross over estimate of the experimentally obtained gains. A second model which considered the pump power saturation caused by the high pump beam intensities within the amplifiers gave reasonable agreement with the data obtained.

Chapter 7 Conclusions/Summary

Introduction

7.1 Nd:YVO₄

7.2 Microchip lasers

7.3 Microchip Amplifiers

7.4 Current and Future Work

Chapter 7

Conclusions / Summary

Introduction

The initial focus of this work involved further study into the operation of a 1.06 μm Nd:YVO₄ microchip laser (initial studies had been reported by Taira *et al.* (1991)). By using the flexibility offered by a Ti:sapphire laser pump source, the performance of the microchip laser at different pump wavelengths was investigated, along with the lasing threshold and slope efficiency at the peak pump wavelength. The temperature tunability of the laser's output was studied, and the conditions under which the laser operated with a single longitudinal mode output were established. The same variables were also investigated for a similar Nd:YVO₄ microchip laser operating for the first time (to the author's knowledge) on the 1.34 μm laser transition. Theoretical predictions of the lasing threshold and slope efficiency, established from rate equations for a four-level lasing system, were compared to those results found experimentally.

Further experiments examined Nd:YVO₄ microchips as miniature small signal single-pass optical amplifiers at both the 1.06 and 1.34 μm wavelengths. The saturation intensity of the material was determined and compared to that theoretically predicted, given a known pump beam diameter. The experimentally measured gain was compared to that modelled theoretically.

Since commencing this thesis there has been considerable research into both the material Nd:YVO₄ and the concept and application of microchip laser technology. The advent of laser diode pumping has renewed interest in Nd:YVO₄ as a laser material and substantial research effort has been directed at improving the quality of the crystals. Commercially available high quality crystals were made available in approximately 1993. Rapid development of commercial products based on the material has occurred since, both in the area of high power laser diode pumped bulk Nd:YVO₄ systems and microchip based Nd:YVO₄ systems.

Summarized through the first part of this chapter are the main conclusions drawn from this work. The results gathered from tests on the Nd:YVO₄ samples themselves are examined first, followed by consideration of the operation and performance achieved from the microchip lasers and amplifiers. In the final section of this chapter other current work, and possible future work with Nd:YVO₄ and/or microchips is briefly described.

7.1 Nd:YVO₄

The non-coated Nd:YVO₄ microchip sample showed several regions of absorption through the visible and near infrared region of the spectrum, as was shown in figure 4.2. The percentage absorption was measured across the 750 nm and 810 nm absorption bands, and these figures were compared to laser performance at different pump wavelengths.

For the 0.5 mm length of Nd:YVO₄ sample tested, and within the 750 nm absorption band, the π polarized incident light showed a maximum absorption of approximately 56% at 742.9 nm, and the σ polarized light a maximum absorption of approximately 41% at 755.3 nm. These percentage figures correspond to absorption co-efficients of 16.3 cm⁻¹ and 10.7 cm⁻¹ respectively. The maximum absorption was however within the 810 nm absorption band, where the maximum absorption was 94.6% for π polarized light at 808.51 nm, and 62.3% for σ polarized light at 808.68 nm. These correspond to absorption co-efficients of 58.2 cm⁻¹ and 19.5 cm⁻¹ respectively. It was shown that in general the best absorption was obtained with π polarized incident light.

The peak absorption co-efficient obtained was shown to be more than six times greater than that for similarly doped Nd:YAG (Table 4.2) and the absorption bandwidth was shown to be approximately six times wider. Therefore when considering a microchip laser system it has been shown that the absorption properties of the laser material Nd:YVO₄ are more suitable than those of Nd:YAG.

The fluorescence measurements revealed gain bandwidths of between 0.86 and 0.93 nm at 1.06 μ m, and a gain bandwidth of \approx 1.6 nm at 1.34 μ m. The expected mode

spacing for a 0.5 mm long microchip of 0.52 nm at 1.06 μm and 0.84 nm at 1.34 μm indicated that either one or two longitudinal laser modes would be expected in the laser output. The microchip laser tests therefore determined under what conditions single longitudinal mode operation was possible with the 0.5 mm long microchips. The Stark sub-levels responsible for the lasing transition were identified by comparing the profile of the fluorescence diagram in the region of the laser transition, with the known energy level values. The main laser transitions were identified as originating from the lowest Stark sub-level of $^4F_{3/2}$ to either the lowest Stark sub-level of $^4I_{11/2}$ (1.06 μm transition) or the lowest Stark sub-level of $^4I_{13/2}$ (1.34 μm transition). In the 1.34 μm case a second transition was frequently observed which corresponded to a transition from the lowest Stark sub-level of $^4F_{3/2}$ to the second lowest Stark sub-level of $^4I_{13/2}$.

7.2 Microchip Lasers

A microchip laser is a very simple laser device which may produce a single longitudinal mode laser output. Its inherent compact size and possibilities for mass production will inevitably see this type of laser device used for many applications.

Low thresholds, in the tens of milliwatts region, were possible with the 1.06 μm laser, correspondingly slope efficiencies up to 56.6% were achieved, therefore producing a very efficient laser source. The 1.34 μm laser exhibited a much higher threshold, in the region of 240 to 275 mW, due to fluorescence competition with the 1.06 μm transition. However, above threshold this laser exhibited high slope efficiency, up to 40%. With the large number, and decreasing price, of higher power laser diodes in the 800 nm region, cost efficient laser diode pumped versions of the Nd:YVO₄ microchip lasers at output wavelengths of 1.06 and 1.34 μm are achievable.

It was necessary to place restrictions on the operating conditions to maintain single longitudinal mode output for the experiments on the 0.5 mm long Nd:YVO₄ microchip lasers. At pump powers well in excess of the threshold pump power, side modes in the laser output

spectra were observed. Approximately 150 to 180 mW above threshold for the 1.06 μm laser, and approximately 100 to 150 mW above threshold for the 1.34 μm laser. The additional modes appeared due to the increase in the gain bandwidth associated with higher pumping powers.

The range of temperatures over which the microchip laser could operate and maintain single mode operation was restricted. The 1.06 μm laser operated with a single mode output of approximately 60 mW over a temperature range of 50°C, and the 1.34 μm laser with a single mode output of approximately 40 mW over 30°C. These were observed whilst testing between 0 and 100°C. Both lasers operated single mode at room temperature, that is, without needing any cooling. To obtain single mode operation with the 1.34 μm laser, it was also found necessary to consider the possible appearance of a second laser transition at around 1346 nm. The limitations described above for single mode operation could be relaxed by having a thinner microchip, and thus broader longitudinal mode spacing. This would result in an increased output power prior to the appearance of any side modes, and a wider single mode tuning range, but would result in a reduced system efficiency resulting from a reduction in the absorbed pump power. In addition, an increase in neodymium concentration to combat the reduced absorption would also result in a reduced fluorescence lifetime (see for example a study of neodymium concentration versus lifetime by DeShazer (1994)).

Changing the temperature of the microchip provides a simple method of tuning the wavelength of the microchip laser output. This has been achieved in the current investigation by controlling the current of a Peltier cooling/heating device mounted against the microchip holder. A tuning range of ≈ 0.6 nm at -1.5 GHz/°C was achieved for the 1.06 μm laser, and ≈ 1.25 nm at -2 GHz/°C for the 1.34 μm laser, over the 0 to 100°C range tested. As described above, single mode operation was observed only over a portion of this range, but given the right thickness of microchip, single mode output could be achieved over the entire gain region.

The quality of the coatings, and possibly the Nd:YVO₄ material itself, needs further improvement above the quality of samples used in this work. Throughout these tests great variability of operation at different locations on the microchips was observed. The Nd:YVO₄

microchip samples used for this work were obtained in 1991-92, since this time it appears the quality and consistency has improved, with recent review articles in laser magazines commenting on this fact[e.g. DeShazer (1994)]. Advertising of the commercial availability of the material from several sources in 1994 and 1995 also gave a strong indication of improved quality.

Simple models, based on rate equations for a four level laser system, were used to predict values for the laser threshold and slope efficiency of the microchip lasers at the two wavelengths studied. In most cases the models were found to be in good agreement with experimental. A predicted threshold value of 24.4 mW was calculated for the 1.06 μm laser, whilst the laser demonstrated threshold values between 20 and 34 mW (π polarization). The predicted slope efficiency was 55.8%, while the laser operated with a maximum slope efficiency of 56.6%. At 1.34 μm the predicted threshold of 211 mW considers the competition of the dominant 1.06 μm fluorescence, however it was still 12 to 25% below the measured threshold which varied between 240 and 280 mW. The predicted slope efficiency of 41.6% is in good agreement with the 40% determined experimentally.

The laser modeling neglects any loss due to upconversion, which may reduce the available gain at high pump powers. While fluorescence from higher levels than the pump level, associated with upconversion, were not observed in the current tests, it is known that upconversion (or Excited State Absorption) is a possible loss mechanism in Neodymium solid-state lasers. [See for example Kliewer *et al.* (1989)]

The Nd:YVO₄ microchip laser may find applications as transmitters or sources in many different systems, be that as a transmitter of signals or information, or in a sensing system. Nd:YVO₄ lasers may replace the less efficient Nd:YAG lasers for many applications particularly as there is a close match between the output wavelengths of Nd:YVO₄ and Nd:YAG near 1.06 μm . Frequency doubled Nd:YVO₄ microchip lasers are already used in applications where the shorter wavelength green output (532 nm) is useful, perhaps including: optical storage, or replacing more-expensive and bulky air or water-cooled argon lasers.

The output wavelength of the 1.34 μm microchip laser may have until recently been considered too long for optimum performance in optical fibre communication systems, where minimum dispersion was nearer 1.30 μm . However, now that silica fibre is being produced which does not show the usual large OH^- absorption peak at around 1.4 μm , the microchips output at 1.34 μm may be an alternative in communications systems. An additional point is that the 1.34 μm output from a microchip laser is easier to couple into an optical fibre (in comparison to the output of a laser diode), and the wavelength is slightly shifted from that already used in 1.3 μm systems. The 1.34 μm microchip laser may be used for lidar and other sensing systems, e.g.; vehicle avoidance and robot vision systems.

7.3 Microchip Amplifier

The same Nd:YVO_4 material that was used to produce the 1.06 and 1.34 μm microchip lasers, was used to produce an effective microchip optical signal amplifier. The investigations looked at the possibility of small signal gain at both 1.06 and 1.34 μm , as provided by the microchip lasers, with a single pass through a 1 mm long Nd:YVO_4 microchip. While the microchip lasers proved to be a very practical device, the microchip amplifiers proved to be a little more difficult, requiring small pump and signal beams, and a high level of overlap between the two.

Tests at 1.06 μm with different signal and pumping powers found the experimental saturation power to be between 7 and 7.75 mW (saturation intensity 1.0 to 1.1 $\times 10^7$ W/m^2), this being in good agreement with the theoretically predicted value of 8.5 mW (1.2 $\times 10^7$ W/m^2). From these tests the small signal region was established. With 30 μm diameter pump and signal beams, single pass gains in excess of 19.6 dB were achieved with an incident pump power of 350 mW. With the 1 mm length of Nd:YVO_4 used, this gain corresponds to a gain co-efficient of 45 cm^{-1} , which is substantially higher than previously reported for any miniature neodymium amplifier. The maximum gain achieved was reduced to a value of 4.8 dB when the pumping diameter was increased to approximately 100 μm . This indicated the need for small diameters (high intensities) to achieve high gains in this system.

Amplification at 1.34 μm proved to be problematic without a means to accurately measure and align the signal and pump beams. This was the case with the signal at 1.34 μm because the beam analyzer used to measure and align the beams contained a silicon detector. Thus, only a single gain measurement was obtained at the 1.34 μm wavelength. A gain of approximately 1.4 was obtained at an incident pump power of approximately 160 mW.

An initial theoretical model which incorporated the small signal gain equation from the laser model predicted small signal gain results for the microchip amplifier. This initial model was found to grossly over estimate the experimentally found gain, and it was found necessary to rewrite the gain equation considering the effect of pump power saturation. This second model was in good agreement with the results obtained at 1.06 μm . The maximum difference between model and experimental results when using both 30 μm pump and signal beams was 3.5 dB (figure 6.6). With the pump beam enlarged to 100 μm the maximum difference was slightly larger (figure 6.7), and this is believe to be because the model assumed unity pump and signal beam overlap. The model was also used to predict expected results with a 1.34 μm signal.

Where small pump and signal beam sizes, and good beam overlap, could be maintained, the microchip amplifier system developed produced high gain results for a 1.06 μm signal. However, given an increase to larger pump sizes, or change to a 1.34 μm signal, the gain results were relatively poor. This fact was confirmed by the related theoretical small signal gain model outcomes.

7.4 Current and Future Work

Laser diodes have brought laser technology to the mass market in many different applications and many different products, however, they have in most instances been simply used as fast light bulbs. Microchip lasers retain this small mass producible nature, but bring with them superior laser properties, like directionality and coherence, that were once only associated with

larger, more complicated laser systems. They introduce low divergence and narrow bandwidth to small, easily produced lasers. Simple pulsed and modulated microchip lasers have also been demonstrated with the addition of other small elements into a microchip arrangement.

The work conducted for this thesis was limited in its ability to optimize a Nd:YVO₄ microchip laser in that only limited crystal samples were available. The microchip laser may have been optimized in terms of output power, or single longitudinal mode tuning range, or both, by considering different microchip thicknesses and/or neodymium concentrations. A reduced microchip thickness would increase the mode spacing, and hence, single mode tuning range and output power before encountering side modes, it would also reduce the absorption and system efficiency. An increased neodymium concentration would have increased the absorption, but also reduced the upper laser level lifetime, and therefore, energy storage capacity. In combination with these tests the effect of different mirror characteristics could have been considered. Different pumping diameters, and its effect on the microchip laser's output power, beam size and divergence, may also be considered, as it was by Zayhowski (March 1990) with Nd:YAG microchip lasers. Such investigations may be considered in further optimizing, or customizing, the Nd:YVO₄ microchip laser system.

The Nd:YVO₄ microchip amplifier would benefit from further development of the single pass small signal model. A closer examination of some of the assumptions within the model would give a more accurate prediction of the gain. While the minimum pump and signal beam diameters were measured in free space, how this transforms to dimensions within the Nd:YVO₄ material could be determined and included in the model, along with the change in the beam diameters through the length of the amplifier. The interplay of the overlap between pump and signal beams may also be incorporated. In addition, as the Nd:YVO₄ has very high absorption it may be beneficial to do an iterative gain calculation along the length of the microchip amplifier considering the pump power absorbed in successive small sections along the length.

The simple co-linear end pumped microchip amplifier configuration used for the present work proved successful in achieving gain (considerable gain in the 1.06 μm signal

case), however different pumping geometry systems utilizing the high gain of the Nd:YVO₄ material may warrant investigation. For example, to improve the gain of the system and possibly ease the stringency of alignment, the Nd:YVO₄ microchip could be side pumped and the signal beam directed through the microchip close to the pumped edge. Here the signal would run through a longer length of gain material that has a high level of absorbed pump power. This type of configuration has been studied by Bernard *et al.* (June 1994) and has achieved small signal single pass gains in excess of 26 dB from a 1 cm long 3% doped Nd:YVO₄ sample with 60 W of laser diode bar power. Another possible pre-amplifier configuration and application may be as shown in figure 7.1, where the amplifier slab wave guide has similar dimensions to the fibre and when side pumped by laser diodes (or laser diode arrays) amplifies the signal prior to detection, producing better signal to noise levels at the detector.

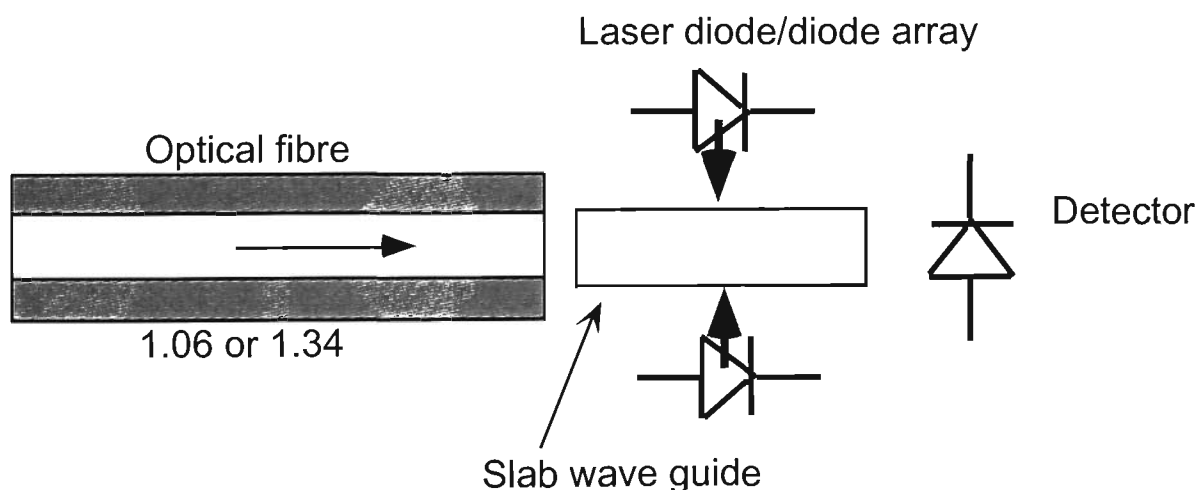


Figure 7.1: Possible Nd:YVO₄ miniature amplifier configuration for pre-amplification.

Further studies have commenced at Victoria University to investigate the development of microchip laser systems at other useful wavelengths. These include wavelengths more suitable for communications or eye-safe sensing systems. To achieve the best performance from a microchip laser material, there needs to be a high conversion of pump energy to useful laser energy (strong pump absorption and conversion to upper laser level population) over the short length of the microchip. While there are many laser materials available, most can not

absorb sufficient pump energy, and therefore achieve appreciable gain, in the short length required to harness the microchip laser advantages. Thus investigations are underway into new laser materials or modification of existing materials, with researchers generally aiming to produce materials with higher dopant concentrations than are presently available. For example, the reader is referred to the work of MacFarlane *et al.* (1997), where high dopant concentration Erbium doped materials are being investigated for microchip applications. If new materials or variations of established materials can be found with high absorption at available laser diode pump wavelengths then simple compact microchip laser systems may be developed at these wavelengths.

Appendix 1

Contained here is a literature review of further research on microchip laser based systems, which is not covered directly within the study of this thesis. It covers the development of Q-switched microchip lasers, microchip laser arrays, dopants other than Nd used in microchips, and second harmonic generation (SHG) with microchips.

Q-Switched Microchip Lasers:

Zayhowski (1991) reported pulsed microchip operation achieved with a pulsed Ti:sapphire pump laser, then demonstrated a Q-switched Nd:YAG microchip with cw laser diode pumping. The output mirror was replaced with a partially reflecting mirror and another partially reflecting mirror mounted a small distant away on a piezoelectric actuator. The change in length between the two mirrors was used to change the Q of the laser to suppress lasing and produce large population inversions, thus producing Q-switched pulses. A polarization-switchable device was also constructed by placing a LiTaO₃ birefringent crystal between the two partially reflecting mirrors.

Zayhowski and Dill (1992) produce an electro-optically Q-switched microchip laser by bonding a thin piece of Nd:YAG crystal to a LiTaO₃ crystal with electrodes deposited on it. The input face of the Nd:YAG is highly reflective coated at 1.064 μm , while at the end of the LiTaO₃ and between the two materials is a partial reflective coating. Q-switched outputs at 1.064 μm with < 2 ns pulse widths and peak powers in excess of 250 W, at repetition rates of 140 Hz were achieved.

A passively Q-switched 1.064 μm microchip laser was created by Zayhowski and Dill (1994) when they bonded a thin piece of Cr:YAG to a thin piece of Nd:YAG. The Cr:YAG operates as an intracavity saturable absorber and prevents the onset of lasing until the average inversion density reaches a nominal value set the properties of the saturable absorber, the laser material and the cavity. The onset of lasing at this point produces a high intracavity optical field that quickly saturates the saturable component of the loss, increasing the cavity Q and

resulting in a Q-switched output pulse. The passively Q-switched microchip laser did not require switching electronics, therefore reducing the size and complexity of the laser. Single longitudinal mode, TEM₀₀ pulses of 337 ps duration, with energies of 11 μJ, were achieved at a repetition rate of 6 kHz.

In a review article in *Laser Focus World*, Aubert (1995) described two saturable absorbers used for Q-switching microchips lasers, and outlined several new applications made possible by the technology. One saturable absorber material was a polymer substance, which was coated onto the Nd:YAG wafers before being diced into microchips. The polymer had drawbacks in that it was difficult to deposit good-quality mirror coatings with standard techniques, and the polymer was easily destroyed at high laser repetition rates. The other saturable absorber material was Cr:YAG, as reported earlier by Zayhowski and Dill (1994). The Cr:YAG allowed standard coating processes to be used, and had good thermal stability to allow high laser peak powers. Applications in range finding, including automotive obstacle avoidance, and laser marking have been outlined.

Microchip Laser Arrays:

Nabor *et al.* (1992) looked at scaling up the output power of microchip lasers by constructing microchip laser arrays. They utilized a 2D array of pump sources (diode lasers) on a Nd:YAG microchip wafer and found that the output beams of such a laser array were parallel and overlapped in the far field, with a divergence of a single element. They indicated that, “While these lasers will not replace a single diffraction-limited-beam laser of the same power, the brightness available from these arrays can be sufficient for numerous uses such as materials processing, radar, and medical applications.”

To gain a better understand of microchip arrays, Harrison and Martinsen (1994) applied Finite-element analysis to the problem of modeling thermal effects in laser diode pumped microchip lasers to predict near-field patterns, local temperatures, and fracture margins. The technique was compared to experimental results from Nd:YAG and Tm,Ho:YLF microchip

arrays, with particular attention to determining the pump powers over which individual lasers in an array would operate in a diffraction-limited mode.

Microchip Lasers using dopants other than Neodymium:

Given the successful and simple design of the microchip laser, it was only a short time before work commenced with different dopants, providing wavelengths other than those achieved using the neodymium doped materials. Storm *et al.* (1990) published results of single mode lasing with different dopant ions in YAG. Lasing at 2.091 μm was achieved with co-doping of Ho and Tm. Single mode laser output powers of up to 10 mW were achieved with a 1 mm flat/flat cavity, when the device was cooled below -15°C . Later Koch, Deyst and Storm (1993) looked at single mode lasing with co-doping of Ho and Tm into the material YLF, with both flat/flat and flat/convex microchip cavities.

Laporta *et al.* (1993) used another popular laser material, Er-Yb:glass, to demonstrate a 200 μm thick microchip laser operating at 1530 nm. The microchip laser had an output power greater than 25 mW, with a bandwidth narrower than 1 kHz.

Lasing at 1.92 μm was obtained from a Tm:YVO₄ microchip laser by Zayhowski *et al.* (1995). This device was developed as an alternative to relatively inefficient 1.9 μm laser diodes for pumping Ho-doped lasers. This device lased at a wavelength away from its peak fluorescence, presumably because of a large thermal population in the lower laser levels, though there was no significant change in the laser wavelength or threshold with decreased temperature. Single mode operation was only achieved just above threshold, with five longitudinal modes present for a pump power of 100 mW above threshold.

Microchip Lasers and Second Harmonic Generation (SHG)

Sasaki *et al.* (Oct 1991, Nov 1991) utilized Kintz and Baer's (1990) findings, of obtaining single mode operation by using a short absorption depth and not necessarily a short cavity length, and demonstrated a small single-mode Nd:YVO₄ laser. They used a 1 mm thick Nd:YVO₄ sample placed at one end of a 10 mm cavity. Sasaki also placed within the cavity

either a KTP crystal or a thienylchalcones crystal to produce SHG of the 1.06 μm light to produce green laser output at 532 nm. This was the first of a number of research projects utilizing this idea to produce compact Nd:YVO₄ SHG green lasers for the predicted application of high density optical storage. (Many of which are listed in the following paragraph).

Tatsuno *et al.* (1992) incorporated a similar Nd:YVO₄ / KTP SHG system into a conventional optical disk head and was able to achieve 3 times higher storage density than with conventional laser diode technology. Honda *et al.* (1993) looked at wavelength tuning of the green output by inserting a Brewster window in the cavity and varying the temperature of the KTP crystal. Nagai *et al.* (1993) examined the noise generation in a laser diode pumped Nd:YVO₄ laser due to optical feedback into the laser diode, and constructed a low-noise Nd:YVO₄ / KTP second-harmonic laser. Kitaoka *et al.* (1994) reported that the output from a Nd:YVO₄ / KTP system can be stabilized by using a transmission-type optical filter in the pumping path, thus locking the laser diode output to the peak absorption of Nd:YVO₄. Later Kitaoka *et al.* (1995) reported improved green output and low noise operation with the use of a grating feedback laser diode for pumping. Suzuki *et al.* (1994) also looked at low-noise operation of a Nd:YVO₄ / KTP system by examining the orientation of the Nd:YVO₄ and KTP crystals to form an inherent birefringent filter.

Taira *et al.* (1995) extended the SHG work by using the frequency doubling KTP crystal to act also as an electro-material for Q-switching. A maximum green peak power of 230 W was obtained with a 8 ns pulse width at a repetition rate of 100 Hz.

Uniphase Corporation have released a compact green laser system, which is based on diode pumped SHG in Nd:YVO₄, called the μGreen . In an article for Laser Focus World, Randolph (1995) outlined the product and reviewed possible new applications. This product was initially developed by the Microchip Laser Research Group at University of St. Andrews, Scotland, from which a number of microchip publication have been produced. [For example: MacKinnon & Sinclair (1994), Conroy *et al.* (1997)]. Several other companies are also beginning to offer products based on SHG in Nd:YVO₄. These systems produce a stable green output, require very little electrical input power, very little space and have predicted long

lifetimes. This makes them attractive to new applications, and in many cases a better alternative for existing applications where air-cooled argon ion lasers, operating in the green, are currently employed.

Harmonic generation in microchip lasers should also be possible in other materials and for other wavelength transitions. If these are achieved with anywhere near the efficiency of SHG in Nd:YVO₄, simple compact efficient microchip laser systems at many and varied wavelengths might be expected.

Appendix 2

Detailed here are calculations to determine the appropriate lens characteristics and position, in order to achieve a required pump diameter. (For example a 200 μm pump diameter is required for a 1.06 μm microchip laser).

Using the specified divergence and beam waist diameter of the Ti:sapphire laser, and following the theory and calculations outlined in section 3.2.1, the lens and lens position required to obtain an approximate 200 μm pump beam diameter may be established .

Specifications for the Ti:sapphire (see Table 3.1) give a beam diameter of 0.95 mm and a divergence of 1 mrad. These figures are specified at a wavelength of 790 nm and are assumed not to vary greatly with a small change in wavelength. Therefore:

$$d_0 = 0.95 \text{ mm and } \theta = 1 \text{ mrad.}$$

Using equation 3.3 the Rayleigh range is:

$$Z_R = d_0/\theta = (0.95 \times 10^{-3} \text{ m} / 1 \times 10^{-3} \text{ rad}) = 0.95 \text{ m.}$$

To obtain a refocused waist of 200 μm the magnification, m , becomes:

$$m = d'_0/d_0 = 200 \mu\text{m}/0.95 \text{ mm} = 0.2105.$$

Then using equations 3.11 and 3.12 the diffraction limited focal length, f_0 , is established.

$$Z_R = 0.95 \text{ m} = 950 \text{ mm} \quad Z'_R = m^2 Z_R = 42.1053$$

$$\therefore f_0^2 = Z_R Z'_R = 950 \times 42.1053 = 40000$$

$$\therefore f_0 = 200 \text{ mm}$$

Choosing a lens with a convenient focal length greater than f_0 we can establish the value of Z_2 , the distance from the old beam waist to the lens, and Z'_1 , the distance from the lens to the new beam waist. This is achieved by using equations 3.13 and 3.14

With a lens of focal length, $f = 250$ mm;

$$Z_2 = f + \frac{1}{m} \sqrt{f^2 - f_0^2}$$

$$Z'_1 = f + m^2(Z_2 - f)$$

$$Z_2 = 250 + \frac{1}{0.2105} \sqrt{(250)^2 - (200)^2}$$

$$Z'_1 = 250 + (0.2105)^2(962.5 - 250)$$

$$Z_2 = 962.5 \text{ mm}$$

$$Z'_1 = 281.6 \text{ mm}$$

Therefore, the distance from the Ti:sapphire laser's beam waist to the lens needs to be 962.5 mm, and the distance from the lens to the focused 200 μm spot will be 281.6 mm.

The Ti:sapphire laser has a Z-fold cavity, with the argon ion pump laser beam focused into the Ti:sapphire crystal in the centre of this cavity. Assuming the beam waist is within the crystal in the centre of the cavity and that the specified beam diameter of 0.95 mm is at this location, the measurement of Z_2 (old beam waist to lens) is taken from the Ti:sapphire cavity centre. The distance from the centre of the Ti:sapphire crystal to the front face panel of the Ti:sapphire laser housing was measured to be approximately 39.5 cm, thus measurements of Z_2 take this distance into account.

Appendix 3

The following is a copy of one of CASIX Inc.'s world wide web pages containing Nd:YVO₄ data which is referenced within this thesis, CASIX (1996). It has been reproduced here due to the changing nature and location of information on the internet.

CASIX laser crystals

<http://www.newsight.com/dcasix/yvobas.htm>

Nd:YVO₄ Crystal Properties

1. Basic Properties (typical for 1.1 atm%, a-cut Nd:Doped YVO₄ crystals)

Atomic Density: $\sim 1.37 \times 10^{20}$ atoms/cm²

Crystal Structure: Zircon Tetragonal, space group D_{4h}, a=b=7.12, c=6.29

Density: 4.22 g/cm³

Mohs Hardness: Glass-like, ~ 5

Thermal Expansion Coefficient: $\alpha_a = 4.43 \times 10^{-6}/K$, $\alpha_c = 11.37 \times 10^{-6}/K$

Thermal Conductivity Coefficient: $\parallel C: 0.0523$ W.cm/K, $\perp C: 0.0510$ W.cm/K

2. Optical Properties

Lasing Wavelength: 1.064 μ m, 1.342 μ m

Crystal class: positive uniaxial, $n_o = n_a = n_b$, $n_e = n_c$,

$n_o = 1.9573$, $n_e = 2.1652$, @ 1064nm

$n_o = 1.9721$, $n_e = 2.1858$, @ 808nm

$n_o = 2.0210$, $n_e = 2.2560$, @ 532nm

Sellmeier Equation (for pure YVO₄ crystals):

$n_o^2 = 3.77834 + 0.069736/(\lambda^2 - 0.04724) - 0.0108133\lambda^2$ (wavelengths in μ m's)

$n_e^2 = 4.59905 + 0.110534/(\lambda^2 - 0.04813) - 0.0122676\lambda^2$

Thermal Optical Coefficient: $dn_a/dT = 8.5 \times 10^{-6}/K$, $dn_c/dT = 3.0 \times 10^{-6}/K$

Stimulated Emission Cross-Section: 25.0×10^{-19} cm² @ 1.06 μ m

Fluorescent Lifetime: 90 μ s (about 50 μ s for 2 atm% Nd doped) @ 0.81 μ m

Absorption Coefficient: 31.4 cm⁻¹ @ 0.81 μ m

Absorption Length: 0.32 mm @ 0.81 μ m

Intrinsic Loss: 0.02 cm⁻¹ @ 1.06 μ m

Gain Bandwidth: 0.96 nm (257 GHz) @ 1.06 μ m

Polarized Laser Emission: polarization; parallel to optic axis (c-axis)

Diode Pumped Optical to Optical Efficiency: > 60%

[Return to CASIX homepage](#)

Thanks for visiting our homepage. Please forward your comments to us by filling out the feedback form or sending email:

CASIX@public.sta.net.cn

©Copyright 1995 NEWSIGHT

Appendix 4

Publications resulting from the work towards this thesis.

Performance of a Nd:YVO₄ microchip laser with continuous-wave pumping at wavelengths between 741 and 825 nm.

Mingxin Qiu, Booth D., Baxter G. & Bowkett G.

Applied Optics 32(12), 2085-2086 (1993)

Single-longitudinal-mode CW operation of a Nd:YVO₄ microchip laser at 1.34 μm .

Bowkett G.C., Baxter G.W., Booth D.J., Taira T., Teranishi H. & Kobayashi T.

Abstract published in Proc. ACOLS 93 Melbourne (Dec) p234 (1993)

Single-mode 1.34 μm Nd:YVO₄ microchip laser with cw Ti:sapphire and diode-laser pumping.

Bowkett G., Baxter G., Booth D., Taira T., Teranishi H. & Kobayashi T.

Optics Letters 19(13), 957-959 (1994)

Optical Amplification at 1.064 μm by a Nd:YVO₄ microchip.

Bowkett G., Baxter G. & Booth D.

Abstract published in Proc. of AOS 95 Brisbane (July) p72 (1995)

References

Arecchi F.T. & Schulz-Dubois E.O. (1972)

'Laser Handbook' Vol.1
North-Holland Publishing, Amsterdam

Aubert J.J. (1995)

Q-switched microchip lasers bring new applications to light
Laser Focus World (June), s11-s13

Baer T.M., Head D.F., Gooding P., Kintz G.J. & Hutchison S. (1992)

Performance of diode-pumped Nd:YAG and Nd:YLF lasers in tightly folded resonator configurations
IEEE J. of Q.E. 28(4),1131-1138

Bagdasarov Kh. S., Kaminskii A.A., Krylov V.S. & Popov V.I. (Feb 1968)

Room-temperature induced emission of tetragonal YVO₄ crystals containing Nd³⁺
Physica Status Solidi PT.27, K1-K3

Bagdasarov Kh. S., Bogomolova G.A., Kaminskii A.A. & Popov V.I. (Dec 1968)

Absorption, luminescence, and stimulated emission on YVO₄-Nd³⁺ crystals
Soviet Physics - DOKLADY 13(6), 516-518

Barnes N.P., Storm M.E., Cross P.L. & Skolaut JR M.W. (1990)

Efficiency of Nd materials with laser diode pumping
IEEE J. of Q.E. 26(3), 558-568

Bernard J.E. & Alcock A.J. (June 1993)

High-efficiency diode-pumped Nd:YVO₄ slab laser
Optics Letters 18(12), 968-970

Bernard J.E., Lokhnygin V.D. & Alcock A.J. (Dec 1993)

Grating-tuned, single-longitudinal-mode, diode-pumped Nd:YVO₄ laser
Optics Letters 18(23), 2020-2022

Bernard J.E., McCullough E. & Alcock A.J. (June 1994)

High gain, diode-pumped Nd:YVO₄ slab amplifier
Optics Comm. 109, 109-114

Bernard J.E. & Alcock A.J. (Nov 1994)

High-repetition-rate diode-pumped Nd:YVO₄ slab laser
Optics Letters 19(22), 1861-1863

Besnard P., Jia X., Dalgliesh R. & May A.D. (1993)

Polarization switching in a microchip Nd:YAG laser using polarized feedback
J. Opt. Soc. Am. B 10(9), 1605-1609

Blows J.L., Omatsu T., Dawes J., Pask H. & Tateda M. (1998)

Heat generation in Nd:YVO₄ with and without laser action
IEEE Photonics Tech. Letts. 10(12), 1727-1729

Bowkett G.C., Baxter G.W., Booth D.J., Taira T., Teranishi H. & Kobayashi T. (1993)

Single-longitudinal-mode CW operation of a Nd:YVO₄ microchip laser at 1.34 μm
Abstract published in Proc. ACOLES 93 Melbourne (Dec) p234

- Bowkett G., Baxter G., Booth D., Taira T., Teranishi H. & Kobayashi T. (1994)**
Single-mode 1.34 μm Nd:YVO₄ microchip laser with cw Ti:sapphire and diode-laser pumping
Optics Letters 19(13), 957-959
- Bowkett G., Baxter G. & Booth D. (1995)**
Optical Amplification at 1.064 μm by a Nd:YVO₄ microchip
Abstract published in Proc. of AOS 95 Brisbane (July) p72
- Brignon A., Feugnet G., Huignard J.P. & Pocholle J.P. (1995)**
Multipass degenerate four-wave mixing in a diode-pumped Nd:YVO₄ saturable amplifier
J. Opt. Soc. Am. B 12(7), 1316-1325
- CASIX (1996)**
World Wide Web page of CASIX, Inc. :- <http://www.newsight.com/dcasix/yvobas.htm>
Shown in Appendix 3
- Chan K. (1987)**
Multiple-pass laser-diode-pumped Nd:YAG amplifier: design
Applied Optics 26(16), 3177-3179
- Chen Y.F., Kao C.F. & Huang T.M. (1998)**
Single-mode operation and frequency doubling of fiber-coupled diode butt-coupling-pumped Nd:YVO₄ lasers
Applied Optics 37(3), 518-521
- Conroy R.S., Kemp A.J., Friel G.J. & Sinclair B.D (1997)**
Microchip Nd:vanadate lasers at 1342 nm and 671 nm
Optics Letters 22(23), 1781-1783
- DeShazer L.G., Bass M., Ranon U., Guha J.K. & Reed E.D. (1974)**
Laser performance of Nd³⁺ and Ho³⁺ in YVO₄, and Nd³⁺ in Gadolinium Gallium Garnet (GGG)
8th Inter. QE Conf. San Francisco (June), 7-8
- DeShazer L. (1994)**
Vanadate crystals exploit diode-pump technology
Laser Focus World (Feb), 88-93
- Fan T.Y. (1994)**
Aperature guiding in quasi-three-level lasers
Optics Letters 19(8), 554-556
- Feugnet G., Schwarz M., Larat C. and Pocholle J.P. (1993)**
TEM₀₀ surface-emitting laser-diode longitudinally pumped Nd:YVO₄ laser
Optics Letters 18(24), 2114-2116
- Feugnet G., Bussac C., Larat C., Schwarz M. and Pocholle J.P. (1995)**
High-efficiency TEM₀₀ Nd:YVO₄ laser longitudinally pumped by a high-power array
Optics Letters 20(2), 157-159
- Fields R.A., Birnbaum M. & Fincher C.L. (1987)**
Highly efficient Nd:YVO₄ diode-laser end-pumped laser
Appl. Phys. Lett. 51(23), 1885-1886
- Fields R.A., Rose T.S., Innocenzi M.E., Yura H.T. & Fincher C.L. (1989)**
Diode laser end-pumped Neodymium lasers: The road to higher power
OSA Proc. on Tunable Solid State Lasers (May1-3) 5, 301-308

- Gavrilovic P., O'Neil M.S., Zarrabi J.H., Singh S., Williams J.E., Grodkiewicz W.H. & Bruce A. (1994)**
High-power, single-frequency diode-pumped Nd:YAG microcavity lasers at 1.3 μm
Appl. Phys. Lett. 65(13), 1620-1622
- Harrison J. & Martinsen R.J. (1994)**
Thermal modeling for mode-size estimation in microlasers with application to linear arrays in Nd:YAG and Tm,Ho:YLF
IEEE J. of QE. 30(11), 2628-2633
- He C. & Killinger D.K. (1994)**
Dual-polarization modes and self-heterodyne noise in a single-frequency 2.1- μm microchip Ho,Tm:YAG laser
Optics Letters 19(6), 396-398
- Higgins T.V. (1993)**
High-quality Nd:YVO₄ crystals available
Laser Focus World (March), 39-41
- Honda T., Morimoto H. & Matsumoto H. (1993)**
Broad tuning of Nd:YVO₄ green laser by temperature control of intracavity KTiOPO₄
Jpn. J. Appl. Phys. 32, 97-98
- Innocenzi M.E., Fincher C.L., Birnbaum M. & Fields R.A. (1988)**
Diode-laser end-pumped 1.34 μm Nd:YVO₄ laser
LEOS 88 Conf. No. 12181, 321-323
- Jain R.K., Sipes D.L., Pier T.J. & Hulse G.R. (1988)**
Diode-pumped 1.34- μm Nd:YVO₄ laser
CLEO 88 Conf. No. 11881 (April) Technical Digest, 298-299
- Johnson L.F. & Nassau K. (1961)**
Infrared fluorescence and stimulated emission of Nd³⁺ in CaWO₄
Proc. IRE 49, 1704-1706
- Kaminskii A.A. (1969)**
Analysis of the Stark structure of TR³⁺ ion spectra by a laser spectroscopy method
Soviet Physics JETP 29(1), 46-48
- Kaminskii A.A., Bogomolova G.A. & Li L. (1969)**
Absorption, luminescence, induced radiation and crystal splitting of the levels of ions of Nd³⁺ in the crystal YVO₄
Inorg. Mater. (USSR) 5, 573-586
- Kaminskii A.A. (1990)**
'Laser Crystals' 2nd Ed.
Springer-Verlag, Berlin 1990
- Kane T.J., Kozlovsky W.J. & Byer R.L. (1986)**
62-dB-Gain Multiple-Pass Slab Geometry Nd:YAG Amplifier
Optics Letters 11, 216-
- Keszenheimer J.A., Balboni E.J. & Zayhowskii J.J. (1992)**
Phase locking of 1.32- μm microchip lasers through the use of pump-diode modulation
Optics Letters 17(9), 649-651
- Kintz G.J. & Baer T. (1990)**
Single-frequency operation in solid-state laser materials with short absorption depths
IEEE J. of QE. 26(9), 1457-1459

Kitaoka Y., Yamamoto K. & Kato M. (1994)

Intracavity frequency doubling of a Nd:YVO₄ laser pumped by a wavelength-locked laser diode using a transmission-type optical filter
Optics Letters 19(11), 810-812

Kitaoka Y., Urairi K., Yamamoto K., Kato M. & Sasaki T. (1995)

High-power green light generation by intracavity frequency doubling using grating feedback optics
Applied Optics 34(24), 5361-5365

Kliewer M.L. & Powell R.C. (1989)

Excited state absorption of pump radiation as a loss mechanism in solid-state lasers
IEEE J. of QE. 25(8), 1850-1854

Koch G.J., Deyst J.P. & Storm M.E. (1993)

Single-frequency lasing of monolithic Ho,Tm:YLF
Optics Letters 18(15), 1235-1237

Koechner W. (1992)

'Solid-State Laser Engineering' 3rd Ed.
Springer-Verlag (Berlin)

Kubodera K. & Otsuka K. (Feb 1979)

Single-transverse-mode LiNdP₄O₁₂ slab waveguide laser
J. Appl. Phys. 50(2), 653-659

Kubodera K., Otsuka K. & Miyazawa S. (March 1979)

Stable LiNdP₄O₁₂ miniature laser
Applied Optics 18(6), 884-890

Kubodera K. & Otsuka K. (Dec 1979)

Efficient LiNdP₄O₁₂ lasers pumped with a laser diode
Applied Optics 18(23), 3882-3883

Laporta P., Taccheo S., Longhi S., Svelto O. & Sacchi G. (1993)

Diode-pumped microchip Er-Yb:glass laser
Optics Letters 18(15), 1232-1234

Leilabady P.A., Anthon D.W. & Sipes D.L. (1990)

Diode laser array pumped cube Nd:YAG laser with stable single-frequency emission
CLEO 90 Technical Digest(May), 6

Leilabady P.A., Anthon D.W. & Gullicksen P.O. (1992)

Single-frequency Nd:YLF cube lasers pumped by laser diode arrays
CLEO 92 (Anaheim) Technical Digest(May)12, 54

Lomheim T.S. & DeShazer L.G. (1978)

Optical-absorption intensities of trivalent neodymium in the uniaxial crystal yttrium orthovanadate
J. Appl. Phys. 49(11), 5517-5522

Longhi S., Cerullo G., Taccheo S., Magni V. & Laporta P. (1994)

Experimental observation of transverse effects in microchip solid-state lasers
Appl. Phys. Lett. 65(24), 3042-3044

Longhi S. & Laporta P. (1995)

Longitudinal-transverse mode interplay and conical emission in microchip lasers
J. Opt. Soc. Am. B 12(8), 1511-1515

- MacFarlane D.R., Jazorniczky J.S., Newman P.J., Bogdanov V., Booth D.J. & Gibbs W.E.K. (1997)**
High Er(III) content ZBN glasses for microchip laser applications
J. Non-Cryst. Solids. Vol 213-214, 158-163
- MacKinnon N. & Sinclair B.D. (1994)**
A laser diode array pumped, Nd:YVO₄/KTP composite material microchip laser
Optics Commun. 105, 183-187
- Mermilliod N., Romero R., Chartier I., Garapon C. & Moncorge R. (1992)**
Performance of various diode-pumped Nd:materials: Influence of inhomogenous broadening
IEEE J. of QE. 28(4), 1179-1186
- Mingxin Qiu, Booth D., Baxter G. & Bowkett G. (1993)**
Performance of a Nd:YVO₄ microchip laser with cw pumping at wavelengths between 741 & 825 nm
Applied Optics 32(12), 2085-2086
- Mooradian A., Wall K. & Keszenheimer J. (1995)**
Microchip lasers and laser arrays: Technology and applications
Optics & Photonics News (Nov), 16-19
- Nabors C.D., Zayhowski J.J., Aggarwal R.L., Ochoa J.R., Daneu J.L. & Mooradian A. (1992)**
High-power Nd:YAG microchip laser arrays
OSA Proc. on Advanced Solid State Lasers (Feb) 13, 234-236
- Nagai H., Kume M., Yoshikawa A. & Itoh K. (1993)**
Low-noise operation (-140dB/Hz) in close-coupled Nd:YVO₄ second-harmonic lasers pumped by single-mode laser diodes
Applied Optics 32(33), 6610-6615
- O'Connor J.R. (1966)**
Unusual crystal-field energy levels and efficient laser properties of YVO₄:Nd
Appl. Phys. Lett. 9(11), 407-409
- O'Shea D.C. (1985)**
'Elements of Modern Optical Design'
Wiley, New York 1985
- Plaessmann H., Re S.A., Alonis J.J., Vecht D.L. & Grossman W.M. (1993)**
Multipass diode-pumped solid-state optical amplifier
Optics Letters 18(17), 1420-1422
- Randolph G. (1995)**
Green microlaser technology promises new applications
Laser Focus World (April), 121-125
- Robrish P. (1994)**
Single-mode electro-optically tuned Nd:YVO₄ laser
Optics Letters 19(11), 813-815
- Sasaki T. (Oct 1991)**
Intracavity second harmonic generation by organic and inorganic materials
Proc. 5th Toyota Conf. on Non-linear Optical Materials (Oct), 445-460
- Sasaki T., Kojima T., Yokotani A., Oguri O. & Nakai S. (Nov 1991)**
Single-longitudinal-mode operation and second-harmonic generation of Nd:YVO₄ microchip lasers
Optics Letters 16(21), 1665-1667

Scheps R., Myers J.F. & Mizell G. (Aug 1994)

High-efficiency 1.06 μm output in a monolithic Nd:YVO₄ laser
Applied Optics 33(24), 5546-5549

Scheps R., Myers J.F., Mizell G. & Yates K. (Sept 1994)

Internally folded Nd:YAG and Nd:YVO₄ lasers pumped by laser diodes
IEEE J. of QE. 30(9), 2132-2135

Siegman A.E. (1986)

'Lasers'
University Science Books, California 1986

Sliney Jr J.R., Leung K.M., Birnbaum M. & Tucker A.W. (1979)

Lifetimes of the 4F_{3/2} state in Nd:YVO₄
J. Appl. Phys. 50(5), 3778-3779

Storm M.E., Koch G.J. & Rohrbach W.W. (1990)

Single-mode lasing of Ho:Tm:YAG at 2.091 μm in a monolithic crystal
OSA Proc. on Advanced Solid State Lasers (March) 6, 140-143

Suzuki K., Shimomura K., Eda A. & Muro K. (1994)

Low-noise diode-pumped intracavity-doubled laser with off-axially cut Nd:YVO₄
Optics Letters 19(20), 1624-1626

Taira T., Mukai A., Nozawa Y. & Kobayashi T. (1991)

Single-mode oscillation of laser-diode-pumped Nd:YVO₄ microchip lasers
Optics Letters 16(24), 1955-1957

Taira T. (1993)

Report on Double-pass Nd:YVO₄ microchip amplifier.
Dept. of Electrical & Electronics Engineering, Fukui University, Japan

Taira T. & Kobayashi T. (1995)

Intracavity frequency doubling and Q switching in diode-laser-pumped Nd:YVO₄ lasers
Applied Optics 34(21), 4298-4301

Tatsuno K., Takahashi M., Muraoka K., Sugiyama H., Nakamura J., Andou T. & Miyai T. (1992)

High storage density optical recording with a stable micro green second harmonic generation laser consisting of Nd:YVO₄ and KTP
Jpn. J. Appl. Phys. 31, 601-604

Tucker A.W., Birnbaum M., Fincher C.L. & DeShazer L.G. (1976)

Continuous-wave operation of Nd:YVO₄ at 1.06 and 1.34 μ
J. Appl. Phys. 47(1), 232-234

Tucker A.W., Birnbaum M., Fincher C.L. & Erler J.W. (1977)

Stimulated-emission cross section at 1064 and 1342 nm in Nd:YVO₄
J. Appl. Phys. 48(12), 4907-4911

Tucker A.W., Birnbaum M. & Fincher C.L. (1981)

Stimulated emission cross section of Nd:YVO₄ and Nd:La₂Be₂O₅ (BeL)
J. Appl. Phys. 52(4), 3067-3068

Yaney P.P. & DeShazer L.G. (1976)

Spectroscopic studies and analysis of the laser states of Nd³⁺ in YVO₄
J. Opt. Soc. Am. 66(12), 1405-1414

Zayhowski J.J. (1990)

Thermal guiding in microchip lasers

OSA Proc. on Advanced Solid State Lasers (March) 6, 9-13

Zayhowski J.J. (1991)

Pulsed operation of microchip lasers

OSA Proc. on Advanced Solid State Lasers (March) 10, 265-269

Zayhowski J.J. & Mooradian A. (Jan 1989)

Single-frequency microchip Nd lasers

Optics Letters 14(1), 24-26

Zayhowski J.J. & Mooradian A. (May 1989)

Microchip lasers

OSA Proc. on Tunable Solid State Laser (May) 5, 288-294

Zayhowski J.J. & Mooradian A. (June 1989)

Frequency-modulated Nd:YAG microchip lasers

Optics Letters 14(12), 618-620

Zayhowski J.J. & Dill C. (1992)

Diode-pumped electro-optically Q-switched microchip lasers

CLEO 92 (Anaheim) Technical Digest (May) 12, 54-55

Zayhowski J.J. & Keszenheimer J.A. (1992)

Frequency tuning of microchip lasers using pump-power modulation

IEEE J. of QE. 28(4), 1118-1122

Zayhowski J.J. & Dill III C. (1994)

Diode-pumped passively Q-switched picosecond microchip lasers

Optics Letters 19(18), 1427-1429

Zayhowski J.J., Harrison J., Dill C. & Ochoa J. (1995)

Tm:YVO₄ microchip laser

Applied Optics 34(3), 435-437